



HAL
open science

Novel cyclodextrin modified electrodes for pharmaceutical and biomedical applications

Luminita Fritea

► **To cite this version:**

Luminita Fritea. Novel cyclodextrin modified electrodes for pharmaceutical and biomedical applications. Materials. Université Grenoble Alpes; Université de médecine et de pharmacie Iuliu Hatieganu (Cluj-Napoca, Roumanie), 2015. English. NNT : 2015GREAI032 . tel-01216123

HAL Id: tel-01216123

<https://theses.hal.science/tel-01216123v1>

Submitted on 15 Oct 2015

HAL is a multi-disciplinary open access archive for the deposit and dissemination of scientific research documents, whether they are published or not. The documents may come from teaching and research institutions in France or abroad, or from public or private research centers.

L'archive ouverte pluridisciplinaire **HAL**, est destinée au dépôt et à la diffusion de documents scientifiques de niveau recherche, publiés ou non, émanant des établissements d'enseignement et de recherche français ou étrangers, des laboratoires publics ou privés.



UMF
UNIVERSITATEA DE
MEDICINĂ ȘI FARMACIE
IULIU HAȚIEGANU
CLUJ-NAPOCA

**UNIVERSITÉ
GRENOBLE
ALPES**

THÈSE

Pour obtenir le grade de

DOCTEUR DE L'UNIVERSITÉ GRENOBLE ALPES

**préparée dans le cadre d'une cotutelle entre
l'Université Grenoble Alpes et**

Université de Médecine et Pharmacie, « Iuliu Hațieganu », Cluj-Napoca

Spécialité : Matériaux, Mécanique, Génie civil, Electrochimie

Arrêté ministériel : le 6 janvier 2005 -7 août 2006

Présentée par

Luminița FRITEA

Thèse dirigée par **Dr. Serge COSNIER**
codirigée par **Prof. Dr. Robert SÂNDULESCU**

préparée au sein des laboratoires
**Biosystèmes Electrochimiques et Analytiques du
Département de Chimie Moléculaire, Grenoble
Département de Chimie Analytique et Analyse Instrumentale,
Cluj-Napoca**
dans les Écoles Doctorales I-MEP2 et UMP Cluj

Novel cyclodextrin modified electrodes for pharmaceutical and biomedical applications

Thèse soutenue publiquement le **14 septembre 2015**,
devant le jury composé de :

Mr, Radu OPREAN

Professeur, UMP Iuliu Hațieganu, Cluj-Napoca, Président

Mrs, Nicole JAFFREZIC-RENAULT

Professeur, Université Claude Bernard, Lyon, Rapporteur

Mr, Dumitru TIȚA

Professeur, UMP Victor Babes, Timișoara, Rapporteur

Mr, Robert SÂNDULESCU

Professeur, UMP Iuliu Hațieganu, Cluj-Napoca, Co-Directeur de thèse

Mr, Serge COSNIER

Directeur de Recherche DCM, Grenoble, Directeur de thèse



ABSTRACT

The cyclodextrin modified electrodes with enhanced analytical performances represent an attractive promise for the future development of electrochemical (bio)sensors and remain a very active field of research for a wide range of applications in many areas, including pharmaceutical and biomedical analysis. The aim of this study was to develop novel cyclodextrin modified electrodes for pharmaceutical and biomedical applications. The β -cyclodextrin influence was investigated both in solution and immobilized at the electrode surface.

The influence of β -cyclodextrin on the electrochemical behavior of some pharmaceuticals (ascorbic acid, uric acid, caffeine, theophylline, aminophylline, and acetaminophen) in aqueous solutions was studied by using electrochemical and spectral methods, which highlighted the inclusion complexes formation.

Various techniques were used for the electrode modification with β -cyclodextrin, such as: the incorporation in carbon paste and the entrapment in polymeric films (polyethylenimine). These sensors allowed the simultaneous determination of ascorbic and uric acids. The modified electrodes were also applied for the dosage of ascorbic acid in two pharmaceutical products and for the ascorbic and uric acids quantification in human urine with good performances.

Two types of biosensors based on a new nanostructured graphene framework were developed with reduced graphene oxide, β -cyclodextrin and tyrosinase by using either layer by layer method or electropolymerization. These new nanocomposites were characterized by spectral, microscopic and electrochemical techniques. The optimized biosensors were successfully applied for catechol and dopamine determination in pharmaceutical products, serum and urine samples with good recoveries.

The solubilization in water of some new fluorophores (four new synthesized tetrazines) by using β -cyclodextrin and gold nanoparticles modified with β -cyclodextrin was reported. The redox supramolecular assemblies were characterized in water by electrochemical and fluorescence measurements. The immobilization of tetrazines onto various types of electrodes modified with polypyrrole-cyclodextrin was also achieved and examined by electrochemical, microscopic and spectroscopic techniques.

Another original contribution is the combination of nanosphere lithography by using latex beads with different diameters (900 and 100 nm), with the electropolymerization of a Ru(II)-pyrrole monomer. The achievement of highly organized micro and nanostructures showed enhanced features for the photosensitive electrogenerated poly-[Ru^{II}-pyrrole] films. Furthermore, poly-[Ru^{II}-pyrrole] film was modified with other types of pyrrole derivatives presenting complexation properties in order to immobilize biomolecules at the electrode surface.

Keywords: β -Cyclodextrin, Polymer, Graphene, (Bio)sensors, Tetrazine, Electrochemistry

RÉSUMÉ

Nouvelles électrodes modifiées avec cyclodextrines pour applications pharmaceutiques et biomédicales

Les électrodes modifiées avec cyclodextrines ayant des grandes performances analytiques représentent une alternative intéressante pour le développement de (bio)capteurs électrochimiques dans un domaine attractif de la recherche pour différentes applications, et notamment les analyses pharmaceutiques et biomédicales. Le but de cette étude a été de développer de nouvelles électrodes modifiées avec β -cyclodextrine pour des applications biomédicales et pharmaceutiques. L'influence de la β -cyclodextrine a été étudiée en solution et à la surface d'électrodes.

L'influence de la β -cyclodextrine en solution aqueuse sur le comportement électrochimique de certaines substances pharmaceutiques (l'acide ascorbique, l'acide urique, la caféine, la théophylline, l'aminophylline et l'acétaminophène) a été étudiée en utilisant des méthodes électrochimiques et spectrales, mettant en évidence la formation de complexes d'inclusion.

Diverses techniques ont été utilisées pour la modification des électrodes avec β -cyclodextrine: l'incorporation de la β -cyclodextrine dans la pâte de carbone et le piégeage dans des films polymères de polyéthylèneimine. Ces capteurs ont permis la détermination simultanée de l'acide ascorbique et de l'acide urique. Les électrodes modifiées ont été aussi appliquées pour le dosage de l'acide ascorbique dans deux produits pharmaceutiques et pour l'évaluation quantitative de l'acide ascorbique et de l'acide urique dans l'urine humaine avec de bonnes performances.

Deux types de biocapteurs basés sur une nouvelle nanostructure de graphène ont été élaborés avec de l'oxyde réduit de graphène, de β -cyclodextrine et de tyrosinase en utilisant la méthode couche par couche et l'électropolymérisation. Les nouveaux nanocomposites ont été caractérisés par des techniques spectrales, microscopiques et électrochimiques. Les biocapteurs optimisés ont été appliqués avec succès pour la détermination du catéchol et de la dopamine dans des produits pharmaceutiques et des échantillons biologiques avec une bonne récupération.

La solubilisation dans l'eau de certains nouveaux fluorophores (quatre nouvelles tétrazines) en utilisant la β -cyclodextrine et de nanoparticules d'or modifiées avec β -cyclodextrine a été signalée. Les assemblages supramoléculaires redox ont été caractérisés dans l'eau par analyses électrochimiques et de fluorescence. L'immobilisation de tétrazines sur différents types d'électrodes modifiées par polypyrrole-cyclodextrine a été également réalisée et examinée par techniques électrochimiques, spectroscopiques et microscopiques.

Une autre contribution originale est la combinaison de la lithographie avec de nanosphères utilisant des billes de latex avec différents diamètres (900 et 100 nm), avec l'électropolymérisation du monomère pyrrole-Ru(II). Des micro et nanostructures très organisées ont été réalisées en présentant de meilleures

propriétés pour le film photosensible de poly [Ru(II)-pyrrole]. Par ailleurs, le film de poly [Ru(II)-pyrrole] a été modifié avec d'autres types de dérivés de pyrrole qui présentent de propriétés de complexation utiles pour l'immobilisation des biomolécules à la surface de l'électrode.

Mots-clés : β -Cyclodextrine, Polymère, Graphène, (Bio)capteurs, Tetrazine, Electrochimie

“A thinker sees his own actions as experiments and questions - as attempts to find out something. Success and failure are for him answers above all.”

Friedrich Nietzsche

*Dedicated to my family,
professeurs
and
friends*

Acknowledgements

“Let us be grateful to the people who make us happy; they are the charming gardeners who make our souls blossom”, Marcel Proust once said. Now, at the end of my doctoral stage, I would like to acknowledge all the persons who have contributed for the completion of my thesis.

Firstly, I would like to express my deepest gratitude to my supervisors Prof. Dr. Robert Săndulescu and Dr. Serge Cosnier for providing me the opportunity to complete my PhD thesis at the University of Medicine and Pharmacy “Iuliu Hațieganu”, Cluj-Napoca, Romania and University Joseph Fourier, Grenoble, France. I want to thank them for receiving me in their prestigious teams and for the opportunity to study and work in their research laboratories. Their confidence, constant support and constructive ideas guided me on the anfractuosity of science outlining my researcher profile. Special thanks to Prof. Dr. Robert Săndulescu for his endless optimism, good humor and also for all the prolific scientific and non-scientific discussions (life lessons).

I am greatly appreciative to Dr. Cecilia Cristea for her guidance, priceless advices, continuous support and her “style”. Special thanks to Prof. Iuliu Marian and to Dr. Ede Bodoki for their scientific advices and availability. I would also like to thank Dr. Alan Le Goff and Dr. Karine Gorgy for their valuable help and guidance in the research lab, for their support and interesting ideas. My sincere thanks go to Dr. Mihaela Tertîș for her friendship, important guidance and essential contribution to my progress.

I am also grateful to all my colleagues and friends from the Department of Analytical Chemistry, Cluj-Napoca and from BEA, Grenoble for their advices, friendship and enjoyable moments spent together (in the lab or on the football field). I also thank to Dr. Liana Tamara Topală for her help concerning the spectral studies.

I am greatly thankful to Prof. Dr. Laura Vicas for her essential impulse which initiated me on this scientific way, for her unending support, confidence, advices, encouragement and inspiration. I would also like to thank to Dr. Adina Popa for her understanding and stimulation.

I would like to thank all my friends, coworkers and other persons I interacted with, for their support and understanding.

Finally, I am deeply thankful to my family for their unconditional support, love, care, encouragement and patience.

For the financial support I am grateful to UMF “Iuliu Hațieganu” for the Erasmus scholarship and for the research project POSDRU.

LIST OF PUBLICATIONS

1. **Fritea L**, Tertiş M, Topală TL, Săndulescu R. Electrochemical and spectral study of cyclodextrins interactions with some pharmaceutical substances. *Farmacia*. 2013;61(6):1054-1068. **ISI Impact Factor 1.251** (*study included in chapter 1 and 2*)
2. **Fritea L**, Tertiş M, Cristea C, Săndulescu R. New β -Cyclodextrin entrapped in polyethyleneimine film-modified electrodes for pharmaceutical compounds determination. *Sensors*. 2013;13:16312-16329. **ISI Impact Factor 2.048** (*study included in chapter 3*)
3. **Fritea L**, Florea A, Tertiş M, Săndulescu R, Cristea C. Polymer based nanostructures for innovative bio and immunosensors development. International Conference on Advancements of Medicine and Health Care through Technology "*MediTech 2014*" *Proceedings*, Simona Vlad, R.V. Ciupa (Eds), Springer, 2014;44:129-134, Print ISBN 978-3-319-07652-2; Online ISBN 978-3-319-07653-9. **ISI Proceedings** (*study included in chapter 4*)
4. **Fritea L**, Haddache F, Reuillard B, Le Goff A, Gorgy K, Gondran C, Holzinger M, Săndulescu R, Cosnier S. Electrochemical nanopatterning of an electrogenerated photosensitive poly-[trisbipyridinyl-pyrrole ruthenium(II)] metallopolymer by nanosphere lithography. *Electrochemistry Communications*. 2014;46:75-78. **ISI Impact Factor 4.847** (*study included in chapter 6*)
5. **Fritea L**, Tertiş M, Cristea C, Cosnier S, Săndulescu R. Simultaneous determination of ascorbic and uric acids in urine using an innovative electrochemical sensor based on β -Cyclodextrin. *Analytical Letters*. 2015;48(1):89-99. **ISI Impact Factor 1.031** (*study included in chapter 3*)
6. **Fritea L**, Tertiş M, Cosnier S, Cristea C, Săndulescu R. A novel reduced graphene oxide/ β -cyclodextrin/tyrosinase biosensor for dopamine detection. *International Journal of Electrochemical Science*. 2015;10:7292-7302. **ISI Impact Factor 1.500** (*study included in chapter 4*)
7. **Fritea L**, Le Goff A, Putaux J-L, Tertis M, Cristea C, Săndulescu R, Cosnier S. Design of a reduced-graphene-oxide composite electrode from an electropolymerizable graphene aqueous dispersion using a cyclodextrin-pyrrole monomer. Application to dopamine biosensing. *Electrochimica Acta*. 2015;178:108-112. **ISI Impact Factor 4.504** (*study included in chapter 4*)
8. **Fritea L**, Audebert P, Galmiche L, Gorgy K, Le Goff A, Săndulescu R, Cosnier S. First occurrence of tetrazines in aqueous solution. *Electrochemistry and fluorescence*. *ChemPhysChem*. 2015, accepted. **ISI Impact Factor 3.419** (*study included in chapter 5*)

Table of Contents

ABBREVIATIONS	15
INTRODUCTION	17
STATE OF THE ART	19
1. Cyclodextrins in pharmaceutical and biomedical electroanalysis	21
1.1. Introduction.....	21
1.2. The electrochemical study of cyclodextrins in solution	25
1.3. Cyclodextrins as electrode modifiers	26
1.3.1. Langmuir-Blodgett technique and Self-Assembly Method	26
1.3.2. Cyclodextrins in plasticized membranes	28
1.3.3. Cyclodextrins modified screen-printed electrodes	29
1.3.4. Cyclodextrins modified carbon paste electrodes.....	29
1.3.5. Nanoparticles coated with cyclodextrins	32
1.3.6. Cyclodextrins in polymeric films	34
1.3.7. Carbon nanomaterials modified with cyclodextrins	38
1.4. Cyclodextrins tagged biomolecules	47
1.5. Cyclodextrins as biomimetic receptors and the comparison with other affinity systems.....	47
1.6. Conclusions.....	50
PERSONAL CONTRIBUTION	51
1. Electrochemical and spectral study of some pharmaceuticals with β-cyclodextrin interactions in solution	53
1.1. Introduction.....	53
1.2. Experimental	53
1.3. Results and discussions	54
1.3.1. The electrochemical behavior of the studied pharmaceuticals in the presence of β-cyclodextrin.....	54
1.3.2. Determination of binding constant K_i for β-CD inclusion complexes with the studied pharmaceuticals.....	57
1.3.3. Infrared spectra of the inclusion complexes.....	58
1.4. Conclusions.....	60
2. β-cyclodextrin modified carbon paste electrodes for ascorbic and uric acids detection	61
2.1. Introduction.....	61
2.2. Experimental	61
2.3. Results and discussions	61
2.4. Conclusions.....	63
3. Glassy carbon electrodes based on β-cyclodextrin entrapped in polyethyleneimine film for ascorbic and uric acids determination	65
3.1. Introduction.....	65
3.2. Experimental	66

3.2.1. Materials and methods.....	66
3.2.2. Preparation of the working electrodes.....	66
3.2.3. Real samples preparation and analysis	66
3.3. Results and discussions	67
3.3.1. Electrochemical, spectral and microscopic analysis	67
3.3.2. Real samples analysis	77
3.4. Conclusions.....	83
4. Novel biosensors for dopamine detection based on GCEs modified with tyrosinase/β-cyclodextrin/ reduced graphene oxide composite	85
4.1. Introduction.....	85
4.2. Experimental	86
4.2.1. Synthesis	86
4.2.2. Reagents and solutions	86
4.2.3. Biosensor preparation.....	87
4.2.4. Electrochemical, spectral and microscopic analysis	87
4.2.4. Real samples preparation	88
4.3. Results and discussions	89
4.3.1. β -cyclodextrin/reduced graphene oxide biosensor.....	89
4.3.2. Reduced graphene oxide/pyrrole- β -cyclodextrin biosensor	94
4.4. Conclusions.....	99
5. Electrochemical and spectral behavior of tetrazines	101
5.1. Introduction.....	101
5.2. Experimental	103
5.2.1. Synthesis	103
5.2.2. Electrochemistry measurements.....	103
5.2.3. UV-visible measurements and fluorescence measurements	103
5.3. Results and discussions	104
5.3.1. Tetrazines behavior in aqueous solution.....	104
5.3.2. Electrochemical, spectral and microscopic studies of the immobilized tetrazines	109
5.4. Conclusions.....	118
6. Nanostructured photosensitive poly-[trisbipyridinyl-pyrrole ruthenium(II)] metallopolymer by nanosphere lithography	119
6.1. Introduction.....	119
6.2. Experimental	120
6.2.1. Methods and Instrumentation	120
6.2.2. Elaboration of electrodes and characterization	120
6.2.3. Photocurrent generation experiments.....	120
6.3. Results and discussions	121
6.3.1. Electrochemical studies	121
6.3.2. Microscopic characterization.....	124
6.3.3. Photoelectrochemical studies	125
6.4. Conclusions.....	128
7. General conclusions	129
8. Originality of the thesis	131
REFERENCES	133

ABBREVIATIONS

Ab/Ag	Antibody/antigen
AuNP CD	Gold nanoparticle modified with cyclodextrin
ACN	Acetonitrile
CD	Cyclodextrin
CNT	Carbon nanotube
CPE	Carbon paste electrode
CV	Cyclic voltammetry
DMF	Dimethylformamide
DMSO	Dimethylsulfoxide
EIS	Electrochemical impedance spectroscopy
Fc	Ferrocene
FTIR	Fourier transform infrared spectroscopy
GCE	Glassy carbon electrode
GO	Graphene oxide
GOX	Glucose oxidase
GOX-CD	Glucose oxidase modified with cyclodextrin
ITO	Indium tin oxide
LBL	Layer by layer
LOD	Limit of detection
LOQ	Limit of quantification
MWCNT	Multiwall carbon nanotube
MIP	Molecularly imprinted polymer
NSL	Nanosphere lithography
NMR	Nuclear magnetic resonance
PBS	Phosphate buffer solution
PEI	Polyethyleneimine
PEDOT	Poly(3,4-ethylenedioxythiophene)
Py-CD	Pyrrole-cyclodextrin

PVC	Polyvinyle chloride
RGO	Reduced graphene oxide
RDE	Rotating disk electrode
SAMs	Self-assembled monolayers
SCE	Saturated calomel electrode
SPE	Screen-printed electrode
SEM	Scanning electron microscopy
SWCNT	Single-wall carbon nanotube
SWV	Square wave voltammetry
TEM	Transmission electron microscopy
THF	Tetrahydrofuran
UV-Vis	Ultraviolet-visible spectroscopy

INTRODUCTION

Cyclodextrins, in their native form or chemically modified, are the subject of extended research in electrochemistry and this is mainly due to their properties, such as: variable size and hydrophobic cavities. The research interest is focused both on their behavior in solutions and embedded in thin films formed at the electrode surface.

The cyclodextrins applications in electrochemistry are based on the inclusion complexes formation, molecular recognition and selective preconcentration of the analyte at the electrode surface leading to the development of highly selective sensors and biosensors. Many techniques can be used for designing the molecular architecture of the electrode/solution interface which supplies various and attractive methods for the preparation of cyclodextrins based electrochemical sensors. The most significant modification methods that involve cyclodextrins are: *Langmuir-Blodgett and Self-Assembly method*; the *incorporation in plasticized membranes*; the *deposition of a film at the surface of solid electrodes*; the *inclusion in carbon paste*; the *use of cyclodextrins for the decoration of metal particles*; and *cyclodextrins embedded in different polymer films*.

The cyclodextrins modified electrodes with enhanced analytical performances represent an attractive promise for the future development of electrochemical (bio)sensors and remain a very active field of research for a wide range of applications in many areas, including pharmaceutical and biomedical analysis.

The first objective of this work was to investigate the influence of β -cyclodextrin in aqueous solutions, on the electrochemical behavior of some pharmaceutical substances: ascorbic acid, uric acid, caffeine, theophylline, aminophylline, and acetaminophen. Electrochemical and spectral studies were used in order to study the formation of inclusion complexes between β -cyclodextrin and these molecules.

Another objective was the elaboration of various types of cyclodextrin based modified electrodes. The first technique used for the electrode modification was the incorporation of β -cyclodextrin in carbon paste, electrodes which were used for the determination of ascorbic acid and uric acid. The second modification method consisted in β -cyclodextrin incorporation in polymeric films of polyethylenimine. This approach aimed to obtain a good separation of the ascorbic and uric acids oxidation peaks for accurate determination of ascorbic acid from pharmaceutical products and for the simultaneous detection and quantification of the two compounds from urine samples.

Dopamine is an important neurotransmitter which is implicated in several nervous system disorders. Many efforts were focused on the development of electrochemical sensors for the fast and sensitive dopamine detection. Another goal of this work consisted in dopamine determination in pharmaceutical products, serum and urine samples. Glassy carbon electrodes were modified with graphene and

β -cyclodextrin through two methods. First modification consisted in layer by layer deposition of reduced graphene oxide, β -cyclodextrin, tyrosinase and polyethyleneimine. The second one used a new nanostructured graphene framework reinforced by a polymer film of pyrrole-cyclodextrin.

Reversible electrochemistry of organic molecules accompanied by an optical change is an important issue nowadays because of the possible applications like electrochromic displays, electro-optical switches or optical sensors. Tetrazines substituted with heteroatoms display interesting fluorescence properties that can be electrochemically monitored, aspect which makes them especially attractive in view of sensing applications. The solubilization in water of some new fluorophores (new synthesized tetrazines) using β -cyclodextrin and their immobilization onto electrodes modified with polypyrrole-cyclodextrin was another aim of this thesis. The formation of supramolecular assemblies between β -cyclodextrin and tetrazine derivatives can be one promising alternative for their occurrence in aqueous medium.

Another interest was the micro and nanostructuring of the photosensitive electrogenerated metallopolymers by using latex beads with different diameters. The combination of nanospheres lithography and electropolymerization represents a powerful technique for the achievement of highly reproducible and homogenous photosensitive nanostructures and interesting platforms for biosensing applications.

STATE OF THE ART

1. Cyclodextrins in pharmaceutical and biomedical electroanalysis

1.1. Introduction

Cyclodextrins (CDs) are non-reducing cyclic oligosaccharides consisting of six (α -cyclodextrin), seven (β -cyclodextrin), eight (γ -cyclodextrin) or more glucopyranose units (chair conformation) linked by α -(1,4) bonds (Figure 1). CDs are also known as cycloamyloses, cyclomaltooses and Schardinger dextrans. They were first obtained by starch digestion with *Bacillus amylobacter* and *Bacillus macerans* by Schardinger after their discovery by Villiers in 1891. They are seminatural products produced by a relatively simple enzymatic conversion (cyclodextrin glucosyl transferase enzyme, CGT-ase). The CDs structures were determined by X-ray crystallography showing that the “truncated cone” has the narrow side formed by the primary hydroxyl groups (C6) and the wider side by secondary hydroxyl groups (C2, C3), the cavity is lined by the hydrogen atoms and the glycosidic oxygen bridges. This results in a relatively hydrophobic (nonpolar) cavity compared to water and with a hydrophilic outside described as a ‘micro heterogeneous environment’ (Figure 2 and 3)¹⁻⁸.

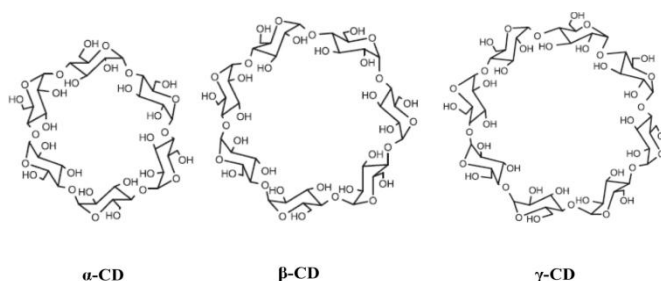


Fig. 1. Chemical structures of native cyclodextrins²

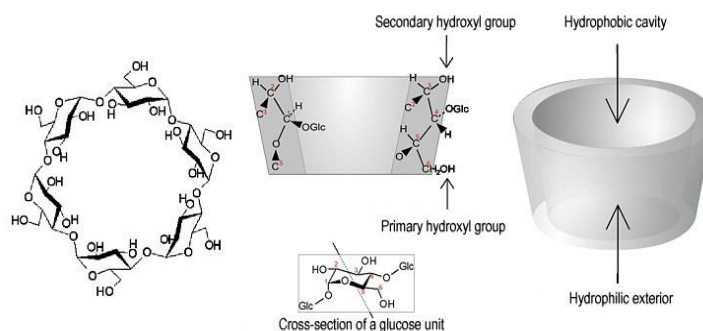


Fig. 2. Chemical structure of β -cyclodextrin⁸

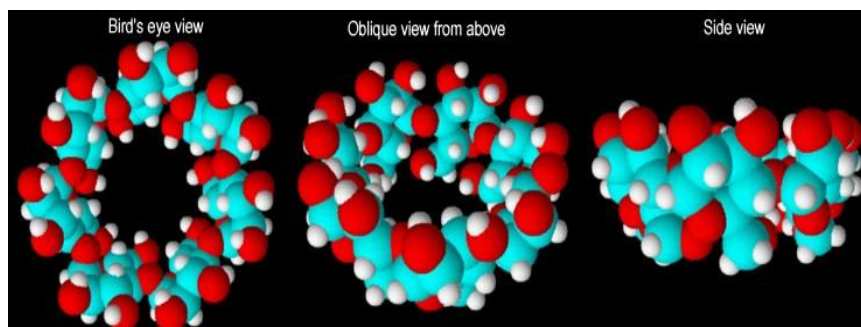


Fig. 3. 3-D representation of β -cyclodextrin⁸

CD molecules have numerous hydroxyl groups (18, 21 and 24 respectively in α -cyclodextrin, β -cyclodextrin and γ -cyclodextrin) which can be derivatized in various ways giving more than 1500 synthesized derivatives. The primary hydroxyl groups are the most reactive, readily modified to other functional groups. Secondary hydroxyl groups at carbons C-2 and C-3 have different reactivities such as: the reactivity of the hydroxyl group at C-3 is much lower than that at C-2. Hydroxyl group at C-2 is the most acidic, OH at C-6 is sterically favored, and OH at C-3 is the least reactive (apparently because of the internal hydrogen bonds). Free electron pairs of oxygen are directed towards the interior of the cavity which produces a high electron density and lending to Lewis base characteristics. The interior cavity is nonpolar in comparison with water.

The hydroxyl groups at C-2 and C-3 carbon atoms of the adjacent glucopyranose units form hydrogen bonds that stabilize the shape of the molecule and, at the same time, significantly influence the water solubility of the cyclodextrin. Through the study of the hydrogen-deuterium exchange in DMSO by NMR spectroscopy, it appears that intramolecular hydrogen bonds are formed by the secondary hydroxyl groups. It was noticed that the strength of the hydrogen bonds increases in the following order: α -, β - and γ -cyclodextrin. This behavior is due to the fact that the α -CD and β -CD protons of hydroxyl groups have lower chemical shifts according to the NMR spectroscopy investigations performed in DMSO-d₆ at 25 °C and 80 °C⁹. The mechanism of simultaneous and reversible change of directions of hydrogen bonds HO₂->O₃ and O₃H->O₂ called “flip-flop” was elucidated by X-ray studies³. Larger CDs (with more than 8 glucose units) have a restricted utilization because they present a “collapsed cylinder” structure, so their real cavity is even smaller than that of γ -cyclodextrin⁶.

The main physico-chemical properties of the native CDs are summarized in Table I^{6,7,11}.

Table I. Cyclodextrins main physico-chemical properties

Physico-chemical property	α -CD	β -CD	γ -CD
Number of glucose units	6	7	8
Molecular weight	972	1135	1297
Internal diameter/Å	4.7-5.2	6.0-6.4	7.5-8.3
Outer diameter/nm	1.53	1.66	1.72
Water solubility at 24C/g*L ⁻¹	145	18.5	232
Water molecules in cavity	6	11	17
pK _a	12.33	12.2	12.08
Height/nm	0.79	0.79	0.79
Volume/nm ³	0.174	0.262	0.472
Melting temperature range/°C	255-260	255-265	240-245

The most notable characteristic of CDs is the inclusion complexes formation with various organic and inorganic molecules (solid, liquid and gaseous compounds) in aqueous, nonaqueous and mixed media. The complex formation consist in a dimensional fit between host cavity and guest molecule when the high enthalpy water molecules from the host cavity are displaced by the more hydrophobic guest molecules leading to a nonpolar–nonpolar association and a decrease of cyclodextrin ring strain with a more stable lower energy state. The main driving forces for the inclusion complexes include Van der Waals interactions, hydrophobic interactions between the guest hydrophobic moiety and the CD cavity, hydrogen bonding between the polar groups of the guest molecules and the CDs hydroxyl groups and electrostatic interactions for ionic guests.

The inclusion of the guest (G) within the host cyclodextrin is not permanent but rather is a thermodynamic equilibrium.



$$K_c = \frac{[GCD]}{[G] \cdot [CD]}$$

The most applied analytical method to calculate the stability constants (K_c) or the dissociation constants (K_d) is the *phase-solubility method* described by Higuchi and Connors¹² (Figure 4).

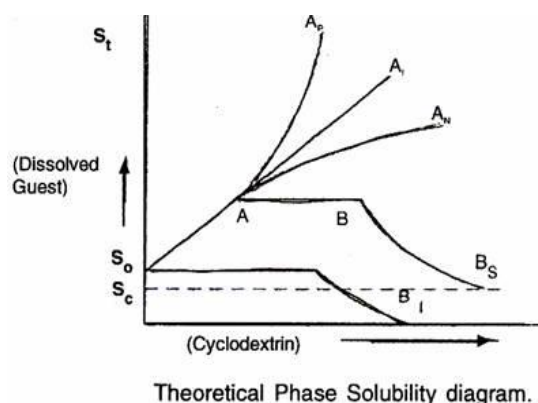


Fig 4. Theoretical phase solubility diagram; **A** - soluble inclusion complex [A_i = linear increases of drug solubility as a function of CD concentration (1:1 stoichiometry); A_p = positively deviating isotherms (higher order complex formation, more CDs molecules); A_n = negatively deviating isotherms (contribution of solute-solvent interaction)]; **B** - sparingly soluble inclusion complex [B_i = insoluble complex in water; B_s = complexes of limited solubility]¹²

β -cyclodextrin often produces type B curve due to its low solubility in water, while its derivatives give soluble compounds of type A. For 1:1 molar ratio the association constant $K_{a:b}$ can be determined from the equation¹²:

$$K_{a:b} = \frac{\text{slope}}{S_0(1 - \text{slope})}$$

S_0 is the intrinsic solubility of the drug.

The inclusion complexation leads to a significant change of the characteristic physico-chemical properties of the guest (solubility, volatility, taste, stability, chemical reactivity, electrochemical and spectral properties) entrapped inside the CD cavity. This unique behavior is responsible for the widespread applications of CDs in agriculture, food, toilet articles, textile industry, environment monitoring, analytical chemistry, pharmaceutical and medical areas¹³.

The main analytical techniques which are used for the characterization of inclusion complexes in solution include:

- Spectroscopic techniques: Ultraviolet/visible spectroscopy (UV-Vis), Circular dichroism, Fluorescence, Nuclear magnetic resonance (NMR), Electron spin resonance (ESR);
- Electroanalytical techniques: Polarography, Voltammetry, Potentiometry, Conductometry;
- Separation techniques: High performance liquid chromatography (HPLC), Capillary electrophoresis (CE);
- Polarimetry;
- Isothermal titration calorimetry (ITC)

The inclusion complexes can be also characterized in solid state by thermoanalytical methods, scanning electron microscopy (SEM), X-ray crystallography, IR spectroscopy, dissolution tests, and thin layer chromatography^{14,15}.

CDs and their derivatives, with or without templates, are widely used as building blocks involved in the construction of one or multidimensional nanostructures such as helix, (pseudo)polyrotaxane, nanotube, nanowire, dendrimer, network, vesicle, nanoparticle with diverse size and morphology. Due to their physico-chemical properties and their ability to interact with bioelements, the CD based nanoarchitectures constructed by molecular assembly became a powerful platform in supramolecular chemistry and nanotechnology¹⁶.

In the last decades, CDs and their derivatives received considerable and increasing attention in the pharmaceutical and biomedical field due to their multiple applications in drug solubility, bioavailability, stability, safety, and delivery.

CDs are also widely used in analytical chemistry as catalysts, enantioselectors and molecular receptors. They were employed for the determination of certain analytes and many results concerning electrochemical sensing devices were published¹⁻³. CDs (natural or chemically modified) with their variable size hydrophobic cavities are the subject of expanded electrochemical research including both their behavior in homogeneous solutions and in thin films attached to the electrode surfaces.

1.2. The electrochemical study of cyclodextrins in solution

The electrochemical investigations of CDs in solution rely on the formation of inclusion complexes using potentiometric titrations and cyclic voltammetry when the binding constants can be determined. The influence of the CD upon the electrochemical behavior of the guest consists in decreased peak currents and shifts in the oxidation and reduction potentials in cyclic voltammetry due to the smaller diffusion coefficients of the complexes than that of the guest alone, and to the relatively high stability of these complexes².

The inclusion of many pharmaceutical substances having various pharmacological effects such as: barbitone sodium, phenylhydrazine hydrochloride, 1,4-benzoquinone, 9,10-anthraquinone, phenothiazine, indomethacin, nalidixic acid, irisquinone, catecholamines (adrenaline, dopamine), hexamethylenetetramine, lumazine, rutin, β -lapachone, steroids (estrone, estradiol), methyl violet and ethyl violet, gliclazide, Pb, chloramine T, chlorpromazine, vitamin K₃, ascorbic acid) within CDs has been investigated using various electrochemical methods (potentiometry, cyclic voltammetry, differential pulse stripping voltammetry, differential liner sweep voltammetry, differential pulse voltammetry using glassy carbon electrodes, hanging mercury drop electrodes or ion-selective electrodes). The interactions of drugs with CDs caused pronounced changes in the electrochemical behavior of the drug. The stoichiometry of most complexes formed in solution is inferred to be 1:1. In the presence of CDs a decrease of the cathodic/anodic peak current with the

increase of the amount of CDs was noticed in all experiments, variation which is attributed to the decrease of concentration of free drug, and to the lower diffusion coefficients of inclusion complexes compared with the free guest^{2,17-20}.

The electrochemical oxidation of the guests in aqueous solutions is not only reduced, but even greatly suppressed by CDs^{21,22}, behavior which can be useful for the protection of the easily oxidative molecules.

The experimental results suggest that both the dimension and polarity of the guest and host molecules influence the inclusion complex stability. Indomethacin presented a higher affinity for β -CD because the guest-host interaction was the most exergonic²³. The same observation was noticed for nalidixic acid revealing 2 recognition elements in the binding process: hydrophobic interaction between 2 methylpyridine sides and the β -CD cavity, and a hydrogen bond between the carboxyl group which remained outside the cavity and the secondary hydroxyl group of β -CD²⁴. Lumazine had a greater affinity for α -CD than for β -CD²⁵.

The influence of the cosolvent on the inclusion complexes formation was also studied. In the presence of acetonitrile, the interactions between steroids and CDs were weakened suggesting a competition of the cosolvent molecules with the guest for CD cavity²⁶. In DMF, CDs generated head-to-tail coupling between the electrogenerated acetophenone anion radicals acting as weak proton donors towards them, meanwhile in water the inclusion complexes formation is favored. Another aspect which was evidenced by experiments is that CDs stabilized the electrogenerated chloroacetophenone and chlorobenzophenone anion radicals and not the bromobenzophenone anion radical (a lower r^* C-X orbital)²⁷. Mertins *et al.* showed that the complexation between the ferrocene moiety of the tamoxifen derivative and the CD cavity became stronger as the solvent polarity increased²⁸.

1.3. Cyclodextrins as electrode modifiers

The CDs applications in electrochemistry are based on the inclusion complexes formation, molecular recognition and selective preconcentration of analyte at the electrode surface leading to the development of highly selective sensors and biosensors. Many techniques can be used for designing the molecular architecture of the electrode/solution interface which offer various and attractive methods for the preparation of CDs electrochemical sensors.

1.3.1. Langmuir-Blodgett technique and Self-Assembly Method

Langmuir-Blodgett (L-B) monolayers are obtained by transferring the monolayers from the air-water interface onto solid substrates requiring amphiphilic CD molecules². CDs modified with organo-sulfur compounds (thiols, disulfides, silanes) are able to chemisorb on metal electrodes (especially gold) forming highly organized monolayers (self-assembled monolayers – SAMs). The number of the thiol groups and the spacer length between the thiol group and the CD cavity influence the density and permeability of CD films: the film of monothiolated CDs is less permeable

than multithiolated films, the packing density of the titled CD cavities increases with spacer length¹⁶. The formation of “nanotube” structures of β -CD was found to be induced by potential-controlled adsorption on Au(III) surfaces².

These types of CDs modified electrodes have many applications in pharmaceutical and medical analysis. A highly sensitive and reproducible sensor based on a cyclodextrin modified gold electrode was elaborated for the measurement of ultra-trace lead concentrations in blood²⁹.

A novel genosensor platform based on CD supramolecular interactions has been developed for the detection of DNA³⁰, while the transglutaminase activity was determined by using an electrochemical sensor based on the patterning of gold electrodes with a mixed self-assembled monolayer of perthiolated β -cyclodextrin and 1-octanethiol³¹. The construction of nanoporous assemblies based on single self-assembled monolayer of mono-(6-deoxy-6-mercapto)- β -cyclodextrin (β -CDSH) and two-component monolayers of β -CDSH and 11-mercaptoundecanoic acid was described and was applied for the investigation of the tricyclic antidepressants drugs, chlorprothixene and imipramine³². A chemically modified electrode based on a suitable thiolate β -cyclodextrin derivative in the form of SAM was elaborated and was used for the evaluation of trimethylcetylammmonium ion and ursodeoxycholic acid. The sensor can work as channel sensor being used for the detection of non electroactive analytes forming a strong inclusion complex with β -CD if a suitable marker able to permeate the β -CD cavity is used³³.

A molecular imprinting method involving a three-step sequential self-assembly procedure was applied to prepare gold electrodes responsive towards ibuprofen based on the competition of ferrocene and ibuprofen for the cyclodextrin cavities in the monolayer³⁴. The gold electrodes modified with cyclodextrin monolayers prepared by sequential method were elaborated for the detection of some selected guest molecules: ferrocene, ibuprofen, methylene blue, dopamine and menadione³⁵.

β -cyclodextrin coated Au electrodes were used for a reversible immobilisation of adamantane modified phenylalanine dehydrogenase by a supramolecular association: the formation of inclusion complexes between CD and adamantane. The biosensor showed a linear amperometric response up to $3 \cdot 10^{-3}$ mol L⁻¹ L-phenylalanine with a detection limit of $15 \cdot 10^{-6}$ mol L⁻¹ ^{36,37}. Dopamine was selectively detected in the presence of ascorbic acid at a gold electrode modified by a β -cyclodextrin/thioctic acid mixed monolayer and on a gold electrode with self-assembled *D,L*-cysteine grafted β -cyclodextrin sulfonic acid^{38,39}. Dopamine which was included in the α -CD cavities anchored to the gold electrode surface by SAM acted as a mediator for the dopamine molecules from the bulk buffer solution diffusing to the electrode⁴⁰. The inclusion complexes between cortisol and cortisone and a self assembled β -cyclodextrin derivative monolayer has been evaluated using electroactive species permeable and impermeable in the β -CD cavity⁴¹.

1.3.2. Cyclodextrins in plasticized membranes

The lipophilic CDs can be incorporated in plasticized PVC membranes and used as ionophores in potentiometric ion-selective electrodes for the detection of a wide range of pharmaceutical/medical analytes (ephedrinium ions, tetraalkylammonium ions, dopaminium ion, local anesthetics, tricyclic antidepressants as imipramine, desipramine, trimipramine, propranolol, ephedrine, amphetamine, guanidinium ions as metformin, phenformin, guanidine, creatinine, choline, acetylcholine, lidocaine); enantioselection for ephedrinium ions and (+) propranolol were also defined. Voltametric and amperometric sensors for dopamine and tricyclic antidepressant drugs were obtained by depositing alkylated CDs in plasticized polymer matrix on screen-printed electrodes. A screen-printed electrode with layers of ferrocene-based redox mediator, enzymes (horseradish peroxidase, choline oxidase and acetylcholine esterase) and alkylated- β -CD in plasticized polyurethane was prepared and applied for the measurement of acetylcholine at subpicomolar levels with negligible interference from ascorbic acid, dopamine and atropine¹⁷.

The benzodiazepine (diazepam and midazolam) ion-selective electrodes for the analysis of pharmaceutical formulations were elaborated by incorporating within polymeric membranes β -cyclodextrin or (2-hydroxypropyl)- γ -cyclodextrin as ionophores, 2-fluorophenyl or 2-nitrophenyl ether as plasticizer and potassium tetrakis(*p*-chlorophenyl) borate as ionic additive⁴².

Novel cyclodextrin-based dextromethorphan potentiometric sensors were developed using 3 types of electrodes: silver coated wire electrode, coated graphite electrode and the conventional PVC membrane electrodes. These electrodes based on CDs ionophores shown a considerable selectivity towards dextromethorphan with Nernstian slopes depending on the type of the electrode and the ionophore used. Silver coated wire electrode incorporated with heptakis (2,3,6-tri-*O*-methyl)- β -CD and sodium tetrakis(4-fluorophenyl) borate with *o*-nitrophenyloctylether as membrane plasticizer, showed the best electroanalytical performances (linear concentration range from 10^{-7} to 10^{-2} mol L⁻¹, Nernstian compliance 59.0 ± 0.22 mV decade⁻¹ and detection limit of $7 \cdot 10^{-8}$ mol L⁻¹)⁴³.

Potentiometric ephedrine-selective membrane sensors were developed using triacetyl- β -cyclodextrin as neutral ionophore, dioctylsebacate as a plasticizer, Na tetraphenyl borate as an anionic excluder and PVC as a polymeric matrix. It provided good analytical performances: wide linear response range ($3.1 \cdot 10^{-5}$ - $7.9 \cdot 10^{-3}$ mol L⁻¹), low detection limit ($5.7 \cdot 10^{-6}$ mol L⁻¹), wide working pH range (3 - 8), fast response (10 s) and better selectivity than those previously reported for ephedrine sensors⁴⁴.

For ibuprofen monitoring in pharmaceuticals and natural water a potentiometric sensor was developed comprising 1.2 % α -cyclodextrin, 65.6 % *o*-nitrophenyloctylether as plasticizer, 42 % mol (relative to the molar concentration of the ionophore) of tetradodecylammonium bromide and 32.8 % PVC. The sensor presented a constant sensitivity of -59.0 mV decade⁻¹ in the concentration range of $3.87 \cdot 10^{-6}$ to 10^{-2} mol L⁻¹ at pH 9 with a practical detection limit of $3.34 \pm 0.03 \cdot 10^{-6}$ mol L⁻¹ for ibuprofen⁴⁵.

The preparation of diclofenac-selective membrane electrodes incorporating β -cyclodextrins as ionophores: (2-hydroxypropyl)- β -cyclodextrin, heptakis(2,3,6-tri-*o*-methyl)- β -cyclodextrin, and heptakis(2,3,6-tri-*o*-benzoyl)- β -cyclodextrin was also reported. After the optimisation of the membrane composition, the best results were obtained by using a heptakis(2,3,6-tri-*o*-benzoyl)- β -cyclodextrin based membrane electrode. The electrode was characterized by a near-Nernstian response slope of -60.0 mV/decade over the linear range of $5.0 \cdot 10^{-5}$ - 10^{-2} mol L⁻¹ and a detection limit of $1.4 \cdot 10^{-5}$ mol L⁻¹. The proposed electrode can easily discriminate diclofenac ions from several inorganic and organic interferences and some common drug excipients⁴⁶.

A high sensitive dopamine potentiometric sensor was elaborated using ultra-thin cobalt oxide (Co₃O₄) nanowires grown on gold coated glass substrates, polyvinyl chloride as plasticized polymer and β -cyclodextrin as ionophore⁴⁷.

1.3.3. Cyclodextrins modified screen-printed electrodes

Carbon-based screen-printed electrodes (SPEs) were modified with thin films of the condensation polymers of β -cyclodextrin (β -CDP) or carboxymethylated β -cyclodextrin (β -CDPA) for determination of tricyclic antidepressive drugs from serum samples. A simple two-step procedure was used comprising a preconcentration step followed by the differential pulse voltammetry quantification. The accumulation properties (120 s accumulation) of the β -CDPA film appeared to be favorable as compared to those of the β -CDP film⁴⁸.

A screen printed graphite electrode with α -CD modified graphite ink has been developed for a simple and sensitive determination of phenolic compounds in an aqueous solution by using cyclic voltammetry, differential pulse voltammetry and square wave voltammetry. Phenols formed inclusion complexes with the α -CD immobilized at the carbon-based SPE surface. The detection limit for phenols was $500 \pm 7 \cdot 10^{-9}$ mol L⁻¹ for DPV, in a linear range of 0.5 - $25 \cdot 10^{-6}$ mol L⁻¹ and $30 \pm 2 \cdot 10^{-9}$ mol L⁻¹ for SWV, in a linear range of $30 \cdot 10^{-9}$ - $50 \cdot 10^{-6}$ mol L⁻¹, respectively⁴⁹.

Dopamine quantification was achieved using a screen-printed electrode modified by electropolymerization of cyclodextrin with glucose oxidase (SPE/MWCNT/ β -CD-GOX). The biosensor displayed a detection limit of $0.48 \cdot 10^{-6}$ mol L⁻¹ in a linear range of 10 - $50 \cdot 10^{-6}$ mol L⁻¹ with a sensitivity of 0.0302 A L mol⁻¹. Dopamine quantification can be performed in the presence of interfering agents such as ascorbic and uric acids⁵⁰.

1.3.4. Cyclodextrins modified carbon paste electrodes

Carbon paste electrodes (CPEs) for a wide range of anodic and cathodic applications can also be modified with cyclodextrins.

A selective and sensitive hydroxypropyl- β -cyclodextrin modified carbon paste sensor was elaborated for the quantification of (+) catechin in some commercial drinks (tea, cocoa, and coffee) and urine samples with recoveries between 98–102 %. Anodic and cathodic voltammetry was used for the electrochemical

characterization of the catechin behavior at the modified electrochemical sensor obtaining linear ranges up to 7.20 and 4.20 $\mu\text{g mL}^{-1}$, 0.12 and 0.30 ng mL^{-1} , detection limits of 1.10 and 2.80 ng mL^{-1} , quantification limits, respectively^{51,52}.

Nitrendipine determination was achieved with a carbon paste electrode modified with β -cyclodextrin. The stripping differential pulse voltammetric analysis presented a significant increase in the peak current of the nitrendipine reduction, probably due to formation of an inclusion complex between β -cyclodextrin and nitrendipine⁵³.

A β -cyclodextrin modified carbon paste electrode presented significantly increased sensitivity and selectivity for donepezil. Thus, donepezil voltammetric determination led to a linear response in the concentration range $3.2 \cdot 10^{-9}$ to $4.2 \cdot 10^{-8}$ mol L^{-1} , with a detection limit of $1.2 \cdot 10^{-9}$ mol L^{-1} and a quantification limit of $0.40 \cdot 10^{-8}$ mol L^{-1} ⁵⁴.

Carbon paste electrodes modified with α - and β -cyclodextrins (CPE α -CD, CPE β -CD) were obtained by applying 30 potential cycles in HClO_4 media, thus forming on the substrate a film with electroactive characteristics. The modified electrodes were used to determine Pb(II) ions in solution within the range from 10^{-5} up to 10^{-3} mol L^{-1} ⁵⁵.

Ascorbic acid was electrocatalytically oxidized at the β -CD–Ferrocene inclusion complex modified carbon paste electrode. The anodic current was proportional to the concentration of ascorbic acid in the range 10^{-3} - $5.0 \cdot 10^{-7}$ mol L^{-1} with the detection limit of 10^{-7} mol L^{-1} ⁵⁶. The electrochemical behavior of the tricyclic antidepressants (imipramine, trimipramine and thioridazine) was investigated on carbon paste electrodes modified with β -cyclodextrin by differential pulse voltammetry with 120 s of accumulation leading to detection limits down to nanomolar concentrations. The modified electrode was applied to the determination of imipramine and thioridazine in pharmaceutical products⁵⁷.

The interaction of dopamine with cyclodextrin on a carbon paste electrode formed with different membranes at different experimental conditions (such as concentrations of perchloric acid and β -cyclodextrin) was studied⁵⁸.

A voltammetric determination of sparfloxacin, ofloxacin, norfloxacin, gatifloxacin and lomefloxacin at a β -cyclodextrin modified carbon paste electrode was described and the increase in the reduction peak currents were attributed to the complex formation of the quinone group of the drugs with β -cyclodextrin at an accumulation time of 160 s. The metal ions interference in the peak current response for the quoted fluoroquinolones was studied. The modified carbon paste electrode exhibited good sensitivity and stability which allowed its application to the determination of the pharmaceutical substances in both commercially available drugs and spiked human urine samples^{59,60}.

Sensitive and accurate voltammetric studies of prednisolone, dexamethasone and hydrocortisone were carried out at β -cyclodextrin modified carbon paste electrode by using cyclic voltammetry and differential pulse voltammetry. The formation of the inclusion complex between the keto-group from the corticosteroid drug and β -cyclodextrin determined the enhancement of the peak current⁶¹.

A carbon paste electrode modified with a β -cyclodextrin-azomethine-H inclusion complex was developed for the potentiometric determination of H_3BO_3 in aqueous solution where azomethine-H plays the role of molecular recognition agent. Glutaraldehyde and nafion were used to avoid the loss of the recognition agent⁶².

A cyclodextrin modified carbon paste electrode exhibited an increased sensitivity and selectivity for anagrelide, the voltammetric method being successfully applied for the drug determination in spiked serum sample, urine samples and pharmaceutical formulations⁶³.

An electrochemical sensor for fluoroquinolones (ciprofloxacin, ofloxacin, norfloxacin and gatifloxacin) based on polymerization of β -cyclodextrin and *l*-arginine (*l*-arg) modified carbon paste electrode was elaborated. The successful modification of the electrode surface was demonstrated by scanning electron microscope images. Electrochemical impedance spectroscopy indicated that the β -CD and *l*-arg copolymer efficiently decreased the charge transfer resistance value of the electrode and improved the electron transfer kinetic. This sensor was successfully applied to detect the concentrations of each drug in pharmaceutical formulations and human serum samples with good reproducibility, long-term stability and fast current response⁶⁴.

The tenoxicam oxidation was studied at a carbon paste electrode modified with a β -cyclodextrin polymer, showing that it is an adsorption controlled process due to formation of a surface inclusion complex with the β -CD molecules from the surface of the polymer. The surface concentration of the tenoxicam's reduced form and the surface inclusion constants were also determined⁶⁵.

A sensor with high sensitivity, low detection limit and excellent reproducibility has been developed for the electrochemical determination of nifedipine using β -CD and CNTs as modifiers in a carbon paste electrode. Cyclic voltammetry, electrochemical impedance spectroscopy and differential pulse adsorptive stripping voltammetry were employed to study the electrochemical behavior of the drug and scanning electron microscopy was utilized for the characterization of the surface morphology of the modified electrodes. The analytical application consisted in determining the concentration of nifedipine in pharmaceutical formulations and biological fluids (urine and serum)⁶⁶.

A CPE modified with a conducting polymer produced by electrochemical polymerization of β -cyclodextrin, influenced drastically the electrochemical response of the dopamine, increasing the peak current density and diminishing the peak potential as a result of the supramolecular interactions between the dopamine and the poly- β -CD. The CPE/poly- β -CD changed the dopamine's redox behavior, from an initially diffusion-controlled process (at the bare CPE) to an adsorption-controlled one. This sensor was tested for the dopamine detection in real samples with 99% recovery, showing satisfactory results even in the presence of its major interfering agent, ascorbic acid⁶⁷.

1.3.5. Nanoparticles coated with cyclodextrins

The recent development of gold nanoparticle based biosensors is accomplished due to the unique properties of gold nanoparticles: immobilization of biomolecules retaining their biological activity and efficient conducting interfaces with electrocatalytic ability generating an intensive used tool for the electrochemical biosensors construction^{68,69}. Other type of metal nanoparticles, such as Co, Fe, Zn, Ti, Cu, Ag with excellent electric conductivity were also functionalized with CDs resulting in new materials with multiple applications in the fields of biosensors, especially for biomedical applications, due to their biocompatibility and to the special inclusion ability of the CD molecules.

A bienzymatic nanoassembly was prepared by the immobilization of catalase modified with 1-adamantane carboxylic acid on β -cyclodextrin-coated gold nanospheres via supramolecular associations and by co-immobilization of β -cyclodextrin-modified superoxide dismutase. The pH range of catalase was increased and the thermal stability was improved, meanwhile the superoxide dismutase was 90-fold more resistant to inactivation by H_2O_2 after co-immobilization on gold nanoparticles⁷⁰.

An electrochemical sensor based on β -cyclodextrin-cobalt ferrite nanocomposite was developed showing an enhanced electrochemical response and excellent analytical performance for catechol detection due to the high catechol-loading capacity on the electrode surface mediated by CD and to the great electric conductivity of cobalt ferrite nanoparticles⁷¹.

Magnetic particle of Fe_3O_4 encapsulated within a shell of SiO_2 and functionalized with folate ligand, fluorescence tag and CD was able to perform a quadruple of activities: magnetic manipulation, bioimaging, cancer cell-targeting and drug storing-and-releasing⁷².

Monochlorotriazinyl- β -cyclodextrin was grafted onto the surface of ZnO nanoparticles through nucleophilic substitution reactions. Characterization of functionalized ZnO nanoparticles were carried out by FTIR, elemental analysis, thermogravimetric analysis, X-ray diffraction, field emission scanning electron microscopy and transmission electron microscopy⁷³.

Fe_3O_4 nanoparticles surface was modified with mono-6-deoxy-6-(*p*-tolylsulfonyl)-cyclodextrin and were employed for detecting uric acid by using cyclic voltammetry. The new materials exhibited excellent molecular recognition ability and shown high electrochemical response due to the combination of individual advantages of magnetic nanoparticles and CDs⁷⁴.

Highly fluorescent and water-soluble CdTe quantum dots (QDs) using β -cyclodextrin as surface-coating agents were fabricated simultaneously possessing unique optical properties of QDs and excellent molecular recognition ability of β -CD⁷⁵. β -cyclodextrin modified CdTe quantum dots were used as fluorescent nanosensor for acetylsalicylic acid determination, also studying the interference effects of its metabolites and ascorbic acid⁷⁶.

The self-assembly of TiO₂ nanoparticles with cyclodextrin molecules into a self-supporting fiber network was studied pointing out the role of dehydration of the cyclodextrin molecules in solution supplying the force that drives self-assembly⁷⁷. Silver nanoparticles surface was modified with β -CD surrounding layer showing a promising bactericidal activity against the microorganism *Escherichia coli*⁷⁸.

Gold nanoparticles embedded in amine functionalized silicate and β -cyclodextrin composite were prepared using a single step synthetic method and were used for the GCE modification. β -CD played a major role both in the synthesis of smaller size nanoparticles and electrocatalytic reduction and sensing of nitroaromatics⁷⁹.

The use of β -cyclodextrin gold nanoparticles as an intermediate layer for the specific anchoring of adamantane tagged enzyme has led to efficient amperometric glucose biosensors with the highest sensitivity and maximum current density. The β -cyclodextrin-modified gold nanoparticles were attached onto the poly(adamantane-pyrrole) functionalized SWCNTs coatings, 3D composite configuration which offers a high-specific surface with an excellent accessibility for the anchoring of enzymes via affinity interactions and represents an attractive way to develop multilayered enzyme assemblies⁸⁰ (Figure 5).

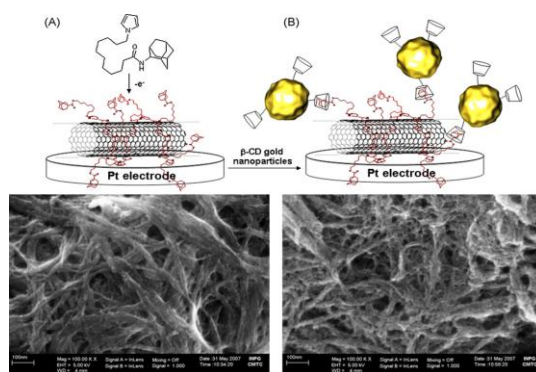


Fig. 5. Schematic presentations and SEM images of the poly(adamantane pyrrole) film electrogenerated on a SWCNT deposit (A) before and (B) after incubation in β -CD modified gold nanoparticles⁸⁰

Au nanoparticles with adjustable sizes (10-50 nm) were controlled synthesized by reducing hydrochloroauric acid with β -cyclodextrin in an alkaline aqueous solution and were used as effective catalyst to activate the reduction of 4-nitrophenol⁸¹. The synthesis of nanometer-sized organic hollow spheres was achieved by the oxidation of gold nanoparticles protected by thiolated β -cyclodextrin molecules. These water-soluble poly-cyclodextrin nanocapsules held together by S–S bonds can find numerous applications in drug delivery, extraction and as nanoreactors⁸².

An amperometric glucose sensor based on inclusion complex of mono-6-thio- β -cyclodextrin/ferrocene capped on gold nanoparticles (GNPs/CD–Fc) and glucose oxidase was elaborated with an excellent sensitivity possibly attributed to the presence of the GNPs/CD–Fc film that can provide a convenient electron tunneling between the protein and the electrode. The sensor showed analytical performances

such as: a relatively fast response time (5 s), low detection limit ($15 \cdot 10^{-6} \text{ mol L}^{-1}$, S/N = 3), high sensitivity (ca. $18.2 \cdot 10^{-3} \text{ A L mol}^{-1} \text{ cm}^{-2}$) with a linear range of $0.08 - 11.5 \cdot 10^{-3} \text{ mol L}^{-1}$ of glucose. The biosensor exhibited a good stability and allowed the detection of glucose at 0.25 V (versus SCE) without almost any interferences⁸³.

Graphene decorated with gold nanoparticles and CDs were deposited on GCE obtaining a sensor with good stability, sensitivity and selectivity to determine dopamine and uric acid in the presence of ascorbic acid. The oxidation peaks of the 3 analytes were well separated by applying SWV which allowed their simultaneous determination⁸⁴.

A superparamagnetic nanomaterial with molecular receptor properties prepared by attaching CD moieties on the surface of silica core-shell Fe_3O_4 nanoparticles was employed as support for the supramolecular immobilization of two different adamantane-modified enzymes, tyrosinase and xanthine oxidase, through host-guest interactions. These biosensors showed excellent electroanalytical behaviors, with linear ranges of $1 \cdot 10^{-7} - 12 \cdot 10^{-6} \text{ mol L}^{-1}$ for catechol and $5.0 - 120 \cdot 10^{-6} \text{ mol L}^{-1}$ for xanthine, sensitivities of $12 \cdot 10^{-3} \text{ A L mol}^{-1}$ and $130 \cdot 10^{-3} \text{ A L mol}^{-1}$, and low detection limits of $22 \cdot 10^{-9}$ and $2.0 \cdot 10^{-6} \text{ mol L}^{-1}$, respectively⁸⁵.

For the ultrasensitive detection of carcino-embryonic antigen (CEA), a non-enzymatic immunoassay was designed using β -cyclodextrin functionalized $\text{Cu@Ag}(\text{Cu@Ag-CD})$ core-shell nanoparticles as labels and β -cyclodextrin functionalized graphene nanosheet as sensor platform. The fabricated immunoassay shows excellent analytical performance for the measurement of CEA with wide linear range, low detection limit, good sensitivity, reproducibility and stability, providing a promising application for CEA in clinical diagnostics⁸⁶.

Gold nanorods and gold nanoparticles, both of them functionalized with β -CD, were employed in the elaboration of a sandwich-type immunosensor for β -fetoprotein detection in a linear range from 0.5 pg mL^{-1} to 0.5 ng mL^{-1} with a detection limit down to 32 fg mL^{-1} . The *in situ* gold superstructures assembly showed excellent performance for the signal amplification⁸⁷.

1.3.6. Cyclodextrins in polymeric films

CDs can form polymers by their own electropolymerization or polycondensation with dialdehyde (giving poly-CD) and they also can be attached to other polymers: poly(*N*-acetylaniline), polypyrrole, poly(*N*-methylpyrrole), polyaniline, poly-3-methylthiophene; polyethyleneimine, chitosan, Nafion (in which CDs are whether covalent bonded to the monomer, or only entrapped in the polymer matrix).

A β -CD modified poly(*N*-acetylaniline) (PAA) electrode has been developed for cinchonine (CCN) sensing using 1,4-hydroquinone (HQ) as a redox probe. Competitive inclusion equilibrium with β -CD was established between HQ and CCN, the decrease in the peak current of HQ is directly proportional to the amount of CCN⁸⁸.

A β -cyclodextrin based Pt sensor (obtained by pyrrole electropolymerization) has been elaborated for a simple and sensitive determination of rifampicin using amperometry. The sensor was applied for the drug determination in pharmaceutical preparations and biological samples with no interferences from other tuberculostatic drugs⁸⁹.

A polypyrrole/ β -cyclodextrin (Ppy/ β -CD) film was prepared by a simple electropolymerization of a 20:1 mixture of the CD and the pyrrole monomer resulting in a functionalized polymer film with interesting electrochemical properties such as selective, simultaneous and quantitative detection of some polyhydroxyphenyls and neurotransmitters derived from pyrogallol and catechol. The detection limit was $4 \cdot 10^{-7}$ and $1.8 \cdot 10^{-6}$ mol L⁻¹ for catechol and pyrogallol, respectively⁹⁰.

The same authors investigated the selective electrocatalytic activity toward the electrochemical oxidation of dopamine and norepinephrine on a glassy carbon electrode modified with an electropolymerized film, made of pyrrole and β -cyclodextrin 1:1. The selectivity of the sensor was achieved even at a concentration 20 times higher than the neurotransmitters⁹¹. The same film was synthesized on gold electrode and used for the electrochemical detection of neurotransmitters giving well resolved and reversible cyclic voltammograms with a negative shift of their oxidation potentials in comparison with the bare electrode. It presented very good selectivity toward interferences such as ascorbic acid at a concentration of more than 500-fold for some neurotransmitters. The same sensor was used to detect concentrations of the muscle relaxant rocuronium bromide with a detection limit of 1 ppm^{92,93}.

Carboxymethylated β -cyclodextrin polymer film was used for the fabrication of a highly selective and sensitive electrochemical sensor for the determination of dopamine in the presence of ascorbic acid, analytical performance which was based on the combination of electrostatic and inclusion interaction of the film for analyte⁹⁴.

Conducting polymer membranes consisting of polypyrrole (PPy) doped with sulfated α -cyclodextrin (α -CDS) or sulfated β -cyclodextrin (β -CDS) were prepared electrochemically providing electrical conductivities of 0.7 S cm^{-1} and 0.4 S cm^{-1} , respectively. Electrochemically controlled transport of alkali metal ions, alkaline earth metal ions and transition metal ions was demonstrated across composite membranes prepared by depositing PPy- α -CDS or PPy- β -CDS onto platinum sputter-coated polyvinylidene filters. PPy- β -CDS coated membranes proved to be significantly more permeable towards most metal ions examined than either PPy- α -CDS coated membranes (excepting copper ions)⁹⁵.

A multi-walled carbon nanotube with incorporated β -cyclodextrin (β -CD-MWNTs) and a polyaniline (PANI) film-modified glassy carbon (GC) electrode has been successfully developed for determination of dopamine in the presence of ascorbic acid. The PANI film showed lack of interference and long term stability. Sensitive detection of dopamine was improved by the acid-treated MWNTs with carboxyl groups which promoted the electron transfer reaction of dopamine and by the preconcentration effect of a supramolecular complex between β -CD and dopamine⁹⁶.

Conducting polypyrrole (PPy) and poly(pyrrole-2,6-dimethyl- β -cyclodextrin) [poly(Py- β -DMCD)] films were prepared by electrode potential cycling on a gold electrode in aqueous and nonaqueous (acetonitrile) electrolyte solutions. The results show that in both solutions in the presence of cyclodextrin, the oxidation potential of pyrrole monomers increased. *In situ* conductivity measurements of the films show that films prepared in acetonitrile solution are more conductive than those synthesized in aqueous solutions. The same results were obtained for poly(*N*-methylpyrrole) and poly(*N*-methylpyrrole-cyclodextrin) films^{97,98}. This seems to indicate the possible insertion of pyrrole groups within the hydrophobic CD cavities in aqueous solutions yielding its oxidation and hence its polymerization more difficult.

A biocompatible hybrid film of β -cyclodextrin and ionic liquids (ILs), 1-butyl-3-methylimidazolium tetrafluoroborate was used for the development of an electrochemical biosensor by immobilizing the horseradish peroxidase (HRP). The electrocatalysis of this biosensor to both quercetin and hydrogen peroxide was characterized. β -CD provided a biocompatible microenvironment for HRP, and ILs accelerated the electron transfer between the enzyme and the electrode. The biosensor exhibited a low operating potential (-0.05 V vs. SCE), fast amperometric response, high sensitivity, good selectivity and submicromolar detection limit⁹⁹.

A stable film of poly-3-methylthiophene combined with γ -cyclodextrin was electropolymerized on gold electrode using a potentiostatic mode. The resulting modified electrode exhibited high sensitivity and selectivity toward electrochemical qualitative and quantitative detection of chlorpromazine and neurotransmitters with low detection limits of $2 \cdot 10^{-7}$, 10^{-6} , and 10^{-7} mol L⁻¹, respectively¹⁰⁰. Simultaneous quantification of serotonin (5-HT) and dopamine using a β -cyclodextrin/poly(*N*-acetylaniline)/carbon nanotube composite (CD/PNAANI/CNT) modified carbon paste electrode was achieved. Synergistic effect of multi-walled carbon nanotube in addition to the preconcentrating effect of β -cyclodextrin, as well as its different inclusion complex stability with 5-HT and dopamine was used to construct an electrochemical sensor for their quantification. The CD/PNAANI/CNT modified CPE exhibited remarkable enhancement effects on the oxidation peak currents, negatively shift of the oxidation potentials and resolved the overlapping anodic peaks of the neurotransmitters into two well-defined peaks. The developed method was tested for their determination in plasma samples with acceptable recoveries¹⁰¹.

Insoluble β -CD polymer was synthesized by β -CD using epichlorohydrin as crosslinking agent under basic conditions. The polymer presented excellent thermal stability, insolubility and catalytic activity for the oxidation of benzyl alcohol to benzaldehyde¹⁰².

Recently, considerable attentions have been paid to molecular imprinting technology which provides a promising alternative to create highly specific recognition sites within a synthetic polymer network via the template polymerization process. CDs have been incorporated in the molecularly imprinted polymers (MIPs) structure improving their selective recognition ability. Formation of MIPs with CD has a major advantage over other MIP polymers due to the benefits brought by the CDs:

binding capacity and binding selectivity. Thus, artificial receptors for versatile nanometer scaled guests can be obtained.

Polymeric receptors for cholesterol and stigmaterol were synthesized by crosslinking β -cyclodextrin and 2,6-di-O-methyl- β -cyclodextrin with hexamethylene diisocyanate or toluene 2,4-diisocyanate in dimethyl sulfoxide. These templates promoted the formation of dimers and trimers of β -CD^{103,104}.

A selective MIP for tryptophan was prepared using bonded β -CD and acrylamide by developing a method for chiral amino acid separation and purification¹⁰⁵. A surface plasmon resonance sensor for dextromethorphan detection was elaborated based on thin layer imprinted β -cyclodextrin polymer¹⁰⁶. The analytical determination of *N*-phenyl-1-naphthylamine was successfully achieved on a molecularly imprinted β -cyclodextrin polymer using β -CD as the building units in the development of an optical sensor receptor¹⁰⁷.

A MIP with good selective adsorption performance for dipentylphthalate from cow milk was prepared using allyl- β -CD and methacrylic acid as the binary functional monomers¹⁰⁸. Another molecularly imprinted photonic polymer using maleic anhydride modified β -cyclodextrin and acrylic acid as functional monomers was developed for *L*-phenylalanine sensing¹⁰⁹.

A protein MIP with cyclodextrin pseudo-polyrotaxanes (CD-PPRs) as pseudo-supports was elaborated demonstrating a highly effective recognition capacity. The recognition specificity of the template relied on the spatial configuration constructed by CD-PPR and metal ions¹¹⁰.

A MIP based on β -CD-MWNTs composite material with imprinted sol-gel film on the PANI layer modified carbon electrode was elaborated for the selective determination of *L*-phenylalanine in blood samples. The response mechanism of the imprinted sensor was based on the inclusion interaction of β -CD and molecular recognition capacity of the imprinted film for *L*-phenylalanine. The interconnected β -CD-MWNTs composites film and the PANI layer possessed superior conductivity, high stability and excellent electrocatalytic ability and inclusion interaction for the determination of *L*-phenylalanine. The electrochemical behavior of the sensor was investigated by cyclic voltammetry, differential pulse voltammetry and amperometry. A linear calibration plot was obtained over the concentration range from $5.0 \cdot 10^{-7}$ to 10^{-4} mol L⁻¹ and a detection limit of 10^{-9} mol L⁻¹. The electrochemical imprinted sensor presented excellent sensitivity, selectivity, stability, reproducibility and recovery¹¹¹.

A molecularly imprinted electrochemical sensor based on gold electrode decorated by β -CD incorporated multiwalled carbon nanotube, gold nanoparticles-polyamide amine dendrimer nanocomposites (Au-PAMAM) and chitosan derivative was developed for selective and convenient determination of chlortetracycline. The electrochemical behavior of the developed sensor was characterised by cyclic voltammetry and amperometry. The linear range of the sensor was from $9.0 \cdot 10^{-8}$ to $5.0 \cdot 10^{-5}$ mol L⁻¹, with the detection limit of $4.95 \cdot 10^{-8}$ mol L⁻¹¹¹².

1.3.7. Carbon nanomaterials modified with cyclodextrins

Carbon nanomaterials consist in various members such as: 0-D nanomaterials (fullerenes) 1-D nanomaterials like carbon nanotubes (CNTs), 2-D nanomaterials (graphene) and 3-D nanomaterials like graphite (Figure 6).

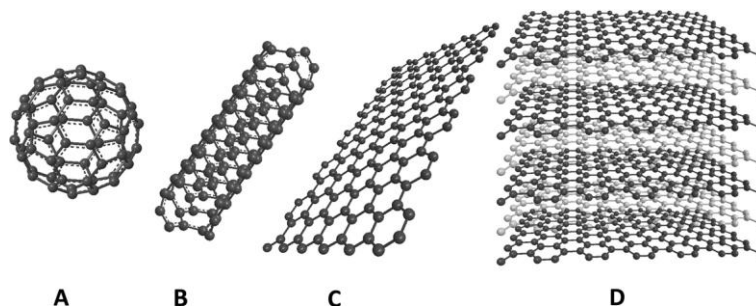


Fig. 6. Different forms of sp^2 hybridized carbon. (A) Fullerene, (B) Single-walled carbon nanotubes, (C) Graphene, (D) Graphite¹¹³

CNTs are formed by one (single-walled carbon nanotubes, SWCNT) or multiple cylindrical layers of graphene sheets (multi-walled carbon nanotubes, MWCNT). Their unique properties such as: high electronic conductivity, high mechanical resistance, increased electrode active surface area which gives rise to enhanced electrochemical responses and a demonstrated anti-fouling capability of electrode surfaces modified with CNTs, allowed their significant applications in many fields, such as: electroanalytical chemistry, including electrochemical (bio)sensors, electronics, medicine, aerospace industry, etc. The CNTs coupling with other materials, possessing well known electrochemical properties (polymers, metal nanoparticles, cyclodextrins, microparticulates, ionic liquids), led to hybrid composite electrode materials that exhibit special properties due to the synergic effect of the individual components. Therefore, CNT based sensors generally have higher sensitivities, lower detection limits, and faster electron transfer kinetics. The electrode performances depend on the nanotube synthesis method, CNT functionalization, addition of electron mediators, and the immobilization method of the CNTs at the electrode surface. The functionalization of CNTs can be achieved by physical (ultrasonic, milling, crushing and friction) and chemical (covalent and non-covalent) approaches. Non-covalent modification uses conjugated polymers, bioactive molecules (DNA, enzyme, and protein) and conjugated polycyclic aromatic hydrocarbons (pyrene and its derivatives) and will not damage the π system of the tubes. Covalent modification *in tip* mainly includes carboxylation and subsequent derivatization, such as amidation and esterification reaction. Covalent modification *in side wall* generally includes fluorination, alkylation reaction and cycloaddition. Covalent modification can improve the CNTs properties, but to a certain extent it will destroy the sp^2 structure of the CNTs, thus influencing their stability and conductivity. Different types of electrochemical methods are used in CNT-based (bio)sensors, including the direct electrochemical detection by amperometry or voltammetry, the indirect detection of an oxidation product using enzyme sensors, and the

detection of conductivity changes using CNT-field effect transistors (FETs). CNT-based (bio)sensors are considered to be a next generation building block for ultrasensitive and ultrafast (bio)sensing systems. CNTs technology is one of the most exciting areas in current material sciences and the development of CNTs for biomolecule detection is particularly important for bioengineering and biomedical applications¹¹⁴⁻¹¹⁸.

Graphene is a two-dimensional (2-D) sheet of carbon atoms in a hexagonal configuration with atoms bonded by sp^2 bonds; it is a one-atom-thick material which resembles a large polyaromatic molecule of semi-infinite size. This configuration is responsible for their extraordinary properties: a very large surface area, a tunable band gap, room-temperature Hall effect, high mechanical strength, high elasticity and thermal conductivity. In comparison with CNTs, graphene is a biocompatible nanomaterial, it does not contain metallic impurities, and its production needs graphite (which is cheap and accessible). Graphene can be functionalized by covalent grafting (using diazonium salts, dienophile compounds, 1-ethyl-3-(3-dimethylaminopropyl) carbodiimide (EDC) or *N,N'*-dicyclohexylcarbodiimide (DCC) and *N*-hydroxysuccinimide (NHS), heteroatom doping (N_2 , B)), by non-covalent (π - π stacking, hydrophilic and hydrophobic interactions) and also by other methods, which meet the specific requirements of different kinds of sensors. The applications of graphene in (bio)sensing are based on electrodes modified with graphene powder or graphene-composite electrodes. Graphene oxide (GO) has been successfully employed in bioelectrochemistry. Proteins retain their structural integrity and biological activity when they form mixtures with GO; this nanomaterial acts as an "electron wire" between the redox centers of the enzyme or protein and the electrode surface, feature which predicts promising applications for GO/protein complexes in biosensor and biofuel cell development. Graphene can be also used as a conductive support for the deposition of electrocatalytic nanoparticles (Pd, Au). Because of its interesting properties, graphene has been used as a transducer in bio-FETs, electrochemical biosensors, impedance biosensors, electrochemiluminescence, and fluorescence biosensors, as well as biomolecular labels^{113,119-122}.

Fullerenes represent a promising class of spheroidally shaped molecules made exclusively of carbon atoms with unique characteristics: broad light absorption in the UV-Visible region, photothermal effect, structural angle strain, the ability to accommodate multiple electrons and endohedral metal atoms, long-living triplet state, singlet oxygen production, as well as ability to act as an electron acceptor with a dual nature of electrophilic and nucleophilic characteristics. Fullerene core enables the design of new macromolecular architectures in order to modify their properties in self-assembled nanostructures. Fullerenes can form well-ordered 2D nanostructures on most semiconductor and metal surfaces; they are also able to form other low dimensional nanostructures such as nanospheres, nanovesicles, nanorods, nanotubes, and even liquid crystals. Fullerene solubility in polar solvents (especially in water) is quite low. So the methods found for their solubilization include: formation of inclusion complexes with cyclodextrins and calixarenes, solubilization using Tween 20, phospholipids, micelles, liposomes, vesicles, polyvinylpyrrolidone

and synthesis of some water soluble fullerene derivatives (having polyamino/polyhydroxy groups, polar side chains).

C60, the most representative among fullerenes with his spherical shape, unequalled in nature, may be reversibly reduced by up to 6 electrons due to its low lying triply degenerate LUMOs (due to their high molecular symmetry, the HOMO-LUMO transition of fullerene is forbidden showing a weak luminescence at room temperature, fullerene have a relatively low energy gap of about 1.8eV). Fullerenes present specific biological application such as: photoinduced enzyme inhibition, antiviral activity, DNA cleavage, photodynamic therapy, electron transfer. Fullerenes have been implemented successfully in biosensors to detect glucose, urea, hemoglobin, immunoglobulin, glutathione in real sample, to identify doping abuse, to analyze pharmaceutical preparations and even to detect cancer and tumor cells at an earlier stage. The main role of fullerene in biosensing devices is as a mediator. Due to their novel structures of high symmetric carbon cages, fullerenes have extensive applications on electronics, magnetics, superconducting materials, medicines, biochemistry, electrochemistry and photophysics¹²³⁻¹²⁷.

Carbon nanotubes, graphenes and fullerenes with their enhanced chemical stability and electrical conductivity, in combination with CDs lead to the improvement of sensing performance with enhanced sensitivity for detecting various analytes taking advantages of the promising properties of both materials. These nanostructured carbon materials can be modified with CDs by two different ways: non covalent (usually sonication) and covalent functionalization (covalent attachment).

1.3.7.1. Carbon nanotubes with cyclodextrins

Multiwalled carbon nanotubes (MWCNTs) were sonicated together with β -CD forming β -CD-MWCNTs nanocomposite which was assembled on GCE using layer-by-layer (LBL) method based on electrostatic interaction of positively charged biopolymer chitosan and negatively charged MWCNTs. The SEM indicated that the β -CD presence lead to the obtaining of more compact multilayer. According to the cyclic voltammetry results, the assembled MWCNTs with β -CD on GCE exhibited lower capacitive background current and higher electrocatalytic activity toward dopamine than the assembled MWCNTs without β -CD. These results may be ascribed to the relatively compact three-dimensional structure of the MWCNTs multilayer films with β -CD and to the excellent molecule recognition function of β -CD¹²⁸.

Glassy carbon, gold and indium tin oxide electrodes were covered by a conductive composite film containing functionalized multi-walled carbon nanotubes (fMWCNTs), gold nanoparticles with hydroxypropyl- β -cyclodextrin (HP β CD) as catalysts which was synthesized by potentiostatic methods. The presence of gold nanoparticles produced an increase in the sensitivity of the modified electrodes and the presence of fMWCNTs and HP β CD in the composite film enhanced the active surface coverage concentration of Au by almost 400 %. These modified electrodes presented well separated voltammetric peaks for tyrosine, guanine, adenine and

thymine¹²⁹. For the simultaneous or individual determination of guanine and adenine other electrodes modified with β -CD incorporated carbon nanotubes were proposed with an accumulation at open circuit for 1 minute presenting a peak potential difference of 300 mV. The marked electrocatalytic activity permitted effective low potential amperometric biosensing of DNA with the detection limits of $0.1 \mu\text{g mL}^{-1}$ for guanine and $0.2 \mu\text{g mL}^{-1}$ for adenine¹³⁰. ITO electrodes coated with β -cyclodextrin modified MWCNTs showed enhanced and selective electrocatalytic effect on the reduction of sodium cholate, while electrochemical response of deoxycholate was not observed¹³¹.

Electrochemical oxidation of norepinephrine was studied on β -CD incorporated CNT modified electrode and the simultaneous determination of norepinephrine and ascorbic acid was successfully achieved, due to a separation peak potential of about 264 mV¹³². An α -cyclodextrin (α -CD) incorporated carbon nanotube-coated electrode with strong catalytic effects for the simultaneous determination of dopamine and epinephrine with a peak potential separation of 390 mV was reported¹³³. Another MWCNTs/ β -cyclodextrin based sensor was elaborated for rutin determination by cyclic voltammetry, showing better analytical performances for the electrocatalytic oxidation and reduction of rutin in comparison with the MWCNTs film and bare glassy carbon electrodes¹³⁴. The selectivity to quercetin and rutin was obtained on succinyl- β -CD-modified MWCNT coated glassy carbon electrode. Succinyl- β -CD separated the peak potential of the two substances by 110 mV and a more favorable complexation between succinyl- β -CD and quercetin was attributed¹³⁵.

MWCNTs were ultrasound-dissolved in 10 % β -CD solution and then were used to modify the glassy carbon electrode elaborating a dopamine electrochemical sensor. β -CD as molecular receptor and MWCNT as enhancer of electron transfer improved the analytical performances and the catalytic oxidation of dopamine with a negatively shifted oxidation potential, a more reversible dopamine redox process, a selectivity toward ascorbic acid, and an excellent sensitivity, repeatability and stability¹³⁶. Aligned carbon nanotubes were functionalized with β -CD diazonium salt through diazotization reaction and the resulting electrode was used to detect DNA hybridization in homogeneous solution based on host-guest recognition. The DNA probe had both ends modified: one with dabcyI (4-((4-(dimethylamino)phenyl)azo) benzoic acid) as guest molecule for the modified electrode capture, and the other end was labeled with a CdS nanoparticle as an electrochemical tag to indicate the occurrence of DNA hybridization. This electrochemical biosensor has high sensitivity and specificity with a detection limit of $5.0 \cdot 10^{-13} \text{ mol L}^{-1}$ for the determination of sequence-specific DNA¹³⁷.

Carbon nanomaterials (including fullerenes, SWCNTs, MWCNTs and graphene sheets) were functionalized with β -cyclodextrin polymer (CDP) obtaining CDP-carbon nanomaterials with high solubility and stability in water. The integrity of carbon nanomaterials was significantly preserved by this noncovalent modification. Furthermore *p*-aminothiophenol used as a guest was trapped in the CDP-modified carbon nanomaterials, after that these complexes interacted with Au or Pt nanoparticles by the formation of thio-Au or thio-Pt bond allowing the highly efficient

nanoparticle assembly onto the surface of MWCNTs. Pt-decorated CDP-carbon nanomaterials can be applied in methanol fuel cells. These carbon nanomaterial-based hybrid materials presented not only the good electrical and large surface area properties of carbon nanomaterials, but also displayed high supramolecular recognition and enriching properties of CDs¹³⁸ (Figure 7).

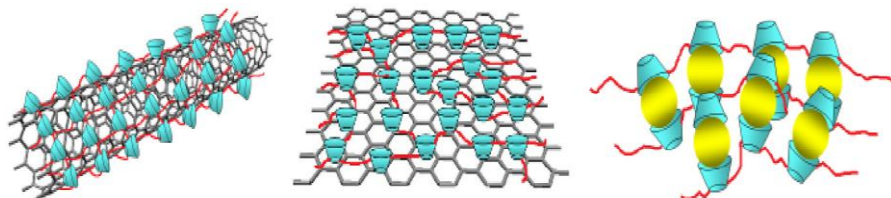


Fig. 7. Schematic illustration of (a) CDP-SWCNTs and CDP-MWCNTs, (b) CDP- CDP-Graphene and (c) CDP-C60s¹³⁸

Gold nanoparticles-poly(luminol) (Plu-AuNPs) hybrid film and multi-walled carbon nanotubes with incorporated β -CD were explored to modify glassy carbon electrode for simultaneous determination of dopamine and uric acid exhibiting good selectivity and sensitivity with well-separated peaks. The gold nanoparticles were dispersed into the porous polymer matrix of poly(luminol) generating additional electrocatalytic sites; β -CD was used as a dispersing reagent for carbon nanotubes. The DPV response of the modified electrode was about 8-fold greater compared to that of the Plu-AuNPs/GCE with a lower detection limit for dopamine. Interferences from ascorbic acid and uric acid were efficiently eliminated and bioanalytical applications such as real sample analysis were investigated¹³⁹.

An insoluble conducting composite film of polycyclodextrin (CDP) and carbon nanotube was obtained by dissolving MWCNTs in a mixed aqueous solution of β -CD and β -CD prepolymer (pre-CDP). For biosensing purpose, glucose oxidase was immobilized on the film, the biosensor presented good sensitivity to glucose within a wide concentration range. β -CD provided a large surface for enzyme and mediator loading, and also a desirable microenvironment to enzyme, while the CNTs could promote the redox reaction of the active center of the oxidase¹⁴⁰.

1.3.7.2. Graphene with cyclodextrins

Hydroxypropyl- β -cyclodextrin-reduced graphene oxide hybrid nanosheets (HP- β -CD-RGO) synthesized by microwave irradiation, Nafion and *in situ* deposited bismuth film, were used as the sensing material for the simultaneous determination of Pb^{2+} and Cd^{2+} . This sensor exhibited high sensitivity (the LOD obtained for Pb^{2+} and Cd^{2+} were $9.42 \cdot 10^{-11}$ and $6.73 \cdot 10^{-11}$ mol L⁻¹, respectively), good stability and reproducibility. It successfully combines the host-guest recognition and enrichment properties of HP- β -CD, the large 2-D electrical conductivity and large-surface-area properties of RGO, the ion-exchange capacity of Nafion and the ability of bismuth film

to form easily alloys with heavy metals in a synergistic effect which improves the analytical performances of the sensor¹⁴¹.

Hydroxypropyl- β -cyclodextrin (HPCD) was covalently grafted onto the surface of graphene oxides (GO) via ester bonds by nucleophilic addition between HPCD and thionyl chloride modified GO. FTIR, Raman and TGA spectra confirmed the synthesis of β -CD functionalized graphene material. The electrochemical interactions between hemoglobin (Hb) and tetraphenyl-porphyrin (TPP) were investigated by cyclic voltammetry showing a detection limit to Hb of $5.0 \cdot 10^{-9}$ mol L⁻¹, indicating high biorecognition capability¹⁴². β -CD@CRG nanocomposite prepared via a simple sonication-induced assembly, in combination with Nafion, was used for the development of a sensitive electrochemical sensor for rutin detection. Its excellent analytical performance was attributed to the high rutin loading capacity on the electrode surface and the outstanding electric conductivity of graphene¹⁴³.

The same simple wet-chemical strategy was used for preparing CD-Gr nanocomposite which was employed for the fabrication of enzyme electrodes via host-guest supramolecular interactions between adamantane-modified horseradish peroxidase (HRP-ADA) and CD-Gr nanocomposites. The biosensor showed good reproducibility and high sensitivity to H₂O₂ with the detection limit of $0.1 \cdot 10^{-6}$ mol L⁻¹ in the range of $0.7 - 35 \cdot 10^{-6}$ mol L⁻¹, revealing that such an electrochemical platform not only preserved the native structure of the immobilized enzyme, but also exhibited good electron transfer properties for HRP¹⁴⁴, (Figure 8).

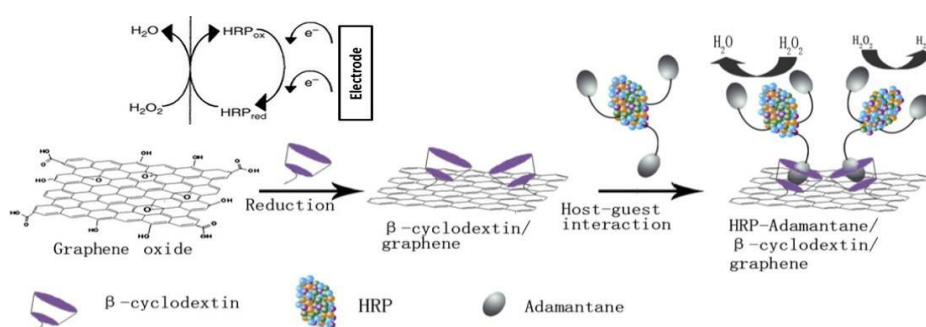


Fig. 8. Schematic representation of fabrication of the HRP-ADA/CD-Gr/GCE and the principle for H₂O₂ determination¹⁴⁴

The electrochemical behavior of dopamine seemed to be more reversible on the electrode modified by β -CD/graphene sheet (GS) compared to GS/GCE (the difference between the two ΔE_p was about 42 mV revealing a faster electron transfer process). By using CV method, the linear current response range of the β -CD/GS/GCE covered the range from $9.0 \cdot 10^{-9}$ to $12.7 \cdot 10^{-6}$ mol L⁻¹, with a detection limit of $5.0 \cdot 10^{-9}$ mol L⁻¹. The sensor also showed a good ability to suppress the background current due to the large excess ascorbic acid¹⁴⁵. A simple method for water-phase synthesis of β -CD modified RGO reduced by *l*-ascorbic acid at room temperature was reported and the β -CD-RGO was used as enhanced material for sensitivity determination of diethylstilbestrol. The developed electrochemical sensor exhibited high selectivity, good stability and reproducibility, performances due to the

excellent electronic properties of RGO sheets and also to the high supramolecular recognition capability of β -CD¹⁴⁶.

A novel method consisting in a cooperation of potentiostatic technique and CV has been employed to prepare the electrodeposited graphene/polymerized β -cyclodextrin (E-Gr/P- β CD) nanocomposite film. Based on the synergistic effect of E-Gr and P- β CD, a highly sensitive electrochemical sensor for quercetin was fabricated with a linear range from 0.005 to $20 \cdot 10^{-6}$ mol L⁻¹, and a detection limit of $1 \cdot 10^{-9}$ mol L⁻¹¹⁴⁷. The electrochemical behaviors of 2-chlorophenol (2-CP) and 3-chlorophenol (3-CP) were investigated on β -CD functionalized graphene modified carbon paste electrode. Well separated oxidation peaks recorded by CVs and DPVs and a higher sensitivity for the oxidation of 3-CP were obtained. These effects may be due to the adsorption of 3-CP into the caves of β -CD. This sensor may also provide a promising new application to detect other isomers¹⁴⁸. Monodisperse AuNPs were anchored onto carboxylic graphene nanosheets (CGS). A dual β -CD functionalized Au@CGS nanohybrid was then fabricated: the NH₂- β -CD was covalently bonded to Au@CGS by combining the amine group of NH₂- β -CD and the carboxyl group of CGS, with the aid of an EDC/NHS coupling agent and then the NH₂- β -CD was strongly attached to the surface of the Au@CGS because of the strong coordinating capability between Au and thiol. The performances of this nanohybrid, for the simultaneous determination of two phenol compounds, hydroquinone and *p*-nitrophenol, were tested by DPV. The proposed electrochemical sensor showed a low detection limit and high selectivity caused by the large surface area, the excellent conductivity, and the high host-guest molecular recognition capability of the β -CD-Au@CGS nanohybrids¹⁴⁹.

A β -CD functionalized graphene nanosheets (GN-CD) assembly was prepared by *in situ* thermal reduction of graphene oxide with hydrazine hydrate in the presence of β -CD, then cytochrome c (Cyt c) was intercalated to the GN-CD assembly to form a layered self-assembled structure, GN-CD-Cyt c, through electrostatic interaction. This assembly combined the specific properties of the modifiers, namely the high conductivity of graphene nanosheets, the selectively binding properties and electronegativity of CDs and the electropositivity of Cyt c. The sensor displayed improved electron transfer rate and high supramolecular recognition capability toward six amino acid probes, among which glycine was chosen as a representative analyte¹⁵⁰. An enhanced electrochemical sensing platform based on the integrating properties of graphene and 2,6-dimethyl- β -cyclodextrin (DM- β -CD) was elaborated for the determination of isoquercitrin and baicalin in real serum samples. The homogeneous graphene oxide dispersion (0.5 mg mL⁻¹) was mixed with 20 mL of DM- β -CD aqueous solution (80 mg) and 300 μ L of ammonia solution, followed by the addition of 20 μ L of hydrazine solution forming well dispersed graphene suspension which showed high supramolecular recognition properties to enrich guest molecules. The linear ranges of isoquercitrin and baicalin were $10 \cdot 10^{-9}$ mol L⁻¹ - $3.0 \cdot 10^{-6}$ mol L⁻¹ and $0.04 \cdot 10^{-6}$ mol L⁻¹ - $3.0 \cdot 10^{-6}$ mol L⁻¹, with the detection limits of $4 \cdot 10^{-9}$ mol L⁻¹ and $10 \cdot 10^{-9}$ mol L⁻¹. The characteristic properties of graphene (large surface area and high conductivity) and of DM- β -CD (high supramolecular recognition and enrichment capability) improved the electrochemical features of the nanocomposite¹⁵¹.

A non-enzymatic electrochemical sensor for micromolar detection of cholesterol was obtained using Graphene- β -Cyclodextrin (Gr- β -CD) hybrid system as the sensing matrix. The graphene oxide was treated with β -CD in presence of ammonia and NaOH, and then the complex was reduced with hydrazine, forming Gr- β -CD. Methylene blue, used as redox probe, was replaced by cholesterol from the host-guest complex formed with β -CD, being detected electrochemically by differential pulse voltammetry¹⁵².

1.3.7.3. Fullerenes with cyclodextrins

Fullerenes have specific and unique chemical and physical features which make them an attractive tool for biological applications. Their well-known lack of solubility in polar solvents can be solved by chemical or supramolecular approaches. The last technique, supramolecular complexation, employed the fullerene entrapment in γ -CD cavity in a molar ratio of 2:1 (CD:fullerene) to form water-soluble fullerene derivatives. The CD ability to mask the fullerene sphere is very important in enhancing solubility in polar solvents and in decreasing aggregation^{153,154}.

C70 solubility was improved by complexation with δ -cyclodextrin using the ball-milling method based on a solid-solid mechano-chemical reaction; the stoichiometric ratio of the complex was 1:2 (C70: δ -CD)¹⁵⁵.

PEG/CD-modified dendrimers have been synthesized and applied for the solubilization of C60 fullerene, obtaining an aqueous solution of fullerene with a concentration of $2.8 \cdot 10^{-6} \text{ mol L}^{-1}$, taking into account that the solubility of C60 in pure water was reported as $2 \cdot 10^{-24} \text{ mol L}^{-1}$ ¹⁵⁶. Stable solutions of fullerene C60 with human serum albumin (C60/HSA) were prepared via the formation of C60/HP- β -CD nanoparticles, in particular by transferring C60 molecules from HP- β -CD to HSA molecules. The resulting C60/HSA presented an excellent stability, antioxidant activity and substantial phototoxicity properties¹⁵⁷.

A supramolecular inclusion complex of C60 and β -CD (1:2) was synthesized; it interacted then with bovine serum albumin giving a $(\beta\text{-CD})_2/\text{C60-BSA}$ water-soluble complex which was characterized by spectroscopic and electrochemical methods in aqueous solutions¹⁵⁸. Triazole-methoxypyridyl γ -CD was used as a successful hydrosolubilizing reagent for C60 resulting in hydrosoluble inclusion complex of C60 with a concentration of more than $70 \cdot 10^{-3} \text{ mol L}^{-1}$ which is approximately 90 times greater than that with non-substituted γ -CD¹⁵⁹. C60 was immobilized through host-guest interaction into the SAMs of bis-pyridine-substituted γ -CD preserving its electronic properties and stabilising the fullerene against photopolymerisation and aggregation¹⁶⁰.

The separation of the different regioisomers of fullerene derivatives using host-guest complexes has been reported. Bis-*N*-methyl-fulleropyrrolidine fullerene derivatives were separated by complexation with γ -CD by controlling the relative amounts of γ -cyclodextrin and dimethyl sulfoxide (DMSO). Using small amount of γ -CD, the trans-1 and trans-2- γ -CD complexes were separated from the trans-3- γ -CD

complex. The explanation for the observed regioselective separation was a competition between the relative stabilities and solubilities of the complexes in water and water-DMSO mixture¹⁶¹. It was proved that host–guest complexes of C60 and its conjugates maintained the electrochemical activity of the fullerene moiety. The determination of redox potentials allowed drawing conclusions on the formation of complexes and determining the binding enhancement due to the redox change on the C60 core¹⁶².

CD-fullerene conjugates were also synthesized by covalent functionalization. In particular, C60 with a notable electron acceptor capability, it was conjugated with azido-CDs via 1,3-dipolar cycloaddition in chlorobenzene, resulting the corresponding azafulleroid with 40–49 % yields. These CD-C60 conjugates are soluble in all the common organic solvents and in THF/H₂O mixtures with up to 90 % of water. Their redox properties determined by cyclic voltammetry in ortho-dichlorobenzene/ acetonitrile (4:1, v:v) mixture and by adding ferrocene as an internal reference, remained totally unaltered. The four reduction processes corresponding to the four quasireversible reductions of the fullerene sphere were displayed in the azafulleroid voltammograms^{163,164}. A bridged bis(β -cyclodextrin)-fullerene conjugate was also synthesized and characterized by UV-Vis, FTIR, NMR, fluorescence, and circular dichroism spectroscopy, techniques which showed that the bis(β -cyclodextrin)-fullerene conjugate displayed an intramolecular capsule type conformation in aqueous solution. Beyond its satisfactory water solubility at physiological temperature and DNA-cleaving ability under visible light irradiation, a specific advantage of the capsule type CD-fullerene conjugate is that the CD cavity can selectively form complexes with certain fragments of the biological substrates, enabling the site specific interaction between the fullerene and target substrate¹⁶⁵.

Another method for synthesizing a water soluble cyclodextrin–fullerene conjugate was based on the Diels–Alder reaction between anthryl-cyclodextrin and fullerene in DMF/toluene solution. The CD-C60 conjugate exhibited water solubility up to 2.5 g L⁻¹ at 25 °C and it could remain stable for several weeks when stored at -10 °C¹⁶⁶. A water-soluble complex of fullerene and β -cyclodextrin [C60(β -CD)₂] was found to act as the mediator for the electrocatalytic conversion of dinitrogen to ammonia, the rate determining step being the reduction of the fullerene–cyclodextrin complex. The EIS data showed a decrease of the charge transfer resistance in the presence of nitrogen¹⁶⁷. A glassy carbon electrode was modified with CD–C60 for *p*-nitrophenol detection. The CD-C60 conjugate was synthesized by 1,3 cycloaddition and 8 μ L of its dichloromethane solution (1 mg mL⁻¹) were casted on the electrode surface. The developed device presented a detection limit of 1.2·10⁻⁹ mol L⁻¹ calculated by square wave voltammetry. The high electrocatalytic performance of the sensor was due to synergetic properties of C60 (microelectrodes) and β -cyclodextrin (acceptor-host system)¹⁶⁸.

1.4. Cyclodextrins tagged biomolecules

Various biomolecules were labelled with CDs whether to be attached at the sensor surface (which will further on express their biological activity when included in the biosensor) or to explore the analytical properties of the inclusion complexes.

An artificial enzyme having a cyclodextrin-peptide hybrid with multiple functional groups on the peptide backbone has been synthesized as a catalyst for ester hydrolysis¹⁶⁹. Another cyclodextrin-peptide conjugates was designed with two β -hairpin peptide chains arranged at the primary hydroxyl group side of β -CD so as to form a hydrophobic site as an additional recognition site¹⁷⁰. For the steroid molecules detection, a cyclodextrin conjugated peptide with two different fluorophores, coumarin and pyrene, was reported¹⁷¹.

A fluorescent thrombin binding aptamer was conjugated with dansyl probe and β -cyclodextrin residue at its extremities. This bis-conjugated aptamer fully retains its G-quadruplex formation ability and thrombin recognition properties resulting in a fluorescence enhancement, due to inclusion of dansyl, attached at the 3'-end, into the apolar cavity of the β -cyclodextrin at the 5'-end¹⁷².

Cosnier *et al.* synthesized glucose oxidase conjugated with β -CD which showed affinity towards adamantane-polypyrrole/pyrene, thus mimicking the biological avidin-biotin interactions. This approach led to the construction of high-performance amperometric biosensors^{80,173,174}.

1.5. Cyclodextrins as biomimetic receptors and the comparison with other affinity systems

The bioreceptor, consisting in the biological recognition system is the most important part of a biosensor. Many bioelements, such as: enzymes, DNA, RNA, antibodies, aptamers, microorganisms, and living cells, were used in biosensor construction, based on different types of interactions between the bioreceptor and the analyte. The major disadvantage of all these biomolecules (poor chemical and physical stability) was the main reason for developing an alternative approach which involves the use of biomimetic receptor systems, capable of binding target molecules with affinities and specificities as natural receptors do. These chiral macrocyclic receptors are also able of stereoselective molecular recognition. Among the biomimetic receptors, the most used are crown ethers, calixarenes, cyclodextrins and molecularly imprinted polymers representing a topic of current interest in supramolecular chemistry¹⁷⁵⁻¹⁷⁷.

The immobilization of bioelements through affinity systems represents a powerful and promising tool in biological devices as biosensors and biofuel cells preserving their biological activity. Affinity systems consist in supramolecular

interactions, including hydrophobic or electrostatic interactions, and coordination chemistry with metal complexes¹⁷⁸.

The first used affinity system is biotin-(strept)avidin system with an association constant comparable to covalent bonds ($K_{\text{ass.}}=10^{15} \text{ L mol}^{-1}$) because avidin forms a highly stable and specific complex with 4 biotin units. Avidin can thus be used to form a bridge between biotinylated proteins or supports. It is still the most used system for the almost irreversible immobilization of many types of bioreceptors. Many (bio)molecules were biotinylated in order to bind an intermediate avidin layer for the biomolecules attachment to the electrode surface. Electrogenerated biotinylated polypyrrole film covered by an avidin bridge formed by affinity interactions was used for the anchoring of biomolecules¹⁷⁹⁻¹⁹⁰.

The second affinity system developed was based on immobilization on metal ions. At the beginning, specific interactions between a chelated Ni^{2+} and histidine tags were observed, lately a new strategy was developed: the coordination of the electropolymerized poly(pyrrole-nitrilotriacetic-acid)-(NTA) film with Cu^{2+} and the coordination of biotin/histidine group¹⁹¹⁻¹⁹⁴. The advantage of this concept is the fact that, in water, the strength of coordinative metal–ligand bonds is superior to almost all other noncovalent interactions. For example, the association constants between carboanhydrase (with 6 surface histidine residues located at specific distances from each other) and Cu^{2+} ions is $K_{\text{ass.}}= 10^5 \text{ L mol}^{-1}$. Proteins which have a different distribution of histidines groups bind more than 100-fold less tightly¹⁹⁵. Another advantage of this affinity system consists in avoiding the intermediate layer of proteins (avidin).

Organic molecules that contain coordinating sites (ethylenediaminetetraacetic acid (EDTA), 1-(2-pyridylazo)-2-naphthol (PAN), 2-aminothiazole, dimethylglyoxime, *N*-phenylcinnaohydroxamic, 4-carboxyphenyl, 1,8-diamino-3,6-dioxaoctane, 4-methoxybenzene diazonium salt) are employed for the preconcentration of metals (Cu^{2+} , Pb^{2+} , Ni^{2+} , Cd^{2+}) by complexation improving the sensibility and selectivity of the electrochemical methods for detection^{196,197}. Other effective and specific ligands for metal ions are the olipeptides (Gly-Gly-His, glutathione, Glu-Cys-Gly, human angiotensin I, etc.) which contain a variety of electron donor atoms giving the ability to complex metallic ions^{198,199}.

Antibodies are complex glycoproteins that specifically recognize and bind an antigen. Their affinity relies on the strength of electrostatic and hydrophobic interactions. An antibody fits its unique antigen in a highly specific way, their 3D dimensional structures being complementary. Immunosensors employ the high Ab/Ag specificity to detect the presence of its analyte by using electrochemical, thermometric, optical, piezoelectric and magnetic transducers. The various applications of these sensors include the biomedical (clinical analysis, diagnosis and treatment monitoring), environmental, public health and safety applications²⁰⁰.

Aptamers are artificial single stranded oligonucleic acid or peptide molecules which can specifically bind to a variety of targets such as: metal ions, pharmaceutical substances, organic dyes, aminoacids, nucleotides and cells. These “chemical antibodies”, called like that due to their method of selection *in vitro* SELEX

(Systematic Evolution of Ligands by EXponential enrichment), possess high selectivity and affinity toward their targets. Compared to antibodies, aptamers have more advantages such as: chemical synthesis, easy modification, high stability, target versatility, easy-to-stock, low immunogenesis and resistance to denaturation and degradation. Aptamers have been widely used as biorecognition elements in electrochemical, optical and mass-sensitive bioassays. The combination of aptamers with novel nanomaterials has significantly improved the performance of aptamer-based sensors. Aptamers show a very high affinity for their targets, with dissociation constants typically from the micromolar to low picomolar range, comparable to those of some monoclonal antibodies. Aptamers have also been selected with a high binding specificity, as demonstrated by an anti-theophyllin aptamer that displays a 10.000-fold discrimination against caffeine, or by an anti-*L*-arginine RNA aptamer which exhibits a 12.000-fold affinity reduction toward *D*-arginine. Aptasensors have been given an increasing attention for analytical, clinical diagnosis, environmental and food analysis²⁰¹⁻²⁰³. Host-guest recognition between CDs and aptamers was used for the development of some biosensors applied for the detection of thrombin and adenosine triphosphate with good analytical performances²⁰⁴⁻²⁰⁷.

Macrocyclic receptors have also been used for the immobilization of inorganic and organic molecules. Crown ethers were employed in preconcentration techniques due to their ability to selectively include molecules into their cage²⁰⁸. Calixarenes, cyclic oligomers of phenol-formaldehyde condensates, and their derivatives with a conformational and structural flexibility supply the basis for molecular and ionic recognition. They were widely used as ionophores increasing the membrane sensitivity and selectivity of the sensors²⁰⁹⁻²¹¹.

CDs with their particular structural properties have been widely used for the inclusion complexes formation with a variety of guest molecules that fitted in their cavity. The immobilization of enzymes through supramolecular complexation between β -CD and adamantane or pyrene tagged molecules was reported for the first time by Villalonga *et al.*²¹² starting the great evolution of the sensors based on this affinity system^{80,173,213}. It is very well known that adamantane derivatives form 1:1 inclusion complexes with β -CD with high stability (association equilibrium constant between 10^4 - 10^5 L mol⁻¹). The association equilibrium constant of $K_{\text{ass}} = 5.2 \cdot 10^4$ L mol⁻¹ for 1:1 inclusion complex between β -CD and adamantane labelled with a fluorescent probe (Ada-A488) was calculated by fluorescence correlation spectroscopy²¹³. The pyrene- β -CD complex has an apparent association constant of $2.3 \cdot 10^4$ L mol⁻¹^{173,214}. Biotin is also a suitable guest for CD forming host-guest complexes with an association constant of 300 L mol⁻¹ used in order to immobilize biomolecules. Due to their high stability, the host-guest complexes have found several important applications in supramolecular chemistry and in biomedical fields²¹⁵⁻²¹⁷.

In the last few years, molecularly imprinted polymers (MIPs) have become an attractive tool for the development of artificial recognition agents. Molecular imprinting technique is achieved by the interaction, either noncovalent or covalent, between complementary groups in a template molecule and

functional monomer units through polymerization or polycondensation. Owing to their advantageous properties (affinity and specificity towards the target molecules and high stability) over natural biological recognition agents, MIPs have been widely employed for diverse applications in diagnostics, separation, purification and quantification processes. One of the most promising applications of MIPs is their use as recognition elements in sensors allowing the highly specific detection of even very dilute molecules in mixtures. Computationally designed MIPs often possess affinity comparable with antibodies. The binding detection was realized using electrochemical, optical and piezoelectric transducers. Two principal types of MIP sensors were developed: affinity sensors (immunosensor and receptor-type sensor devices) and catalytic sensors²¹⁸⁻²²⁰.

1.6. Conclusions

The cyclodextrins ability to form inclusion complexes is the main reason of their wide spread utilization in various areas such as: pharmaceutical technology, agriculture, food, toilet articles, textile industry and environment monitoring. During the last decades, cyclodextrins found an increasing interest in analytical chemistry, multiple applications in pharmaceutical and biomedical analysis being reported in literature. The interactions between cyclodextrins and/or their derivatives with many electroactive molecules (as guest) modify the electrochemical behavior of the last ones, determining the decrease of the anodic/cathodic peak currents and shifts in the oxidation/reduction potentials. This is the reason why cyclodextrins have been widely employed as electrode modifiers by using various methods for their immobilization onto the electrode surface. The cyclodextrin based (bio)sensors showed increased performances such as marked sensitivity, selectivity and molecular recognition.

PERSONAL CONTRIBUTION

1. Electrochemical and spectral study of some pharmaceuticals with β -cyclodextrin interactions in solution

1.1. Introduction

Cyclodextrins (CDs) find various applications in pharmaceutical formulations where they are used in order to enhance the solubility, stability and bioavailability of drug molecules^{2,3}. The main subject of many scientific articles consists in the study of the formation of inclusion complexes between CDs and various molecules^{20,221-224}. The formation of host-guest complexes with CDs was characterized by electrochemical, chromatographic, calorimetric and spectral methods such as: NMR^{27,225,226}, UV-Vis spectrophotometry²²⁶, IR spectroscopy^{27,226}, fast atom bombardment mass spectrometry²²⁶, X-ray crystallography²²⁷, differential scanning calorimetry²²⁸, thermogravimetry/differential thermal analysis^{221,229} and electrochemical methods^{18,20,27,226,230}. Several electrochemical methods such as potentiometry, cyclic voltammetry, differential pulse voltammetry and square wave voltammetry were used for the investigation of CDs behavior in solution. The influence of the CD addition on the electrochemical behavior of the guest molecules mainly consists in the decrease of the peak current and also in a shift to more positive potential values, due to the formation of inclusion complexes with smaller diffusion coefficients^{18,20}.

The influence of β -cyclodextrin (β -CD) in aqueous solutions, on the electrochemical behavior of some pharmaceutical substances, such as: ascorbic acid ((5R)-[(1S)-1,2-dihydroxyethyl]-3,4-dihydroxyfuran-2(5H)-one), uric acid (7,9-Dihydro-1H-purine-2,6,8(3H)-trione), caffeine (1,3,7-trimethyl-1H-purine-2,6(3H,7H)-dione-3,7-dihydro-1,3,7-trimethyl-1H-purine-2,6-dione), caffeine citrate (1,3,7-trimethylpurine-2,6-dione; 2-hydroxypropane-1,2,3-tricarboxylic acid), theophylline (1,3-dimethyl-7H-purine-2,6-dione), aminophylline (1,3-dimethyl-7H-purine-2,6-dione; ethane-1,2-diamine) and acetaminophen (*N*-(4-hydroxyphenyl)acetamide) was investigated with carbon paste electrodes (CPEs) by using square wave voltammetry (SWV)²³¹. The inclusion complexes were characterized by FTIR spectra²³¹.

1.2. Experimental

β -CD was purchased from Merck, acetaminophen from Sigma, caffeine, caffeine citrate, theophylline, uric acid, ascorbic acid, aminophylline were purchased from Fluka. The 0.1 mol L⁻¹ phosphate buffer solutions (PBS) at pH 7.4 and pH 7.2 were prepared using sodium dihydrogen phosphate and sodium monohydrogen phosphate from Fluka. The 0.1 mol L⁻¹ acetate buffer at pH 4 was prepared using acetic acid and

sodium acetate from Fluka. All the reagents were used without further purification and were of analytical grade. All aqueous solutions were prepared with ultrapure water. All the measurements were performed at room temperature (22 – 25 °C)²³¹.

The electrochemical experiments were carried out with an Autolab PGSTAT 12 potentiostat equipped with GPES 4.9 software, using a traditional three electrodes system. The carbon paste electrode was used as the working electrode, with an Ag/AgCl, KCl 3 mol L⁻¹ as reference electrode and a platinum wire as the counter electrode. The FTIR spectra were measured in a Jasco FT/IR-4100 spectrophotometer equipped with Jasco Spectra Manager Version 2 software on wavenumber 550 - 4000 cm⁻¹. The solid samples were obtained after evaporation of the same solvent used in electrochemical analysis²³¹.

The carbon paste (CP) was prepared by hand-mixing graphite powder with melted solid paraffin in a ratio of 3:1 (w/w) to ensure easy manipulation. The electrode was constructed by packing the carbon paste into the tip of the Teflon cavity (d = 4 mm; h = 5 mm), provided with a copper wire which assures electric contact. The surface was then smoothed with a smooth white paper while a light manual pressure was applied to the electrode tip until a shiny surface was obtained²³¹.

The optimal parameters for SWV were: frequency 15 Hz, amplitude 25 mV and step potential 2 mV, and for cyclic voltammetry (CV) a scan rate of 100 mV s⁻¹ was used. The mixtures were obtained by vortexing the solutions 5 minutes at 400 rpm in order to allow the formation of inclusion complexes. The uric acid solution was prepared by ultrasonication during 10 minutes and heating up to 60 °C to solve the powder. All the other solutions were prepared by ultrasonication for 3 minutes²³¹.

1.3. Results and discussions

1.3.1. The electrochemical behavior of the studied pharmaceuticals in the presence of β -cyclodextrin

The square wave and cyclic voltammetry behavior of increasing concentrations of β -CD with 10⁻³ mol L⁻¹ solutions of uric acid, ascorbic acid, aminophylline, caffeine, caffeine citrate and theophylline was investigated with CPE. A shift towards positive values of potential and in the same time a decrease of the current intensity after β -CD addition in the solution, which can be attributed to the formation of inclusion complexes between the β -CD host cavity and the analyte guest molecule, are presented in Figures 9-12²³¹.

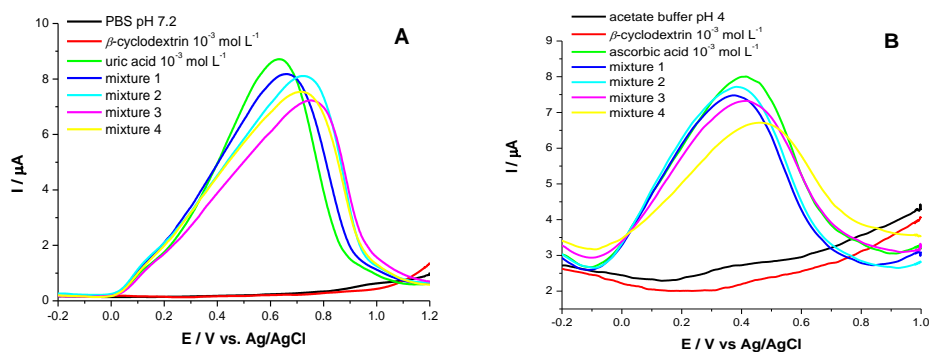


Fig. 9. SWVs of (A) 10^{-3} mol L $^{-1}$ uric acid in PBS pH 7.2 (green line) and (B) 10^{-3} mol L $^{-1}$ ascorbic acid in acetate buffer pH 4 (green line) with β -CD: 10^{-3} (dark blue), $2 \cdot 10^{-3}$ (light blue), $3 \cdot 10^{-3}$ (purple), $4 \cdot 10^{-3}$ (yellow) mol L $^{-1}$ 231

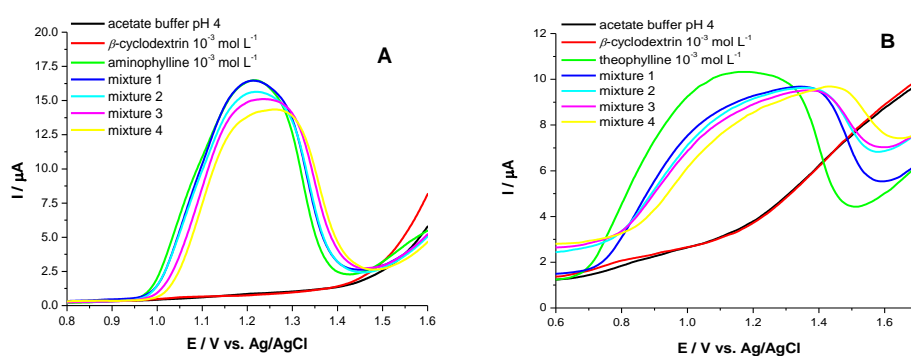


Fig. 10. SWVs of (A) 10^{-3} mol L $^{-1}$ aminophylline (green line) in acetate buffer pH 4 with β -CD: 10^{-3} (dark blue), $3 \cdot 10^{-3}$ (light blue), $5 \cdot 10^{-3}$ (purple), $7 \cdot 10^{-3}$ (yellow) mol L $^{-1}$; (B) 10^{-3} mol L $^{-1}$ theophylline monohydrate (green line) in acetate buffer pH 4 with β -CD: 10^{-3} (dark blue), $3 \cdot 10^{-3}$ (light blue), $5 \cdot 10^{-3}$ (purple), $6 \cdot 10^{-3}$ (yellow) mol L $^{-1}$ 231

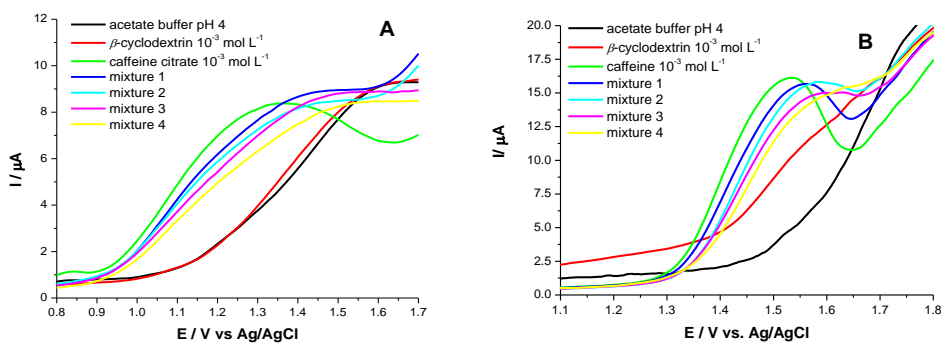


Fig. 11. SWVs of (A) 10^{-3} mol L $^{-1}$ caffeine citrate in acetate buffer pH 4 with β -CD: 10^{-3} (dark blue), $3 \cdot 10^{-3}$ (light blue), $5 \cdot 10^{-3}$ (purple), $8 \cdot 10^{-3}$ (yellow) mol L $^{-1}$; (B) 10^{-3} mol L $^{-1}$ caffeine in acetate buffer pH 4 with β -CD: 10^{-3} (dark blue), $5 \cdot 10^{-3}$ (light blue), $6 \cdot 10^{-3}$ (purple), $9 \cdot 10^{-3}$ (yellow) mol L $^{-1}$ 231

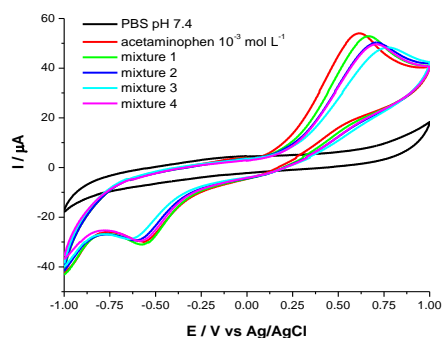


Fig. 12. CVs of 10^{-3} mol L $^{-1}$ acetaminophen in PBS pH 7.4 with β -CD: 10^{-3} (dark blue), $2 \cdot 10^{-3}$ (light blue), $3 \cdot 10^{-3}$ (purple), $4 \cdot 10^{-3}$ (yellow) mol L $^{-1}$ ²³¹

The current intensity depends on the concentration of free molecules and on their diffusion coefficient. The decrease in current intensity after addition of β -CD is attributed to the decrease in concentration of free analyte molecules. It was observed that the guest molecules entrapment in the host cavity hinders their oxidation (electron transfer does not involve the encapsulated substrate, the complex dissociation usually takes place before the electron transfer step)^{18,20}. The positive shift of the E_p also indicates that the oxidation center of the analyte is included in the β -CD cavity leading to a more difficult oxidation. Another reason for the decrease in current intensity may be a smaller diffusion coefficient of the inclusion complexes compared to the free drug, taking into consideration that the complexes usually present smaller diffusion coefficients and the analyte reaches the surface electrode harder^{18,20}.

The relationships between the oxidation peak currents and the concentration of caffeine in acetate buffer at pH 4 in the presence of 10^{-4} mol L $^{-1}$ β -CD was examined by SWV (Figure 13 A). The values of the maximum current intensity were read at different potentials according to the shift registered for each complex. The concentration shows a linear variation range from 10^{-4} to $5 \cdot 10^{-4}$ mol L $^{-1}$ expressed by the following equation: $I_p(\mu A) = 0.75 \pm 0.158 + 6.30 \pm 0.578 \cdot C_{\text{caffeine}}$ (mmol L $^{-1}$); $R^2 = 0.983$ (4 points), Figure 13 B. The current variation is not linear for concentrations greater than $5 \cdot 10^{-4}$ mol L $^{-1}$. The oxidation peak corresponding to the caffeine is growing proportional to the amount added suggesting that the molar ratio of 1:1 is convenient for the complexation (Figure 13 A).

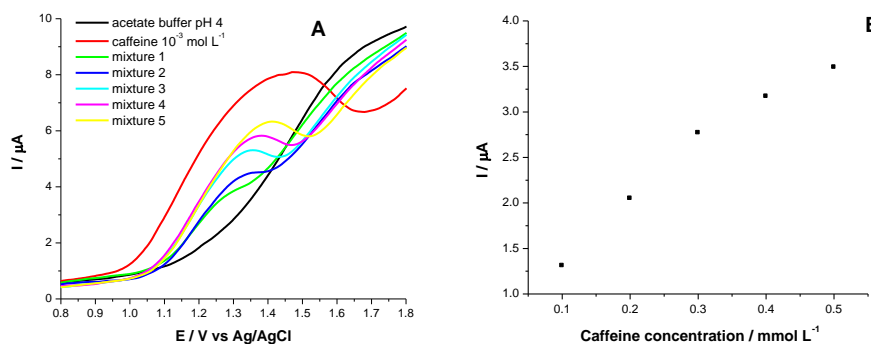


Fig. 13. (A) SWVs of $10^{-3} \text{ mol L}^{-1}$ caffeine (red) and mixtures of $10^{-4} \text{ mol L}^{-1}$ β -CD with increasing concentration of caffeine in acetate buffer pH 4: $1 \cdot 10^{-4}$ (green), $2 \cdot 10^{-4}$ (dark blue), $3 \cdot 10^{-4}$ (light blue), $4 \cdot 10^{-4}$ (purple), $5 \cdot 10^{-4}$ (yellow) mol L^{-1} ; **(B)** Variation of current intensity with caffeine concentration in presence of $10^{-4} \text{ mol L}^{-1}$ β -CD²³¹

1.3.2. Determination of binding constant K_i for β -CD inclusion complexes with the studied pharmaceuticals

The binding constants of the inclusion complexes between β -CD and the studied pharmaceuticals were calculated according to the following equation²³²:

$$I_{cp}^2 = \frac{K_D}{[\beta - CD]_0} (I_{cp,s}^2 - I_{cp}^2) + I_{cp,\beta-CD-s}^2$$

where $I_{cp,s}$ is the limited diffusion current of the guest in the absence of β -CD; I_{cp} is the detected current of the guest molecule in the presence of different concentrations of β -CD; $I_{cp,\beta-CD-s}$ is the limited diffusion current of the guest included by β -CD.

Table II. K_i values of β -CD inclusion complexes²³¹

Host molecule	Guest molecule	$I_{cp}^2 = f(K_D)$	$K_i (\text{L mol}^{-1})$
β -CD	Ascorbic acid	$I_{cp}^2 = -0.0041 K_D + 27.80$	243.90
	Uric acid	$I_{cp}^2 = 0.0015 K_D + 46.48$	666.66
	Acetaminophen	$I_{cp}^2 = 0.0061 K_D - 290.808$	161.29
	Aminophylline	$I_{cp}^2 = -0.0124 K_D + 294.62$	80.65
	Teophylline	$I_{cp}^2 = 0.0011 K_D + 4.387$	909.09
	Caffeine	$I_{cp}^2 = 0.009 K_D + 7.394$	1111.11

The plots of I_{cp}^2 vs. $(I_{cp,s}^2 - I_{cp}^2)/[\beta\text{-CD}]_0$ are straight lines with the slopes being equal to the corresponding dissociation constants K_D . The equations for these straight lines and the values for the binding constants for all the inclusion complexes are presented in Table II. The binding constant K_i was calculated from the inverse of the slope K_D . The obtained values for K_i are in agreement with the results presented in literature for other inclusion complexes of $\beta\text{-CD}$ ²³².

1.3.3. Infrared spectra of the inclusion complexes

FTIR measurements for $\beta\text{-CD}$, guests alone and also for the inclusion complexes were performed. The solid samples were prepared by evaporation of the same solvent used in electrochemical analysis. Two supplementary peaks, at 1583 cm^{-1} and 1400 cm^{-1} corresponding to the COO^- asymmetric and symmetric stretches, can be observed when acetate buffer is used; meanwhile PBS presents no remarkable influence in FTIR spectra. Major modifications of the absorption bands such as shifts, attenuations and disappearances of some bands can be easily observed in the FTIR spectra of the inclusion complexes.

In the FTIR spectra of ascorbic acid inclusion complexes (in two molar ratio 1:1 and 1:4) can be observed that some bands of the guest are diminished: 1752 cm^{-1} (C=O stretch in carbonyl), 1652 cm^{-1} (C=C stretch), 1023 cm^{-1} (C-O stretch in alcohols and ethers), 754 cm^{-1} (=C-H bend), 628 cm^{-1} (C-O bend in ether). Other bands of ascorbic acid are not observable in complexes: 3005 cm^{-1} (=C-H stretch), 1496 cm^{-1} (C-C stretch in-ring), 1455 cm^{-1} (C-H bend), and $1312\text{-}1110\text{ cm}^{-1}$ (C-O stretch), $987\text{-}683\text{ cm}^{-1}$ (=C-H bend). The four small O-H stretches from 3523 , 3406 , 3310 , 3206 cm^{-1} disappear in complexes being hidden in the broad band at 3277 cm^{-1} from $\beta\text{-CD}$. The specific bands of $\beta\text{-CD}$ from 3313 cm^{-1} (O-H stretch, H-bonded), 2924 cm^{-1} (C-H stretch in alkanes), $1338\text{-}1020\text{ cm}^{-1}$ (C-O stretch in alcohols and ethers), $946\text{-}754\text{ cm}^{-1}$ (carbohydrates bends), $605\text{-}574\text{ cm}^{-1}$ (ether bend) are attenuated and shifted in the complexes spectra (Figure 14 A).

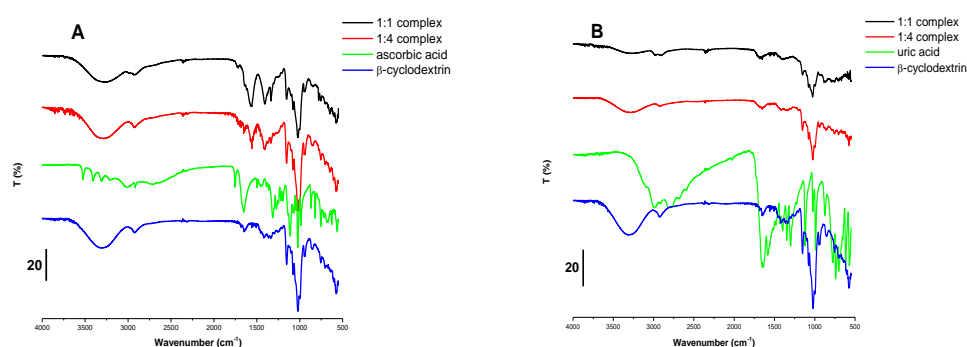


Fig. 14. FTIR spectra of $\beta\text{-CD}$, ascorbic acid (**A**), uric acid (**B**) and their inclusion complexes²³¹

The FTIR spectra of uric acid- $\beta\text{-CD}$ complexes are presented in Figure 14 B where it can be easily observed the marked modifications of uric acid spectra: some bands of uric acid from 2986 cm^{-1} , 2916 cm^{-1} (CH_3 asymmetric and N-H stretch

in imidazol), 1024 cm^{-1} (N-H stretching, C-N stretch in pirimidine), 874 cm^{-1} (N-H out-of-plane bending) are strongly diminished and shifted in complexes, meantime other bands have disappeared: 2817-2024 cm^{-1} (ν CH_3 asymmetric and N-H stretch, asymmetric stretch of C=C), 1652-1435 cm^{-1} (C=O stretch in unsaturated carbonyl, asymmetric deformation of NH_3 , CH_2 -CO bending, δ CH_2 scissoring), 1398-1348-1299 cm^{-1} (CH_2 -CO deformation, ν C=O, ν CN in imidazole), 1120 cm^{-1} (N-H stretching, C-N stretch in pirimidine), 989-572 cm^{-1} (C-C stretch, N-H out-of-plane bending, C-N stretching of aromatic). The modification of β -CD absorption bands is almost the same like in the case of ascorbic complexes.

In the caffeine and caffeine citrate complexes spectra (Figures 15 A and 15 B) some vibration bands of citrate caffeine from 1753-1696-1646 cm^{-1} (C=O stretch in unsaturated cetones, carboxylic acid), 1239 cm^{-1} (CN stretch in imidazole), 911 cm^{-1} (O-H bend in carboxylic acid), 849-673 cm^{-1} (δ CH) are attenuated. Other peaks of citrate caffeine disappear in complexes: 3471-3215-3167 cm^{-1} (O-H, NH stretch, H-bonded), 3119 cm^{-1} (CH stretch in imidazole), 1761-1706 cm^{-1} (C=O stretch), 1374 cm^{-1} (δ CH in citrate), 1313 cm^{-1} (C-N stretch in imidazole), 1208-1189 cm^{-1} (C-O stretch), 1172-1032 cm^{-1} (C-N stretch in pyrimidine), 977-763 cm^{-1} (δ CH, NH, ring). In the case of inclusion complexes between caffeine and β -CD many bands of caffeine are strongly attenuated and shifted: 3112 cm^{-1} (C-H stretch in imidazole), 1692 cm^{-1} (C=O stretch), 1480-1455 cm^{-1} (C-C stretch in-ring), 1283-1237 cm^{-1} (C-N stretch in imidazole), 924 cm^{-1} (δ NH), 758 cm^{-1} (δ CH). Other bands disappear: 1598-1402 cm^{-1} (ν CC), 1187-1073 cm^{-1} (ν CN), 972-608 cm^{-1} (δ CH, ring, NH).

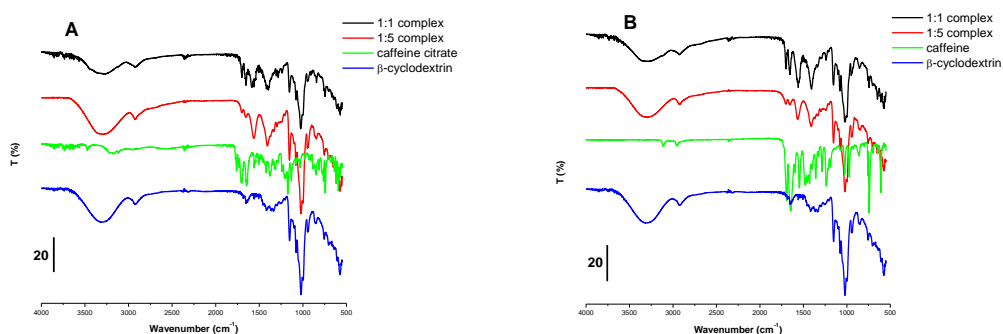


Fig. 15. FTIR spectra of β -CD, caffeine citrate (A), caffeine (B) and their inclusion complexes²³¹

The β -CD's inclusion complexes with theophylline (Figure 16 A) also revealed that most of the theophylline bands are attenuated and shifted: 3120 cm^{-1} (ν CH in imidazole), 2982-2924 cm^{-1} (ν NH imidazole), 1705-1661 cm^{-1} (C=O stretch), 1284-1239 cm^{-1} (C-N stretch imidazole), 1186 cm^{-1} (C-N stretch pirimidine), 846-609 cm^{-1} (δ CH, NH)²³³. Some peaks of theophylline from 3058-2822-2597 cm^{-1} (C-H stretch imidazole), 1047 cm^{-1} (C-N stretch in pirimidine), and 913 cm^{-1} (δ NH) have disappeared in the complexes spectra. The spectral behavior of aminophylline complexes (Figure 16 B) is similar to that of theophylline ones.

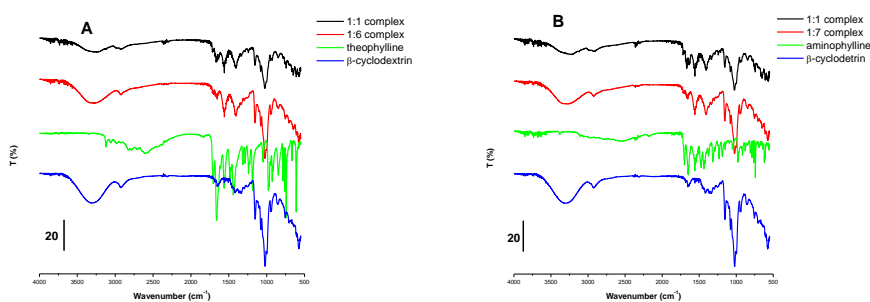


Fig. 16. FTIR spectra of β -CD, theophylline (A), aminophylline (B) and their inclusion complexes²³¹

In the case of acetaminophen complexes (Figure 17) the peaks of acetaminophen are very strong attenuated and some of them completely disappear: 3321 cm^{-1} (O–H stretch, H-bonded in phenols), 3160 cm^{-1} (N–H stretch in amides), 3109 cm^{-1} (C–H stretch in aromatics), $3035\text{--}2492\text{ cm}^{-1}$ ($\nu\text{ CH}_3$), 1258 cm^{-1} (C–N stretch in aromatic amine), $1172\text{--}968\text{ cm}^{-1}$ (δ phenyl, δ COH, δ CH₃), 835 cm^{-1} (δ CH in phenyl), 710 cm^{-1} (δ CH₃). The specific bands of β -CD are a little shifted and diminished.

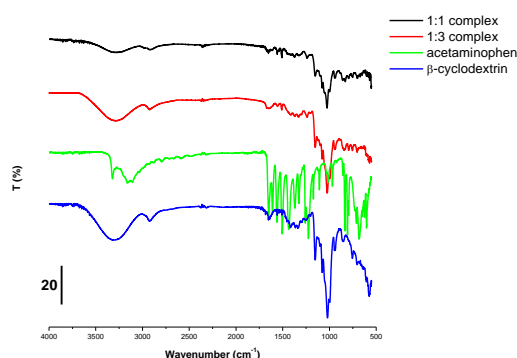


Fig. 17. FTIR spectra of β -CD, acetaminophen and their inclusion complexes²³¹

1.4. Conclusions

The effect of β -CD on the electrochemical behavior of the guest molecules which were studied, namely uric acid, ascorbic acid, aminophylline, caffeine, caffeine citrate, theophylline and acetaminophen, highlights a decrease in the peak current and a positive shift in the anodic peak potential. The formation of inclusion complexes between β -CD and these molecules may be responsible for these results which can be explained by the concentration decrease of the free analyte and by the decrease of the diffusion coefficient for the inclusion complexes.

The FTIR spectra revealed the modifications of vibration bands of the analytes and of β -CD consisting in shift, attenuation and disappearance of some bands in the complexes spectra, thus confirming the formation of inclusion complexes.

2. β -cyclodextrin modified carbon paste electrodes for ascorbic and uric acids detection

2.1. Introduction

Cyclodextrins can be used as carbon paste electrodes modifiers with the purpose of enhancing the sensitivity and selectivity of the analyte determination in pharmaceuticals, biological samples and soft drinks. The preconcentration of the substance on the electrode surface is based on the formation of inclusion complexes between the cyclodextrin host and the analyte guest^{51-57,59-61,234}. The advantages of carbon paste electrodes modified with β -cyclodextrin for the determination of ascorbic acid and uric acid are presented and commented²²³.

2.2. Experimental

The 5 % β -CD modified carbon paste was prepared in two different ways. Solid β -CD powder was mixed with graphite powder and melted solid paraffin (3:1) until the paste was homogenous. This composition was packed into the tip of Teflon tube. The electrode surface is brushed up whenever necessary by removing a small layer of carbon paste and replacing with a new one²³¹.

An aqueous solution of β -CD 10^{-2} mol L⁻¹ (2.2 mL of β -CD solution was added to 475 mg of carbon paste in order to obtain 5 % β -CD modified carbon paste) was added to melted solid paraffin and graphite powder in a ratio of 1:3. The mixture was homogenized in a mortar and the aqueous phase was allowed to evaporate at about 70 °C.

The optimal parameters for SWV were: frequency 15 Hz, amplitude 25 mV and step potential 2 mV, and for CV a scan rate of 100 mV s⁻¹ was used. The mixtures were obtained by stirring the solutions 5 minutes at 400 rpm in order to allow the formation of inclusion complexes. The uric acid solution was prepared by ultrasonication during 10 minutes and heating up to 60 °C to solubilize the powder. All the other solutions were prepared by ultrasonication for 3 minutes²³¹.

2.3. Results and discussions

Ascorbic acid and uric acid were analyzed at β -CD/CPEs by using SWV. Ascorbic acid was detected at carbon paste electrode having a peak height of 5.14 μ A and a peak potential of 0.414 V (Table III). With both β -CD/CPEs the peak height increased significantly and the potential was strongly shifted to more negative values indicating the formation of inclusion complexes between the β -CD and the analytes, complexation which leads to a preconcentration of the analyte on the electrode

surface. Ascorbic acid accumulation within the β -CD cavity is revealed by the increase of the anodic peak currents with 0.39 μ A and 0.93 μ A compared to those obtained at unmodified electrode. The results indicate that the best response was achieved with the β -CD/CPE prepared with β -CD solution, suggesting higher complexation efficiency due to the higher homogeneity of the carbon paste than the one prepared with β -CD added as powder²³¹.

Table III. SWV parameters for ascorbic acid 10^{-3} M with different CPEs²³¹

Electrode	Peak height (μ A)	Peak potential (V)
CPE	5.14	0.414
β -CD/CPE (β -CD powder)	5.53	0.28
β -CD/CPE (β -CD solution)	6.07	0.323

In the case of uric acid determination, the peak height is higher with 0.50 μ A only on the β -CD/CPE obtained with the addition of β -CD as solution and the potential shift is about 0.042 V (Table IV) in comparison with the unmodified electrode. These differences can be attributed to the immobilization of β -CD on the carbon paste which leads to the modification of the electrode surface, that cause an increased signal due to the substance accumulation, probably by formation of uric acid- β -CD inclusion complex. The inclusion complex formed may be responsible for the preconcentration of the uric acid to the electrode surface, thus facilitating the oxidation²³¹.

Table IV. SWV parameters for 10^{-3} M uric acid with different CPEs²³¹

Electrode	Peak height (μ A)	Peak potential (V)
CPE	8.31	0.631
β -CD/CPE (β -CD powder)	7.20	0.605
β -CD/CPE (β -CD solution)	8.81	0.589

Even if the best response concerning the current intensity for the ascorbic acid determination is obtained on β -CD(solution)/CPE, it can be noticed that the negative potential shift is bigger on β -CD(powder)/CPE ($\Delta E = 0.134$ V). The anodic potential in the case of ascorbic acid is shifted with 0.134 V and 0.091 V to more negative values in comparison with the bare CPE. This behavior can be explained by the formation of inclusion complexes which maintain the analyte to the electrode surface, making it easier to be oxidized. Briefly, both β -CD/CPEs present better electrochemical signals for ascorbic and uric acids, compared with the unmodified CPE (Figure 18 A and B)²³¹.

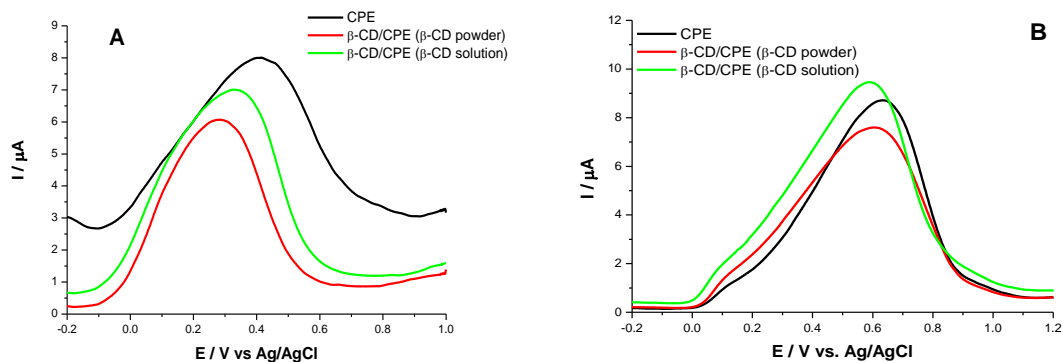


Fig. 18. SWVs of $10^{-3} \text{ mol L}^{-1}$ ascorbic acid **(A)** and $10^{-3} \text{ mol L}^{-1}$ uric acid **(B)** solutions with unmodified and β -CD modified CPEs²³¹

2.4. Conclusions

Among the β -CD/CPEs advantages for the determination of ascorbic and uric acids can be mentioned: enhanced sensitivity, simple, fast and low cost procedure. Neither accumulation time, nor accumulation potential is required for the sensitive measurements of ascorbic and uric acids. No electrochemical pretreatment of the electrode is necessary. The increase of current intensity and negative potential shift are attributed to the inclusion complexes formation which leads to the preconcentration of the analytes at the electrode surface.

3. Glassy carbon electrodes based on β -cyclodextrin entrapped in polyethyleneimine film for ascorbic and uric acids determination

3.1. Introduction

Ascorbic acid has a tremendous antioxidant effect playing an important role in bioelectrochemistry, neurochemistry and clinical diagnostics applications²³⁵. Uric acid, the primary end product of purine metabolism, is a marker for diseases such as gout, hyperuricaemia and Lesch-Nyhan syndrome in abnormal concentrations. Colorimetric, enzymatic and electrochemical methods were used for the detection and quantification of the two substances²³⁶. The electrochemical methods are less expensive, less time consuming and more sensitive, but less selective. The major problem is the interference between ascorbic and uric acids due to the very close oxidation potential values²³⁷. This inconvenient was overcome by developing various modified electrodes for simultaneous selective determination of the two species with and without other interferences²³⁵⁻²⁵⁵. In many cases, the cyclodextrins inclusion as electrode modifier generated an enhancement of the sensitivity and selectivity of ascorbic acid and uric acid determinations^{84,139,256,257}. For their detection and quantification in biological samples, various ascorbic acid and uric acid analytical procedures have been reported, including high-performance liquid chromatography (HPLC) methods with UV-Vis and electrochemical detection²⁵⁸⁻²⁶⁰.

Polyethyleneimine (PEI), a cationic polymer, was often used for the entrapment of several molecules in various biosensors due to its advantages: retaining the biomolecule at the surface of the electrode without stressing it with any supplementary electropolymerization process, and partial solubility in water²⁶¹⁻²⁶³.

A simple method for the modification of GCE with the polymeric films of PEI with β -cyclodextrin (β -CD) for the analysis of ascorbic and uric acids, separately and in mixture, is reported. A very good separation of the ascorbic acid and uric acid peaks, increased signals and shifted oxidation potentials to more negative values were obtained, results which highlight the advantages of this modified electrode compared with the bare one. These modified electrodes were applied successfully to the monitoring of ascorbic acid from pharmaceutical products and for the quantification of ascorbic and uric acids in urine offering possible applications in biomedical analysis^{264,265}.

3.2. Experimental

3.2.1. Materials and methods

β -CD was purchased from Merck, uric acid, ascorbic acid, sodium dihydrogen phosphate, sodium monohydrogen phosphate and methanol for HPLC ($\geq 99.9\%$) were purchased from Sigma. The 0.1 mol L^{-1} phosphate buffer solution (PBS) at pH 7.2 was used. The uric acid solution was prepared by 10 minutes ultrasonication and heating it up to $60\text{ }^{\circ}\text{C}$. All the reagents were used without further purification and they were all of analytical grade. All aqueous solutions were prepared with ultrapure water. All the measurements were performed at room temperature²⁶⁴.

The electrochemical experiments were carried out with an Autolab PGSTAT 12 potentiostat equipped with GPES 4.9 software, using a traditional three-electrode system. GCE purchased from Bioanalytical Systems (BAS), was used as the working electrode, with Ag/AgCl as reference electrode and a platinum wire as the counter electrode. For SWV experiments, a frequency of 15 Hz and amplitude of 25 mV were employed. CV was performed by sweeping the potential between -0.1 V and 0.6 V vs Ag/AgCl for uric acid, and between 0 V and 0.8 V for ascorbic acid, at different scan rates. The mixtures were obtained by vortexing the solutions for 3 minutes at 400 rpm. For the real sample analysis the square wave voltammograms were obtained by scanning potential from -0.3 V to 1.0 V with frequency of 25 Hz and amplitude of 25 mV ²⁶⁴.

The FTIR spectra were measured with Jasco FT/IR-4100 spectrophotometer equipped with Jasco Spectra Manager Version 2 software in the wave number range of $550 - 4000\text{ cm}^{-1}$. The solid samples were obtained after evaporation of the same solvent used in the electrochemical analysis. The RAMAN spectra of the modified electrodes were obtained using a confocal Raman microscope (Alpha 300R from WiTec) with 532 nm wavenumber of the laser and 60 seconds time accumulation. For the chromatographic method a LC-10AS Shimadzu was used. The conditions for the chromatographic analysis were: reverse phase (RP) C 18 column ($5\mu\text{m}$), mobile phase - isocratic elution with methanol 2.5 % in NaH_2PO_4 pH 4.75, UV detection at 265 nm for ascorbic acid, 292 nm for uric acid, temperature $35\text{ }^{\circ}\text{C}$, flow rate 0.5 mL min^{-1} ^{258-260,265}. The spectrophotometry determinations were performed with SPECORD 250 PLUS spectrophotometer (Analytik Jena Germany) equipped with WinAspect software. Ascorbic acid was determined in UV domain at 243 nm. The microscopic characterization of the modified electrodes surface was achieved by using a confocal Raman microscope (Alpha 300R from WiTec)^{264,265}.

3.2.2. Preparation of the working electrodes

Solutions of 5 mg mL^{-1} and 1 mg mL^{-1} were prepared by dissolving the necessary weight of PEI in the solvent composed of water: alcohol 1:1. The solution of 5 mg mL^{-1} PEI and 1 % β -CD was obtained by dissolving the necessary amount of β -CD in the solvent in which then PEI was dissolved. The other solution of 1 mg mL^{-1} PEI and 0.2 % β -CD was prepared by diluting 5 times the above mentioned solution^{264,265}.

5 types of working electrodes were used: bare GCE, GCE modified with 5 mg mL⁻¹ PEI, GCE modified with 1 mg mL⁻¹ PEI, GCE modified with 5 mg mL⁻¹ PEI and 1 % β -CD, and GCE modified with 1 mg mL⁻¹ PEI and 0.2 % β -CD. 6 μ L of the PEI solution, simple and modified with β -CD, were dropped on the electrode and then was dried for 30 minutes at room temperature^{264,265}.

3.2.3. Real samples preparation and analysis

The 10⁻² mol L⁻¹ ascorbic acid stock solution was prepared by mixing together for homogenization ten vials of Vitamina C[®] injectable solution (Arena), by adding the appropriate volume of PBS (pH 7.2, 0.1 mol L⁻¹). In the case of ascorbic acid oral solution from the second analyzed pharmaceutical formulation, Vitamina C[®] (Biofarm), five bottles were mixed together following the same procedure mentioned above for the injection solution. The stock solutions were prepared daily and maintained in the dark, protected from light and at constant temperature. In order to quantify the ascorbic acid concentration from the pharmaceutical samples, the analytical data obtained from the calibration curves were used²⁶⁴.

Urine samples were collected from healthy voluntaries before and during the treatment with ascorbic acid (1 g/day, 7 days) (UPSAVIT VITAMIN C 1g, Bristol-Myers Squibb[®], Hungary). The urine probes were collected each day at 6 hours after medicine administration. Before analysis, the urine was filtered with dense, narrow pores filter (FILTRAK 390, Germany), then diluted 1:500 with phosphate buffer (0.1 mol L⁻¹, pH 7.2)²⁶⁵.

3.3. Results and discussions

3.3.1. Electrochemical, spectral and microscopic analysis

3.3.1.1. Square wave voltammetry of uric and ascorbic acids at β -CD/PEI modified GCEs and FTIR spectra of their inclusion complexes

When the two acids were tested at GCEs modified with β -CD/PEI films using SWV, obvious differences in peak potential and peak height were noticed in comparison with bare GCEs and PEI/GCEs. Uric acid was detected on bare GCE at 0.684 V vs Ag/AgCl, the peak potential was shifted with 0.150 V vs Ag/AgCl at 1 % β -CD/PEI(5 mg mL⁻¹)/GCE and with 0.144 V at 0.2 % β -CD/PEI(1 mg mL⁻¹)/GCE (Figure 19 B), due to the complexation between β -CD from the film and uric acid from solution. The guest molecule, uric acid, entrapped in the cavity of the CD is easier to oxidize because it is retained on the film at the surface of the electrode. M. Ramirez Berriozabal *et al.*²³⁷ obtained a positive shift for the oxidation peak of the uric acid on β -CD/CPE²⁶⁴.

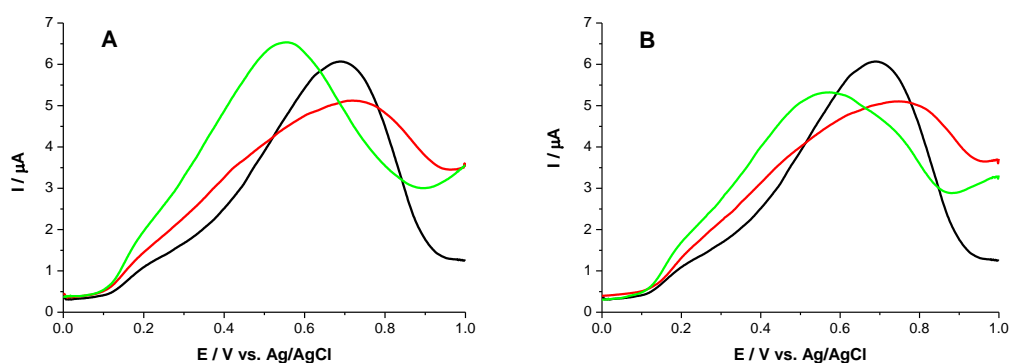


Fig. 19. SWVs of 10^{-3} mol L $^{-1}$ uric acid in PBS (0.1 mol L $^{-1}$; pH 7.2) at bare GCE (black); PEI/GCE (red); β -CD/PEI/GCE (green); **(A)** 5 mg PEI mL $^{-1}$; 1 % β -CD; **(B)** 1 mg PEI mL $^{-1}$; 0.2 % β -CD²⁶⁴

Concerning the peak height and peak area of uric acid on bare GCE, they were bigger than those obtained on the modified GCEs. In the case of uric acid, even the 1 % β -CD/PEI (5 mg mL $^{-1}$)/GCE did not improve the current response (Table V), in contrast with the ascorbic acid behavior²⁶⁴.

Table V. SWV parameters for 10^{-3} mol L $^{-1}$ uric acid on different electrodes²⁶⁴

Electrode type	Peak potential (V)	Peak height (μ A)	Peak area (μ C)
GCE	0.684	5.11	2.03
PEI(1 mg mL $^{-1}$)/GCE	0.674	2.42	1.24
PEI(5 mg mL $^{-1}$)/GCE	0.661	2.62	1.35
0.2 % β -CD/PEI(1 mg mL $^{-1}$)/GCE	0.54	3.46	1.52
1 % β -CD/PEI(5 mg mL $^{-1}$)/GCE	0.534	4.64	1.89

Ascorbic acid presented an oxidation peak at 0.611 V vs. Ag/AgCl and an intensity current of 3.81 μ A at bare GCE. At the modified GCEs the peak potential was shifted to more negative values, the most remarkable shift being noticed for 1 % β -CD/PEI(5 mg mL $^{-1}$)/GCE with a value of 0.316 V vs. Ag/AgCl, (Figure 20)²⁶⁴. For the ascorbic acid oxidation peak, M. Ramirez Berriozabal *et al.* have reported a negative shift of 0.260 V by using β -CD/CPE, while J. J. Colleran and C. B. Breslin obtained a cathodic shift of 0.080 - 0.135 V at PEDOT/S- β -CD/Au electrode^{237,256}.

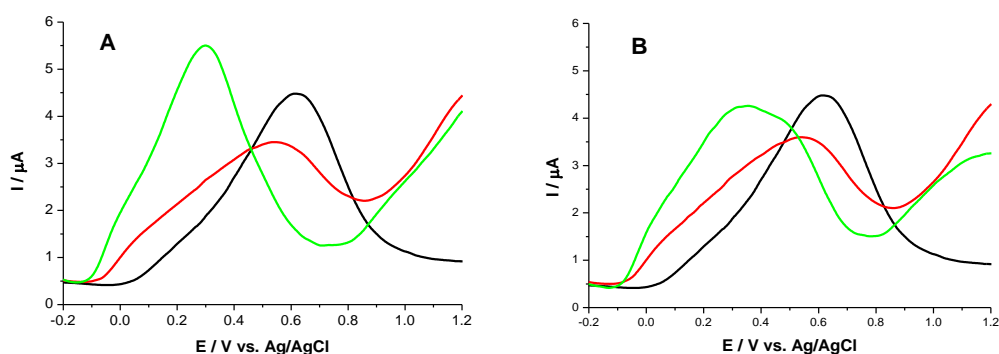


Fig. 20. SWVs of 10^{-3} mol L $^{-1}$ ascorbic acid in PBS (0.1 mol L $^{-1}$; pH 7.2) on bare GCE (black); PEI/GCE (red); β -CD/PEI/GCE (green). **(A)** 5 mg PEI mL $^{-1}$; 1 % β -CD; **(B)** 1 mg PEI mL $^{-1}$; 0.2 % β -CD²⁶⁴

In Table VI it can be observed that the ascorbic acid current intensity was grown only at 1 % β -CD/PEI(5 mg mL $^{-1}$)/GCE with 0.82 A compared to bare GCE indicating that β -CD concentration plays an important role. This behavior can be explained by the inclusion complexes formed between ascorbic acid and β -CD, complexation which seems to be more effective for ascorbic acid than for uric acid. The increase of the current intensity can be attributed to the preconcentration of the analyte at the electrode surface due to the complexation with cyclodextrin which retains more molecules at the surface of the electrode. The negative shift of peak potential can be explained by the mediator effect of cyclodextrin: its cavity acts like a “tunnel” which directs the electrons to the electrode surface for the redox process²⁶⁴.

Table VI. SWV parameters for 10^{-3} mol L $^{-1}$ ascorbic acid at different electrodes²⁶⁴

Electrode type	Peak potential (V)	Peak height (μ A)	Peak area (μ C)
GCE	0.611	3.81	1.76
PEI(1 mg mL $^{-1}$)/GCE	0.513	2.06	1.09
PEI(5 mg mL $^{-1}$)/GCE	0.505	1.85	0.99
0.2 % β -CD/PEI(1 mg mL $^{-1}$)/GCE	0.321	3.29	1.65
1 % β -CD/PEI(5 mg mL $^{-1}$)/GCE	0.295	4.63	1.78

Spectral studies were performed in order to understand the electrochemical behavior of the two analytes at the β -CD/PEI modified GCEs. In the spectra of the two complexes presented in Figure 21, it can be observed that some specific bands of cyclodextrin were attenuated and shifted: 3313 cm $^{-1}$ (O–H stretch, H–bonded), 2924 cm $^{-1}$ (C–H stretch in alkanes), 1338-1020 cm $^{-1}$ (C–O stretch in alcohols and ethers), 946-754 cm $^{-1}$ (carbohydrates bends), 605-574 cm $^{-1}$ (ether bend)²⁶⁴.

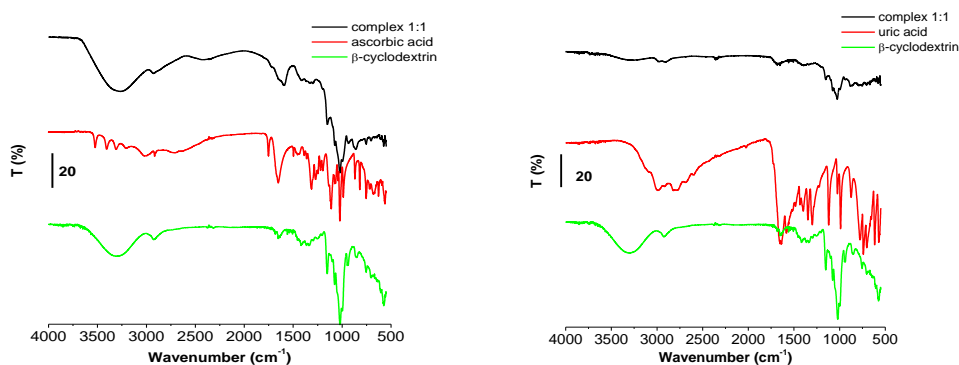


Fig. 21. FTIR spectra of ascorbic acid (A), uric acid (B), β -CD, and their inclusion complexes²⁶⁴

Some bands of ascorbic acid were diminished and shifted in the inclusion complex spectra (1652 cm^{-1} (C=C stretch), 683 cm^{-1} (=C-H bend)), while many bands disappeared: 3523 , 3406 , 3310 , 3206 cm^{-1} (four O-H stretches are hidden in the broad band at 3277 cm^{-1} from β -CD), 3005 cm^{-1} (=C-H stretch), 1752 cm^{-1} (C=O stretch in carbonyl), 1496 cm^{-1} (C-C stretch in-ring), 1455 cm^{-1} (C-H bend), 1387 cm^{-1} (C-H rock in alkanes), 1312 - 1110 cm^{-1} (C-O stretch), 987 - 683 cm^{-1} (=C-H bend) (Figure 21 A). In the case of uric acid, some absorption bands were diminished and shifted in the spectra of the complex: 2986 cm^{-1} , 2916 cm^{-1} (CH_3 asymmetric and N-H stretch in imidazole), 1024 cm^{-1} (N-H stretching, C-N stretch in pirimidine), 874 cm^{-1} (N-H out-of-plane bending). Other bands of the analyte have disappeared: 2817 - 2024 cm^{-1} ($\nu\text{ CH}_3$ asymmetric and N-H stretch, asymmetric stretch of C=C), 1652 - 1435 cm^{-1} (C=O stretch in unsaturated carbonyl, asymmetric deformation of NH_3 , CH_2 -CO bending, $\delta\text{ CH}_2$ scissoring), 1398 - 1348 - 1299 cm^{-1} (CH_2 -CO deformation, $\nu\text{ C=O}$, $\nu\text{ CN}$ in imidazole), 1120 cm^{-1} (N-H stretching, C-N stretch in pirimidine), 989 - 572 cm^{-1} (C-C stretch, N-H out-of-plane bending, C-N stretching of aromatic) (Figure 21 B). The modifications in the FTIR spectra indicate the formation of inclusion complexes between uric acid and β -CD, ascorbic acid and β -CD respectively²⁶⁴.

3.3.1.2. Square wave voltammetry of ascorbic and uric acids mixture at β -CD/PEI/GCEs and FTIR spectra of their inclusion complexes

0.2 mmol L^{-1} solutions of ascorbic acid and uric acid were analysed with 3 types of electrodes: bare GCE, GCE modified with polyethyleneimine film and GCE modified with β -cyclodextrin and polyethyleneimine film (Figure 22). In the case of ascorbic acid solution, the PEI film deposition leads to a decrease of the oxidation peak intensity. At the electrode modified with β -CD and PEI film, the ascorbic acid peak potential is negatively shifted of about 350 mV and for uric acid the potential shift being about 250 mV (Figure 22 A and B)²⁶⁵.

The electrochemical behavior of an equimolar mixture of ascorbic acid and uric acid in phosphate buffer at a bare GCE is illustrated by a single peak corresponding to the two merged oxidation peaks. The coverage of GCE by a PEI film leads also to a merged peak, negatively shifted by almost 50 mV but with a lower intensity than at

bare GCE, which may reflect the steric hindrances towards the permeation of uric acid and ascorbic acid. In contrast, at the β -CD and PEI/GCE, the voltammogram presents two obvious peaks separated by more than 250 mV corresponding to ascorbic and uric acids oxidation (Figure 22 C)²⁶⁵.

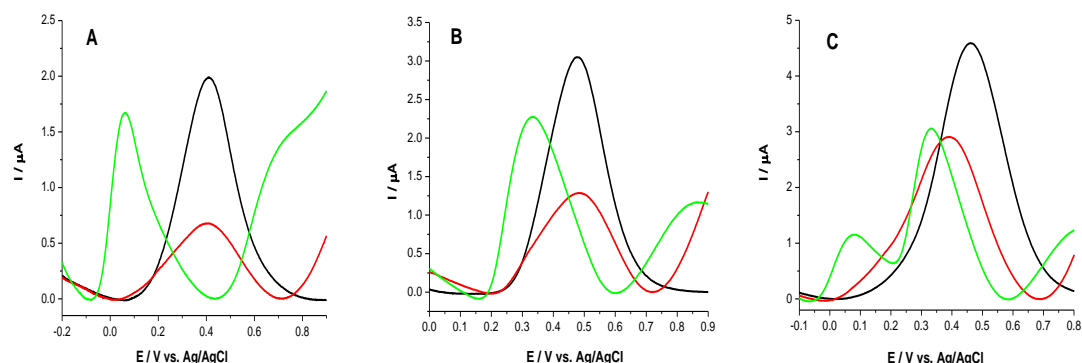


Fig. 22. SWVs of 0.2 mmol L^{-1} ascorbic acid (A), 0.2 mmol L^{-1} uric acid (B) and their 0.2 mmol L^{-1} mixture (C) in 0.1 mol L^{-1} PBS (pH 7.2) at bare GCE (black), 5 mg mL^{-1} PEI/GCE (red), and $1\% \beta\text{-CD/PEI}(5 \text{ mg mL}^{-1})/\text{GCE}$ (green)²⁶⁵

The scan rate influence on the current intensity and the potential of the oxidation peaks was investigated, in the range $5 - 500 \text{ mV s}^{-1}$, for the two analytes. The current intensity increased linearly with the square root of the scan rate while the peak potential is shifted in anodic direction, suggesting that both processes are controlled by the diffusion of molecules towards the electrode surface. Also in both cases during the cathodic potential scan no significant currents were detected indicating that both electrochemical oxidation processes are irreversible. The mechanisms related to the irreversible oxidations of ascorbic acid and uric acid imply the 2 protons and 2 electrons transfer in each case being similar with those obtained by other authors using other working electrodes^{265,266}.

The equation obtained in the case of ascorbic acid is: $I_p(\text{A}) = 6.83 \cdot 10^{-7} \pm 7.66 \cdot 10^{-8} + 3.21 \cdot 10^{-7} \cdot v^{1/2} \pm 6.61 \cdot 10^{-9} (V^{1/2} \text{ s}^{-1/2})$, $R^2 = 0.999$; while for uric acid the equation is: $I_p(\text{A}) = 7.54 \cdot 10^{-7} \pm 1.48 \cdot 10^{-7} + 4.53 \cdot 10^{-7} \cdot v^{1/2} \pm 1.28 \cdot 10^{-8} (V^{1/2} \text{ s}^{-1/2})$, $R^2 = 0.996$ (Figure 23).

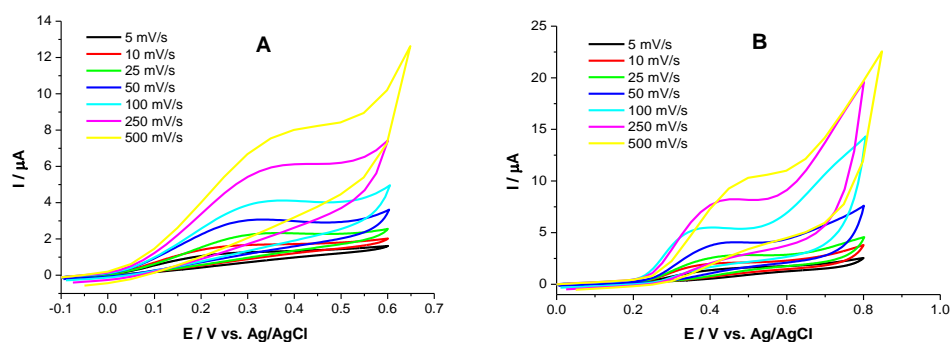


Fig. 23. CVs of 0.2 mmol L^{-1} ascorbic acid (A) and 0.2 mmol L^{-1} uric acid (B) at $1\% \beta\text{-CD/PEI}(5 \text{ mg mL}^{-1})/\text{GCE}$ at different scan rates: 5 (black); 10 (red); 25 (green); 50 (dark blue); 100 (light blue); 250 (purple); 500 mV s^{-1} (yellow)²⁶⁵

a) Interference study for 10^{-3} mol L⁻¹ uric acid with different concentrations of ascorbic acid

The interference between ascorbic and uric acids is the main problem in the electrochemical analysis of biological samples. In order to overcome this drawback and to separate the electrochemical signal of the two compounds in the same solution, GCEs modified with β -CD/PEI films in two concentrations were used. First time these modified electrodes were tested in solutions of a constant concentration in uric acid and at different concentrations of ascorbic acid (Figure 24). The results were compared with those obtained with other electrodes (bare GCE, PEI/GCE, β -CD/CPE). Voltammograms with the two separate peaks corresponding to these two analytes were obtained only with β -CD/PEI/GCEs²⁶⁴.

The peaks separation noticed on the GCEs modified with 1 % β -CD/PEI(5 mg mL⁻¹) films was greater than 0.42 V, namely for mixture 1 it was 0.422 V and grew up until 0.695 V for mixture 5 (Figure 24 A). The first peak, corresponding to ascorbic acid oxidation, grew linearly with the concentration in ascorbic acid ($I_p(\mu\text{A}) = 1.637 + 638.167 \cdot C_{\text{ascorbic acid}} (\text{mmol L}^{-1})$; $R^2 = 0.996$). The second peak attributed to uric acid which maintained the same concentration in all mixtures, remained almost constant (relative deviation for mixtures 2-5 was $\pm 2.38 \%$)²⁶⁴.

At 0.2 % β -CD/PEI(1 mg mL⁻¹)/GCE the peak potential separation is of more than 0.43 V: for mixture 2 the difference was 0.432 V and it reached 0.742 V in mixture 5 (Figure 24 B). The ascorbic acid peak height was not as large as at the 1 % β -CD/PEI(5 mg mL⁻¹)/GCE, the slope of the calibration line being 2.5 times smaller ($I_p(\mu\text{A}) = 1.464 + 256.173 \cdot C_{\text{ascorbic acid}} (\text{mmol L}^{-1})$; $R^2 = 0.994$). The uric acid peak remained almost constant only in the first 3 mixtures and then it raised, behavior which may be interpreted as follows: if the CD concentration is low and the ascorbic acid concentration is increased, ascorbic acid is forming more easily the complex with CD than the uric acid, then increasing concentrations of uric acid remain in solution and the uric acid, in its uncomplexed form, is detected by the electrode²⁶⁴.

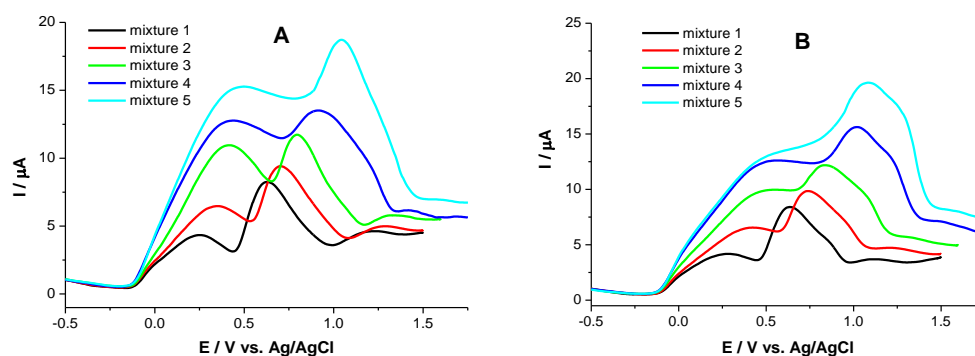


Fig. 24. SWVs recorded at 1 % β -CD/PEI(5 mg mL⁻¹)/GCE (A) and 0.2 % β -CD/PEI(1 mg mL⁻¹)/GCE (B) for 10^{-3} mol L⁻¹ uric acid with: 10^{-3} (black), $2 \cdot 10^{-3}$ (red), $4 \cdot 10^{-3}$ (green), $6 \cdot 10^{-3}$ (dark blue), and $8 \cdot 10^{-3}$ (light blue) mol L⁻¹ ascorbic acid²⁶⁴

Different sensors developed by other authors were able to discriminate between the voltammetric signals of ascorbic acid and uric acid, but most of them needed a laborious method of modification: carbon paste electrode with β -CD incorporated ($\Delta E = 0.376$ V)²³⁷; gold nanoparticles- β -cyclodextrin-graphene-modified electrode ($\Delta E = 0.324$ V)⁸⁴ and β -cyclodextrin modified copolymer of sulfanilic acid and *N*-acetylaniline on glassy carbon electrode ($\Delta E = 0.275$ V)²⁵⁷.

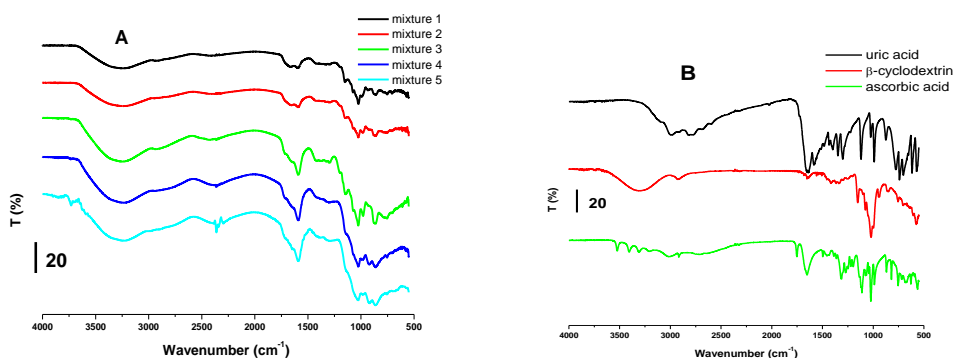


Fig. 25. (A) FTIR spectra for β -CD:uric acid: ascorbic acid mixtures in the following ratios: 1:1:1 (black), 1:1:2 (red), 1:1:4 (green), 1:1:6 (dark blue), 1:1:8 (light blue); **(B)** FTIR spectra for uric acid (black), β -CD (red), and ascorbic acid (green)²⁶⁴

The formation of inclusion complexes which were electrochemically analyzed before was also investigated by spectral method. From the FTIR spectra it can be observed that the growing concentration of ascorbic acid determined the growth of the band from 1590 cm^{-1} which was the shift of the uric acid peak from 1580 cm^{-1} (asymmetric deformation of NH_3) (Figure 25 B). A possible explanation could be the fact that ascorbic acid is preferentially allowed to enter the cavity of the CD leading to an increasing accumulation of uncomplexed uric acid. The bands of ascorbic acid molecules inside the cavity are screened, meanwhile the uric acid molecules which were left outside to the cavity (partially or totally), present bands which become stronger with the ascorbic acid increasing concentration (Figure 25 A)²⁶⁴.

b) Interference study for 10^{-3} M ascorbic acid with different concentrations of uric acid

The peak potential separation was 0.411 V for the first mixture, reaching 0.575 V for the fifth mixture when the solutions were analyzed at 1% β -CD/PEI (5 mg mL^{-1})/GCE. For the first three mixtures the current intensity of uric acid grew linearly ($I_p(\mu\text{A}) = 3.695 + 1275 \cdot C_{\text{uric acid}} (\text{mmol L}^{-1})$; $R^2 = 0.976$) (Figure 26 A). When the voltammograms were recorded at 0.2% β -CD/PEI (1 mg mL^{-1})/GCE, the difference in peaks potential was 0.457 mV for the second mixture and 0.611 mV for the last one. The increasing current intensity of uric acid was linear having the following equation: $I_p(\mu\text{A}) = 3.146 + 638.076 \cdot C_{\text{uric acid}} (\text{mmol L}^{-1})$; $R^2 = 0.992$ (Figure 26 B)²⁶⁴.

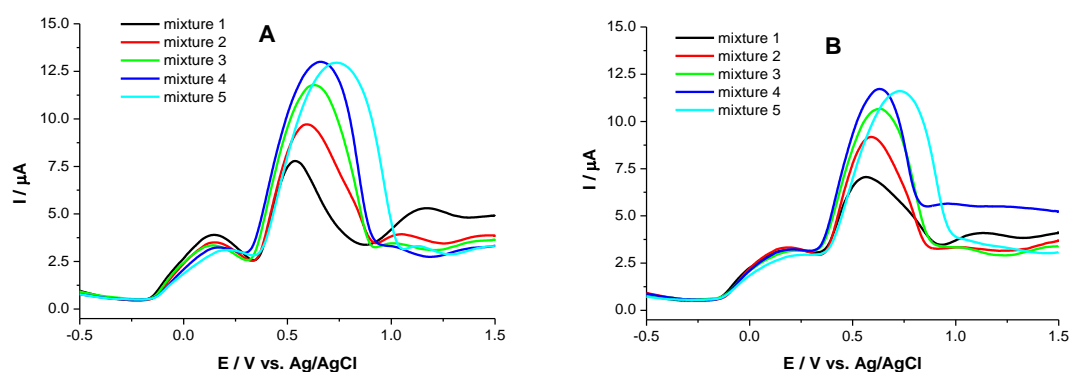


Fig. 26. SWVs recorded at 1 % β -CD/PEI(5 mg mL⁻¹)/GCE (A) and 0.2 % β -CD/PEI(1 mg mL⁻¹)/GCE (B) for 10⁻³ mol L⁻¹ ascorbic acid with: 10⁻³ (black), 2·10⁻³ (red), 4·10⁻³ (green), 6·10⁻³ (dark blue), and 8·10⁻³ (light blue) mol L⁻¹ uric acid²⁶⁴

In the FTIR spectra for the five complexes formed in the mixtures can be observed two bands (at 1600 cm⁻¹ and 1660 cm⁻¹) that were increasing gradually with the concentration of uric acid. The uric acid peaks from 1580 cm⁻¹ (asymmetric deformation of NH₃) and 1640 cm⁻¹ (C=O stretch) were shifted in the case of the complexes and appeared at 1600 cm⁻¹ and 1660 cm⁻¹ (Figure 27)²⁶⁴.

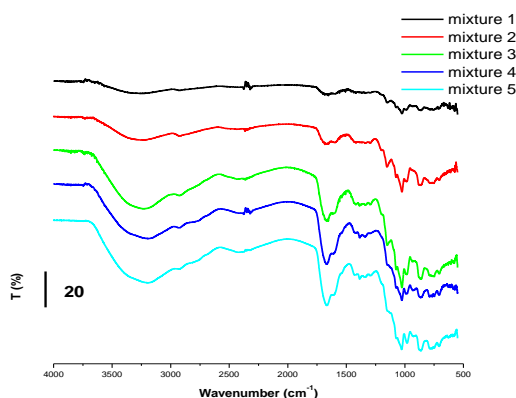


Fig. 27. FTIR spectra for β -CD: ascorbic acid: uric acid mixtures in the following ratios: 1:1:1 (black), 1:1:2 (red), 1:1:4 (green), 1:1:6 (dark blue), 1:1:8 (light blue)²⁵⁶

3.3.1.3. Microscopic images and RAMAN spectra of the modified electrode surface

The 5 mg mL⁻¹ PEI/GCEs and 1 % β -CD/PEI(5 mg mL⁻¹)/GCEs were characterized by using a confocal Raman microscope (Figure 28 A and B). The images reveal an obvious difference between the two types of modified electrodes due to the presence of β -CD. In the case of the electrode modified with 1 % β -CD/PEI(5 mg mL⁻¹) it can be observed that the β -CD structures were uniformly and homogeneously distributed in the PEI film²⁶⁴.

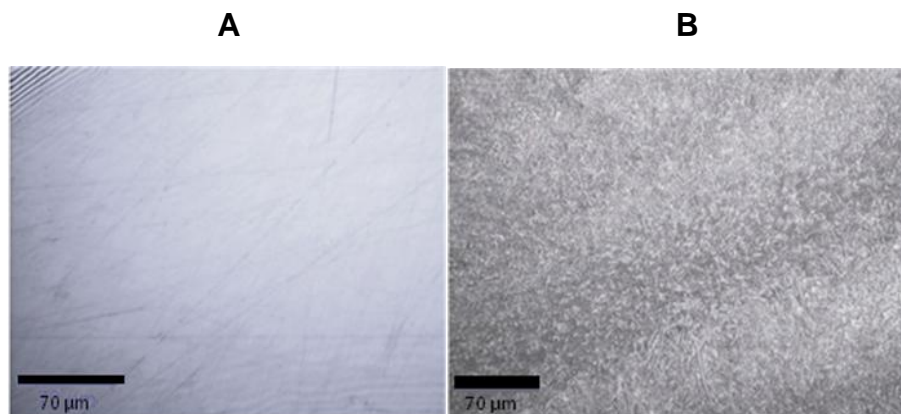


Fig. 28. Microscopic images for: **(A)** 5 mg mL⁻¹ PEI/GCE and **(B)** 1 % β -CD/PEI(5 mg mL⁻¹)/GCE²⁶⁴

The Raman spectra recorded before and after the modification of GCE by PEI film with or without β -CD are presented in Figure 29. The deposition of the PEI film on the GCE does not induce the appearance of a novel peak compared to the Raman spectrum of GCE (Figure 29 A), but the two sharp peaks recorded for glassy carbon at 1345 cm⁻¹ and 1597 cm⁻¹ are diminished indicating a complete coverage of the GCE surface by PEI film (Figure 29 B). The homogenous incorporation of β -CD inside the PEI film is clearly indicated by the intensity increase of its characteristic peaks⁴⁰⁻⁴² from 2906 cm⁻¹ to 2944 cm⁻¹ (Figure 29 E), while those related to GCE and PEI drastically decreased (Figure 29 C). In the case of β -CD/PEI/GCE (Figure 29 C) the signals are even weaker. The characteristic peaks of β -CD (Figure 29 E) between 0-1250 cm⁻¹ (C-H bending and C-O stretch) decreased and the region 3200-3400 cm⁻¹ (OH and H bonded stretches) is much flattened. The peaks of β -CD from 2906 cm⁻¹ and 2944 cm⁻¹ (ν C-H) are strongly diminished, but two shoulders still remain. The GCE peak from 2687 cm⁻¹ is the most reduced (Figure 29 A)^{265,267-269}.

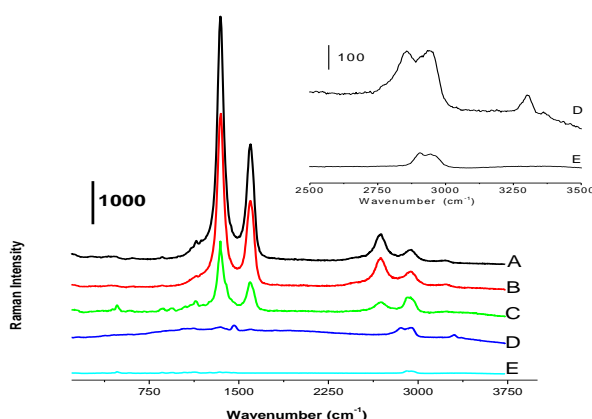


Fig. 29. RAMAN spectra of: bare GCE **(A)**, 5 mg mL⁻¹ PEI/GCE **(B)**, 1 % β -CD/PEI (5 mg mL⁻¹)/GCE **(C)**, PEI **(D)**, and β -CD **(E)**; (Inset: details of PEI **(D)** and β -CD **(E)** spectra)²⁶⁵

3.1.3.4. Electrochemical impedance spectroscopy analyses

The impedance spectroscopy determinations confirmed the modification of the electrode surface with β -CD/PEI. Figure 30 shows the Nyquist plots of bare and modified GCEs in the range 100 kHz to 10 mHz. An equivalent circuit was modeled for the bare and modified GCE in contact with the redox probe consisting in 10 mmol L⁻¹ K₃[Fe(CN)₆] and K₄[Fe(CN)₆] prepared in phosphate buffer (0.1 mol L⁻¹; pH 7.2). The circuit is: $R_{sol}(C_{dl}(R_{ct}[R_fW]))$, (see the inset of Figure 30), and contains the solution resistance (R_{sol}), the double layer capacitance (C_{dl}), the charge transfer resistance (R_{ct}), a resistance related to the diffusion process (R_f) and the Warburg impedance (W).

The Nyquist plots obtained for all types of electrodes show a semicircle portion at higher frequencies (lower Z values), corresponding to the electron transfer limited process, and a linear part in the lower frequency range (higher Z values) for the diffusion limited process. The semicircle diameter is related to charge transfer resistance. In the proposed equivalent circuit, C_{dl} with R_{ct} and with Warburg impedance (W) express the accessibility of ions within the porous structures and surface functionalities or polarization resistance. A series resistance (R_{sol}) is introduced in order to quantify the resistance of the electrolyte and the contact resistance of the current collector²⁷⁰⁻²⁷².

The EIS spectra showed that the bare GCE has the lowest conductivity, while the charge transfer resistance (R_{ct}) decreased in the case of the modified electrodes (Figure 30 A). For the bare GCE the value of R_{ct} is 922.3 Ω and it decreases at 112.5 Ω when PEI film covers the surface of the electrode (Figure 30 B). The sharp decreasing of the R_{ct} value in the case of the electrode modified with PEI can be explained by the positive charge of the polyethyleneimine which facilitates the negative charged species accumulation at the interface. In the case of β -CD/PEI/GCE an additional decrease of the R_{ct} to 95.1 Ω is observed, probably due to the fact that the β -CD presence disturbs the film homogeneity which becomes more permeable (Figure 30 C).

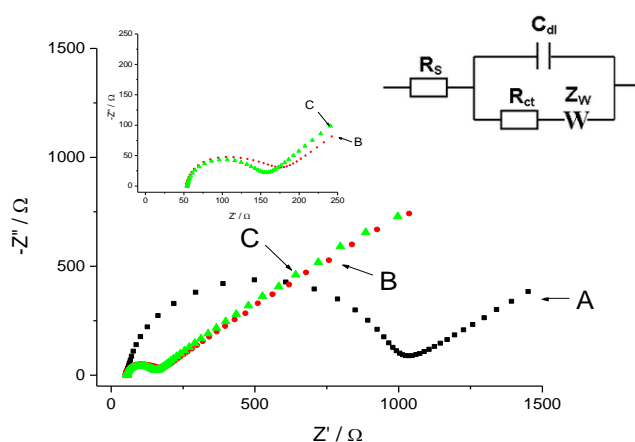


Fig. 30. Nyquist plots for 10 mmol L⁻¹ [Fe(CN)₆]³⁻/[Fe(CN)₆]⁴⁻ in 0.1 mol L⁻¹ PBS (pH 7.2) at: (A) bare GCE (black); (B) PEI/GCE (red); (C) β -CD/PEI/GCE (green); (61 frequencies, 100 kHz - 10 mHz; Amp. 0.01 V; (Inset: the equivalent circuit and the detail for PEI/GCE (red), β -CD/PEI/GCE (green)

3.3.2. Real samples analysis

3.3.2.1. Pharmaceutical samples analysis

The electrodes modified with β -CD/PEI were applied for the assay of ascorbic acid in two commercial drug formulations: oral solution Vitamina C[®] Biofarm (dietary supplement) and injectable solution Vitamina C[®] Arena.

The ascorbic acid injectable solution from Arena Group SA[®] contains in 1 vial of 5 mL: 750 mg vitamin C, NaOH, 3.75 mg sodium metabisulphite and water for injections. A study of electrochemical interference from sodium metabisulphite was initiated in the same ratio as in Vitamina C[®] Arena: 215.26 $\mu\text{mol L}^{-1}$ solution of ascorbic acid with 116 $\mu\text{mol L}^{-1}$ solution of sodium metabisulphite. We considered that the interference was negligible if the average signal for ascorbic acid in the presence of the interferent was altered by less than $\pm 5\%$ in comparison with the one for ascorbic acid alone²⁷³⁻²⁷⁵. In this case the sodium metabisulphite slightly influenced the ascorbic acid signal decreasing it with 2.61% (Figure 31 A), so its interference was negligible. This is the reason why the calibration curve was obtained using standard ascorbic acid without sodium metabisulphite. The calibration curve was determined by adding equal aliquots of ascorbic acid pro analysis (2.5 μL and 10.10 μL) obtaining the following equation for the calibration curve: $I_p(\mu\text{A}) = 0.035 + 0.007 \cdot C_{\text{ascorbic acid}} (\mu\text{mol L}^{-1})$; $R^2 = 0.999$ (Figure 31 B)²⁶⁴.

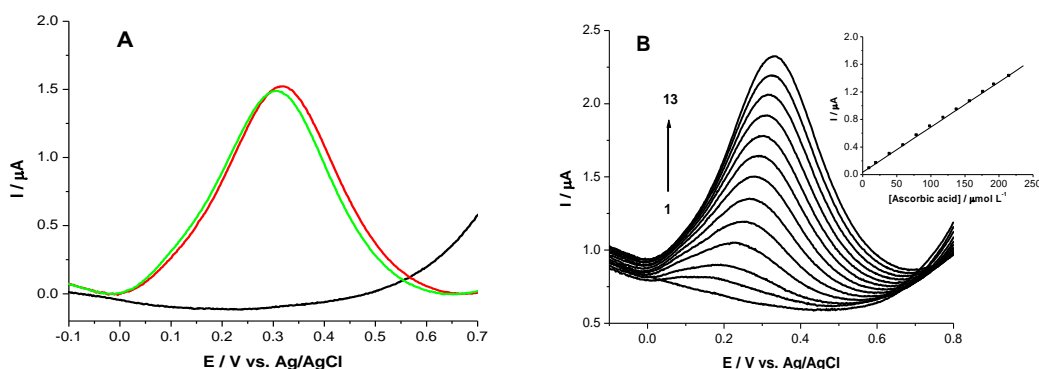


Fig. 31. (A) SWVs for 215.26 $\mu\text{mol L}^{-1}$ ascorbic acid solution without (red) and with 116 $\mu\text{mol L}^{-1}$ of sodium metabisulphite (green) compared with the blank (0.1 mol L^{-1} PBS; pH 7.2) (black); **(B)** SWVs for different concentrations of ascorbic acid: 0 (1), 9.99 (2), 19.96 (3), 39.84 (4), 59.64 (5), 79.36 (6), 99 (7), 118.5 (8), 138.06 (9), 157.48 (10), 176.81 (11), 193.07 (12) and 215.26 $\mu\text{mol L}^{-1}$ (13); (Inset: calibration curve)²⁶⁴

In Table VII are presented the recovery rates of the active substance in Vitamina C[®] Arena containing ascorbic acid which were between 98.25% and 101.02%²⁶⁴.

Table VII. Ascorbic acid determination in pharmaceuticals at β -CD/PEI/GCE by SWV²⁶⁴

Pharmaceutical product	Theoretical concentration ($\mu\text{mol L}^{-1}$)	Found concentration ($\mu\text{mol L}^{-1}$)	Recovery (%)	RSD (%)
Vitamina C[®](Arena)	157.48	154.72	98.25	1.41
	176.81	175.45	99.23	
	193.07	195.04	101.02	
Vitamina C[®](Biofarm)	157.48	156.01	99.06	1.02
	176.81	173.20	97.29	
	193.07	191.14	99.00	

In Romanian Pharmacopoeia the method specified for the dosage of ascorbic acid from the injectable solution is polarimetry. Ascorbic acid concentration calculated with this method gave a result of 95.3 % compared with the quantity declared by the manufacturer, in agreement with the imposed limits (± 5 % deviation)²⁷⁶.

Ascorbic acid from Vitamin C[®] oral solution (Biofarm) contains in one vial of 10 mL: 1000 mg vitamin C dissolved in 10 mL propylene glycol and water. Another calibration curve obtained in the presence of propylenglycol was used in this case because this cosolvent influenced the oxidation peak of ascorbic acid shifting it to a more negative potential with almost 0.04 V and increased the peak intensity with 1.87 % (Figure 32 A). The equation for the calibration curve was: $I_p(\mu\text{A}) = -0.031 + 0.008 \cdot C_{\text{ascorbic acid}} (\mu\text{mol L}^{-1})$; $R^2 = 0.999$ (Figure 32 B)²⁶⁴.

The recovery rates found were between 97.29 % and 99.06 % in good accordance with the Romanian Pharmacopoeia specification (± 5 % deviation) (Table VI)²⁷⁶.

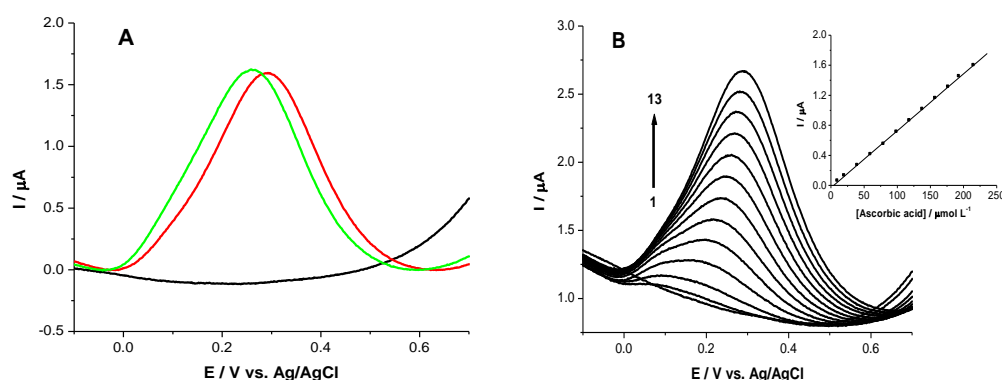


Fig. 32. (A) SWVs for $215.26 \mu\text{mol L}^{-1}$ ascorbic acid solution without (red) and with $215.26 \mu\text{mol L}^{-1}$ propylene glycol (green) compared with the blank (0.1 mol L^{-1} PBS; pH 7.2) (black); **(B)** SWVs for different concentrations of ascorbic acid: 0 (1), 9.99 (2), 19.96 (3), 39.84 (4), 59.64 (5), 79.36 (6), 99 (7), 118.5 (8), 138.06 (9), 157.48 (10), 176.81 (11), 193.07 (12) and $215.26 \mu\text{mol L}^{-1}$ (13) in the presence of propylene glycol; (Inset: calibration curve)²⁶⁴

This sensor presented a detection limit of $0.22 \mu\text{mol L}^{-1}$ ($S/N = 3$) over the concentration range of $9.99 - 215.26 \mu\text{mol L}^{-1}$ ²⁶⁴. The detection limit value is comparable with the lowest LOD reported in literature, being 50 times lower than other methods employing electrodes modified with CDs, Table VIII^{84,139,235,240-257}.

Table VIII. The β -CD/PEI/GCE sensitivity compared with previously reported sensors²⁶⁴

Analyte	Electrode/Method	Ascorbic acid LOD ($\mu\text{mol L}^{-1}$)	Ref.
ascorbic acid, uric acid, dopamine, tryptophan	GNP/PIlox/GCE ^a ; DPV	2.00	[240]
ascorbic acid, uric acid	GNP/LC/GCE ^b ; DPV	-	[241]
ascorbic acid, uric acid, dopamine	CDDA/GCE ^c ; DPV	1.43	[242]
ascorbic acid, uric acid, epinephrine	PCAC/GCE ^d	0.40	[243]
ascorbic acid, uric acid, dopamine	P-4-ABA/GCE ^e ; DPV	5.00	[244]
ascorbic acid, uric acid, dopamine	GRA/Pt/GCE ^f ; CV, DPV	-	[245]
ascorbic acid, uric acid, dopamine	NG/GCE ^g ; CV, DPV	2.20	[246]
ascorbic acid, uric acid, dopamine	GRA/SPE ^h ; CV, DPV	0.95	[247]
ascorbic acid, uric acid	GA/TC-GNP/Au ⁱ ; CV	-	[248]
ascorbic acid, uric acid, dopamine	PDDA-HCNTs/GCE ^j ; DPV	0.12	[235]
ascorbic acid, uric acid, dopamine	PS(III)/GCE ^l ; DPV	0.17	[249]
ascorbic acid, uric acid	OC/GCE ^m ; CV, amperometry	10	[251]
ascorbic acid, uric acid, dopamine	AuNPs- β -CD-Gra/GCE ⁿ ; SWV	10	[84]

ascorbic acid, dopamine	(PEDOT/S- β -CD) films/Au ^o ; CV, Amperometry, Hydrodynamic voltammetry	-	[256]
ascorbic acid, uric acid	β -CD/p-ASA+SPNAANI/GCE ^p	-	[257]
ascorbic acid, uric acid	β -CD/PEI/GCE; SWV	0.22	[254]

CV = cyclic voltammetry; SWV = square wave voltammetry; DPV = differential pulse voltammetry

^aGNP/PI/mox/GCE = gold nanoparticles/overoxidized-polyimidazole composite modified GCE

^bGNP/LC/GCE = gold nanoparticles and L-cysteine onto GCE

^cCDDA/GCE = poly(3-(5-chloro-2-hydroxyphenylazo)-4,5-dihydroxynaphthalene-2,7-disulfonic acid) film modified GCE

^dPCAC/GCE = poly(3,3'-bis[N,N-bis(carboxymethyl)aminomethyl]-o-cresolsulfonephthalein) modified GCE

^eP-4-ABA/GCE = poly(4-aminobutyric acid) modified GCE

^fGRA/Pt/GCE = graphene/Pt-modified GCE

^gNG/GCE = Nitrogen doped graphene/GCE

^hGRA/SPE = screen-printed electrode using an ink containing graphene

ⁱGA/TC-GNP/Au = guanine/thiocyosine-gold nanoparticles/Au

^jPDDA-HCNTs/GCE = poly(diallyl dimethylammonium chloride functionalised helical CNTs onto GCE

^kPS(III)/GCE = poly(sulfonazo III) modified GCE

^mOC/GCE = organoclay film modified GCE

ⁿAuNPs- β -CD-Gra/GCE = Graphene decorated with gold nanoparticles and β -CD onto GCE

^o(PEDOT/S- β -CD)films/Au = Poly(3,4-ethylene dioxythiophene)/sulphated β -CD films, deposited onto gold

^p β -CD/p-ASA+SPNAANI/GCE = β -CD modified copolymer membrane of sulfanilic acid and N-acetylaniline onto GCE

Spectrophotometric studies at 266 nm (the characteristic ascorbic acid wavelength) were done in order to compare the electroanalytical results obtained for ascorbic acid solutions (standard and obtained with the investigated pharmaceutical Vitamina C[®] Arena). The calibration curve in the range 1 - 100 $\mu\text{mol L}^{-1}$ had the following equation: $A = 0.151 + 0.145 (R^2 = 0.994; \text{RSD} = 2.22 \%)$. The recovery rates for the pharmaceutical samples were between 100.23 % and 103.89 %, RSD = 3.21 %, results which were in good agreement with those obtained by the electrochemical method²⁶⁴. The UV-Vis method for the determination of the ascorbic acid in solution is the standard method recommended also by European Pharmacopoeia and used by the pharmaceutical companies²⁷⁷.

3.3.2.2. Real samples analysis

Ascorbic acid presents a characteristic pharmacokinetic feature: it is eliminated by kidney filtration predominantly unchanged and another part as metabolites, especially as oxalic acid²⁷⁸.

The β -CD/PEI/GCE based sensor was applied for urine samples monitoring during the ascorbic acid treatment for 7 days. Real samples were analysed in order to quantify the ascorbic and uric acids. In Figure 33 it can be noticed that

before the treatment with ascorbic acid there is a lack of any electrochemical signal for ascorbic acid at β -CD/PEI/GCE. The performance of this sensor consisting in simultaneous detection of ascorbic acid and uric acid due to the obvious anodic peak separation of the two studied substances ($\Delta E = 0.22$ V) permitted their quantification. The SWVs of the diluted urine samples showed a continuous increase in ascorbic acid concentration until the fifth day²⁶⁵.

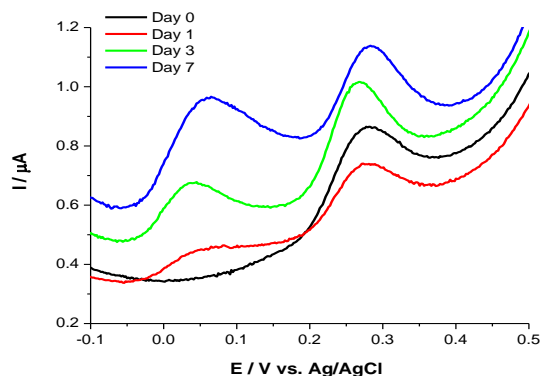


Fig. 33. SWVs of the diluted urine samples collected before (day 0) and during the treatment with ascorbic acid at 1 % β -CD/PEI(5 mg mL⁻¹)/GCE²⁶⁵

The addition of increasing concentrations of ascorbic acid induces the proportional increase of the corresponding oxidation peak (Figure 34).

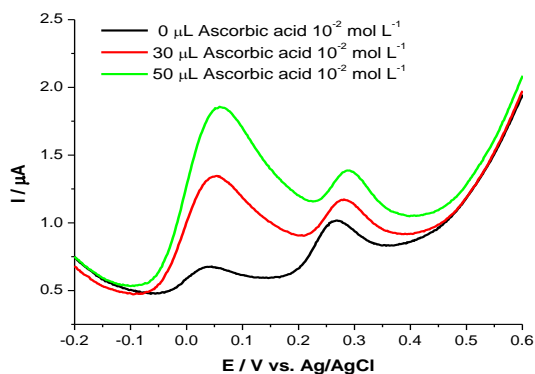


Fig. 34. SWVs of the diluted urine sample collected in the third day, spiked with ascorbic acid at 1 % β -CD/PEI(5 mg mL⁻¹)/GCE

The concentrations of ascorbic acid and uric acid in the diluted urine samples in PBS 0.1 mol L⁻¹, pH 7.2 were calculated using the following equations: $I_p(\mu A) = 0.007 \cdot C_{\text{ascorbic acid}} (\mu\text{mol L}^{-1}) + 0.035$; ($R^2 = 0.999$); $I_p(\mu A) = 0.008 \cdot C_{\text{uric acid}} (\mu\text{mol L}^{-1}) + 0.097$, ($R^2 = 0.994$), respectively (Table IX).

Table IX. Ascorbic and uric acids data recorded at 1% β -CD/PEI(5 mg mL⁻¹)/GCE by SWV in diluted urine samples²⁶⁵

Urine sample	Detected analyte concentration ($\mu\text{mol L}^{-1}$)		RSD (%)	
	Ascorbic Acid	Uric Acid	Ascorbic Acid	Uric Acid
Day 0	0.00	18.99	-	2.55
Day 1	2.07	9.11	2.58	1.06
Day 2	15.83	0.60	3.06	2.61
Day 3	16.55	22.68	4.02	2.29
Day 4	33.86	28.45	2.65	3.57
Day 5	41.52	15.11	2.06	2.83
Day 6	26.60	20.36	1.84	2.74
Day 7	39.07	17.02	2.44	3.45

The real samples were spiked with 30 μL and 50 μL of 10^{-2} mol L⁻¹ ascorbic acid solution and then, taking into account the initial detected concentration, the total values were calculated. The recovery of the ascorbic acid in urine samples was between 95.45 % and 103.67 % (Table X)²⁶⁵.

Table X. Ascorbic acid data recorded at 1% β -CD/PEI(5 mg mL⁻¹)/GCE by SWV in urine samples²⁶⁵

Urine sample	Ascorbic acid initially detected ($\mu\text{mol L}^{-1}$)	Added 10^{-2} mol L ⁻¹ ascorbic acid solution (μL)	Added ascorbic acid ($\mu\text{mol L}^{-1}$)	Total ascorbic acid found ($\mu\text{mol L}^{-1}$)	Recovery ascorbic acid (%)
Day 1	2.07	30	59.64	59.76	96.73
		50	99.00	100.04	98.95
Day 4	33.86	30	59.64	95.69	103.67
		50	99.00	131.49	98.61
Day 6	26.6	30	59.64	86.73	100.82
		50	99.00	121.1	95.45

The diluted urine samples were also analyzed using reverse phase high performance liquid chromatography with ultraviolet spectroscopy detection. In the optimized conditions, the retention time for ascorbic acid (standard substance) was 2.5 minutes and for uric acid 4 minutes. The identification of the peaks in the real samples was made by comparing the retention times with those corresponding to the pure substances which were spiked to the urine sample. We were able to trace the following calibration curves for the two compounds: Area = 31341 · C_{ascorbic acid} ($\mu\text{mol L}^{-1}$) + 2452.1; ($R^2 = 0.998$); Area = 208039 · C_{uric acid} ($\mu\text{mol L}^{-1}$) + 11791; ($R^2 = 0.999$), in a linear range between 1.4 - 50 $\mu\text{mol L}^{-1}$.

These equations were used to determine the concentrations of ascorbic acid and uric acid in urine samples. The recovery rates obtained for ascorbic acid were $97.66 \pm 1.5 \%$ and for uric acid $100.17 \pm 0.31 \%$. The results of the electrochemical measurements for ascorbic acid and uric acid were in good agreement with those obtained by the chromatographic method²⁶⁵.

3.4. Conclusions

The glassy carbon electrodes modified with β -cyclodextrin in polyethyleneimine film were elaborated for the investigation of the electrochemical behavior of ascorbic acid and uric acid. This sensor allowed the separation of the voltammetric signals and the shifting to more negative of the oxidation peaks potential for the two compounds. The intensity of the oxidation peak for ascorbic acid increased linearly with its concentration at constant concentration of uric acid. When the concentration of the ascorbic acid was constant, the intensity of the oxidation peak for uric acid increased linearly with its concentration. An important performance of this sensor is the simultaneous determination of ascorbic acid and uric acid due to the well separation of signals corresponding to the electrochemical oxidation processes of these compounds.

The electrochemical behavior of ascorbic acid and uric acid in solution was also explained by FTIR measurements. The increasing concentration of ascorbic acid resulted in a growth of the band corresponding to the asymmetric deformation of N-H in uric acid. This behavior is probable due to the fact that ascorbic acid was "preferentially" incorporated into β -CD cavity forming an inclusion complex, while the uric acid concentration increased in solution.

These modified electrodes were applied for the detection and dosage of ascorbic acid in two pharmaceutical products with reliable performance: low detection limit, good linear range, the absence of interferences in the case of injectable solution. Taking advantage of the privileged permeation of ascorbic acid and uric acid through the β -CD and PEI film, via the host-guest interaction between β -CD and ascorbic and uric acids, the simultaneous detection of the two compounds from urine samples was successfully achieved. The sensor main advantage of clearly distinguishing binary mixtures of ascorbic acid and uric acid, allowed their simultaneous determination in real samples. Good recoveries were obtained using electrochemical methods which were confirmed by using spectrophotometric method in the case of the pharmaceutical samples and chromatographic method for the urine samples.

4. Novel biosensors for dopamine detection based on GCEs modified with tyrosinase/ β -cyclodextrin/ reduced graphene oxide composite

4.1. Introduction

Graphene, a two-dimensional carbon-based nanomaterial, has attracted tremendous interest in recent years. Its unique features, such as: exceptional thermal and mechanical properties, high specific surface area and excellent electrochemically catalytic activity, generated their broad use in electrochemical sensing and biosensing^{113,279,280}.

They can be obtained by covalent functionalization (by using diazonium salts, dienophile compounds, 1-ethyl-3-(3-dimethylaminopropyl) carbodiimide (EDC) or *N,N'*-dicyclohexylcarbodiimide (DCC) and *N*-hydroxysuccinimide (NHS), heteroatom doping (N_2 , B)), and by non-covalent functionalization (π - π stacking, hydrophilic and hydrophobic interactions). Because of its interesting properties, graphene has been used as a transducer in bio-FETs, electrochemical biosensors, impedance biosensors, electrochemiluminescence and fluorescence biosensors, as well as biomolecular labels. The applications of graphene in (bio)sensing are based on electrodes modified with graphene powder or graphene-composite electrodes. Similar to CNTs, graphene is a biocompatible nanomaterial, it does not contain metallic impurities, and its production needs graphite (which is cheap and accessible)^{113,119-122}.

A challenging aspect in this area is the elaboration of hybrid electrodes based on the combination of graphene and conductive polymers leading to the design of novel nanocomposites with (bio)sensing properties. Up to now, electropolymerizable CNT-modified monomers were synthesized by using covalent and non-covalent functionalization with pyrrole derivatives such as: pyrrole alcohol, pyrene-pyrrole and metallopolymers based on polypyridinyl ruthenium (II)^{281,282}.

Dopamine is an important neurotransmitter being related to several diseases such as schizophrenia, Parkinson's disease and Huntington's disease. Update, many electrochemical sensors were elaborated for dopamine detection. Many other biological molecules, normally found in biological samples, such as ascorbic and uric acids, glucose, etc. interfere in the accurate determination of dopamine^{283,284}.

Many types of modifiers such as Nafion, organic redox mediators, nanoparticles, polymers, self-assembled monolayers, and carbon nanotubes were used to modify the electrodes for dopamine detection²⁸³⁻²⁹².

In the last years, the electrodes modified with graphene and cyclodextrins have been widely employed for the detection of dopamine, alone or in the presence of various interferents^{84,145,283,293-299}.

In order to improve the thermal, mechanical and electrical properties, the graphene oxide (GO) was reduced with ascorbic acid, by a simple *green chemistry method*, avoiding thus the environmentally harmful reducing agents¹⁴⁶.

The GCE was modified with reduced graphene oxide (RGO), β -CD and polyethylenimine (PEI) by using layer by layer method (LBL). The obtained nanocomposite was then characterized by Raman and FTIR spectroscopy and optical microscopy. The electrochemical behavior of dopamine was investigated by electrochemical methods with a series of modified electrodes during the optimization process and the best results were obtained with the GCE modified with single layers of RGO, β -CD and PEI. This nanoplatform was used to immobilize tyrosinase obtaining a biosensor applied for the dopamine determination in pharmaceutical products, serum and urine samples with good recoveries, enhanced sensitivity (LOD of 3.9 $\mu\text{mol L}^{-1}$) and good selectivity (tested in the presence of glucose, ascorbic and uric acids)^{300,301}.

A new non-covalent modification of RGO was obtained by using a new synthesized pyrrole derivate bearing a β -CD moiety which led to a non-destructive functionalization method: β -CD is involved in a better solubilization of graphene in aqueous medium as an efficient aqueous dispersant³⁰² and pyrrole is responsible for generating an electropolymerized coating, both aspects being important for the graphene electrodeposition. This new nanocomposite was characterized by spectral, microscopic and electrochemical techniques. Moreover, this functionalized graphene was used in combination with an amphiphilic pyrrole derivative and tyrosinase for catechol and dopamine determination³⁰³.

4.2. Experimental

4.2.1. Synthesis

[12-(pyrrol-1-yl) dodecyl] triethylammonium tetrafluoroborate (amphiphilic pyrrole) and *N*-succinimide-11-pyrrolyl-1-undecyl carboxylic acid ester (NHS-pyrrole) were synthesized according to Cosnier *et al.*^{80,304}.

Synthesis of: β -cyclodextrin-11-pyrrolyl-1-undecyl carboxylic acid amide (Py-CD): The NHS-pyrrole (90 mg, 0.26 mmol L^{-1}) was dissolved in 5 mL of DMF. 1-adamantylamine (370 mg, 0.32 mmol L^{-1}) and an excess of tetraethylamine (150 mg, 1.5 mmol L^{-1}) were added and the resulting mixture was stirred overnight at 80 °C. The crude solution was evaporated to dryness and the residue was washed with water and Et_2O . 330 mg (0.24 mmol L^{-1}) of a white powder was obtained in 92 % yield³⁰³.

¹H NMR: $\delta\text{H/ppm}$ (400 MHz, DMSO): 1.3-1.5 (m, 16H), 1.66 (t, $j = 6.4\text{Hz}$, 2H), 2.07 (t, $J = 7.2\text{Hz}$, 2H), 3.30 (m, 12H), 3.55(m, 28H),), 3.63 (t, $j = 6.4\text{Hz}$, 2H), 4.42

(m, 7H), 4.82 (m, 7H), 5.64-5.70 (m, 14H), 5.92 (s, 2H), 1.44 (m, 2H), 6.71 (s, 2H), 7.55 (m, 1H)³⁰³.

MS (ESI+): 1367.5+ (M+)

4.2.2. Reagents and solutions

β -CD was purchased from Merck and graphene oxide, tyrosinase, normal human serum and dopamine hydrochloride from Sigma Aldrich. Phosphate buffer solutions were prepared with sodium dihydrogen phosphate, sodium monohydrogen phosphate from Sigma (pH 7.2; pH 6.5; 0.1 mol L⁻¹). All aqueous solutions were prepared with ultrapure water (MilliQ Barnstead EASY pureRodi). All the measurements were performed at room temperature.

The RGO modified with β -CD (RGO-CD) was prepared as follows: 30 mg graphene oxide was dispersed in 60 mL water and were sonicated for 2 hours, 60 mL of β -CD solution (4 mg mL⁻¹) was then added and stirred together for 30 minutes. Then 600 mg of ascorbic acid was dissolved and the final suspension was stirred for 48 hours. The preparation of the unmodified RGO was similar to the procedure mentioned above without the addition of β -CD^{146,300,301,305}.

The suspension was centrifuged and washed with ultrapure water for the removal of ascorbic acid. The RGO powder was dried in oven and suspended in water (1 mg mL⁻¹). The suspension was sonicated for 1 hour before its use for the electrode modification. The 1 mg mL⁻¹ β -CD and 1 mg mL⁻¹ tyrosinase solutions were prepared with ultrapure water, while 1 mg mL⁻¹ PEI solution was prepared in water:ethanol (1:1) mixture^{300,301}.

For preparing RGO/Py-CD solution, 1 mg mL⁻¹ RGO and 1 mmol L⁻¹ Py-CD were sonicated together for 3 hours in water to give a stable black solution. For preparing amphiphilic pyrrole/tyrosinase solution, 10 mg mL⁻¹ enzyme was dissolved in 3 mmol L⁻¹ amphiphilic pyrrole aqueous solution³⁰³.

4.2.3. Biosensor preparation

GCEs (d = 3 mm) were purchased from BASInc. (Lafayette, USA) and were polished using 2 μ m diamond paste and then washed successively with water and ethanol. The electrode modification was carried out by LBL deposition of the different modifiers. Thus, two successive layers of 5 μ L of 1 mg mL⁻¹ RGO, 5 μ L of 1 mg mL⁻¹ β -CD, each of them followed by solvent evaporation in the oven at 40 °C for 10 - 15 minutes, were dropped onto the electrode surface. After that, 5 μ L of 1 mg mL⁻¹ tyrosinase and 5 μ L of 1 mg mL⁻¹ PEI were dropped and dried at room temperature. Different configurations of bioelectrode materials were elaborated by varying the numbers of 5 μ L RGO and tyrosinase layers^{300,301}.

The GCEs were prepared by drop casting 5 μ L of RGO/Py-CD aqueous suspension, dried under vacuum and then electropolymerized by controlled potential electrolysis (0.85 V, 5 min) in 0.1 mol L⁻¹ LiClO₄/ACN. A defined amount of

tyrosinase/ amphiphilic pyrrole aqueous solution (containing 0.3 mg of enzyme) with and without RGO/Py-CD was spread on the electrode surface and dried under vacuum. The adsorbed coating was then electropolymerized by controlled potential electrolysis for 20 min at 0.85 V in 0.1 mol L⁻¹ LiClO₄/H₂O³⁰³.

4.2.4. Electrochemical, spectral and microscopic analysis

Electrochemical measurements were carried out with an Autolab PGSTAT100 potentiostat (Metrohm/Eco Chemie Netherlands) controlled by Nova 1.10.4 software using a three-electrode cell with GCE as working electrode, Ag/AgCl and SCE as reference electrodes and a platinum wire as the counter electrode^{300,301}.

The optimized parameters for SWV are: frequency 25 Hz, amplitude 25 mV, initial potential -0.3 V, end potential 1 V. The amperometric determinations were made at -0.2 V stirring the solution with 200 rpm. Electrochemical impedance spectroscopy (EIS) measurements were carried out in the presence of 10 mmol L⁻¹ [Fe(CN)₆]^{3-/4-} in PBS (10 mmol L⁻¹, pH 7.4) as redox probe. The impedance was measured in a frequency range from 100 mHz to 100 KHz using the open circuit potential (OCP) and the experimental data were fitted with proper equivalent circuits using Nova 1.10.4 software^{300,301}.

The Raman spectra of the modified electrodes were acquired with Alpha 300R (WiTec) confocal Raman microscope, at 532 nm for laser and 60 seconds time accumulation and using a WiTec Control software for data interpretation (1000 - 3600 cm⁻¹, resolution > 0.5 cm⁻¹). The microscopic images were obtained with the same microscope³⁰¹.

The FTIR spectra of the GO and RGO were recorded with Jasco FT/IR-4100 spectrophotometer (Jasco) equipped with Jasco Spectra Manager Version 2 software in the wave number range from 550 to 4000 cm⁻¹³⁰¹. The FTIR spectra of Py-CD, Py-CD/RGO were recorded with a Thermo Scientific Nicolet iS10 in the wave number range from 650 to 4000 cm⁻¹. TEM images were recorded using a Philips CM200 microscope operating at an accelerating voltage of 200 kV³⁰³.

4.2.4. Real samples preparation

The solution from 10 vials of solution for injection of dopamine hydrochloride 0.5 % (Zentiva, Romania) was mixed together for homogenization and then were diluted to obtain a 10⁻² mol L⁻¹ stock solution by adding an appropriate volume of PBS (pH 7.2, 0.1 mol L⁻¹). The stock solutions were prepared daily and maintained in the dark, protected from light, at 4 °C to avoid dopamine oxidation. In order to quantify the dopamine hydrochloride concentration from the pharmaceutical samples, calibration curve was obtained using standard dopamine hydrochloride substance³⁰¹.

The urine was collected from a healthy patient and was filtered (paper filter FILTRAK 390) before analysis, then diluted 1:100 with phosphate buffer (0.1 mol L⁻¹, pH 7.2). The human serum was prepared as follows: the lyophilized powder was

dissolved in 2 mL of distilled water resulting 60 mg mL⁻¹ of proteins and then diluted 1:100 with phosphate buffer (0.1 mol L⁻¹, pH 7.2)³⁰¹.

4.3. Results and discussions

4.3.1. β -cyclodextrin/reduced graphene oxide biosensor

4.3.1.1. Spectral and microscopic characterization

In accordance with recent scientific papers³⁰⁶, the Raman spectra of GO revealed three characteristic bands: two strong bands close to 1353 cm⁻¹ (D band) and 1598 cm⁻¹ (G band), and a weaker one in the region 2500 - 3000 cm⁻¹ (2D band) (Figure 35 A). The reduction of oxygen containing groups from GO sheets may be responsible for the pronounced decreasing of D, G and 2D characteristic bands intensity in the Raman spectra of RGO/CD and RGO-CD, due to the restoration of the *sp*² graphene structure after the reduction reaction^{145,307}.

Taking into consideration the GO FTIR spectra, some specific signals, corresponding to different functional groups: 1001 cm⁻¹ u(C-O), 1174 cm⁻¹ u(C-O, carboxyl, ethers, alcohols), 1507 cm⁻¹ u(C-C, aromatics), 1656 cm⁻¹ u(C=C) and 1750 cm⁻¹ u(C=O, carboxyl), also reported by other authors, can be observed^{306,308-310}.

In the FTIR spectrum of the RGO the bands at 2908 and 2990 cm⁻¹ u(C-H) presents weaker intensities due to the disappearance of C-H bonds during the aromatization of the graphene core. The characteristic bands for oxygen containing groups (3500 - 3900 cm⁻¹), from the GO spectrum are diminished indicating that those groups were partially eliminated by reduction process^{311,312}. All the modifications observed in the FTIR spectra of RGO and RGO-CD reveal that the GO sheets were successfully reduced (Figure 35 B).

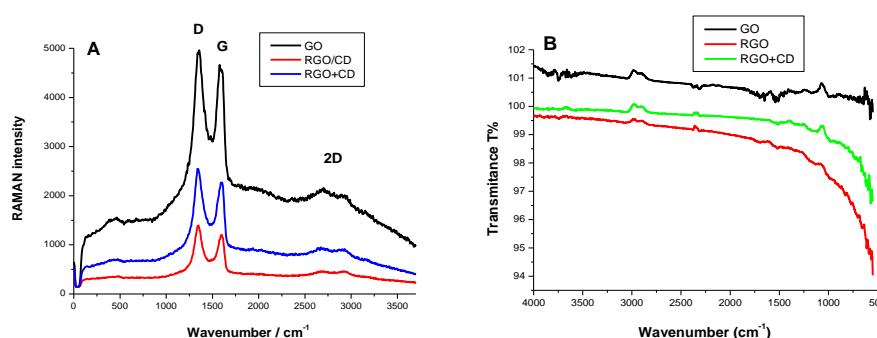


Fig. 35. Raman spectra (A) registered for: GO (black), RGO/CD (red), RGO-CD (blue) and FTIR spectra (B) registered for: GO (black), RGO (red), RGO-CD (green)³⁰¹

The electrodes modified with thin films of GO, RGO/CD and RGO-CD on PEDOT were characterized with a confocal Raman microscope (Figure 36). It can be observed the difference between the two types of modified electrodes due to the presence of RGO. In the case of the electrode modified with RGO, the graphene structure was more distinguishable covering the electrode surface (Figure 36 B).

On the electrode modified with RGO-CD, the graphene sheets were more homogeneously distributed over the electrode surface (Figure 36 C)³⁰¹.

The PEDOT substrate was used for Raman and optical microscopic characterization in order to avoid the superposition of the characteristic signals given by GCE and graphene at the same wavenumber value.

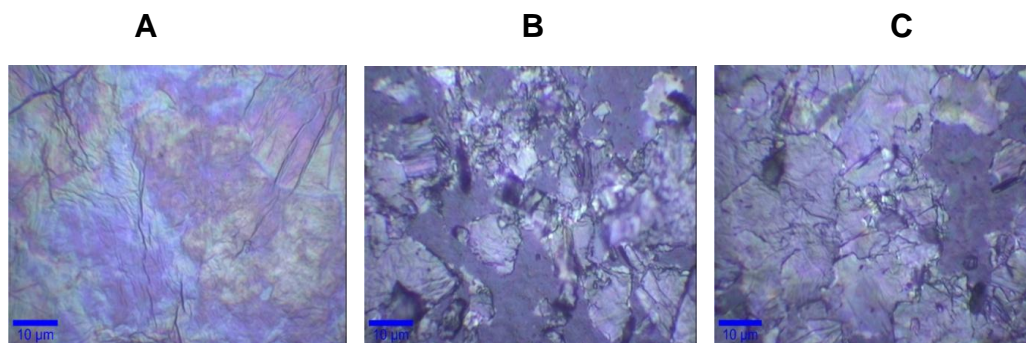


Fig. 36. Microscopic images for: (A) GO/PEDOT, (B) RGO/CD/PEDOT and (C) RGO-CD/PEDOT³⁰¹

4.3.1.2. Electrochemical characterization of the nanostructured electrode material

The influence of different types of graphene: RGO, RGO modified with β -CD (RGO-CD) and RGO covered with a β -CD layer (RGO/CD), on the voltammetric response of dopamine was investigated. LBL method was chosen because the current intensity of dopamine peak was 4.5 times bigger in comparison with the spin coating method of deposition. The best sensitivity to dopamine electrooxidation was recorded with the configuration consisting in single layers of RGO/CD and PEI (RGO/CD/PEI), respectively (Figure 37 A)³⁰¹. Comparing the RGO and the RGO/CD, it can be observed that the oxidation potential is slightly shifted towards cathodic values due to the cavity of β -CD which facilitate the dopamine oxidation, and the peak area is smaller because the graphene proportion is smaller in the β -CD/graphene nanocomposite¹⁴⁵.

The effect of the number of RGO layers deposited on GCE towards dopamine oxidation current intensity was also examined. It appears that increasing the number of RGO layers, the height and area of the oxidation peak decreased, while the potential was slightly shifted towards more anodic potential (Table XI). This behavior may be due to a possible compaction of the graphene structure with the increasing deposited amount of graphene, slowing thus the electron transfer process. The most sensitive configuration for the direct determination without any preconcentration time is based on single layer of RGO (Figure 37 B)³⁰¹. For three and five graphene layers, the intensity of the oxidation signal is higher after the accumulation at open circuit during 1 minute, indicating that the penetration of dopamine through the graphene layers is hindered.

Table XI. SWV data for dopamine registered at GCE modified with different numbers of RGO layers³⁰¹

Electrochemical parameters	RGO layers number			
	0	1	3	5
Oxidation potential	0.213	0.195	0.219	0.241
Peak height (μA)	92.37	508.19	174.10	87.58
Peak area (μC)	25.35	95.14	22.74	10.02

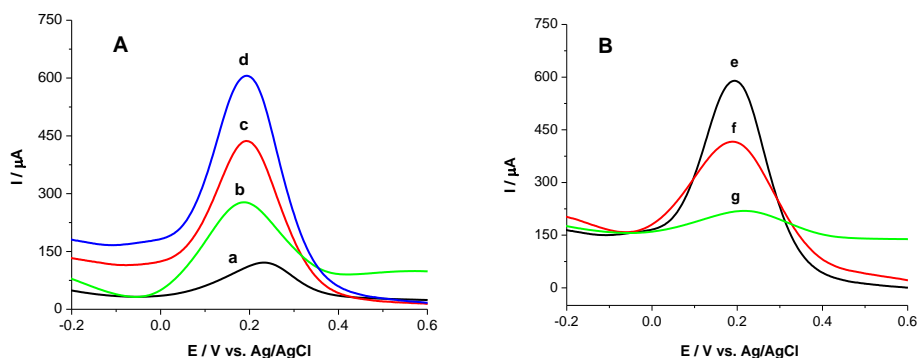


Fig. 37. (A) SWVs for 10^{-3} mol L^{-1} dopamine solution obtained at: (a) bare GCE; (b) single layers RGO-CD/PEI modified GCE; (c) single layers RGO/PEI modified GCE; (d) single layers of RGO/CD/PEI modified GCE; (B) SWVs for 10^{-3} mol L^{-1} dopamine solution at single layer RGO modified GCE after (e) 0 min, (f) 1 min and (g) 5 min of preconcentration³⁰¹

4.3.1.3. Electrochemical performance of the biosensor

The biosensor was assembled by depositing successive layers of RGO, β -CD and tyrosinase entrapped in polymeric film onto GCE (PEI/TYR/ β -CD/RGO/GCE), (Figure 38)³⁰¹.

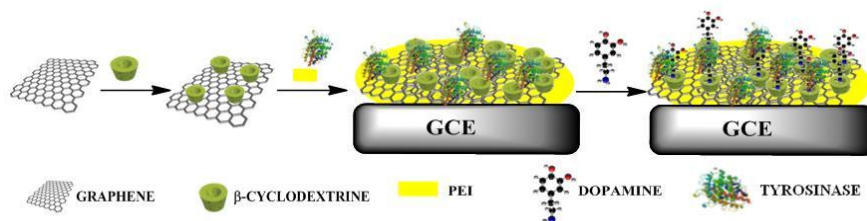


Fig. 38. The biosensor development for dopamine detection³⁰¹

Taking into account that the quantity of enzyme immobilized at the surface influences the amperometric performance of the biosensor, different amounts of tyrosinase (15, 25 and 50 μg) were tested, the optimum configuration being obtained with 50 μg of tyrosinase (above this quantity the amperometric response is not significantly increased). The enzyme layer was finally covered by a PEI film in order to avoid the enzyme detachment during the amperometric analysis under stirring.

In addition, hydrophobic residues of appropriate size of the tyrosinase shell can lead to host-guest interactions with the β -CD groups reinforcing its adsorption onto the graphene layer³⁰¹.

The biosensor elaboration process was studied using electrochemical impedance spectroscopy. Each step was followed by the variation of the charge transfer resistance (R_{ct}) represented in the Nyquist plots (Figure 39 A). The β -CD presence determined the increase of the R_{ct} , while RGO layer increased the sensor conductivity (Figure 39 B)³⁰⁰.

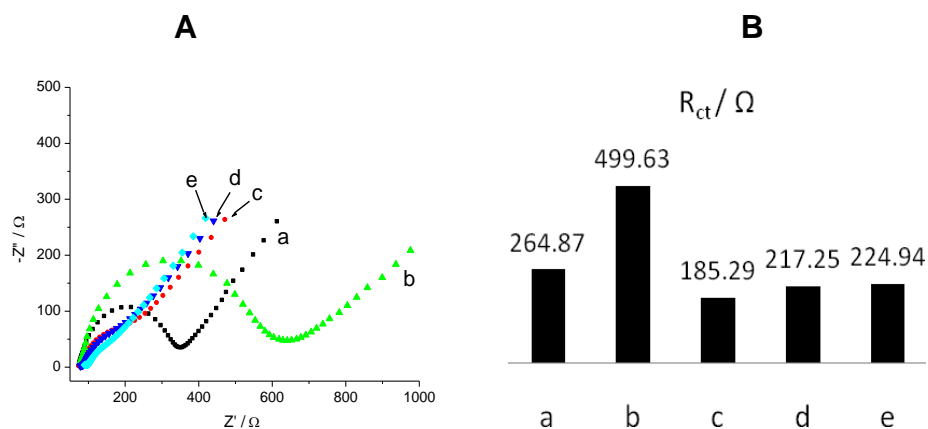


Fig. 39. (A) Nyquist plots of 10 mmol L⁻¹ [Fe(CN)₆]^{3-/4-} in PBS (0.02 mol L⁻¹; pH 7.4); **(B)** R_{ct} variation for: (a) bare GCE; (b) 1 mg mL⁻¹ β -CD/GCE; (c) 1 mg mL⁻¹ RGO/GCE; (d) β -CD/RGO/GCE and (e) PEI/TYR/ β -CD/RGO/GCE

The proposed circuit for GCE and β -CD/GCE is a Randles type one: $R_{sol}(C_{dl}[R_{ct}W])$. R_{sol} represents the electrolyte resistance followed by the double-layer capacitance C_{dl} , charge transfer resistance R_{ct} and impedance of a faradaic reaction W . In the presence of RGO layer the equivalent circuit changed to a Voight type one: $R_{sol}(R_{ref}C_{ref})(R_{ads}C_{ads})(C_{dl}[R_{ct}W])$, circuit which includes components referring to the contribution of the external reference electrode (R_{ref} and C_{ref}) and to the adsorption process (C_{ads} and R_{ads}) that may occur to the electrode surface^{271,313}.

The performance of the elaborated biosensor for the detection of dopamine in pharmaceutical and biological samples was examined by potentiostating the modified electrode at -0.2 V. Figure 40 shows the resulting calibration curve exhibiting a linear part ranging from 3.9 to 328.8 μ mol L⁻¹ ($I_p(\mu A) = 0.0121 \cdot C_{dopamine}(\mu mol L^{-1})$; $R^2 = 0.999$), with a LOD of 3.9 μ mol L⁻¹ and a sensitivity of $12.1 \cdot 10^{-3} A L mol^{-1}$. In the absence of β -CD, the LOD is markedly increased, namely 12.74 μ mol L⁻¹, highlighting the sensitivity improvement conferred by the presence of the β -CD³⁰¹.

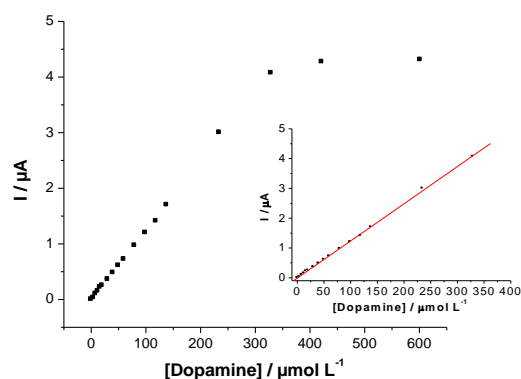


Fig. 40. Calibration data for different concentrations (from 3.9 to 601.5 $\mu\text{mol L}^{-1}$) of dopamine solutions obtained with PEI/TYR/ β -CD/RGO/GCE; (Inset: linear part of the calibration curve obtained for dopamine with amperometry)³⁰¹

4.3.1.4. Analytical performance of the biosensor in real samples

The optimized biosensor was tested for the amperometric detection of dopamine hydrochloride[®] 0.5 % (Zentiva) at -0.2 V. The results are in good agreement with the Romanian Pharmacopoeia³¹⁴ and the recovery rates were between 96.96 % and 100.77 % (RSD \pm 1.65 %). The potential interferences with the excipients in the same concentration as in the commercial product were also evaluated. Propylene glycol 25 % and ethanol 25 % did not show any interference with the dopamine signal, meanwhile 0.01 % sodium metabisulphite decreased the dopamine electrochemical response with 2.2 %³⁰¹.

The urine and human serum samples, prepared by 100 times dilution before testing, were spiked with different volumes of 10^{-2} mol L⁻¹ standard dopamine solution and the amperometric measurements revealed good recoveries (Table XII)³⁰¹.

Table XII. Dopamine amperometric detection from urine and serum³⁰¹

Probe	Vol. of 10^{-2} mol L ⁻¹ dopamine spiked (μL)	Peak intensity (μA)	Recovery (%)	RSD (%)
PBS	5	0.520	-	-
	10	1.10	-	
Urine samples	5	0.521	100.19	1.46
	10	1.07	97.27	
Serum samples	5	0.530	101.92	1.87
	10	1.08	98.18	

No significant interferences were observed when dopamine was determined by using amperometry, in the presence of equal concentrations of uric or ascorbic acids, and for equal and 10 times higher concentrations of glucose (Figure 41)³⁰¹.

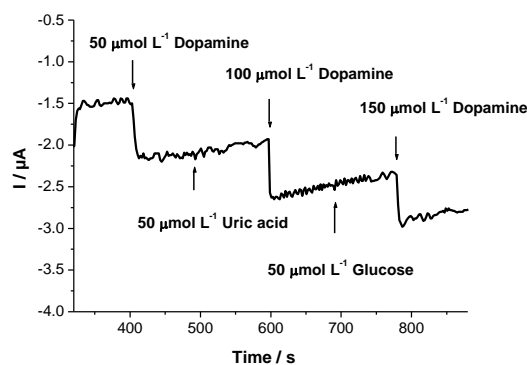


Fig. 41. Amperometric current response of PEI/TYR/ β -CD/RGO/GCE to successive injections of equal volumes ($25 \mu\text{L}$) of $10^{-2} \text{ mol L}^{-1}$ of dopamine, uric acid and glucose solutions in PBS ($\text{pH } 7.2$; 0.1 mol L^{-1})³⁰¹

4.3.2. Reduced graphene oxide/pyrrole- β -cyclodextrin biosensor

4.3.2.1. Spectral and microscopic characterization

The design of the graphene polymer framework is presented in Figure 42 A.

The Py-CD spectrum indicates the functionalization of pyrrole with β -CD; in comparison with β -CD spectrum, there appear some new peaks: $2850\text{-}2900 \text{ cm}^{-1}$ (C-H stretch from the aliphatic chain of pyrrole), 1540 cm^{-1} (C-C stretch for aromatic ring of pyrrole). The characteristic peaks for N containing groups (amide and amine) from 3300 cm^{-1} are overlapped by the broad and intensive band of OH groups from β -CD. The other bands of β -CD ranging between 700 cm^{-1} and 1650 cm^{-1} can be noticed in the functionalized monomer spectrum. In the case of the RGO/Py-CD spectrum, the bands for hydroxyl groups (3313 cm^{-1}) and for carboxylic groups (1633 cm^{-1}) are diminished due to the reduction process of the graphene oxide. In addition, there appear some new bands at: 2928 cm^{-1} (C-H stretch in alkanes), 1201 cm^{-1} , 1148 cm^{-1} , 1075 cm^{-1} , 1020 cm^{-1} (C-O stretch in alcohols and ethers) attributed to β -CD molecule providing the evidence that the RGO were successfully functionalized with Py-CD (Figure 42 B)³⁰³.

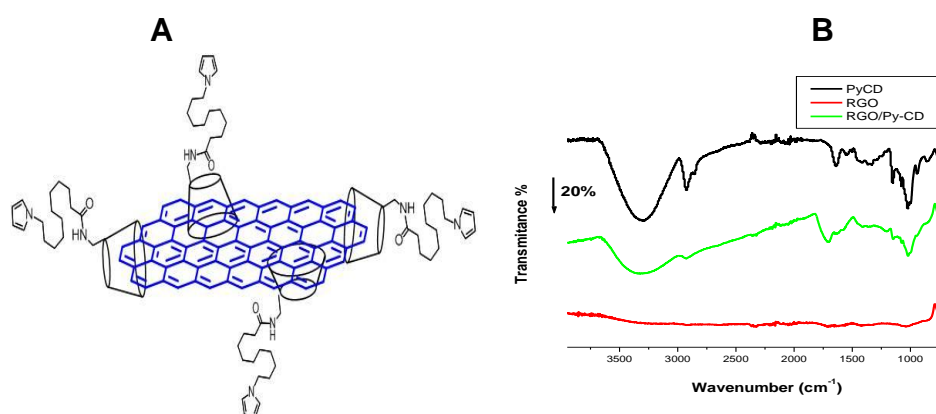


Fig. 42. (A) The structure of RGO/Py-CD; (B) FTIR spectra of Py-CD (black), RGO (red) and RGO/Py-CD (green)³⁰³

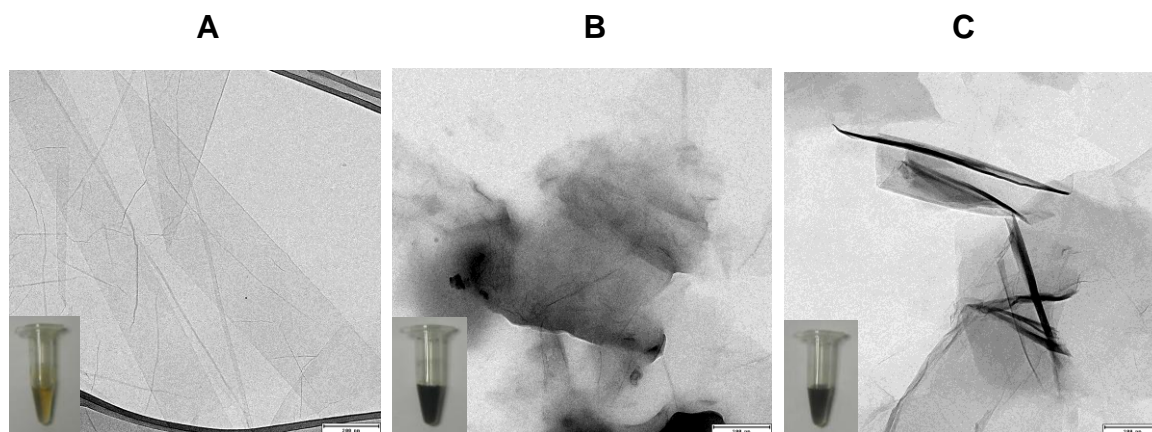


Fig. 43. TEM images of: GO (A), RGO (B), and RGO/Py-CD (C) (Insets: photos of corresponding aqueous solutions)³⁰³

The TEM images also prove the RGO functionalization: reduced graphene oxide was compared with reduced graphene oxide modified with Py-CD. It was observed that the reduced graphene oxide sheets are more aggregated in “black flakes” in comparison with the reduced graphene oxide modified with Py-CD, aspect that could be also noticed for its solution which was darker. The RGO/Py-CD sheets are more exfoliated presenting an excellent individualization due to the presence of Py-CD which acts as a dispersing agent for graphene (Figure 43)³⁰³.

4.3.2.2. Electrochemical characterization of the nanostructured electrode material

After drop-coating of 5 μL RGO/Py-CD solution on GCE, electropolymerization was performed in 0.1 mol L⁻¹ LiClO₄/ACN by controlled potential electrolysis at 0.85 V for 5 min (Figure 44 A). The electrogeneration of poly-[RGO/Py-CD] is confirmed by the decrease of the irreversible oxidation peak corresponding to the irreversible pyrrole oxidation at $E_p = 1.1$ V. The appearance of a small reversible redox system at $E_{1/2} = 0.50$ V is attributed to the polypyrrole electroactivity (Figure 44 A)³⁰³.

The electrochemical properties of poly-[RGO/Py-CD]/GCEs were investigated by using Ru(NH₃)₆Cl₃ as redox probe (Figure 44 B). After the electropolymerization of several layers (1, 3, 5 and 10 layers) of poly-[RGO/Py-CD], it can be observed that the Ru(III)/Ru(II) redox peak intensities increase with the increasing number of layers. The maximum improvement for Ru(III)/Ru(II) peak intensity was achieved with 5 layers of RGO/Py-CD, after that no significant changes were observed (maybe too much layers of graphene lead to the graphite structure and behavior). The most notable difference for increased intensity was observed for 1 layer of RGO/Py-CD (almost twice in comparison with bare GCE). Using the Randles-Sevick equation, electroactive area was increased from 0.07 cm² (the geometrical area of GCE) to 0.2 cm², which is obtained above 5 layers of poly-[RGO/Py-CD]. This is consistent with an increase of electroactive area caused by the immobilization of RGO by electropolymerization of Py-CD. Film thicknesses were measured

by laser scanning microscopy, showing values around 1 μm for single layer and 8 μm for ten layers electrodeposited³⁰³.

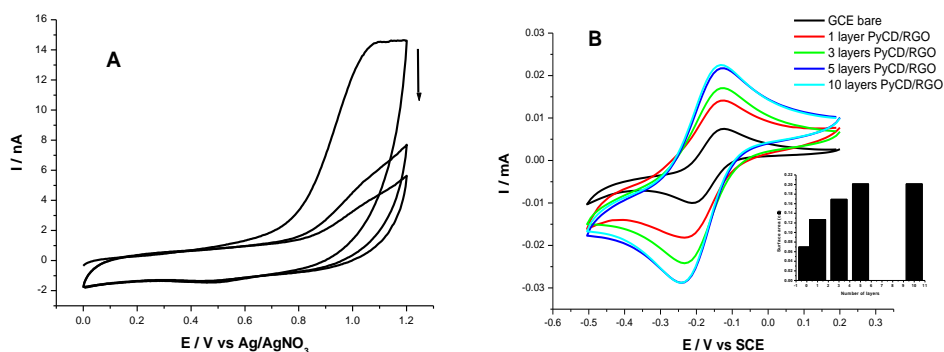


Fig. 44. (A) CVs for 3 layers of RGO/Py-CD at GCE (0.1 mol L^{-1} , $\text{LiClO}_4/\text{ACN}$, 3 scans, 50 mV s^{-1}); (B) CVs of 1 mmol L^{-1} $\text{Ru}(\text{NH}_3)_6\text{Cl}_3$ at bare and poly-[RGO/Py-CD] modified GCEs (1, 2, 3, 5 and 10 layers, 100 mV s^{-1}); (Inset: Electrode surface area increase with the number of layers)³⁰³

4.3.2.3. Electrochemical performances of the biosensor

The electrochemical behavior of the electrodes towards dopamine (1 mmol L^{-1} in PBS pH 6.5) was also investigated by CV at bare GCE, poly-[RGO/Py-CD] and poly-Py-CD electrodes (Figure 45). For poly-[RGO/Py-CD], the reversible peak system of dopamine exhibits higher current intensities, accompanied with lower ΔE of 190 mV, compared to bare GCE ($\Delta E = 260 \text{ mV}$). GCE modified with poly-Py-CD exhibits a higher ΔE value of 440 mV, which underlines the insulating properties of poly-Py-CD, compared to the RGO-doped poly-Py-CD³⁰³.

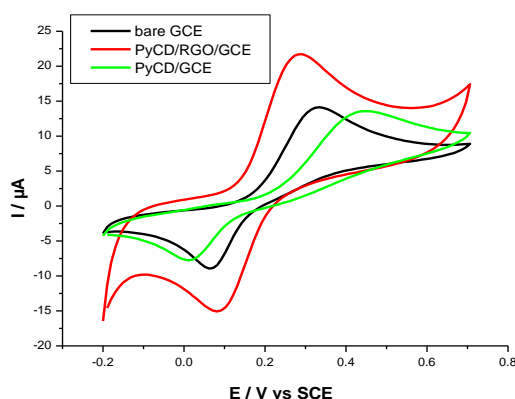


Fig. 45. CVs of 1 mmol L^{-1} dopamine at bare GCE (black), single layer of RGO/Py-CD/GCE (red) and poly-Py-CD/GCE (green); (100 mV s^{-1} , 0.1 mol L^{-1} PBS, pH 6.5)³⁰³

The tyrosinase biosensor was elaborated by using two methods. The first two-step technique consisting in a single layer electrodeposition of poly-[RGO/Py-CD] onto GCE, followed by the co-electropolymerization of the amphiphilic pyrrole monomer and tyrosinase, was achieved according to Cosnier *et al.*³⁰⁴.

The second procedure was performed by electropolymerization of a mixture of RGO/Py-CD, amphiphilic pyrrole and tyrosinase. This poly-[RGO/Py-CD/amphiphilic pyrrole] composite bioelectrode was compared with the layer-by-layer electrodeposition and with the GCE modified with poly-[amphiphilic pyrrole]/tyrosinase (Figure 46). In Figures 46 A and 46 C are presented the calibration curves for catechol and dopamine recorded by chronoamperometric measurements at $E_p = -0.2$ V after successive addition of substrates. The linear part of the calibration curves is displayed in Figures 46 B and 46 D for catechol and dopamine respectively³⁰³.

The combination of RGO/Py-CD with tyrosinase/amphiphilic pyrrole led to an improvement of the biosensor performances. First, in the case of layer-by-layer electrodeposition, the best configuration for the biosensor was obtained after the electrodeposition of a single layer of poly-[RGO/Py-CD]. For catechol oxidation the I_{max} for monolayer of RGO/Py-CD was 12 μ A, for three layers 11.23 μ A and for ten layers 7.9 μ A, respectively. In the case of dopamine oxidation, the monolayer of RGO/Py-CD generated an I_{max} of 1.22 μ A and three layers of RGO/Py-CD an I_{max} of 0.8 μ A. This effect can be attributed to the steric hindrances induced by thick electropolymerized films (consisting in many layers of RGO/Py-CD) towards the permeation of both substrate and oxygen, despite the higher electroactive area²⁸⁴. In both one-step and layer-by-layer configurations, the combination of poly-[RGO/Py-CD] and poly-amphiphilic pyrrole/tyrosinase at the electrode leads to a two fold increase in maximum current intensities (in the absence of RGO/Py-CD the I_{max} was 6.7 μ A for catechol oxidation and 0.5 μ A for dopamine oxidation). This is explained by a higher quantity of immobilized enzyme per surface unit, thanks to the nanostructuration of the surface functionalized with poly-[RGO/Py-CD]. Especially in the case of dopamine sensing, the sensitivity and LOD were improved for these graphene-based electrodes³⁰³.

All the electrochemical parameters of the biosensors for the three different electrodes are presented in Table XIII and Table XIV. It is noteworthy that the addition of ascorbic acid, uric acid and glucose as interferences did not show any significant current change for all types of electrodes³⁰³.

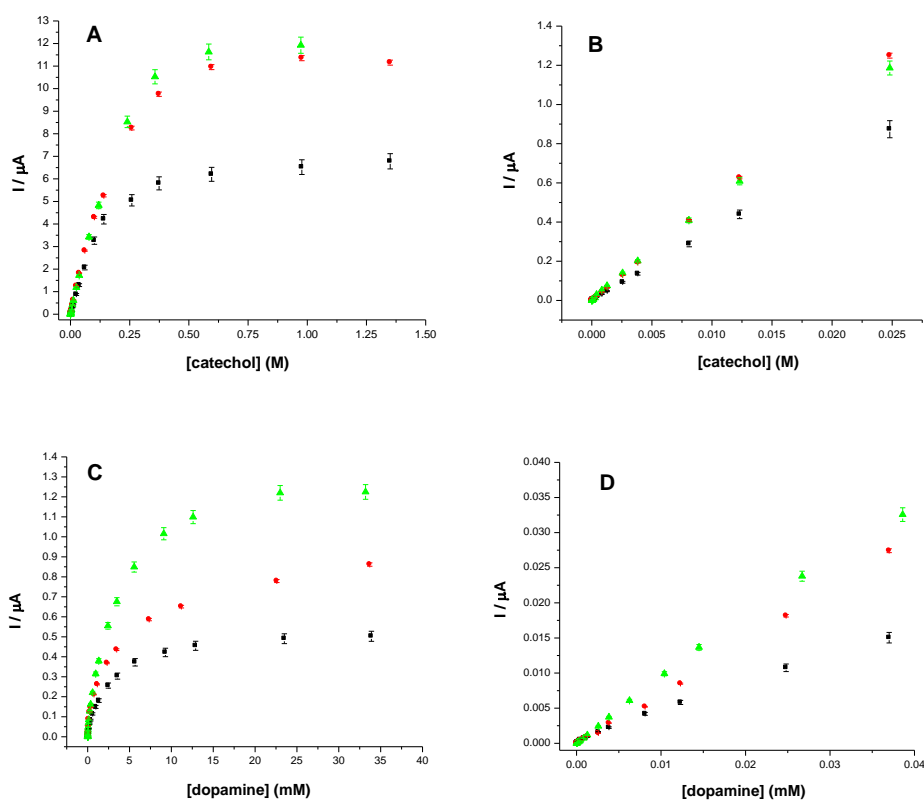


Fig. 46. Plots of normalized current intensities towards catechol (A, B) and dopamine (C, D) concentration at poly-amphiphilic pyrrole/tyrosinase (black), poly-[Py-CD/amphiphilic pyrrole/RGO]/tyrosinase (red) and LBL poly-[RGO/Py-CD]/poly-amphiphilic pyrrole/tyrosinase (green) electrodes (-0.2 V, 0.1 mol L⁻¹ PBS pH 6.5)³⁰³

Table XIII. Electroanalytical parameters of the biosensors for catechol determination³⁰³

Modified electrode	I_{max} (μA)	Sensitivity (mA L mol^{-1})	LOD (nmol L^{-1})	Linear range (nmol L^{-1} - $\mu\text{mol L}^{-1}$)	R^2	RSD (%)
Amphiphilic pyrrole/ Tyrosinase	6.7	40	2.44	2.44 – 25	1	5%
RGO/Py-CD/ Amphiphilic pyrrole/ Tyrosinase (one-step technique)	11.35	50	1	1 – 25	1	1%
RGO/Py-CD/ Amphiphilic pyrrole/ Tyrosinase (two-step technique)	12	50	2.8	2.8 – 25	0.99	3%

Table XIV. Electroanalytical parameters of the biosensors for dopamine determination³⁰³

Modified electrode	I_{\max} (μA)	Sensitivity (mA L mol^{-1})	LOD (nmol L^{-1})	Linear range (nmol L^{-1} - $\mu\text{mol L}^{-1}$)	R^2	RSD (%)
Amphiphilic pyrrole/ Tyrosinase	0.5	0.04	40	40 – 37	0.994	5%
RGO/Py-CD/ Amphiphilic pyrrole/ Tyrosinase (one-step technique)	0.92	0.07	27	27 – 37	0.998	1%
RGO/Py-CD/ Amphiphilic pyrrole/ Tyrosinase (two-step technique)	1.22	0.09	27	27 – 38.6	0.997	3%

4.4. Conclusions

The biosensor elaborated through LBL deposition of reduced graphene oxide and β -cyclodextrin was tested for the sensitive and selective determination of dopamine. The optimization process included: the layers number and the type of graphene (reduced graphene oxide vs. β -cyclodextrin functionalized reduced graphene oxide), the accumulation time and the deposition method. The modification of graphene oxide and the formation of the nanocomposite at the surface of GCE were confirmed by spectral and microscopic techniques. The optimized biosensor was successfully applied for dopamine determination in pharmaceutical products, serum and urine samples with good recoveries.

A new nanostructured graphene framework reinforced by a polymer film was elaborated. Py-CD plays a double role due to its structure: β -CD is used in order to improve graphene dispersion in water, while the pyrrole group is used for its ability to form electropolymerized coatings. These electropolymerizable graphene sheets were electrodeposited on GCEs and demonstrate excellent nanostructured support for the fabrication of a tyrosinase-based composite bioelectrode for catechol and dopamine sensing. The controlled electropolymerization of such nano-objects on surfaces is very promising for amperometric biosensors miniaturization, which can be applied for *in vivo* measurements of low levels of neurotransmitters.

5. Electrochemical and spectral behavior of tetrazines

5.1. Introduction

Tetrazines (TZ) are 6-membered aromatic heterocycles with 4 nitrogen atoms symmetrically arranged in the ring with a strong electron-deficient character. They have a very high electron affinity, making them reducible at high to very high potentials (potentials depending on the electron affinity of the substituent); actually they are the electron poorest C–N heterocycles. They can be electrochemically reduced to a stable anion radical state and a second time to an unstable dianion state in solution. There are three possible tetrazine isomers: **1,2,3,4-tetrazines**, **1,2,3,5-tetrazines** and **1,2,4,5-tetrazines**.

One of the most remarkable aspects of tetrazine chemistry is the presence of a very low-lying π^* molecular orbital, with as consequence a low energy $n-\pi^*$ transition in the visible range, which makes them highly colored. Tetrazines are colorful compounds ranging from purple to orange or red because of a weak $n-\pi^*$ transition located in the visible with its maximum between 510 and 530 nm. The position of the absorption band corresponding to this transition is weakly influenced by the nature of the substituents and was shown not to be solvatochromic. A second intense band appears in the UV region being a $\pi-\pi^*$ transition whose position is strongly dependent on the substituents, and it correlates linearly with their electron donating or withdrawing character. A large number of tetrazines are fluorescent. The position of the maximum of emission ranges between 550 and 590 nm. The quantum yields are strongly dependent on the nature of the substituents^{315,316}.

Because of their optical and oxidizing properties, they are very promising candidates to examine electrochemical fluorescence switching, in which the fluorescence of the neutral state could be reversibly switched on and off by converting the molecules successively to their reduced form (possibly non fluorescent) and back to the neutral (fluorescent) state. An optical change is an important issue in organic electronics such as electrochromic displays or electro-optical switches and such devices might find application in large size display panels using UV light³¹⁷⁻³¹⁹.

s-Tetrazines substituted with heteroatoms display interesting fluorescence properties that can be electrochemically monitored placing them among the smallest organic fluorophores in the visible range ever prepared. This makes them especially attracting in view of sensing applications³²⁰⁻³²².

Most 1,2,4,5-tetrazines are almost as reducible as quinones. The presence of at least four nitrogen donor atoms in tetrazines and their derivatives confers them rich coordination possibilities for metal complexes formation³²³. Organic compounds with high-nitrogen content currently attract significant attention from many researchers

due to their novel energetic properties. Therefore, many symmetrical and unsymmetrical substituted tetrazines were synthesized³²⁴.

Tetrazines are widely used for industrial and medical applications as they exhibit particular coordination chemistries, characterized by electron and charge transfer phenomena. Some compounds containing the 1,2,4,5-tetrazine skeleton have been claimed for pharmaceutical effects due to their high potential for biological activity: antiinflammatory and analgesic (hexahydro-s-tetrazines), antimalarial (3-amino-6-aryl-1,2,4,5-tetrazines), antibacterial and antifungal (tetrahydro-s-tetrazines), antiviral and antitumoral activities (1,4-dihydro-s-tetrazine derivative)³²⁵⁻³²⁷. A covalent labeling of live cancer cells on the basis of the cycloaddition of a tetrazine to a highly strained trans-cyclooctene was reported^{328,329}. s-tetrazine can be an excellent candidate for constructing anion receptors due to π -interaction of anions with the aromatic ring of the s-tetrazine unit³³⁰. New nanocomposites materials have been obtained by reaction of s-tetrazines with fullerene C60 or carbon nanotubes. Multi-walled carbon nanotubes have been modified with 3,6-diaminotetrazine under heating involving π - π interactions, cycloaddition (Diels-Alder) and cross-linking reactions. This functionalization can open new approaches for the preparation of carbon nanotube interconnects³³¹. A conducting polymer with a tetrazine pendant functional group was obtained proving anti-corrosion efficiency³³².

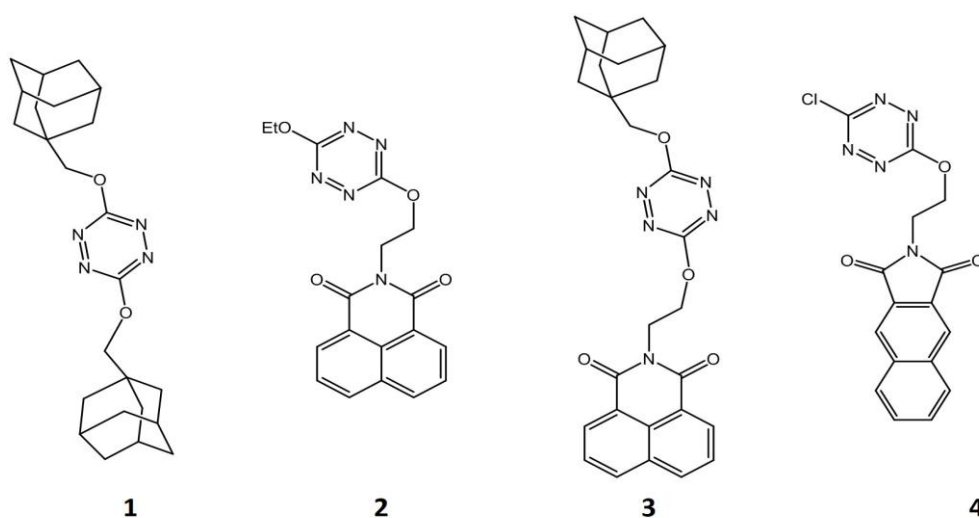


Fig. 47. The chemical structures of the new four synthesized tetrazines

Like most organic compounds, tetrazines are only very weakly soluble in water. Their behavior and solubilization in water has not yet been studied. The formation of supramolecular assemblies between β -cyclodextrin and tetrazine derivatives can be one promising alternative. Four tetrazines were synthesized bearing different substituents specially adapted to the inclusion inside a cyclodextrin (Figure 47)³³³. Tetrazines were functionalized with adamantane groups and naphthalimide antennas, organic anchoring groups which may also fit the requirements for inclusion within cyclodextrin³³⁴⁻³³⁶. On the other hand, the tetrazine itself is small enough to be efficiently included in the cyclodextrin cavity.

The solubilization of these new fluorophores in water, as well as the electrochemical behavior and the fluorescence of these compounds in aqueous solutions are presented³³³. The immobilization of tetrazines onto electrodes modified with polypyrrole-cyclodextrin is also presented. The immobilization of tetrazines was examined by electrochemical (on glassy carbon electrodes), microscopic (on gold microelectrodes) and spectroscopic methods (on indium tin oxide electrodes).

5.2. Experimental

5.2.1. Synthesis

All tetrazines derive from the reaction between dichlorotetrazine and alcohols. The first substitution is catalyzed by collidine³³⁷, while the second one is catalyzed by an additional equivalent of 4-dimethylaminopyridine³³⁸, sequentially added. For tetrazine 2, the monosubstitution product was not isolated. For tetrazine 3 and 4, the starting synthon was the naphthalimide tetrazine (NITZ) molecule, already described in several previous articles^{333,339,340}.

The amphiphilic pyrrole derivative, [12-(pyrrol-1-yl) dodecyl] triethylammonium tetrafluoroborate (amphiphilic pyrrole) and β -cyclodextrin-11-pyrrolyl-1-undecyl carboxylic acid amide (Py-CD), were synthesized according to previously described procedures^{303,304}.

5.2.2. Electrochemistry measurements

The electrochemical experiments were carried out in the three-electrode electrochemical cell under dry argon atmosphere using an Autolab PGSTAT 100 potentiostat. All potentials were measured against SCE or Ag/AgCl reference electrodes in aqueous solutions and against a silver wire immersed in 0.01 mol L⁻¹ AgNO₃ and 0.1 mol L⁻¹ LiClO₄ in ACN for organic solutions. The working electrodes are GCEs from BAS, diameter of 3 mm, Pt electrodes (\varnothing 5 mm), rotating disk electrodes (RDE, \varnothing 3 mm), polished with diamond paste (2 μ m), then rinsed with ethanol and distilled water. The indium tin oxide (ITO) electrodes were modified and used for spectral studies.

The chemical products LiClO₄, β -CD, K₂HPO₄, KH₂PO₄ were purchased from Sigma Aldrich and used as received. ACN was purchased from HPLC – VWR Chemicals (HPLC grade).

5.2.3. UV-visible measurements and fluorescence measurements

Absorption spectra were recorded with a Perkin Elmer UV-Lamba 650 spectrophotometer in glass cuvettes (Huet, 1 cm, 1 mm) at room temperature. Fluorescence measurements were done by using the Fluorescence Spectrometer Perkin Elmer LS 55 in quartz cuvettes (Huet, 1 cm) at a 518 nm excitation wavelength and room temperature³³³.

Dispersions containing 0.1 mg mL^{-1} of tetrazine were prepared by ultrasonication for 1 hour in: water, $10^{-2} \text{ mol L}^{-1}$ β -CD aqueous solution and 0.5 mg mL^{-1} β -CD modified gold nanoparticles (CD-AuNP) solution. The obtained dispersions were let overnight for sedimentation and then the limpid liquid was analysed³³³.

5.3. Results and discussions

5.3.1. Tetrazines behavior in aqueous solution

5.3.1.1. Electrochemical study

The electrochemical behavior of the four tetrazines has been investigated in ACN + 0.1 mol L^{-1} LiClO_4 . As it can be observed in Figure 48, the reversible anion-radical formation is observed around -0.75 V to -0.80 V , with the exception for tetrazine 4 where the potential is shifted to -0.6 V , due to the stronger electron-withdrawing power of the substituted chlorine. The dianion formation observed around -1.2 V , barely or not reversible, is due to its high reactivity towards adventitious water. The reduction of the naphtalimide moiety of tetrazines 2, 3, and 4 can be observed at more negative potentials (around -1.5 V) as previously was reported for analogous molecules³³³.

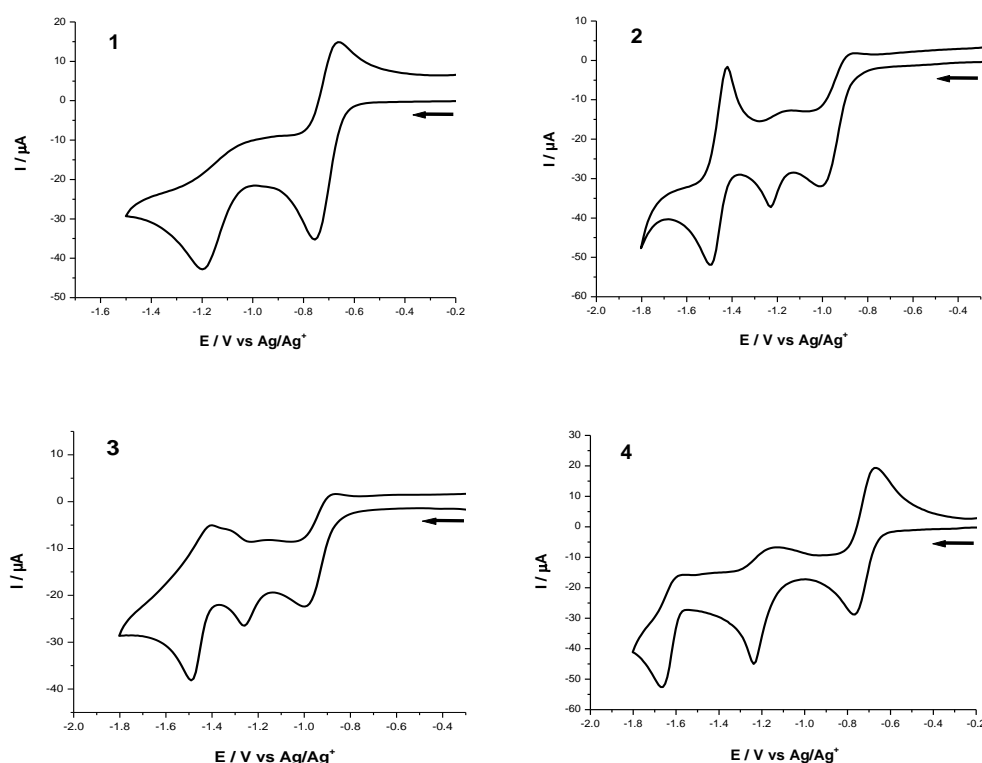


Fig. 48. CVs of 1 mmol L^{-1} tetrazines 1, 2, 3 and 4 in 0.1 mol L^{-1} $\text{LiClO}_4/\text{ACN}$ (100 mV s^{-1})³³³

All four tetrazines have been solubilized in aqueous phosphate buffer, in the presence or absence of $10^{-2} \text{ mol L}^{-1}$ β -CD. For all electrodes, a reversible redox system can be observed at -0.17 V (Figure 49).

Tetrazine 1 substituted by two adamantane groups is not soluble in water. This behavior is explained by the high hydrophobic character of the two adamantanyl groups, which surprisingly help quite moderately the solubilization process in aqueous solutions. The other three tetrazines with small groups (like Cl, OEt) are more soluble in water, entering more easily inside the β -CD cavity. In addition, tetrazines themselves are good “keys” for β -CD³³³. The CD effect consisted in the improvement of the tetrazines solubilisation and in the increase of the current intensity recorded in the following CVs.

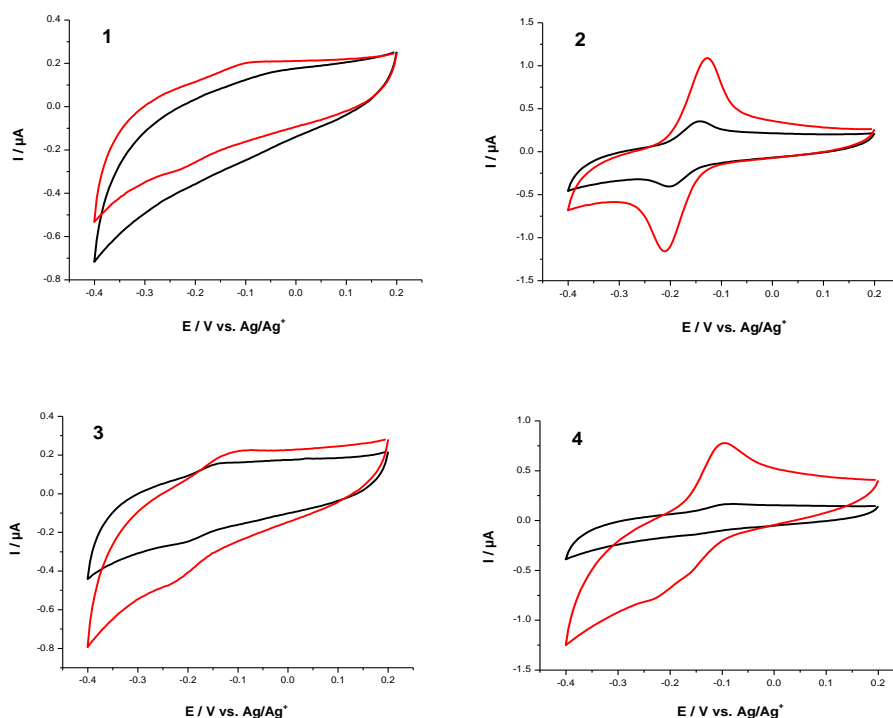


Fig. 49. CVs of tetrazines 1, 2, 3 and 4 in PBS, with (red) or without (black) $10^{-2} \text{ mol L}^{-1} \beta\text{-CD}$ (50 mV s^{-1})³³³

Tetrazines are chemically reduced by two-protons, two-electrons process into 1,4-dihydropyridazines (Figure 50), behavior which is very close to the quinones ones in similar conditions³³³.

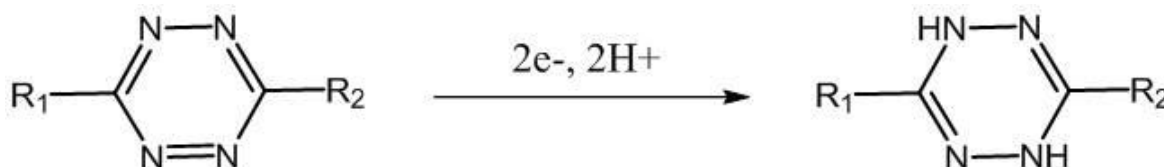


Fig. 50. Two-electrons, two-protons reduction of a tetrazine ring³³³

5.3.1.2. Spectroscopic study

Tetrazines are colorful substances: in visible light they appear pink and orange, and under UV irradiation they appear yellow (Figure 51 A and 51 B).



Fig. 51. Visible (left) and UV 365 nm (right) photos of 10^{-3} mol L⁻¹ tetrazine 1 (A), 2 (B), 3 (C) and 4 (D) in ACN

The UV-Vis absorption and fluorescence of the tetrazines have been recorded in ACN (Figure 52). Tetrazines absorb in UV-Vis region presenting two characteristic bands: a weak one around 500-530 nm ($n-\pi^*$ transition), and an intensive one around 300-360 nm, ($\pi-\pi^*$ transition) (Figure 52 A).

Tetrazines present also fluorescence at 560–568 nm when excitation wavelength is 518 nm. While the three dialkoxytetrazines show the classical spectra already observed for this family of compounds, the last compound exhibits the strongest fluorescence of the chloroalkoxytetrazines with a slightly hypsochromic shift (Figure 52 B)³³³.

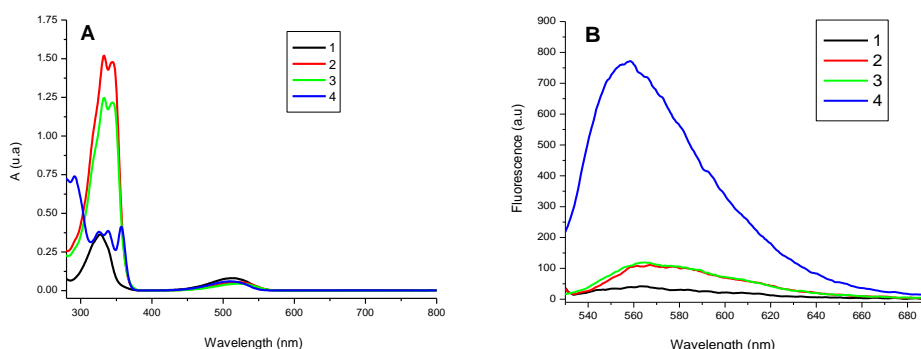


Fig. 52. (A) UV-Vis spectra of 10^{-4} mol L⁻¹ and (B) fluorescence spectra of 10^{-6} mol L⁻¹ tetrazines 1 (black), 2 (red), 3 (green), and 4 (blue) in ACN ($\lambda_{\text{ex}} = 518$ nm; 1 cm cuvettes)³³³

Taking into account that fluorescence is a more sensitive technique than cyclic voltammetry, and that there is no electrolyte salt that might influence the solubilization, the fluorescence of the four tetrazines has been examined in the absence and presence of β -CD (10^{-2} mol L $^{-1}$). It can be clearly observed that the fluorescence response of the fluorophore is almost negligible or very weak in the absence of the β -CD (Figure 53). Tetrazines 2 and 4 are less hydrophobic (without any adamantane groups) and consequently they are slightly soluble in water in comparison with tetrazines 1 and 3³³³.

In the presence of β -CD in all cases the fluorescence response is enhanced (Figure 53). For tetrazines 1 and 3 bearing hydrophobic adamantanyl groups, the fluorescence response increased from zero to a strong emission demonstrating the inclusion in CD cavity. Tetrazines 2 and 4 also experience an enhancement of their solubility in water, showing again the ability of the tetrazine to enter the CD cavity with a reasonable efficiency.

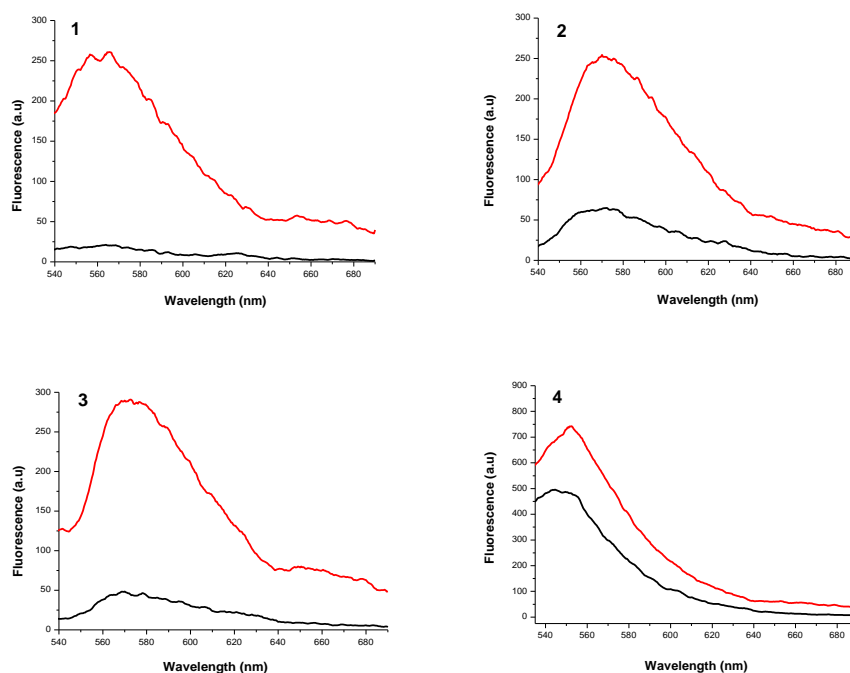


Fig. 53. Fluorescence spectra of tetrazines 1-4 in H₂O (black) and 10^{-2} mol L $^{-1}$ β -CD solution (red) (518 nm)³³³

The solubilization effect of β -CD on tetrazines can be observed only in UV region proving thus, the enhanced tetrazine solubilization by the inclusion in β -CD cavity (Figure 54).

The influence of the ultrasonication time (30 minutes, 1 h, 1 h 30 minutes, 2 h, 2 h 30 minutes), upon the solubilization of the tetrazines in the β -CD solution was also investigated. Above 1 h of ultrasonication the fluorescence response was not significantly enhanced.

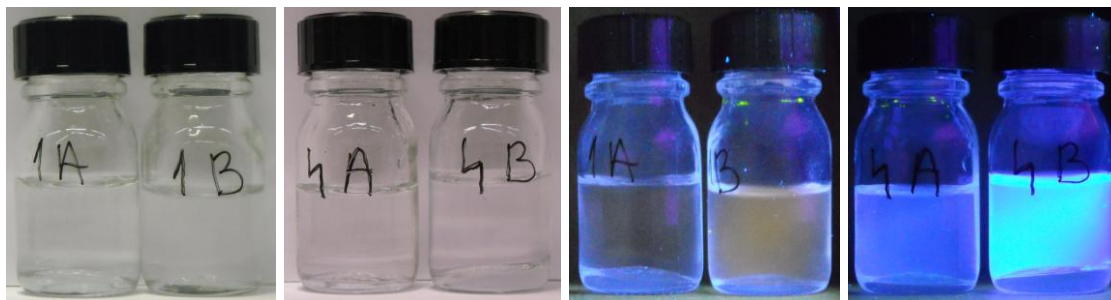


Fig. 54. Visible (left) and UV 365 nm (right) photos of tetrazines 1 and 4 in **(A)** water and **(B)** $10^{-2} \text{ mol L}^{-1}$ β -CD solution (after 1 h of sonication)

According to the UV-Vis spectra of tetrazines in β -CD aqueous solutions, only tetrazines 2 and 4 presented evident absorption in UV region (Figure 55).

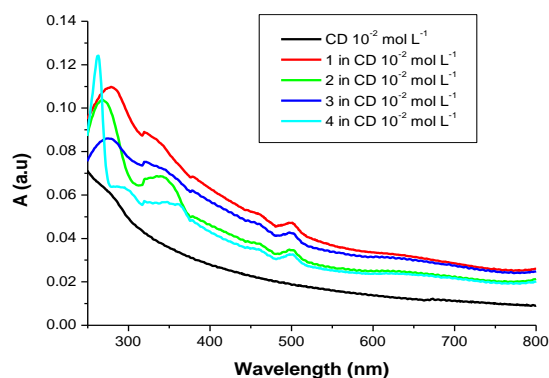


Fig. 55. UV-Vis spectra of tetrazines 1 (red), 2 (green), 3 (dark blue), and 4 (light blue) in $10^{-2} \text{ mol L}^{-1}$ β -CD (black)

The influence of AuNPs modified with β -CD (CD-AuNP) upon the tetrazines solubilization was also studied by fluorescence and absorption spectra. The CD-AuNP suspension is not fluorescent, but it absorbs in UV-Vis region (Figure 56 A and 56 B). The fluorescence response of the tetrazines solubilised in CD-AuNP aqueous solution is observed being weaker in comparison with the spectra registered only in presence of β -CD. The fluorescence spectra of all inclusion complexes of tetrazines with β -cyclodextrin, either in solution, or grafted onto AuNP are presented in Figure 56 A. In the presence of β -CD, only for tetrazines 2 and 4 was recorded an evident absorption in UV region (Figure 56 B)³³³.

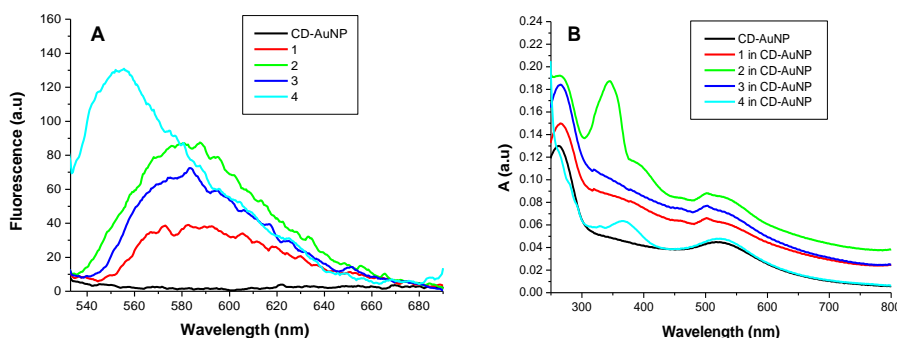


Fig. 56. Fluorescence spectra (A) and (B) UV-Vis spectra of tetrazines in CD-AuNP solutions³³³

The molar absorption coefficient for tetrazine 2 ($22187 \text{ L mol}^{-1} \text{ cm}^{-1}$) was calculated. The concentration of tetrazine 2 solubilized in CD-AuNP solution was $6.7 \cdot 10^{-5} \text{ mol L}^{-1}$, which means that 33.5 % of the tetrazine initial amount was solubilized. In the case of the solubilization in β -CD solution, the tetrazine concentration was $2.1 \cdot 10^{-5} \text{ mol L}^{-1}$, meaning that 10.5 % of the initial amount was solubilized.

5.3.2. Electrochemical, spectral and microscopic studies of the immobilized tetrazines

5.3.2.1. Immobilization by using pyrrole-cyclodextrin

The pyrrole-cyclodextrin monomer (Py-CD) was electropolymerized on the GCE by CV with different parameters (potential window between 0.0 V to 0.9 V or to 1.2 V, and number of scans between 5 and 15). Due to the poor solubility of the Py-CD, the electrochemical behavior has been studied in a mixture of ACN/DMSO (4:1.5). Upon oxidation, an irreversible peak, characteristic for the irreversible oxidation of pyrrole, is detected at 1.0 V. The electropolymerization of the monomer was achieved by cycling the potential of the electrode between 0.0 V and 1.2 V for 15 scans. Although the electroactivity of the polypyrrole is not detected, a decrease of the oxidation peak of the pyrrole is in agreement with the electrodeposition of a polymeric layer at the electrode surface (Figure 57).

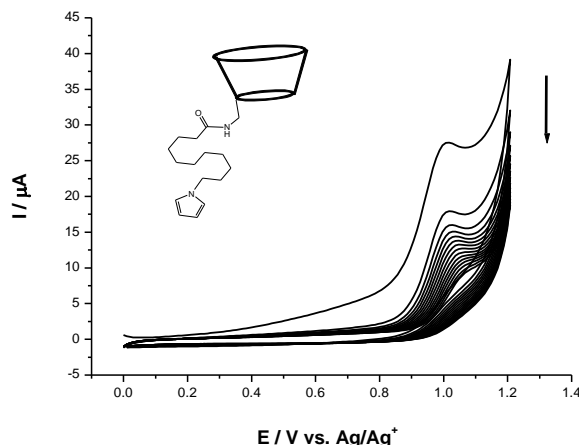


Fig. 57. CV polymerization of 1 mmol L^{-1} Py-CD in $0.1 \text{ mol L}^{-1} \text{ LiClO}_4$ (ACN/DMSO) at GCE (100 mV s^{-1} , 15 scans); (Inset: Structure of Py-CD)

In addition, in order to demonstrate the polymer presence at the electrode surface, the complexation with ferrocene and tetrazine was investigated. The optimization tests made with ferrocene revealed that the best electropolymerization parameters are: CV (15 scans) between 0.0 V and 1.2 V, with 100 mV s^{-1} scan rate. After the electropolymerization step the modified electrodes were kept in 1 mmol L^{-1} tetrazine dissolved in ACN for 45 minutes. The electrodes were rinsed with ACN and then transferred in 0.1 mol L^{-1} phosphate buffer, pH 7. Reversible redox systems were detected for all four tetrazines at -0.12 V , -0.16 V , -0.15 V and -0.14 V potentials, respectively, indicating the tetrazine immobilization onto the electrodes through the inclusion complexes formation with β -CD from the polymeric film (Figure 58).

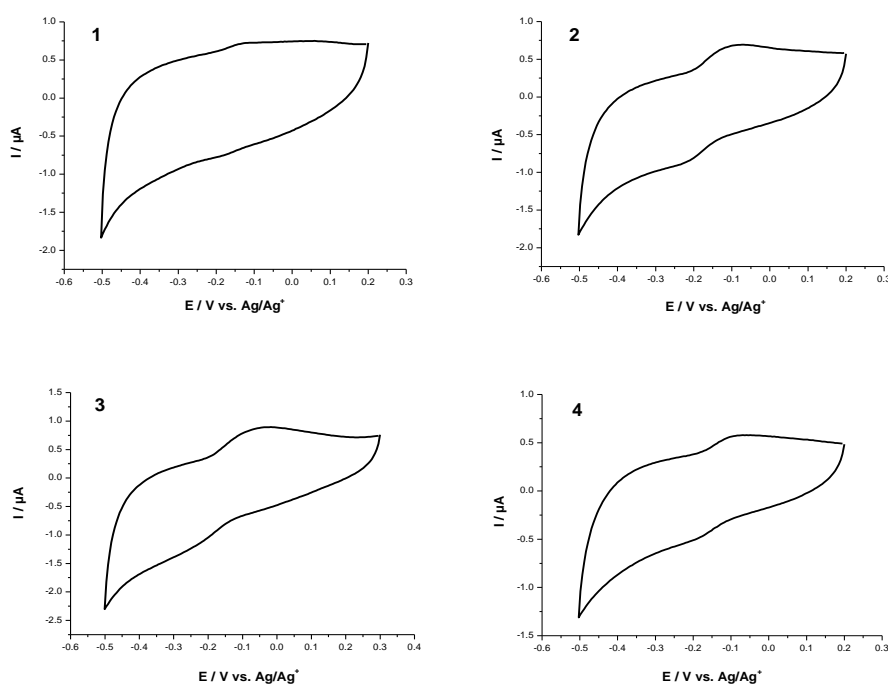


Fig. 58. CVs of tetrazines 1-4 in PBS (pH 7, 50 mV s^{-1}) at Py-CD/GCEs (kept in 1 mmol L^{-1} tetrazine/ACN for 45 min)

Moreover, the linear variation of the current in function of the scan rate (between 25 mV to 150 mV) is in agreement with the fact that tetrazines are immobilized at the electrode surface (Figure 59 A). Furthermore, a linear variation of the redox potential towards pH was observed with a slope of 50 mV between pH 5 to 9, being closed to the theoretical value of 58 mV for a H^+/e^- ratio of 1 (Figure 59 B).

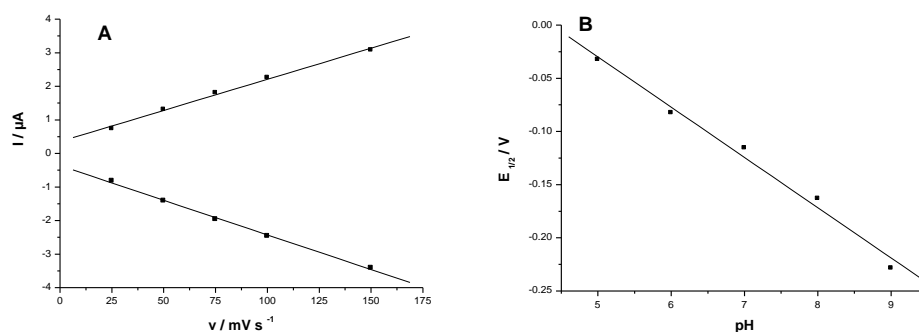


Fig. 59. (A) The current variation of tetrazine 3 immobilized on Py-CD/GCE in function of the scan rate; **(B)** The variation of $E_{1/2}$ of tetrazine 1 immobilized on Py-CD/GCE in function of pH

The diffusion of $\text{Fe}^{\text{II}}(\text{CN})_6$ is detected at 0.30 V onto GCE. The successive steps of electropolymerization and complexation with tetrazine 1 induce a positive shift of the anodic peak potential from 0.30 V to 0.45 V and 0.55 V. Similarly, the cathodic peak potential was negatively shifted in association with an increase of ΔE_p . These phenomena illustrate the increase of the steric hindrances due to the successive formation of polymer and immobilization of tetrazine at the electrode surface (Figure 60 A). The permeability of the modified electrode before and after tetrazine 1 immobilization was investigated by rotating disk electrode (RDE, \varnothing 3 mm) experiments with $2 \text{ mmol L}^{-1} \text{ Fe}^{2+}$ in PBS, as redox probe. The rotating disk voltammograms were recorded at 10 mV s^{-1} in the range from 0.0 V to 0.8 V corresponding to the oxidation of the redox probe at 250, 500, 750, 1000, 1250, 1500 rpm. The decrease of the permeability of the organic material from $1.4 \cdot 10^{-5} \text{ cm s}^{-1}$ to $7.2 \cdot 10^{-6} \text{ cm s}^{-1}$ indicates that the immobilization of tetrazine via the polymer was successful (Figure 60 B).

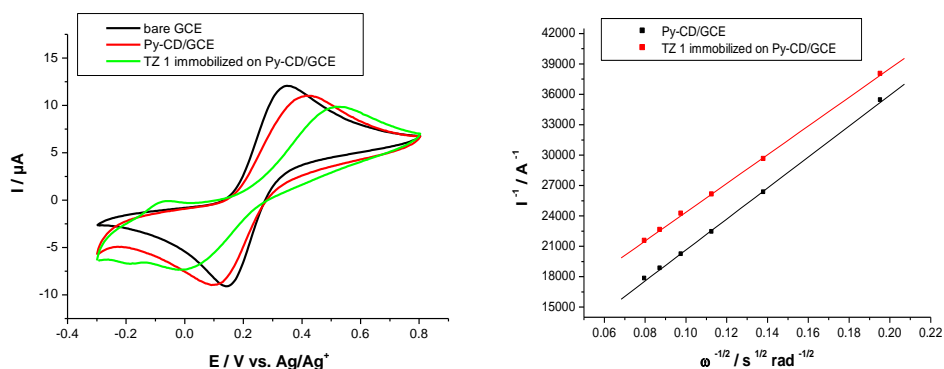


Fig. 60. (A) CVs (50 mV s^{-1}) and **(B)** Koutecky-Levich plots for $2 \text{ mmol L}^{-1} \text{ Fe}^{2+}$ in $0.1 \text{ mol L}^{-1} \text{ PBS}$ (pH 7, 10 mV s^{-1})

The amount of tetrazine immobilized onto the modified electrodes was calculated by integrating the charge recorded under the reduction signal considering one electron for the reduction of tetrazine. The low recovering of the surface

by tetrazine varying from 0.8 pmol cm^{-2} to 4.6 pmol cm^{-2} is probably due to the difficulty to get an homogeneous film at the electrode surface.

The modified GCEs were also maintained for 45 minutes in 0.1 mg mL^{-1} tetrazine aqueous solutions, previously sonicated in $10^{-2} \text{ mol L}^{-1}$ β -CD and 0.5 mg mL^{-1} CD-AuNP solutions for 1 h. Then, the electrodes were transferred in a PBS solution and the signal of the immobilized tetrazine was recorded (Figure 61 A and 61 B).

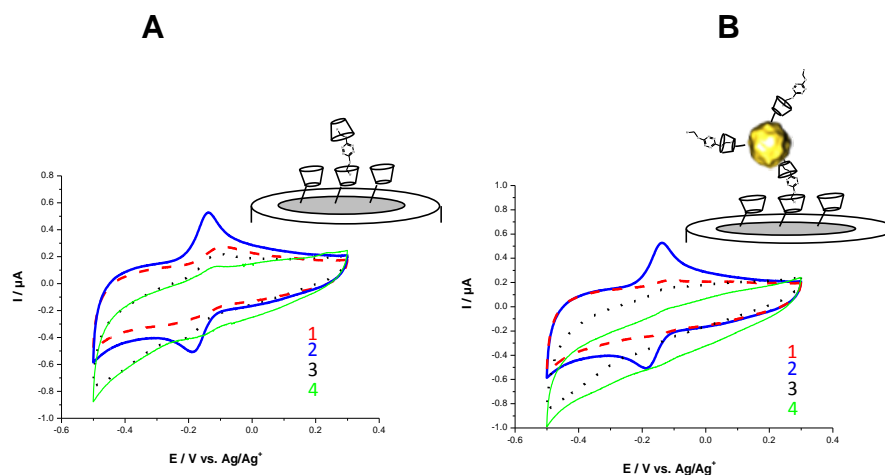


Fig. 61. CVs of tetrazines 1-4 in PBS (0.1 mol L^{-1} , pH 7, 10 mV s^{-1}) at Py-CD/GCEs kept in aqueous solutions of tetrazines with **(A)** $10^{-2} \text{ mol L}^{-1}$ β -CD and **(B)** 0.5 mg mL^{-1} CD-AuNPs for 45 min

The ITO electrodes were also modified with poly-Py-CD by CV (15 scans) in the range from 0 V to 1.2 V, with 100 mV s^{-1} , and were kept for 45 minutes in 0.1 mg mL^{-1} tetrazine aqueous solutions, previously sonicated in $10^{-2} \text{ mol L}^{-1}$ β -CD and 0.5 mg mL^{-1} CD-AuNP solutions for 1 h. The UV-Vis spectroscopy (Figure 62) revealed the absorption band around 420 nm indicating the tetrazine immobilization on the polymeric film covering the electrode surface.

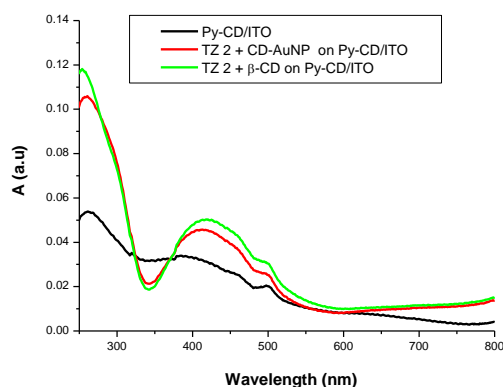


Fig. 62. UV-Vis spectra of Py-CD/ITO kept in aqueous solutions of tetrazine 2

The polymerization of 1 mmol L⁻¹ Py-CD and 1 mmol L⁻¹ tetrazines in mixture on GCEs for tetrazine immobilization was also studied (Figure 63). The best configuration for the mixture electropolymerization was achieved employing the parameters presented in table XV.

Table XV. Electropolymerization parameters for 1 mmol L⁻¹ Py-CD and 1 mmol L⁻¹ tetrazines mixture

Tetrazines	Potential (V)	Number of scans	Scan rate (mV s ⁻¹)
Tetrazine 1	0.0 V -1 V +1.2 V	10 scans	100 mV s ⁻¹
Tetrazine 2	0.0 V -1.4 V +1.2 V		
Tetrazine 3			
Tetrazine 4			

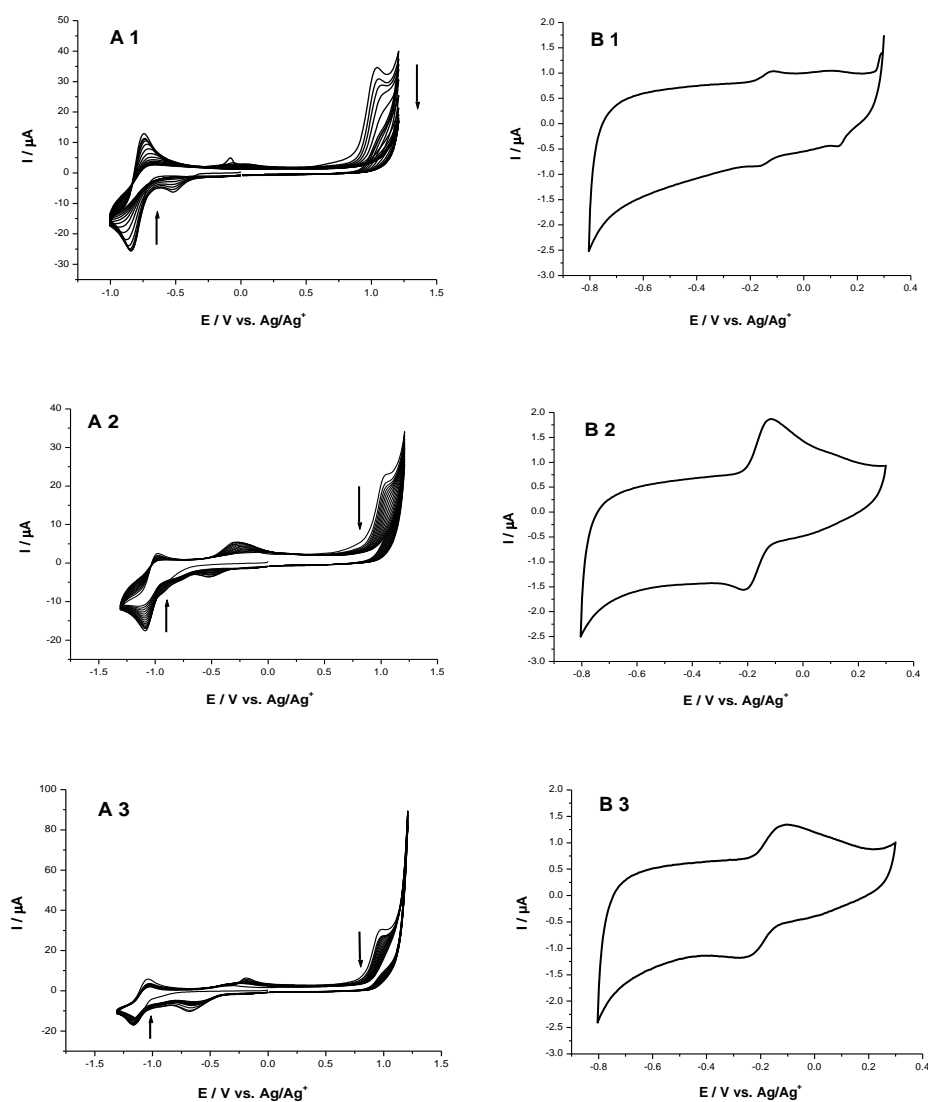


Fig. 63. (A) Polymerization of 1 mmol L⁻¹ Py-CD and 1 mmol L⁻¹ tetrazines 1-3 by CV in 0.1 mol L⁻¹ LiClO₄ (ACN) at GCEs (15 scans, 100 mV s⁻¹); **(B)** CVs of tetrazines 1-3/Py-CD/GCE in 0.1 mol L⁻¹ PBS (pH 7, 50 mV s⁻¹)

The stability of the modified electrodes was evaluated by scanning the electrode from -0.5 V to 0.2 V. The electrode keeps about 90 % of its signal after 400 cycles. The stability of the immobilized tetrazines was examined as a function of time, the modified electrode being stored in 0.1 mol L⁻¹ PBS. It appears that the signal decreases with 14 % during the first 100 hours and then becomes stable during more than 130 hours.

The tetrazines were used for biomolecule immobilization through inclusion complexes between tetrazine and CD cavity. The Pt electrodes electropolymerized with 1 mmol L⁻¹ Py-CD and 1 mmol L⁻¹ tetrazines (parameters presented in table XV) were incubated with 20 μL of 1 mg mL⁻¹ β-cyclodextrin modified glucose oxidase (CD-GOX) for 45 minutes in the refrigerator, then were washed 10 minutes in 0.1 mol L⁻¹ PBS under stirring. These modified electrodes were tested towards the amperometric detection of glucose (Figure 64) obtaining the analytical parameters presented in table XVI.

Table XVI. Electroanalytical parameters for glucose oxidation

Modified electrode	I_{\max} ($\mu\text{A cm}^{-2}$)	Sensitivity ($\mu\text{A L mol}^{-1} \text{cm}^{-2}$)	Linear range ($\mu\text{mol L}^{-1}$ - mmol L^{-1})	R^2
1 mmol L ⁻¹ Py-CD/Pt	4.23	149.04	40 – 3.83	0.998
1 mmol L ⁻¹ Py-CD/ 1 mmol L ⁻¹ tetrazine 1/Pt	14.87	367.85	132 – 8.11	0.993
1 mmol L ⁻¹ Py-CD/ 1 mmol L ⁻¹ tetrazine 2/Pt	38.07	1484.1	8.61 – 3.83	0.997
1 mmol L ⁻¹ Py-CD/ 1 mmol L ⁻¹ tetrazine 3/Pt	12.24	374.11	13.3 – 8.11	0.992
1 mmol L ⁻¹ Py-CD/ 1 mmol L ⁻¹ tetrazine 4/Pt	9.03	285.7	86.6 – 8.11	0.994

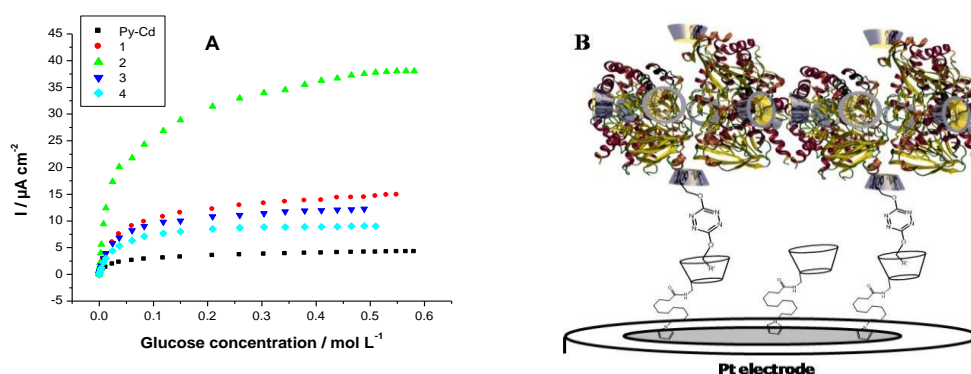


Fig. 64. (A) Calibration curves for glucose oxidation obtained with Pt electrodes polymerized with 1 mmol L⁻¹ Py-CD and 1 mmol L⁻¹ tetrazines; (B) Schematic representation of the biosensor

The Pt electrodes polymerized with Py-CD were also kept in the aqueous solution of tetrazine (previously sonicated 1 h) followed by the incubation in 1 mg mL^{-1} CD-GOX. The biosensor response proves that the enzyme was immobilized at the electrode surface through the inclusion complexes formed between the tetrazine and the β -cyclodextrin (Figure 65).

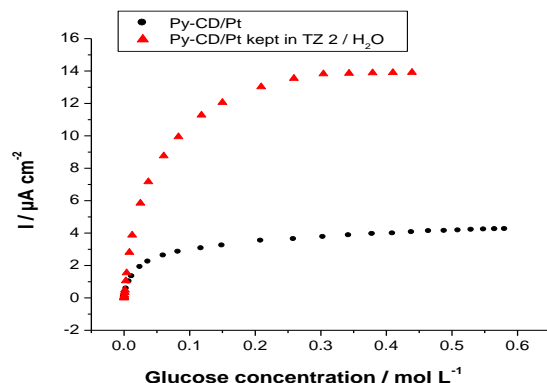


Fig. 65. Calibration curves for glucose oxidation obtained at Py-CD/Pt

It was also examined the immobilization of tetrazines on gold microelectrodes and carbon fibers modified with poly-Py-CD by fluorescence microscopy using an appropriate filter. For this purpose, the modified electrodes were kept in tetrazine solution. In the images below (Figure 66 and 67) the tetrazines immobilized on the film are represented as white/yellow-green spots due to their fluorescence.

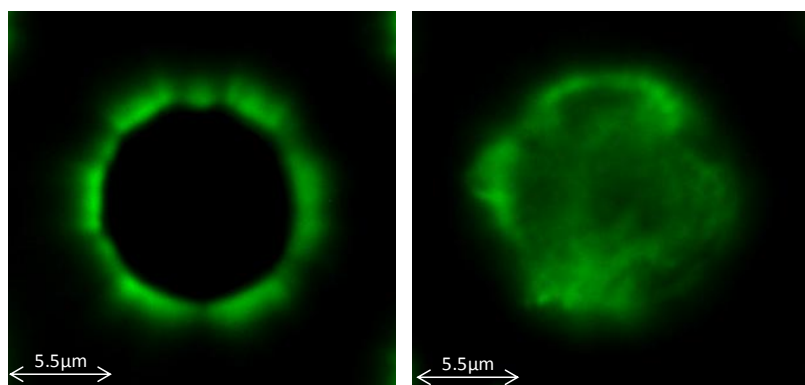


Fig. 66. Microscopic images of gold microelectrodes modified with poly-Py-CD before (left) and after (right) the treatment with 1 mmol L^{-1} tetrazine 2 in ACN (excitation filter HQ 530/30 CHROMA, emission filter ET 575Lp)

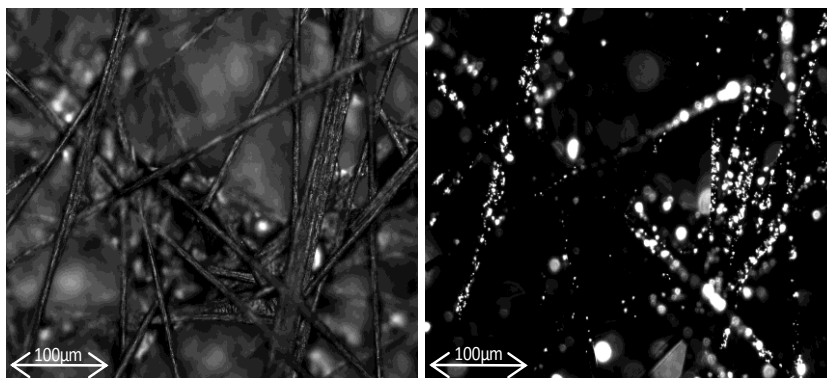


Fig. 67. Microscopic images of carbon fibres treated with 1 mmol L^{-1} tetrazine 2 (ACN) without (left) and with fluorescent filter (right) (excitation filter HQ 530/30 CHROMA, emission filter ET 575Lp)

5.3.2.2. Tetrazines immobilization using an amphiphilic pyrrole derivative

For tetrazine immobilization, the electropolymerization of a mixture containing tetrazine and an amphiphilic pyrrole derivative, [12-(pyrrol-1-yl) dodecyl] triethylammonium tetrafluoroborate (amphiphilic pyrrole) was also achieved. Different concentrations of tetrazine (1 , 3 , and 10 mmol L^{-1}) were mixed with 2.5 mmol L^{-1} monomer in ACN and then were electropolymerized at the electrodes surface by using electrolysis (0.76 V vs SCE) and cyclic voltammetry ($0.0 \text{ V} + 0.75 \text{ V}$, 100 mV s^{-1}). After the polymer electrogeneration and rinsing with ACN, the electrodes were tested in PBS when the peak of the immobilized tetrazine can be observed (Figure 68).

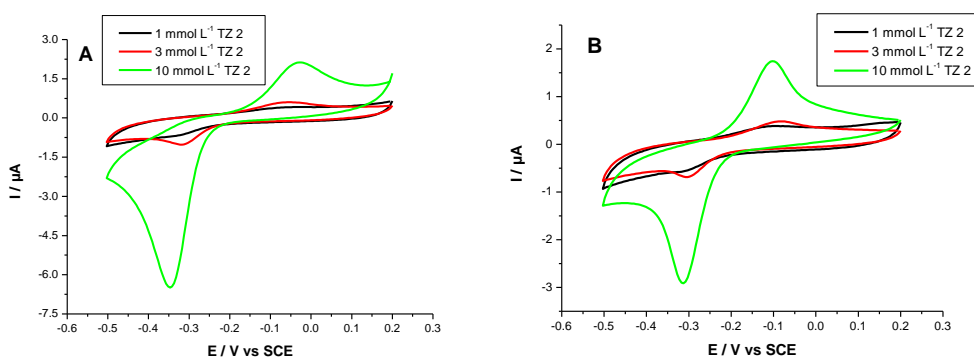


Fig. 68. CVs of tetrazine 2 in 0.1 mol L^{-1} PBS at GCE polymerized with 2.5 mmol L^{-1} amphiphilic pyrrole and 1 , 3 and 10 mmol L^{-1} tetrazine 2 by **(A)** electrolysis (0.4 mC) and **(B)** cyclic voltammetry (10 scans)

The same mixture was electropolymerized for tetrazine immobilization at ITO electrodes and the electrochemical and spectral studies showed the successful entrapment of tetrazine in the polymeric film. In the CV scans (Figure 69 A) the tetrazine 2 peak can be observed at -0.2 V . The absorption bands at 500 nm and 340 nm in UV spectrum (Figure 69 B) also indicates the tetrazine immobilization in the film.

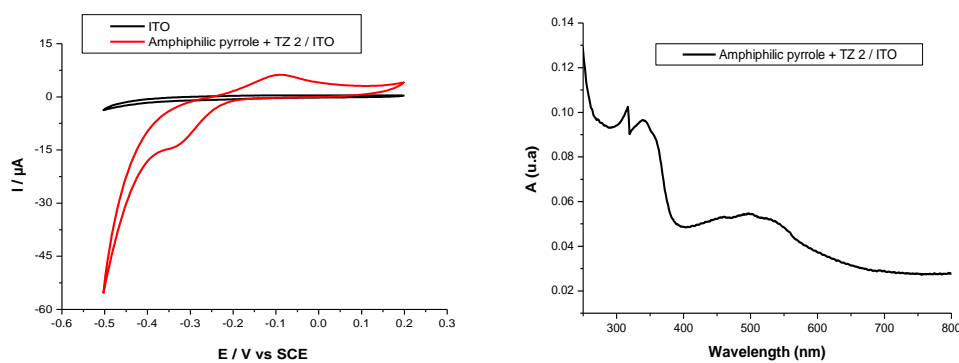


Fig. 69. (A) CVs in PBS (50 mV s^{-1}) and (B) UV-Vis spectrum of the ITO electrode modified with 2.5 mmol L^{-1} amphiphilic pyrrole and 10 mmol L^{-1} tetrazine 2 by electrolysis (0.8 V , 3 mC)

Furthermore, the tetrazine entrapment in the polymeric film was also used for CD-GOX immobilization indicating the complexation between tetrazine and β -CD cavity (Figure 70).

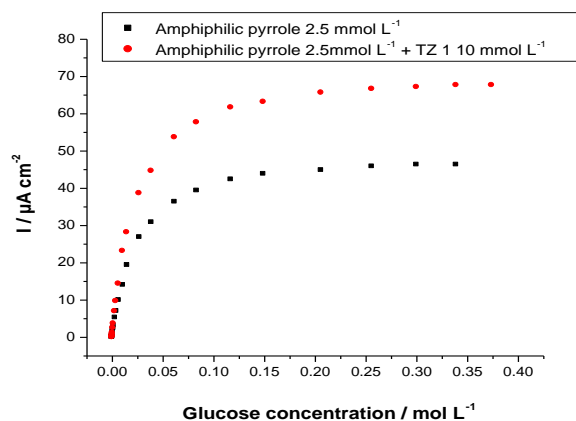


Fig. 70. Calibration curves for glucose oxidation obtained at Pt electrodes polymerized with (black) 2.5 mmol L^{-1} amphiphilic pyrrole and (red) 2.5 mmol L^{-1} amphiphilic pyrrole and 10 mmol L^{-1} tetrazine 1 by electrolysis (0.76 V , 1 mC)

The electropolymerization of a mixture containing 10 mmol L^{-1} tetrazine 1 and 2.5 mmol L^{-1} amphiphilic pyrrole was also achieved onto gold microelectrodes which were examined at fluorescent microscope. The fluorescent spots indicated the entrapment of tetrazine in the polymeric film (Figure 71).

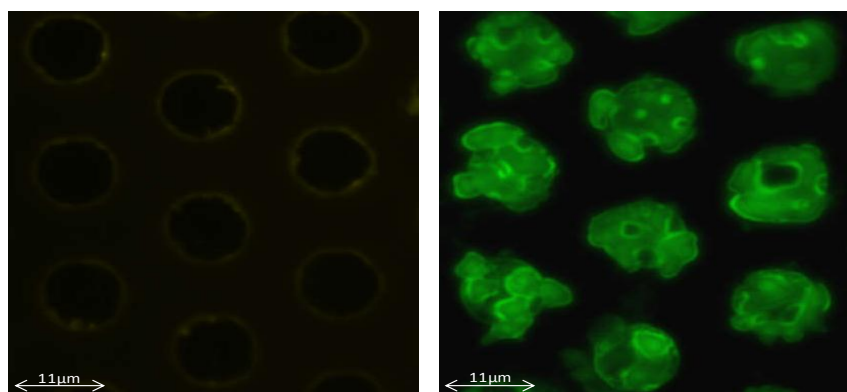


Fig. 71. Microscopic images of gold microelectrodes modified with poly-Py Amphiphile (left) and poly-Py Amphiphile and tetrazine 1 (right) (excitation filter HQ 530/30 CHROMA, emission filter ET 575Lp)

5.4. Conclusions

Different substituted tetrazines (functionalized with adamantane and naphthalimide groups) were solubilized in aqueous solutions by using β -CD and β -CD modified gold nanoparticles, due to the inclusion complexes formation between β -CD cavity and the organic groups, as well as the tetrazine itself. These redox supramolecular assemblies were characterized in water by electrochemical and fluorescence measurements. A poly-pyrrole-cyclodextrin film electrogenerated onto the electrodes surface was also used for the tetrazine immobilization. Immobilization of tetrazine was examined by electrochemical (on glassy carbon electrodes), microscopic (on gold microelectrodes) and spectroscopic methods (on indium tin oxide electrodes). Tetrazines were also entrapped into a polymeric film of an amphiphilic pyrrole derivative. These fluorophores were used for glucose oxidase immobilization at the electrode surface through the inclusion complexes formed between tetrazine and cyclodextrin.

6. Nanostructured photosensitive poly-[trisbipyridinyl-pyrrole ruthenium(II)] metallopolymer by nanosphere lithography

6.1. Introduction

Metallopolymers are a particular class of redox polymers having a wide range of applications, ranging from molecular electronics to sensing or energy conversion^{341,342}. Among them, electrogenerated metallopolymers demonstrated attractive properties in photovoltaics³⁴³, photoelectrochemical immunosensors or aptasensors³³⁴ and electrogenerated chemiluminescence³⁴⁵. The functionalization of pyrrole monomers and their subsequent electropolymerization represent a versatile and controllable approach to create modified electrodes with precise spatial resolution. An important parameter for photocurrent enhancement is the nanostructuring of photosensitive surface. Thus, the combination of polymers with different nanomaterials, such as: carbon nanotubes, metal or metal oxide nanoparticles^{173,282,346-348} was used in order to form photosensitive highly porous nanostructures.

Nanosphere lithography (NSL) is a technique used for nano- and micro-structuration. It employs latex or silica beads to control the nano- and micro-structuration of deposited materials such as metals³⁴⁹⁻³⁵¹ or conducting polymers³⁵²⁻³⁵⁵. The micro- or nano-beads can form highly ordered templates when the latter are deposited on planar surfaces. After materials deposition by using various techniques (chemical vapor deposition or electropolymerization), latex beads are easily removed by simple dissolution in organic solvents, leaving a highly porous and highly ordered surface with controlled nanostructure³⁵⁶. The porosity of functional electrogenerated polypyrroles has been controlled for immobilization of enzymes¹⁹³.

The NSL was combined with electropolymerization of a Ru(II)-pyrrole monomer, *tris[4,4 bis(3-pyrrol-1-ylpropyloxy)bipyridinyl] ruthenium(II) hexafluorophosphate*. By using different bead diameters (900 and 100 nm), the successful use of NSL to achieve highly ordered porosity in photosensitive metallopolymers was demonstrated. Enhanced photocurrent was observed being inversely proportional to the polystyrene bead diameter size³⁵⁷.

6.2. Experimental

6.2.1. Methods and Instrumentation

All reagents were purchased from Sigma Aldrich, excepting ACN (Rathburn, HPLC grade), were of analytical grade and used as received. *Tris[4,4 bis(3-pyrrol-1-ylpropyloxy)bipyridinyl] ruthenium(II) hexafluorophosphate* (Ru^{II} -pyrrole) was synthesized according to the procedure reported by Le Goff *et al.*²⁸².

All electrochemical studies were performed with a conventional three-electrode system using Ag/AgCl reference in ACN or a saturated calomel electrode (SCE) in water. A Pt wire electrode was used as counter electrode. The working electrodes were glassy carbon (5 mm diameter), both polished with 2 μm diamond paste followed by rinsing with distilled water and ethanol. Electrochemical experiments were conducted on an Autolab PGstat100 potentiostat³⁵⁷.

6.2.2. Elaboration of electrodes and characterization

The template was created on GCEs by drop casting a 0.5 wt % ethanol suspension of latex spheres with 900 nm (5 μL) and 100 nm (3x5 μL) diameter and allowed to dry at room temperature for 10 - 30 minutes. After the formation of poly- $[\text{Ru}^{\text{II}}$ -pyrrole] film by scanning the potential repeatedly (5 - 10 scans) from 0.0 V to 1.1 V vs Ag/AgCl at 0.1 V s^{-1} in a 2 mmol L^{-1} $\text{Ru}(\text{II})$ -pyrrole and 0.1 mol L^{-1} LiClO_4 dissolved in ACN, the resulting electrodes were immersed for 15 - 20 h in tetrahydrofuran (THF) in order to remove the latex template. The electrodes were rinsed with ethanol and distilled water. The morphology of the modified electrodes was investigated by scanning electron microscopy (SEM) using an ULTRA 55 FESEM based on the GEMINI FESEM column with beam booster (Nanotechnology Systems Division, Carl Zeiss NTS GmbH, Germany) and tungsten gun. 3D and profile images were taken by using a Keyence VK-X200 laser microscope³⁵⁷.

6.2.3. Photocurrent generation experiments

In these experiments, an electrochemical cell with a quartz window was used. The modified GCE was placed in front of the quartz window and irradiated with a 200 W Hg lamp through UV and IR cutoff filters below 420 nm and beyond 630 nm with a surface light intensity of 11.2 $\mu\text{W cm}^{-2}$. In order to monitor the photogenerated currents, the modified electrodes were potentiostated at 0 V³⁵⁷.

6.3. Results and discussions

6.3.1. Electrochemical studies

Nanostructured poly-[Ru^{II}-pyrrole]-modified electrodes were prepared in two successive steps. Firstly, a solution of Latex beads (900 nm and 100 nm) was drop-casted on GCEs forming a closely-packed and highly ordered nanosphere homogenous network. Then, Ru^{II}-pyrrole (Figure 72) was electropolymerized onto the deposited nanobeads using cyclic voltammetry for a precise control over electropolymerization conditions. In Figure 73 are shown ten successive CV scans for Ru^{II}-pyrrole (2 mmol L⁻¹) performed at bare GCE and GCEs covered with nanospheres with 900 or 100 nm diameters, respectively. These conditions were purposely chosen because it allows the reproducible and homogenous electrodeposition of a 0.5 μm thick polymer film onto GCE. The electrogeneration of poly-[Ru^{II}-pyrrole] onto the GCE surface is confirmed by the continuous increase in current intensity of the quasi-reversible monoelectronic metal-centered Ru(III)/Ru(II) oxidation at $E_{1/2}^{\text{ox}} = +0.91$ V. The poorly reversibility of this system is due to the irreversible catalytic oxidation of the pyrrole groups by the electrogenerated Ru(III) species. On the contrary, for GCEs modified by the reproducible and homogenous electrodeposition of a 0.5 μm thick polymer film onto adsorbed nanospheres (diameter: 900 or 100 nm), the irreversible oxidation of pyrrole decreases after successive scans due to the insulating properties of closely-packed nanobeads deposited on GCEs³⁵⁷. The irreversible oxidation of the six pyrrole groups at $E_p^{\text{ox}} = +0.9$ V overlaps the reversible metal-centered oxidation²⁸².

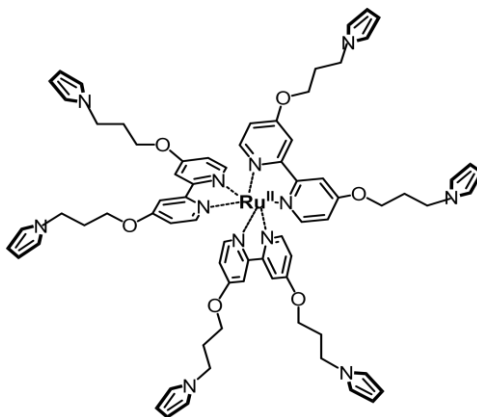


Fig. 72. Structure of Tris[4,4 bis(3-pyrrol-1-ylpropyloxy)bipyridinyl] ruthenium(II) complex³⁵⁷

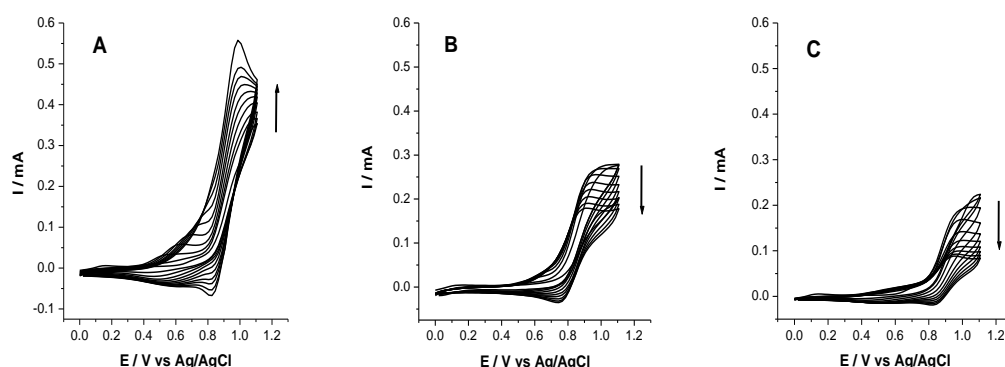


Fig. 73. CVs (10 scans) of Ru^{II}-pyrrole (2 mmol L⁻¹) in ACN + 0.1 mol L⁻¹ LiClO₄ recorded at: **(A)** bare GCE, **(B)** GCE covered with 900 nm and **(C)** with 100 nm diameter nanospheres ($v = 0.1 \text{ V s}^{-1}$)³⁵⁷

After the electropolymerization step, the modified GCEs were tested in ACN + 0.1 mol L⁻¹ LiClO₄ (Figure 74). The bare GCE exhibits a well-shaped reversible system at $E_{1/2} = +0.91 \text{ V}$, corresponding to the immobilized poly-[Ru^{II}-pyrrole] (Figure 74 C). An irreversible prepeak is observed at $E_p^{ox} = +0.82 \text{ V}$ corresponding to a charge trapping phenomenon especially encountered in redox polymer films²⁸².

For nanosphere covered electrodes, the CV scans before and after dissolution of the nanospheres were compared (Figures 74 A and 74 B). In both cases, an increase of the peak intensity was observed after dissolution of the beads, especially in the case of dissolution of 100 nm-diameter nanobeads. This behavior is explained by the insulating properties of the latex beads and by the fact that the presence of high concentration of latex nanobeads in the polymer film prevents from the diffusion of ions necessary for charge compensation during CV scans. The beads dissolution leaves a highly porous structure that greatly enhances redox site accessibility for the diffusion of the electrolyte and the excellent heterogeneous electron transfer is recovered³⁵⁷.

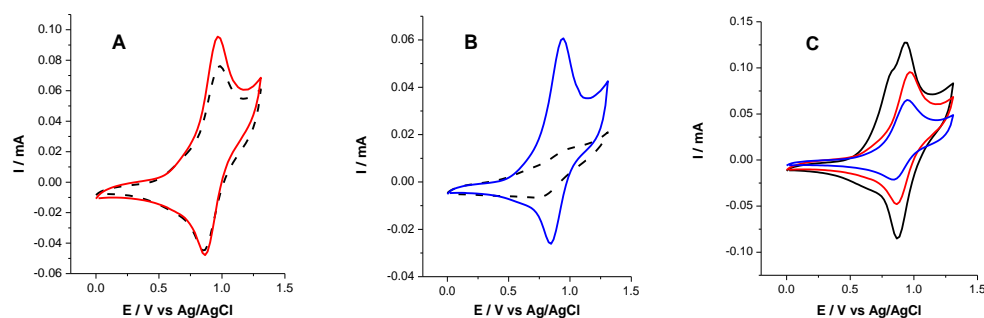


Fig. 74. CVs recorded at microstructured **(A)** and nanostructured poly-[Ru^{II}-pyrrole]/GCE **(B)**, before (dashed) and after (solid) beads dissolution; **(C)** CVs recorded at bare GCE of poly-[Ru^{II}-pyrrole] (black), microstructured poly-[Ru^{II}-pyrrole]/GCE (900 nm beads, red) and nanostructured poly-[Ru^{II}-pyrrole]/GCE (100 nm beads, blue) in ACN + 0.1 mol L⁻¹ LiClO₄ ($v = 0.05 \text{ V s}^{-1}$)³⁵⁷

This is also confirmed by experiments made in the presence of ferrocene (Fc) as redox probe (Figure 75). In this case, the barrier effect of a conventional planar polymer deposit was compared with both nanostructured polymers. While the $\Delta E = 310$ mV, peak-to-peak separation is measured for a 0.5 μm -thick metallopolymer film, ΔE for 900 nm and 100 nm templated metallopolymer are 200 mV and 190 mV, respectively (Figure 75). These experiments confirm the excellent diffusion of both the electrolyte and redox species through the mesoporous polymer layer, also confirmed by the permeability tests³⁵⁷.

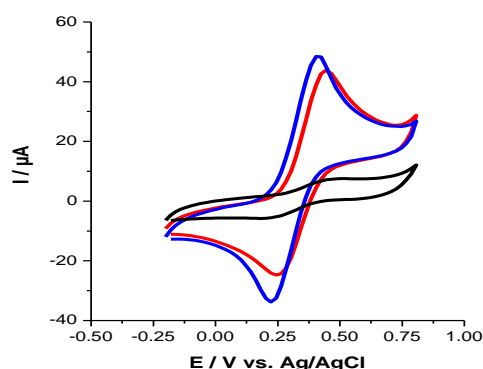


Fig. 75. CVs of 1 mmol L⁻¹ Fc recorded at a conventional poly-[Ru^{II}-pyrrole]/GCE (black), microstructured (red) and nanostructured poly-[Ru^{II}-pyrrole]/GCE (blue); ($v = 0.05$ V s⁻¹)³⁵⁷

The permeability of the polymeric film was investigated with 1 mmol L⁻¹ Fc as redox probe, in ACN by using RDE. The voltammograms for the 3 types of modified electrodes were recorded in the range of 0.0 V to +0.8 V, corresponding to the Fc oxidation, with a 50 mV s⁻¹ scan rate and at different rotation speeds (from 500 to 1500 rpm). After the polystyrene beads removal, the micro and nanostructured films obtained by using NSL (Figure 76), presented a higher permeability (0.11 cm s⁻¹ and 0.12 cm s⁻¹ for 900 nm and 100 nm, respectively) than the planar film (permeability value of 0.07 cm s⁻¹).

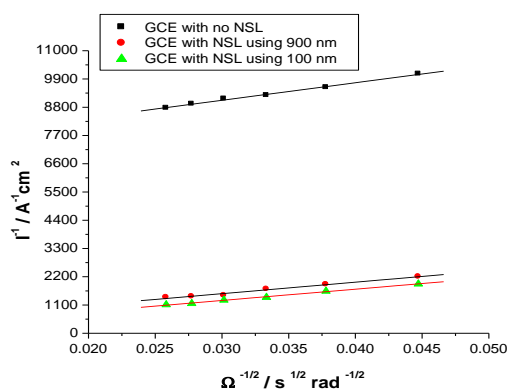


Fig. 76. Koutecky-Levich plots for 1 mmol L⁻¹ Fc in ACN + LiClO₄ (0.1 mol L⁻¹) at the poly-[Ru^{II}-pyrrole]/GCEs

The experiments in a monomer free solution were performed at different scan rates from 10 to 500 mV s^{-1} (Figure 77). The peak of Ru(II)/Ru(III) from poly-[Ru^{II}-pyrrole] showed a linear dependence of oxidation and reduction currents over scan rate for all modified electrodes. This is a proof of the film immobilization at the electrodes surface, being characteristic for a surface-controlled redox system. It can be observed that on the micro and nanostructured poly-[Ru^{II}-pyrrole]/GCEs the linear dependence of currents intensity is improved ($R^2 = 0.98$) in comparison with flat poly-[Ru^{II}-pyrrole]/GCE ($R^2 = 0.94$) indicating a better diffusion of the electrolyte through the porous film.

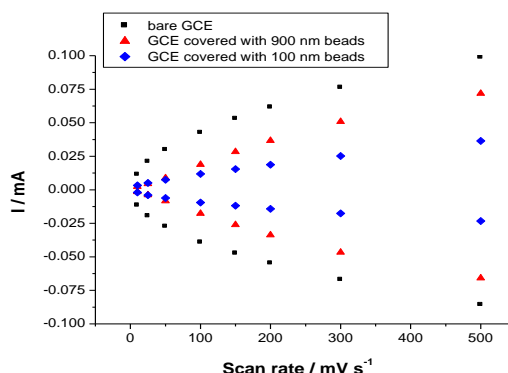


Fig. 77. The variation of the Ru (II)/Ru (III) peak intensity at flat, microstructured and nanostructured poly-[Ru^{II}-pyrrole]/GCEs at different scan rate

The amount of electropolymerized Ru(II) complexes was calculated from the charge recorded under the Ru(III)/Ru(II) oxidation. As expected, the maximum surface coverage was obtained for non-patterned modified GCE with $2.2 \cdot 10^{-8} \text{ mol cm}^{-2}$, while 900 nm and 100 nm templated poly-[Ru-pyrrole] exhibit surface coverages of $1.5 \cdot 10^{-8}$ and $8.7 \cdot 10^{-9} \text{ mol cm}^{-2}$, respectively, indicating that the polymerization is less effective in the presence of beads³⁵⁷.

6.3.2. Microscopic characterization

The surface morphology of the electrogenerated metallopolymer obtained with 900 nm diameter beads was characterized by laser scanning microscopy, while SEM was used when the 100 nm diameter nanobeads were employed. The characterization of poly-[Ru^{II}-pyrrole] after dissolution of the 900 nm diameter beads is shown in Figure 78, where the electrochemical patterning of the poly-[Ru^{II}-pyrrole] is confirmed by optical and 3D images. Well-organized micropores with a highly-reproducible honeycomb structure can be observed demonstrating the controlled deposition of the metallopolymer (Figure 78 A and 78 B). Furthermore, profile from Figure 78 C indicates the presence of pores of 250 nm depth accompanied with the unexpected presence of a 450 nm diameter hemisphere located in the centre of the pores. This hemispheric shape arises, perhaps, from a two-step electropolymerization process: in the first step, the hexagonal structure is formed by electropolymerization occurring around the beads and

in the second step the electropolymerization takes place on the top of the beads, forming a centered hemispheric structure³⁵⁷.

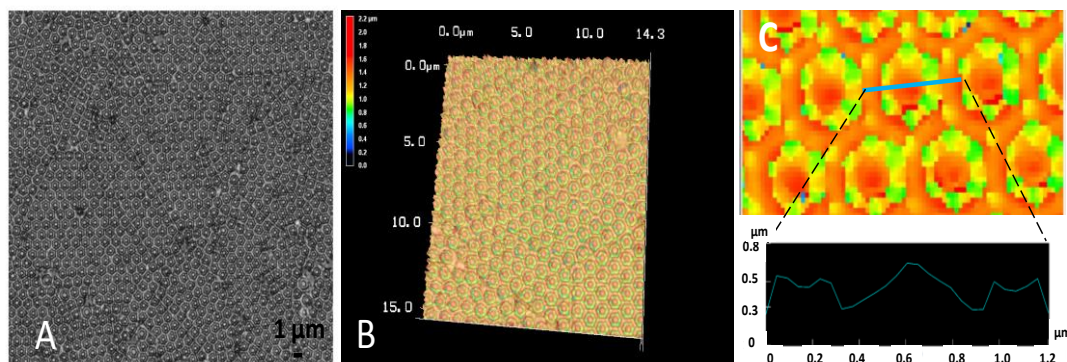


Fig. 78. Confocal 3D microscope images of a poly-[Ru^{II}-pyrrole]/GCE electrogenerated with 900 nm beads: **(A)** laser image; **(B)** 3D image and **(C)** height image accompanied with a pore profile image³⁵⁷

In the case of the metallopolymer obtained after dissolution of the 100 nm diameter nanobeads, an average thickness of 250 nm for the metallopolymer was measured, underlining the multilayered structure. In this case the average pore size is close to 100 nm, confirming the efficient dissolution of 100 nm nanobeads. SEM images (Figures 79 A and 79 B) indicate the achievement of a highly porous and reproducible electrogenerated metallopolymer³⁵⁷.

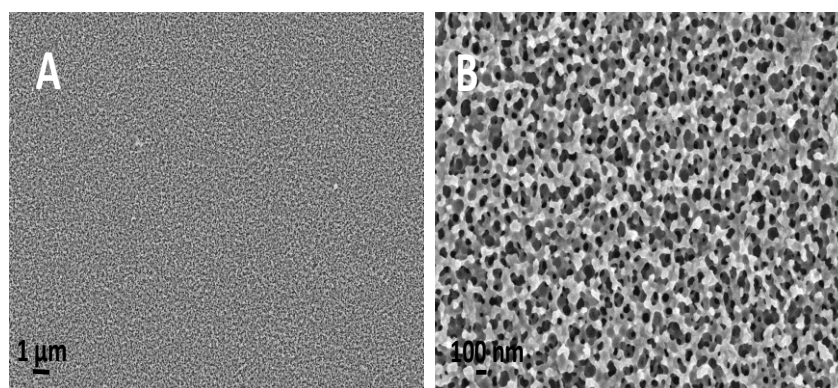


Fig. 79. SEM images of poly-[Ru^{II}-pyrrole]/GCE electrogenerated with 100 nm beads³⁵⁷

6.3.3. Photoelectrochemical studies

Due to the metal to ligand charge transfer transition band of the Ru^{II}-pyrrole complex, photoelectrochemical studies were performed by irradiation in the visible region, using filters absorbing light below 420 nm and beyond 630 nm (Figure 80).

Cathodic photocurrents were measured for 0.5 μm-thick metallopolymer, 900 nm and 100 nm beads nanopatterned metallopolymer in the presence of an oxidative quencher, pentaaminechloro cobalt(III) chloride. Maximum photocurrents of 0.25 μA cm⁻² and shortest time responses of 8 s were observed for the nanostructured (100 nm) mesoporous metallopolymer.

The microstructured polymer (900 nm) exhibits photocurrents of $0.12 \mu\text{A cm}^{-2}$ and time responses of 65 s. Thick-planar metallopolymer shows photocurrents of $0.09 \mu\text{A cm}^{-2}$ and time responses of 95 s. These experiments confirmed the excellent photoelectrochemical properties of nanostructured poly[Ru-pyrrole] obtained by using NSL, properties arisen from the excellent accessibility of the electrolyte, and preventing Ru^{II} photosensitive unit from self-quenching phenomenon^{347,357}.

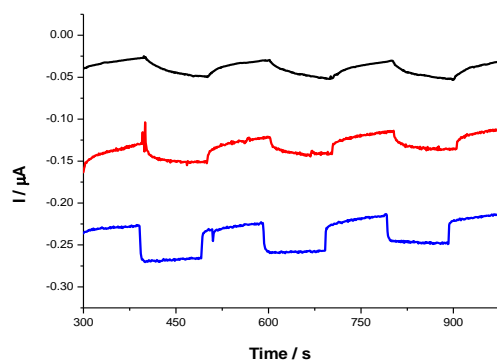


Fig. 80. Cathodic photocurrent obtained in the presence 15 mmol L^{-1} pentaaminechloro cobalt(III) chloride in 0.1 mol L^{-1} acetate buffer (pH 5), with flat poly-[Ru^{II} -pyrrole]/GCE (black), 900 nm beads microstructured poly-[Ru^{II} -pyrrole]/GCE (red) and 100 nm beads nanostructured poly-[Ru^{II} -pyrrole]/GCE (blue)³⁵⁷

This metallopolymer can be used with other types of pyrrole-monomers, such as: pyrrole-nitrilotriacetic acid (Py-NTA), pyrrole-cyclodextrin (Py-CD), in order to immobilize biomolecules at the electrode surface taking advantages of both specific characteristics: photoelectrochemical and anchoring properties.

In the case of the combination with Py-NTA, after the immobilization of proteins (albumins, toxin and antibody) on the copolymer film surface (using Cu^{2+} coordinated to NTA groups attached to pyrrole), the cathodic photocurrent intensity decreased after each step indicating that the immobilization of the bioelements hindered the access of the electron acceptor to the electrode (Figure 81). The photocurrent response after incubation with bovine serum albumin (BSA) was $0.053 \mu\text{A cm}^{-2}$, value which decreased at $0.038 \mu\text{A cm}^{-2}$ after incubation with biotin cholera toxin and furthermore at $0.024 \mu\text{A cm}^{-2}$ after the last step of incubation with anticholera toxin antibody. The decrease in photocurrent intensity was caused by the increase in steric hindrances towards the diffusion of the quencher molecules to the Ru^{II} -pyrrole film due to the biomolecules binding. Pyrrole functionalized with NTA moieties was used as immobilization system for biotin-tagged cholera toxin via Cu^{2+} coordination system, while Ru^{II} -pyrrole was employed as a photoelectrochemical transducing molecule.

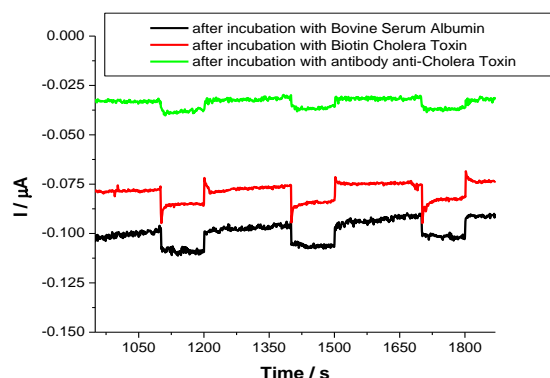


Fig. 81. Cathodic photocurrent measurements on GCEs modified by electropolymerization of a mixture of 2 mmol L^{-1} Ru^{II} -pyrrole and Py-NTA in 1:10 molar ratio (electropolymerization conditions: $0.0 \text{ V} - 1.1 \text{ V}$, 10 scans, 100 mV s^{-1}) in the presence 15 mmol L^{-1} of pentaaminechloro cobalt(III) chloride in acetate buffer 0.1 mol L^{-1} , pH 5

The other possibility consisted in the electrogeneration of poly-[Ru^{II} -pyrrole] which was followed by the electrodeposition of poly(Py-CD). The pyrrole monomer functionalized with CD was used for the complexation properties of CD due to its cavity which can act as a host for biomolecules tagged with appropriate molecules such as adamantane or biotin. A good coverage with poly(Py-CD) is indicated by both CV scans in electrolyte solution and anodic photocurrent response generated in the presence of sodium ascorbate (Figure 82). The current intensity for the $\text{Ru}(\text{II})/\text{Ru}(\text{III})$ peak from poly-[Ru^{II} -pyrrole] was reduced with almost 50 % after the electropolymerization of Py-CD, while ΔE of 60 mV for poly-[Ru^{II} -pyrrole] was increased at $\Delta E = 100 \text{ mV}$ (Figure 82 A). These modifications are caused by the poly(Py-CD) film which acts as a barrier for the electrolyte diffusion through poly-[Ru^{II} -pyrrole] film. The same behavior was observed for photocurrent measurements when the electrodeposition of poly(Py-CD) film decreased the photocurrent value with 50 % hindering the diffusion and thus the accessibility of the quencher molecules through the poly-[Ru^{II} -pyrrole] film (Figure 82 B).

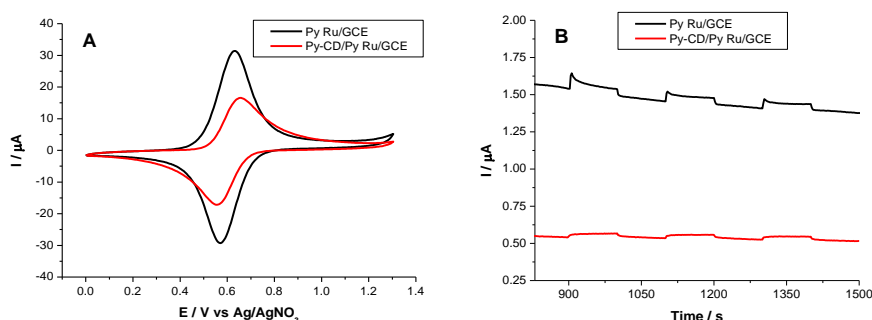


Fig. 82. (A) CVs in 0.1 mol L^{-1} LiClO_4 (ACN, 50 mV s^{-1}) for the modified GCEs; **(B)** anodic photocurrent response in 10 mmol L^{-1} sodium ascorbate in phosphate buffer 0.1 mol L^{-1} , pH 7 for the modified GCEs (polymerization conditions: 1 mmol L^{-1} of monomers, $0.0 \text{ V} - 1.1 \text{ V}$, 10 scans, 100 mV s^{-1})

The pyrrole monomer functionalized with CD was used for the complexation between CD cavity and adamantane tagged glucose oxidase (GOX-Ad) and then it was tested for glucose oxidation by chronoamperometry. The biosensor response to glucose corroborated the enzyme immobilization by host-guest inclusion complex formation (Figure 83).

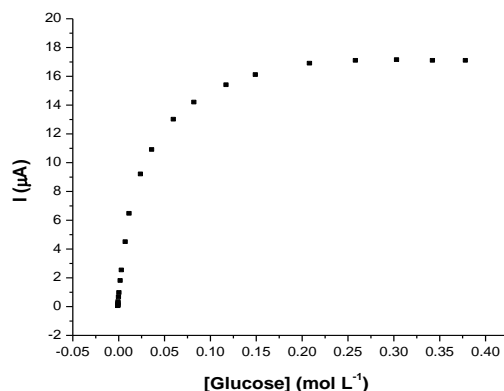


Fig. 83. Calibration curves for glucose oxidation obtained at Pt electrode electropolymerized with 1 mmol L^{-1} Py Ru and 1 mmol L^{-1} Py-CD by electrolysis (0.5 mC), incubation 1 h with $20 \text{ }\mu\text{L}$ GOX-Ad 1 mg mL^{-1}

6.4. Conclusions

The achievement of highly organized micro and nanostructures showed enhanced features for the photosensitive electrogenerated poly-[Ru^{II}-pyrrole] films. By using different nanosphere diameters, various morphologies at micro and nanoscale could be obtained and characterized. The poly-[Ru^{II}-pyrrole] film was further modified with other types of pyrrole derivatives presenting complexation properties in order to immobilize biomolecules at the electrode surface taking advantages of both specific features: photoelectrochemical and anchoring properties. The combination of NSL and electropolymerization represents a powerful technique for the achievement of highly reproducible and homogenous photosensitive nanostructures and interesting platforms for biosensing applications. As perspectives, the nanosphere lithography can be used as a promising step towards 3D films of cyclodextrins.

7. General conclusions

The aim of this study was to develop novel cyclodextrin modified electrodes for pharmaceutical and biomedical applications. The cyclodextrin influence was investigated both in solution and on the electrode modification.

The first objective of this work was to study the β -cyclodextrin effect on the electrochemical behavior of the pharmaceutical substances as guest molecules (uric acid, ascorbic acid, aminophylline, caffeine, caffeine citrate, theophylline, acetaminophen). The formation of inclusion complexes between β -cyclodextrin and these molecules caused a decrease in the peak current and a positive shift in the anodic peak potential, results which were explained by the concentration decrease of the free analyte and by the decrease of the diffusion coefficient for the inclusion complexes. The FTIR spectra confirmed the formation of inclusion complexes through the vibration bands modifications of the analytes and of β -cyclodextrin consisting in shift, attenuation and disappearance of some bands in the complexes spectra.

The sensitive determination of ascorbic and uric acids was achieved by using carbon paste electrodes modified with β -cyclodextrin. The increase of current intensity and negative potential shift were attributed to the inclusion complexes formation which led to the preconcentration of the analytes at the electrode surface.

The glassy carbon electrodes modified with β -cyclodextrin in polyethyleneimine film were elaborated for the investigation of the electrochemical behavior of ascorbic acid and uric acid by using square wave voltammetry. The modified electrodes were characterized by RAMAN and electrochemical impedance spectroscopy and optical microscopy. This sensor allowed a well separation of the voltammetric signals and the shifting to more negative of the oxidation peaks potential for the two compounds. An important performance of this sensor was the simultaneous determination of ascorbic acid and uric acid due to the well separation of signals of these compounds. These modified electrodes were applied for the detection and determination of ascorbic acid in two pharmaceutical products with good performances: low detection limit, good linear range, the absence of interferences in the case of injectable solution. The sensor main advantage was the simultaneous determination of uric and ascorbic acids in urine samples. Good recoveries were obtained using electrochemical methods which were confirmed using spectrophotometric method in the case of the pharmaceutical samples and chromatographic method for the urine samples.

The biosensor elaborated by using layer-by-layer deposition of reduced graphene oxide, β -cyclodextrin, polyethylenimine and tyrosinase was tested for the sensitive and selective determination of dopamine. The optimization process included: the layers number and the type of graphene, the accumulation time and the deposition method. The obtained nanocomposite was then characterized by Raman and FTIR spectroscopy and optical microscopy.

The optimized biosensor was successfully applied for dopamine determination in pharmaceutical products, serum and urine samples with good recoveries, enhanced sensitivity and good selectivity.

A new synthesized pyrrole derivative bearing a cyclodextrin moiety was used for a non-covalent modification of reduced graphene oxide. Cyclodextrin was involved in a better solubilization of graphene in water as an efficient aqueous dispersant, meanwhile pyrrole was responsible for generating an electropolymerized coating, both aspects being important for the graphene electrodeposition. This new nanocomposite was characterized by spectral, microscopic and electrochemical techniques. These electropolymerizable graphene sheets were electrodeposited on glassy carbon electrodes doubling their active surface area. Furthermore, the functionalized graphene in combination with an amphiphilic pyrrole derivative and tyrosinase were used for the elaboration of a biosensor tested for catechol and dopamine determination.

β -cyclodextrin was used for the solubilization in water of new synthesized tetrazines functionalized with adamantane and naphthalimide groups, organic anchoring groups which fit the requirements for inclusion within cyclodextrin. The tetrazine ring itself is hydrophobic and small enough to be also included in the cyclodextrin cavity. The behavior of these compounds in aqueous solutions, in the presence or absence of cyclodextrin, was investigated by electrochemical and fluorescence methods. The immobilization of tetrazines onto various types of electrodes modified with poly-pyrrole-cyclodextrin was also reported and was examined by electrochemical, microscopic and spectroscopic techniques. Tetrazines were also entrapped into a polymeric film of an amphiphilic pyrrole derivative. These fluorophores were used for glucose oxidase immobilization at the electrode surface through the inclusion complexes formed between tetrazine and cyclodextrin.

The electropolymerization of a Ru(II)-pyrrole monomer by using cyclic voltammetry was combined with nanospheres lithography obtaining highly ordered porosity in photosensitive metallopolymers. By using latex beads with different diameters (100 nm and 900 nm), various morphologies at micro and nanoscale were obtained and characterized by microscopy. The achievement of highly organized micro and nanostructures showed enhanced features for the photosensitive electrogenerated poly-[Ru^{II}-pyrrole] films. Furthermore, poly-[Ru^{II}-pyrrole] film was modified with other types of pyrrole derivatives presenting complexation properties in order to immobilize biomolecules at the electrode surface taking advantages of both specific features: photoelectrochemical and anchoring properties.

8. Originality of the thesis

The originality of the thesis consists in the development of a sensor modified with β -cyclodextrin entrapped in polyethyleneimine film which allowed a well separation of the voltammetric signals of ascorbic acid and uric acid. An important performance of this sensor was the simultaneous determination of ascorbic acid and uric acid due to the well separation of signals corresponding to the electrochemical oxidation processes of these compounds. These modified electrodes were applied for the detection and determination of ascorbic acid in two pharmaceutical products with good performances: low detection limit, good linear range, absence of interferences in the case of injectable solution. The sensor main advantage was the simultaneous determination of uric and ascorbic acids in urine samples. Taking advantage of the permeation of ascorbic acid and uric acid through the β -cyclodextrin and polyethyleneimine film, via the host-guest interaction between β -cyclodextrin and ascorbic acid and uric acid, the simultaneous detection of the two compounds from urine samples was successfully achieved.

The elaboration of two types of biosensors based on reduced graphene oxide and β -cyclodextrin is a new approach for dopamine detection. The first one was elaborated through layer-by-layer deposition of reduced graphene oxide and β -cyclodextrin and then it was tested for the sensitive and selective determination of dopamine. The optimized biosensor was successfully applied for dopamine determination in pharmaceutical products, serum and urine samples with good recoveries. The second one consisted in a new nanostructured graphene framework with electropolymerizable properties. A new synthesized pyrrole derivate bearing a cyclodextrin moiety was used for a non-covalent modification of reduced graphene oxide. Cyclodextrin was involved in a better solubilization of graphene in water as an efficient aqueous dispersant, meanwhile pyrrole was responsible for generating an electropolymerized coating, both aspects being important for the graphene electrodeposition. These electropolymerizable graphene sheets were electrodeposited on glassy carbon electrodes and demonstrated excellent nanostructured support for the fabrication of a tyrosinase-based composite bioelectrode for sensing of catechol and dopamine.

Another element of novelty is, to our knowledge, for the first time, the solubilisation of tetrazines in water and their electrochemical characterization in this unusual medium. 4 tetrazines functionalized with different substituents like adamantane and naphthalimide groups, specially adapted to the inclusion inside a cyclodextrin cavity, were synthesized and characterized. In addition, the tetrazine ring itself may also fit the requirements for inclusion within cyclodextrin. These fluorophores were solubilised in aqueous solutions using β -cyclodextrin and gold nanoparticles modified with CD. These redox supramolecular assembly were characterized in water by electrochemical and fluorescence measurements. The immobilization of tetrazines onto various types of electrodes modified with poly-pyrrole-cyclodextrin was also reported and was examined by electrochemical,

microscopic and spectroscopic techniques. Tetrazines were also entrapped into a polymeric film of an amphiphilic pyrrole derivative. These fluorophores were used for the immobilization of glucose oxidase modified by CD groups at the electrode surface through the inclusion complexes formed between tetrazine and cyclodextrin.

Another original contribution is the combination of nanosphere lithography with electropolymerization of a Ru(II)-pyrrole monomer. By using latex beads with different diameters (900 nm and 100 nm), highly ordered porosity in photosensitive metallopolymers was achieved. Enhanced photocurrent was observed, being inversely proportional to the polystyrene bead diameter size. Furthermore, poly-[Ru^{II}-pyrrole] film was modified with other types of pyrrole derivatives presenting complexation properties in order to immobilize biomolecules at the electrode surface taking advantages of both specific features: photoelectrochemical and anchoring properties.

REFERENCES

1. Del Valle MEM. Cyclodextrins and their uses. *Process Biochemistry*. 2004;39(9):1033-1046.
2. Abd-Elgawad R, Shima E. Electrochemistry of cyclodextrin inclusion complexes of pharmaceutical compounds. *The Open Chemical and Biomedical Methods Journal*. 2010;3:74-85.
3. Dodziuk H. Cyclodextrins and their complexes. Wiley-VCH Verlag GmbH & Co. KGaA, Weinheim. 2006.
4. Szejtli J, Osa T. *Comprehensive supramolecular chemistry*. Vol. 3. Cyclodextrins. Elsevier Science Ltd. Oxford, 1996.
5. Szejtli J. Past, present and future of cyclodextrin research. *Pure and Applied Chemistry*. 2004;10(76):1825-1845.
6. Szejtli J. Introduction and general Overview of cyclodextrin chemistry. *Chemical Reviews*. 1998;98:1743-1753.
7. Connors KA. The Stability of cyclodextrin complexes in solution. *Chemical Reviews*. 1997;97:1325-1357.
8. http://www.chemiedidaktik.uni-wuppertal.de/disido_cy/cyen/info/nav/nav_info_en.html
9. Suflet DM, Chitanu GC, Aldea G, Anghelescu-Dogaru AG, Popescu I. Noi materiale funcționale din resurse regenerabile. Grant CNCSIS, tip At, 33527/2003.
10. Popovici I, Lupuleasa D. *Tehnologie Farmaceutică*. Editura Polirom. Colecția Bios. vol. 1, Ediția III, Iași. 2011;290-292.
11. Zhou JW, Ritter H. Cyclodextrin functionalized polymers as drug delivery systems. *Polymer Chemistry*. 2010;1:1552-1559.
12. Higuchi T, Connors KA. Phase-solubility techniques. *Advances in Analytical Chemistry and Instrumentation*. 1965; 4:117-122.
13. Singh M, Sharman R, Banerjee UC. Biotechnological applications of cyclodextrins. *Biotechnology Advances*. 2002;20:341-359.
14. Mura P. Analytical techniques for characterization of cyclodextrin complexes in aqueous solution: A review. *Journal of Pharmaceutical and Biomedical Analysis*. 2014;101:238-250.
15. Singh R, Bharti N, Madan J, Hiremath SN. Characterization of cyclodextrin inclusion complexes - A review. *Journal of Pharmaceutical Science and Technology*. 2010;2(3):171-183.
16. Chen Y, Zhang YM, Liu Y. Multidimensional nanoarchitectures based on cyclodextrins. *Chemical Communications*. 2010;46:5622-5633.
17. Ferancová A, Labuda J. Cyclodextrins as electrode modifiers. *Fresenius Journal of Analytical Chemistry*. 2001;370:1-10.
18. Song JP, Guo YJ, Shuang SM, Dong C. Study on the supramolecular systems of two basic violets with cyclodextrins by MWNTs/Nafion modified glassy carbon electrode. *Chinese Chemical Letters*. 2009;20:981-984.
19. Roa-Morales G, Galicia L, Hernandez AR, Ramirez-Silva MT. Electrochemical study on the selective formation of [Pb(cyclodextrin)²⁺] surface inclusion complexes at the carbon paste electrode/CIO₄⁻ 1M interphase. *Electrochimica Acta*. 2005;20:1925-1930.

20. Radi AE, Eissa S. Electrochemical study of gliclazide and its complexation with β -cyclodextrin. *Electroanalysis*. 2010;22(24):2991-2996.
21. Gao Z-N, Li H-L. Spectroscopic and electrochemical studies of phenylhydrazine β -cyclodextrin inclusion complex and its adsorption behaviors. *Acta Physico-Chimica Sinica*. 1999;15(11):1005-1010.
22. Gao ZN, Wen XL, Li HL. Study of the inclusion complexes of catecholamines with β -cyclodextrin by cyclic voltammetry. *Polish Journal of Chemistry*. 2002;76:1001-1007.
23. Shehata IS, Ibrahim MS. Binding of anti-inflammatory drug indomethacin with cyclodextrin and DNA: Solubility, spectroscopic, and voltammetric studies. *Canadian Journal of Chemistry*. 2001;79:1431-1438.
24. Shehata IS, Ibrahim MS, Sultan MR. The antimicrobial nalidixic acid as a probe for molecular recognition of α - and β -cyclodextrins. *Canadian Journal of Chemistry*. 2002;80:1313-1320.
25. Ibrahim MS, Shehata IS, Al-Nayeli AA. Voltammetric studies of the interaction of lumazine with cyclodextrins and DNA. *Journal of Pharmaceutical and Biomedical Analysis*. 2002;28:217-225.
26. Yáñez C, Zamora C, Jara P. In Electrochemical study of inclusion complexes cyclodextrin/steroids. *Proceedings of 208th Meeting of The Electrochemical Society; Los Angeles, CA, October 16-21, 2005*;2137.
27. Amatore C, Buriez O, Labbe E, Verpeaux JN. Supramolecular effects of cyclodextrins on the electrochemical reduction and reactivity of aromatic carbonyl compounds. *Journal of Electroanalytical Chemistry*. 2008;621:134-145.
28. Mertins O, Buriez O, Labbé E, Fang PP, Hillard E, Vessières A, Jaouen G, Tian ZQ, Amatore C. Further insights into hydrophobic interactions between ferrocenyl-tamoxifen drugs and non-polar molecular architectures at electrode surfaces. *Journal of Electroanalytical Chemistry*. 2009;635:13-19.
29. Li W, Jin GY, Chen H, Kong JL. Highly sensitive and reproducible cyclodextrin-modified gold electrodes for probing trace lead in blood. *Talanta*. 2009;78:717–722.
30. Ortiz M, Torrén M, Alakulppi N, Strömbom L, Frago A, O'Sullivan KC. Amperometric supramolecular genosensor self-assembled on cyclodextrin-modified surfaces. *Electrochemistry Communications*. 2011;13:578–581.
31. Fernández I, Araque E, Martínez-Ruiz P, Di Pierro P, Villalonga R, Pingarrón JM. Gold surface patterned with cyclodextrin-based molecular nanopores for electrochemical assay of transglutaminase activity. *Electrochemistry Communications*. 2014;40:13–16.
32. Damos FS, Luz RCS, Kubota LT. Electrochemical properties of self-assembled monolayer based on mono-(6-deoxy-6-mercapto)- β -cyclodextrin toward controlled molecular recognition. *Electrochimica Acta*. 2007;57:1945–1953.
33. D'Annibale A, Regoli R, Sangiorgio P, Ferri T. Preparation and electrochemical characterization of a β -cyclodextrin-based chemically modified electrode. *Electroanalysis*. 1999;11(7):505-510.
34. Chmurski K, Temeriusz A, Bilewicz R. Measurement of ibuprofen binding to mixed monolayers containing β -cyclodextrin active sites. *Journal of Inclusion Phenomena and Macrocyclic Chemistry*. 2004;49:187–191.
35. Chmurski K, Majewska UE, Bilewicz R. Analytical applications of gold electrodes modified with monolayers of thiolated cyclodextrins. *Journal of Inclusion Phenomena and Macrocyclic Chemistry*. 2007;57:385–389.
36. Villalonga R, Tachibana S, Cao R, Ortiz PD, Gomez L, Asano Y. Supramolecular-mediated immobilisation of L-phenylalanine dehydrogenase on β -cyclodextrin-modified gold nanospheres. *Journal of Experimental Nanoscience*. 2006;1(2):249–260.
37. Villalonga R, Fujii A, Shinohara H, Asano Y, Cao R, Tachibana S, Ortiz P. Supramolecular-mediated immobilization of L-phenylalanine dehydrogenase on

- cyclodextrin-coated Au electrodes for biosensor applications. *Biotechnology Letters*. 2007;29:447-452.
38. Fragoso A, Almirall E, Cao R, Echegoyen L, González-Jonte R. A supramolecular approach to the selective detection of dopamine in the presence of ascorbate. *Chemical Communications*. 2004;10(19):2230-2231.
 39. Li J, Wu X, Yu Y, Le S. Self-assembled sulfonated β -Cyclodextrin layer on gold electrode for the selective electroanalysis of dopamine. *Journal of Solid State Electrochemistry*. 2009;13:1811-1818.
 40. Majewska UE, Chmurski K, Biesiada K, Olszyna AR, Bilewicz R. Dopamine oxidation at per(6-deoxy-6-thio)- α -cyclodextrin monolayer modified gold electrodes. *Electroanalysis*. 2006;18:1463-1470.
 41. Frasconi M, Mazzei F. Electrochemical and surface Plasmon resonance characterization of β -cyclodextrin-based self-assembled monolayers and evaluation of their inclusion complexes with glucocorticoids. *Nanotechnology*. 2009;20(28):285502.
 42. Amorim CG, Araujo AN, Montenegro MCBSM, Silva VL. Cyclodextrin-based potentiometric sensors for midazolam and diazepam. *Journal of Pharmaceutical and Biomedical Analysis*. 2008;48:1064–1069.
 43. Khaled E, Kamel MS, Hassan HNA, Aboul-Enein HY. Cyclodextrin-based dextromethorphan potentiometric sensors. *Journal of Electroanalytical Chemistry*. 2011;661:239–244.
 44. Hassan SSM, Kamel AH, El-Naby HA. New potentiometric sensors based on selective recognition sites for determination of ephedrine in some pharmaceuticals and biological fluids. *Talanta*. 2013;103:330–336.
 45. Sousa TFA, Amorim CG, Montenegro MCBSM, Araújo AN. Cyclodextrin based potentiometric sensor for determination of ibuprofen in pharmaceuticals and waters. *Sensors and Actuators B*. 2013;176:660-666.
 46. Lenik J. A new potentiometric electrode incorporating functionalized β -cyclodextrins for diclofenac determination. *Material Science and Engineering: C*. 2014;45:109–116.
 47. Elhag S, Ibupoto ZH, Liu XJ, Nur O, Willander M. Dopamine wide range detection sensor based on modified Co_3O_4 nanowires electrode. *Sensors and Actuators B*. 2014;203:543–549.
 48. Ferancová A, Korgová E, Buzinkaiová T, Kutner W, Stepanek I, Labuda J. Electrochemical sensors using screen-printed carbon electrode assemblies modified with the β -cyclodextrin or carboxymethylated β -cyclodextrin polymer films for determination of tricyclic antidepressive drugs. *Analytica Chimica Acta*. 2001;447:47–54.
 49. Kim H, Chang SC, Shim YB. α -Cyclodextrin modified screen printed graphite electrodes for detection of phenols. *Bulletin of the Korean Chemical Society*. 2002;23(3):427-431.
 50. Alarcón-Ángeles G, Guix M, Silva WC, Ramírez-Silvad MT, Palomar-Pardavé M, Romero-Romoe M, Merkoci A. Enzyme entrapment by β -cyclodextrin electropolymerization onto a carbon nanotubes-modified screen-printed electrode. *Biosensors and Bioelectronics*. 2010;26:1768–1773.
 51. El-Hady DA. Selective and sensitive hydroxypropyl- β -cyclodextrin based sensor for simple monitoring of (+)-catechin in some commercial drinks and biological fluids. *Analytica Chimica Acta*. 2007;593:178–187.
 52. El-Hady D, El-Maali N. Selective square wave voltammetric determination of (+)-catechin in commercial tea samples using β -cyclodextrin modified carbon paste electrode. *Microchimica Acta*. 2008;161:225-231.
 53. Yanez C, Nunez-Vergara LJ, Squella JA. Determination of nitrendipine with β -cyclodextrin modified carbon paste electrode. *Electroanalysis*. 2002;14:559-562.

54. Rao CN, Subbarayudu K, Rao CCN, Venkateswarlu P. Electrochemical reduction behaviour of donepezil at β -cyclodextrin modified carbon paste electrode. *Port Electrochimica Acta*. 2010;28(5):349-357.
55. Morales RG, Ramirez T, Galicia SL. Carbon paste electrodes electrochemically modified with cyclodextrins. *Journal of Solid State Electrochemistry*. 2003;7:355–360.
56. Guorong Z, Xiaolei W, Xingwang S, Tianling S. β -cyclodextrin–ferrocene inclusion complex modified carbon paste electrode for amperometric determination of ascorbic acid. *Talanta*. 2000;51:1019–1025.
57. Ferancová A, Korgová E, Mikó R, Labuda J. Determination of tricyclic antidepressants using a carbon paste electrode modified with β -cyclodextrin. *Journal of Electroanalytical Chemistry*. 2000;492:74-77.
58. Ramírez-Silva MT, Corona-Avendaño S, Alarcón-Ángeles G, Rojas-Hernández A, Romero-Romo M, Palomar-Pardavé M. Dopamine electrochemical behavior onto an electrode modified with a β -cyclodextrin polymer. *ECS Transactions*. 2009;20(1):151-157.
59. Reddy TM, Sreedhar M, Reddy SJ. Electrochemical determination of sparfloxacin in pharmaceutical formulations and urine samples using a β -cyclodextrin modified carbon paste electrode. *Analytical Letters*. 2003;36:1365-1379.
60. Reddy TM, Balaji K, Reddy SJ. Voltammetric behavior of some fluorinated quinolone antibacterial agents and their differential pulse voltammetric determination in drug formulations and urine samples using a β -cyclodextrin-modified carbon paste electrode. *Journal of Analytical Chemistry*. 2007;62(2):168–175.
61. Balaji K, Reddy GVR, Reddy TM, Reddy SJ. Determination of prednisolone, dexamethasone and hydrocortisone in pharmaceutical formulations and biological fluid samples by voltammetric techniques using β -cyclodextrin modified carbon paste electrode. *African Journal of Pharmacy and Pharmacology*. 2008;2(8):157-166.
62. Ramirez OD, Ramirez SMT, Palomar PM, Alarcón-Ángeles G, Rojas HA, Romero RM. Development a boron potentiometric determination methodology using a carbon paste electrode modified with a β -Cyclodextrine-Azomethine-H inclusion complex. *ECS Transactions*. 2009;20(1):13-19.
63. Narasimha RC, Madhavi G, Venkateswarlu P. Electrochemical behavior of anagrelide and its determination. *Oriental Journal of Chemistry*. 2009;25:425-428.
64. Zhang FF, Gu SQ, Ding YP, Zhang Z, Li L. A novel sensor based on electropolymerization of β -cyclodextrin and l-arginine on carbon paste electrode for determination of fluoroquinolones. *Analytica Chimica Acta*. 2013;770:53–61.
65. Guzmán-Hernández DS, Palomar-Pardavé M, Rojas-Hernández A, Corona-Avendano S, Romero-Romo M, Ramírez-Silva MT. Electrochemical quantification of the thermodynamic equilibrium constant of the tenoxicam- β -cyclodextrin inclusion complex formed on the surface of a poly- β -cyclodextrin-modified carbon paste electrode. *Electrochimica Acta*. 2014;140:535–540.
66. Reena R. Gaichore, Ashwini K. Srivastava. Voltammetric determination of nifedipine using a β -cyclodextrin modified multi-walled carbon nanotube paste electrode. *Sensors and Actuators B*. 2013;188:1328– 1337
67. Palomar-Pardavé M, Corona-Avendaño S, Romero-Romo M, Alarcón-Ángeles G, Merkoçi A, Ramírez-Silva MT. Supramolecular interaction of dopamine with β -cyclodextrin: An experimental and theoretical electrochemical study. *Journal of Electroanalytical Chemistry*. 2014;717-718:103–109.
68. Pingarron JM, Yanez-Sedeno P, Gonzalez-Cortes A, Gold nanoparticle-based electrochemical biosensors. *Electrochimica Acta*. 2008;53:5848–5866.
69. Guo SJ, Wang EK. Synthesis and electrochemical applications of gold nanoparticles. *Analytica Chimica Acta*. 2007;598:181–192.

70. Villalonga R, Cao R, Fragoso A, Damia AE, Ortiz PD, Caballero J. Supramolecular assembly of β -cyclodextrin-modified gold nanoparticles and Cu, Zn-superoxide dismutase on catalase. *Journal of Molecular Catalysis B: Enzymatic*. 2005;35:79–85.
71. Han JT, Huang KJ, Li J, Liu YM, Yu M. β -cyclodextrin-cobalt ferrite nanocomposite as enhanced sensing platform for catechol determination. *Colloids and Surfaces B: Biointerfaces*. 2012;98:58–62.
72. Badruddoza AZM, Rahman MT, Ghosh S, Hossain MZ, Shi JZ, Hidajat K, Uddin MS. β -cyclodextrin conjugated magnetic, fluorescent silica core-shell nanoparticles for biomedical applications. *Carbohydrate Polymers*. 2013;95:449–457.
73. Abdolmaleki A, Mallakpour S, Borandeh S. Tailored functionalization of ZnO nanoparticle via reactive cyclodextrin and its bionanocomposite synthesis. *Carbohydrate Polymers*. 2014;103:32–37.
74. Zhu J, He J, Du XY, Lu RH, Huang LZ, Ge X. A facile and flexible process of β -cyclodextrin grafted on Fe_3O_4 magnetic nanoparticles and host-guest inclusion studies. *Applied Surface Science*. 2011;257:9056–9062.
75. Chen XF, Zhou M, Chang YP, Ren CL, Chen HL, Chen XG. Novel synthesis of β -cyclodextrin functionalized CdTe quantum dots as luminescent probes. *Applied Surface Science*. 2012;263:491–496.
76. Algarra M, Campos BB, Aguiar FR, Rodriguez-Borges JE, Esteves da Silva JCG. Novel β -cyclodextrin modified CdTe quantum dots as fluorescence nanosensor for acetylsalicylic acid and metabolites. *Materials Science and Engineering C*. 2012;32:799–803.
77. Yoon S, Nichols WT. Cyclodextrin directed self-assembly of TiO_2 nanoparticles. *Applied Surface Science*. 2013;285:517–523.
78. Andrade PF, Fonseca de Faria A, Soares da Silva D, Bonacin AJ, do Carmo Goncalves M. Structural and morphological investigations of β -cyclodextrin-coated silver nanoparticles. *Colloids and Surfaces B: Biointerfaces*. 2014;118:289–297.
79. Manivannan S, Ramaraj R. Synthesis of cyclodextrin-silicate sol-gel composite embedded gold nanoparticles and its electrocatalytic application. *Chemical Engineering Journal*. 2012;210:195–202.
80. Holzinger M, Bouffier L, Villalonga R, Cosnier S. Adamantane/ β -cyclodextrin affinity biosensors based on single-walled carbon nanotubes. *Biosensors and Bioelectronics*. 2009;24:1128–1134.
81. Huang T, Meng F, Qi LM. Facile synthesis and one-dimensional assembly of cyclodextrin-capped gold nanoparticles and their applications in catalysis and surface-enhanced Raman scattering. *The Journal of Physical Chemistry C*. 2009;113:13636–13642.
82. Sun L, Crook RM, Chechik V. Preparation of polycyclodextrin hollow spheres by templating gold nanoparticles. *Chemical Communications*. 2001:359–360.
83. Chen M, Diao GW. Electrochemical study of mono-6-thio- β -cyclodextrin/ferrocene capped on gold nanoparticles: Characterization and application to the design of glucose amperometric biosensor. *Talanta*. 2009;80:815–820.
84. Tian XQ, Cheng CM, Yuan HY, Du JA, Xiao D, Xie SP, Choi MMF. Simultaneous determination of l-ascorbic acid, dopamine and uric acid with gold nanoparticles- β -cyclodextrin-graphene-modified electrode by square wave voltammetry. *Talanta*. 2012;93:79–85.
85. Díez P, Villalonga R, Villalonga ML, Pingarrón JM. Supramolecular immobilization of redox enzymes on cyclodextrin-coated magnetic nanoparticles for biosensing applications. *Journal of Colloid and Interface Science*. 2012;386:181–188.
86. Gao JA, Guo ZK, Su FJ, Gao L, Pang XH, Cao W, Du B, Wei Q. Ultrasensitive electrochemical immunoassay for CEA through host-guest interaction of β -cyclodextrin

- functionalized graphene and Cu@Ag core-shell nanoparticles with adamantine-modified antibody. *Biosensors and Bioelectronics*. 2015;63:465–471.
87. Lin DJ, Wu J, Ju HX, Yan F. Signal amplification for electrochemical immunosensing by in situ assembly of host-guest linked gold nanorod superstructure on immunocomplex. *Biosensors and Bioelectronics*. 2013;45:195–200.
 88. Yu Y, Xin Y, Feng YH, Min LZ, Li LY, Li SG, Qin YR. Electrochemical sensor for cinchonine based on a competitive host-guest complexation. *Analytica Chimica Acta*. 2005;528:135–142.
 89. Alonso LMA, Dominguez RO, Arcos MMJ. Optimization of a cyclodextrin-based sensor for rifampicin monitoring. *Electrochimica Acta*. 2005;50:1807–1811.
 90. Izaoumen N, Bouchta D, Zejli H, El Kaoutit M, Stalcup AM, Tamsamani KR. Electrosynthesis and analytical performances of functionalized poly(pyrrole/ β -cyclodextrin) films. *Talanta*. 2006;66:111–117.
 91. Izaoumen N, Bouchta D, Zejli H, El Kaoutit M, Tamsamani KR. The electrochemical behavior of neurotransmitters at a poly (pyrrole- β -cyclodextrin) modified glassy carbon electrode. *Analytical Letters*. 2005;38:1869-1885.
 92. Bouchta D, Izaoumen N, Zejli H, El Kaoutit M, Tamsamani KR. Electroanalytical properties of a novel PPY/ γ -cyclodextrin coated electrode. *Analytical Letters*. 2005;38:1019-1036.
 93. Luk HN, Jheng RF, Tsai TC, Wu RJ. Novel electrochemical impedance detection for rocuronium by using polypyrrole and cyclodextrin as the sensing material. *Sensors Letters*. 2009;7:1093-1099.
 94. Yang Y, Lei CX, Liu ZM, Liu YL, Shen GL, Yu RQ. Highly selective dopamine determination by using carboxymethylated β -cyclodextrin polymer film modified electrode. *Analytical Letters*. 2004;37:2267-2282.
 95. Reece DA, Ralph SF, Wallace GG. Metal transport studies on inherently conducting polymer membranes containing cyclodextrin dopants. *Journal of Membrane Science*. 2005;249:9–20.
 96. Tanji Y, Wanzhi W, Jinxiang Z. Selective detection of dopamine in the presence of ascorbic acid by use of glassy-carbon electrodes modified with both polyaniline film and multi-walled carbon nanotubes with incorporated β -cyclodextrin. *Analytical and Bioanalytical Chemistry*. 2006;386:2087–2094.
 97. Arjomandi J, Holze R. Spectroelectrochemistry of conducting polypyrrole and poly(pyrrole-cyclodextrin) prepared in aqueous and nonaqueous solvents. *Journal of Solid State Electrochemistry*. 2007;11:1093–1100.
 98. Arjomandi J, Holze R. In situ characterization of N-methylpyrrole and (N-methylpyrrole-cyclodextrin) polymers on gold electrodes in aqueous and nonaqueous solution. *Synthetic Metals*. 2007;157:1021–1028.
 99. Cao AP, Ai HH, Ding YL, Dai CY, Fei JJ. Biocompatible hybrid film of β -cyclodextrin and ionic liquids: A novel platform for electrochemical biosensing. *Sensors and Actuators B*. 2011;155:632–638.
 100. Bouchta D, Izaoumen N, Zejli H, El Kaoutit M, Tamsamani KR. A novel electrochemical synthesis of poly-3-methylthiophene- γ -cyclodextrin film. Application for the analysis of chlorpromazine and some neurotransmitters. *Biosensors and Bioelectronics*. 2005;20:2228–2235.
 101. Abbaspour A, Noori A. A cyclodextrin host-guest recognition approach to an electrochemical sensor for simultaneous quantification of serotonin and dopamine. *Biosensors and Bioelectronics*. 2011;26:4674-4680.
 102. Jiang HG, Yang ZJ, Zhou XT, Fang YX, Ji HB. Immobilization of β -cyclodextrin as insoluble β -cyclodextrin polymer and its catalytic performance. *Chinese Journal Chemical Engineering*. 2012;20(4):784-792.

103. Asanuma H, Kakazu M, Shibata M, Hishiya T, Komiyama M. Synthesis of molecularly imprinted polymer of β -cyclodextrin for the efficient recognition of cholesterol. *Supramolecular Science*. 1998;5:417-421.
104. Hishiya T, Asanuma H, Komiyama M. Spectroscopic anatomy of molecular-imprinting of cyclodextrin. Evidence for preferential formation of ordered cyclodextrin assemblies. *Journal of the American Chemical Society*. 2002;124(4):570-575.
105. Qin L, Hea XW, Li WY, Zhang YK. Molecularly imprinted polymer prepared with bonded β -cyclodextrin and acrylamide on functionalized silica gel for selective recognition of tryptophan in aqueous media. *Journal of Chromatography A*. 2008;1187:94-102.
106. Roche PJR, Ng SM, Narayanaswamy R, Goddard N, Page KM. Multiple surface plasmon resonance quantification of dextromethorphan using a molecularly imprinted β -cyclodextrin polymer: A potential probe for drug-drug interactions. *Sensors and Actuators B*. 2009;139:22-29.
107. Ng SM, Narayanaswamy R. Molecularly imprinted β -cyclodextrin polymer as potential optical receptor for the detection of organic compound. *Sensors and Actuators B*. 2009;139:156-165.
108. Kang YF, Duan WP, Li YN, Kang JX, Xie J. Molecularly imprinted polymers of allyl- β -cyclodextrin and methacrylic acid for the solid-phase extraction of phthalate. *Carbohydrate Polymers*. 2012;88:459-464.
109. Liu XY, Fang HX, Yu LP. Molecularly imprinted photonic polymer based on β -cyclodextrin for amino acid sensing. *Talanta*. 2013;116:283-289.
110. Guo MJ, Hu X, Fan Z, Liu J, Wang XC, Wang Y, Mi HF. Imprinted polymers with cyclodextrin pseudo-polyrotaxanes as pseudo-supports for protein recognition. *Talanta*. 2013;105:409-416.
111. Hu YF, Zhang ZH, Zhang HB, Luo LJ, Yao SZ. Electrochemical determination of L-phenylalanine at polyaniline modified carbon electrode based on β -cyclodextrin incorporated carbon nanotube composite material and imprinted sol-gel film. *Talanta*. 2011;84:305-313.
112. Lian WJ, Huang JD, Yu JH, Zhang XM, Lin Q, He XR, Xing XR, Liu S. A molecularly imprinted sensor based on β -cyclodextrin incorporated multiwalled carbon nanotube and gold nanoparticles-polyamide amine dendrimer nanocomposites combining with water-soluble chitosan derivative for the detection of chlortetracycline. *Food Control*. 2012;26:620-627.
113. Pumera M, Ambrosi A, Bonanni A, Chng ELK, Poh HL. Graphene for electrochemical sensing and biosensing. *Trends in Analytical Chemistry*. 2010;29:954-965.
114. Jacobs CB, Peairs MJ, Venton BJ. Review: Carbon nanotube based electrochemical sensors for biomolecules. *Analytica Chimica Acta*. 2010;662:105-127.
115. Yanez-Sedeno P, Riu J, Pingarron JM, Rius FX. Electrochemical sensing based on carbon nanotubes. *Trends in Analytical Chemistry*. 2010;29:939-953.
116. Yang N, Chen X, Ren T, Zhang P, Yang D. Carbon nanotube based biosensors. *Sensors and Actuators B*. 2015;207:690-715.
117. Saha A, Jiang C, Marti AA. Carbon nanotube networks on different platforms. *Carbon*. 2014;79:1-18.
118. Agui L, Yanez-Sedeno P, Pingarron JM. Role of carbon nanotubes in electroanalytical chemistry, a review. *Analytica Chimica Acta*. 2008;622:11-47.
119. Kuila T, Bose S, Khanra P, Mishra AK, Kim NH, Lee JH. Recent advances in graphene-based biosensors. *Biosensors and Bioelectronics*. 2011;26:4637-4648.
120. Pumera M, Graphene in biosensing. *Materials Today*. 2011;14:308-315.
121. Liu J, Liu Z, Barrow CJ, Yang W. Molecularly engineered graphene surfaces for sensing applications: A review. *Analytica Chimica Acta*. 2015;859:1-19.

122. Lawal AT. Synthesis and utilization of graphene for fabrication of electrochemical sensors. *Talanta*. 2015;131:424–443.
123. Jensen AW, Wilson SR, Schuster DI. Biological applications of fullerenes. *Bioorganic and Medicinal Chemistry*. 1996;4:767-779.
124. Prato M. [60]Fullerene chemistry for materials science applications. *Journal of Materials Chemistry*. 1997;7:1097–1109.
125. Da Ros T, Prato M. Medicinal chemistry with fullerenes and fullerene derivatives. *Chemical Communications*. 1999;8:663–669.
126. Zhang EY, Wang CR. Fullerene self-assembly and supramolecular nanostructures. *Current Opinion in Colloid & Interface Science*. 2009;14:148–156.
127. Afreen S, Muthoosamy K, Manickam S, Hashim U. Functionalized fullerene (C60) as a potential nanomediator in the fabrication of highly sensitive biosensors. *Biosensors and Bioelectronics*. 2015;63:354–364.
128. Kong B, Zeng J, Luo G, Luo S, Wei W, Li J. Layer-by-layer assembled carbon nanotube films with molecule recognition function and lower capacitive background current. *Bioelectrochemistry*. 2009;74:289–294.
129. Yogeswaran U, Thiagarajan S, Chen SM. Pinecone shape hydroxypropyl- β -cyclodextrin on a film of multi-walled carbon nanotubes coated with gold particles for the simultaneous determination of tyrosine, guanine, adenine and thymine. *Carbon*. 2007;45:2783–2796.
130. Wang Z, Xiao S, Chen Y. β -Cyclodextrin incorporated carbon nanotubes-modified electrodes for simultaneous determination of adenine and guanine. *Journal of Electroanalytical Chemistry*. 2006;589:237-242.
131. Kang SZ, Cui Z, Mu J. Electrochemical behavior of sodium cholate and deoxycholate on an electrode modified with multi-walled carbon nanotubes (MWNTs) linked up with cyclodextrin. *Diamond & Related Materials*. 2007;16:12–15.
132. Wang G, Liu X, Yu B, Luo G. Electrocatalytic response of norepinephrine at a β -cyclodextrin incorporated carbon nanotube modified electrode. *Journal of Electroanalytical Chemistry*. 2004;567:227-231.
133. Wang GY, Liu XJ, Luo GA, Wang ZH. α -Cyclodextrin incorporated carbon nanotube-coated electrode for the simultaneous determination of dopamine and epinephrine. *Chinese Journal of Chemistry*. 2005;23:297-302.
134. He JL, Yang Y, Yang X, Liu YL, Liu ZH, Yu RQ. β -Cyclodextrin incorporated carbon nanotube-modified electrode as an electrochemical sensor for rutin. *Sensors and Actuators B: Chemical*. 2006;114:94-100.
135. Joon-Hyung J, Hyunmyung K, Seunho J. Electrochemical selectivity enhancement by using monosuccinyl β -cyclodextrin as a dopant for multi-wall carbon nanotube-modified glassy carbon electrode in simultaneous determination of quercetin and rutin. *Biotechnology Letters*. 2009;31:1739–1744.
136. Alarcon-Angeles G, Perez-Lopez B, Palomar-Pardave M, Ramirez-Silva MT, Alegret S, Merkoci A. Enhanced host–guest electrochemical recognition of dopamine using cyclodextrin in the presence of carbon nanotubes. *Carbon*. 2008;46:898-906.
137. Yang LZ, Xu Y, Wang XH, Zhu J, Zhang RY, He PA, Fang YZ. The application of β -cyclodextrin derivative functionalized aligned carbon nanotubes for electrochemically DNA sensing via host–guest recognition. *Analytica Chimica Acta*. 2011;689:39–46.
138. Zhang W, Chen M, Gong XD, Diao GW. Universal water-soluble cyclodextrin polymer–carbon nanomaterials with supramolecular recognition. *Carbon*. 2013;61:154-163.
139. Jia D, Dai JY, Yuan HY, Lei L, Xiao D. Selective detection of dopamine in the presence of uric acid using a gold nanoparticles-poly(luminol) hybrid film and multi-walled carbon nanotubes with incorporated β -cyclodextrin modified glassy carbon electrode. *Talanta*. 2011;85:2344– 2351

140. Yang HP, Zhu YF, Chen DC, Li CH, Chen SG, Ge ZC. Electrochemical biosensing platforms using poly-cyclodextrin and carbon nanotube composite. *Biosensors and Bioelectronics*. 2010;26:295-298.
141. Lv MJ, Wang XB, Li J, Yang XY, Zhang CA, Yang J, Hu H. Cyclodextrin-reduced graphene oxide hybrid nanosheets for the simultaneous determination of lead(II) and cadmium(II) using square wave anodic stripping voltammetry. *Electrochimica Acta*. 2013;108:412-420.
142. Xu CH, Wang XB, Wang JC, Hu HT, Wan L. Synthesis and photoelectrical properties of β -Cyclodextrin functionalized graphene materials with high bio-recognition capability. *Chemica Physics Letters*. 2010;498:162–167.
143. Liu K, Wei J, Wang C. Sensitive detection of rutin based on β -cyclodextrin@chemically reduced graphene/Nafion composite film. *Electrochimica Acta*. 2011;56:5189–5194
144. Lu LM, Qiu XL, Zhang XB, Shen GL, Tan WH, Yu RQ. Supramolecular assembly of enzyme on functionalized graphene for electrochemical biosensing. *Biosensors and Bioelectronics*. 2013;45:102–107.
145. Tan L, Zhou KG, Zhang YH, Wang HX, Wang XD, Guo YF, Zhang HL. Nanomolar detection of dopamine in the presence of ascorbic acid at β -cyclodextrin/graphene nanocomposite platform. *Electrochemistry Communications*. 2010;12:557–560.
146. Lu DB, Lin SX, Wang LT, Shi XZ, Wang CM, Zhang Y. Synthesis of cyclodextrin-reduced graphene oxide hybrid nanosheets for sensitivity enhanced electrochemical determination of diethylstilbestrol. *Electrochimica Acta*. 2012;85:131-138.
147. Zhang Z, Gu SQ, Ding AP, Shen MJ, Jiang L. Mild and novel electrochemical preparation of β -cyclodextrin/graphene nanocomposite film for super-sensitive sensing of quercetin. *Biosensors and Bioelectronics*. 2014;57:239–244.
148. Wei MC, Tian D, Liu S, Zheng XL, Duan S, Zhou CL. β -Cyclodextrin functionalized graphene material: A novel electrochemical sensor for simultaneous determination of 2-chlorophenol and 3-chlorophenol. *Sensors and Actuators B*. 2014;195:452–458.
149. Yang L, Zhao H, Li YC, Li CP. Electrochemical simultaneous determination of hydroquinone and p-nitrophenol based on host–guest molecular recognition capability of dual β -cyclodextrin functionalized Au@graphene nanohybrids. *Sensors and Actuators B*. 2015;207:1-8.
150. Gong CB, Guo CC, Jiang D, Tang Q, Liu CH, Ma XB. Graphene–cyclodextrin–cytochrome c layered assembly with improved electron transfer rate and high supramolecular recognition capability. *Materials Science Engineering: C*. 2014;39:281–287.
151. Liu ZG, Zhang A, Guo YJ, Dong CA. Electrochemical sensor for ultra sensitive determination of isoquercitrin and baicalin based on DM- β -cyclodextrin functionalized graphene nanosheets. *Biosensors and Bioelectronics*. 2014;58:242–248.
152. Agnihotri N, Chowdhury AD, De A. Non-enzymatic electrochemical detection of cholesterol using β -cyclodextrin functionalized graphene. *Biosensors and Bioelectronics*. 2015;63:212–217.
153. Bosi S, Da Ros T, Spalluto G, Prato M. Fullerene derivatives: an attractive tool for biological applications. *European Journal of Medicinal Chemistry*. 2003;38:913-923.
154. Kato S, Aoshima H, Saitoh Y, Miwa N. Highly hydroxylated or γ -cyclodextrin-bicapped water-soluble derivative of fullerene: The antioxidant ability assessed by electron spin resonance method and β -carotene bleaching assay. *Bioorganic & Medicinal Chemistry Letters*. 2009;19:5293–5296.
155. Furuishi T, Fukami T, Nagase H, Suzuki T, Endo T, Ueda H, Tomono K. Improvement of solubility of C70 by complexation with cyclomaltonaose(δ -cyclodextrin). *Pharmazie*. 2008;63:54-57.

156. Kojima C, Toi Y, Harada A, Kono K. Aqueous solubilization of fullerenes using poly(amidoamine) dendrimers bearing cyclodextrin and poly(ethyleneglycol). *Bioconjugate Chemistry*. 2008;19:2280–2284.
157. Abdulmalik A, Hibah A, Zainy BM, Makoto A, Daisuke I, Masaki O, Kaneto U, Fumitoshi H. Preparation of soluble stable C60/human serum albumin nanoparticles via cyclodextrin complexation and their reactive oxygen production characteristics. *Life Science*. 2013;93:277–282.
158. Zhang MF, Fu L, Wang J, Xu ZQ, Jiang FL, Liu Y. Spectroscopic and electrochemical studies on the interaction of an inclusion complex of β -cyclodextrin/fullerene with bovine serum albumin in aqueous solution. *Journal of Photochemistry and Photobiology A: Chemistry*. 2012;228:28–37.
159. Nobusawa K, Payra D, Naito M. Pyridyl-cyclodextrin for ultra-hydrosolubilization of [60]fullerene. *Chemical Communications*. 2014;50:8339-8342.
160. McNally A, Forster RJ, Keyes TE. Interfacial supramolecular cyclodextrin-fullerene assemblies: host reorientation and guest stabilization. *Physical Chemistry Chemical Physics*. 2009;11:848–856.
161. Ikeda A, Ishikawa M, Aono R, Kikuchi J, Akiyama M, Shinoda W. Regioselective recognition of a [60]fullerene-bisadduct by cyclodextrin. *Journal of Organic Chemistry*. 2013;78:2534–2541.
162. Pospíšil L, Hromadová M, Gál M, Bulíčková J, Sokolová R, Filippone S, Yang J, Guan Z, Rassat A, Zhang YM. Redox potentials and binding enhancement of fullerene and fullerene–cyclodextrin systems in water and dimethylsulfoxide. *Carbon*. 2010;48:153-162.
163. Giacalone F, D'Anna F, Giacalone R, Gruttadauria M, Riela S, Noto R. Cyclodextrin-[60]fullerene conjugates: synthesis, characterization, and electrochemical behavior. *Tetrahedron Letters*. 2006;47:8105–8108.
164. Yuan DQ, Koga K, Kourogi Y, Fujita K. Synthesis of fullerene-cyclodextrin conjugates. *Tetrahedron Letters*. 2001;42:6727–6729.
165. Liu Y, Liang P, Chen Y, Zhao YL, Ding F, Yu A. Spectrophotometric study of fluorescence sensing and selective binding of biochemical substrates by 2,2'-bridged bis(β -cyclodextrin) and its water-soluble fullerene conjugate. *Journal of Physical Chemistry B*. 2005;109:23739-23744.
166. Liu Y, Zhao YL, Chen Y, Liang P, Li L. A water-soluble β -cyclodextrin derivative possessing a fullerene tether as an efficient photodriven DNA-cleavage reagent. *Tetrahedron Letters*. 2005;46:2507–2511.
167. Pospíšil L, Hromadová M, Gál M, Bulíčková J, Sokolová R, Fanelli N. Electrochemical impedance of nitrogen fixation mediated by fullerene–cyclodextrin complex. *Electrochimica Acta*. 2008;53:7445–7450.
168. Rather JA, Debnath P, De Wael K. Fullerene– β -cyclodextrin conjugate based electrochemical sensing device for ultrasensitive detection of p-nitrophenol. *Electroanalysis*. 2013;25(9):2145–2150.
169. Tsutsumi H, Hamasaki K, Mihara H, Ueno A. Cyclodextrin-peptide hybrid as a hydrolytic catalyst having multiple functional groups. *Bioorganic & Medicinal Chemistry Letters*. 2000;10:741-743.
170. Tsutsumi H, Ikeda H, Mihara H, Ueno A. Enantioselective ester hydrolysis catalyzed by β -cyclodextrin conjugated with b-hairpin peptides. *Bioorganic & Medicinal Chemistry Letters*. 2004;14:723–726.
171. Hossain MA, Mihara H, Ueno A. Fluorescence Resonance Energy Transfer in a novel cyclodextrin–peptide conjugate for detecting steroid molecules. *Bioorganic & Medicinal Chemistry Letters*. 2003;13:4305–4308.
172. De Tito S, Morvan F, Meyer A, Vasseur JJ, Cummaro A, Petraccone L, Pagano B, Novellino E, Randazzo A, Giancola C, Montesarchio D. Fluorescence enhancement

upon

G-quadruplex folding: synthesis, structure, and biophysical characterization of a dansyl/cyclodextrin-tagged thrombin binding aptamer. *Bioconjugate Chemistry*. 2013;24: 1917-1927.

173. Le Goff A, Gorgy K, Holzinger M, Haddad R, Zimmerman M, Cosnier S. Biofunctionalization of Carbon Nanotubes via Tris(bispyrene-bipyridine)iron(II): A supramolecular bridge for the π -stacking and pyrene/ β -cyclodextrin host-guest interactions. *Chemistry – A European Journal*. 2011;17:10216-10221.
174. Haddad R, Holzinger M, Villalonga R, Neumann A, Roots J, Maaref A, Cosnier S. Pyrene-adamantane- β -cyclodextrin: An efficient host-guest system for the biofunctionalization of SWCNT electrodes. *Carbon*. 2011;49:2571–2578.
175. Dinh TV, Cullum B. Biosensors and biochips: advances in biological and medical diagnostics. *Fresenius Journal of Analytical Chemistry*. 2000;366:540–551.
176. Shahgaldian P, Pieles U. Cyclodextrin derivatives as chiral supramolecular receptors for enantioselective sensing. *Sensors*. 2006;6:593-615.
177. Cosnier S, Marks R, Lellouche J-P, Perie K, Folgea D, Szunerits. Electrogenerated poly(chiral dicarbazole) films for the reagentless grafting of enzymes. *Electroanalysis*. 2000;12(14):1107-1112.
178. Prieto-Simon B, Campas M, Marty JL. Biomolecule immobilization in biosensor development: tailored strategies based on affinity interactions. *Protein and Peptide Letters*. 2008;15:757–763.
179. Cosnier S. Affinity biosensors based on electropolymerized films. *Electroanalysis*. 2005;17(19):1701-1715.
180. Dupont-Filliard A, Roget A, Livache T, Billon M. Reversible oligonucleotide immobilisation based on biotinylated polypyrrole film. *Analytica Chimica Acta*. 2001;449:45-50.
181. Cosnier S, Novoa A, Mousty C, Mark RS. Biotinylated alginate immobilization matrix in the construction of an amperometric biosensor: application for the determination of glucose. *Analytica Chimica Acta*. 2002;453:71-79.
182. Dupont-Filliard A, BillonM, Livache T, Guillerez S. Biotin/avidin system for the generation of fully renewable DNA sensor based on biotinylated polypyrrole film. *Analytica Chimica Acta*. 2004;515:271–277.
183. Torres Rodriguez LM, Billon M, Roget A, Bidan G. Electrosynthesis of a biotinylated polypyrrole film and study of the avidin recognition by QCM. *Journal of Electroanalytical Chemistry*. 2002;523:70–78.
184. Cosnier S, Galland B, Gondran C, Le Pellec A. Electrogeneration of biotinylated functionalized polypyrroles for the simple immobilization of enzymes. *Electroanalysis*. 1998;10:808-813.
185. Cosnier S, Stoytcheva M, Senillou A, Perrot H, Furriel RPM, Leone FA. A biotinylated conducting polypyrrole for the spatially controlled construction of amperometric biosensor. *Analytical Chemistry*. 1999;71:3692-3697.
186. Cosnier S, LE Pellec A. Poly(pyrrole-biotin): a new polymer for biomolecule grafting on electrode surfaces. *Electrochimica Acta*. 1999;44:1833-1836.
187. Anzai J, Hoshi T, Osa T. Avidin-biotin complexation for enzyme sensor applications. *Trends in Analytical Chemistry*. 1994;73(5):205-210.
188. Cosnier S. Biomolecule immobilization on electrode surfaces by entrapment or attachment to electrochemically polymerized films. A review. *Biosensors & Bioelectronics*. 1999;14:443-456.
189. Ouerghi O, Touhami A, Jaffrezic-Renault N, Martelet C, Ben Ouada H, Cosnier S. Impedimetric immunosensor using avidin-biotin for antibody immobilization. *Bioelectrochemistry*. 2002;56:131– 133.

190. Da Silva S, Grosjean L, Ternan N, Mailley P, Livache T, Cosnier S. Biotinylated polypyrrole films: an easy electrochemical approach for the reagentless immobilization of bacteria on electrode surfaces. *Bioelectrochemistry*. 2004;63:297–301.
191. Davis J, Glidle A, Cass AEG, Zhang J, Cooper JM. Spectroscopic evaluation of protein affinity binding at polymeric biosensor films. *Journal of the American Chemical Society*. 1999;121(17):4302–4303.
192. Haddour N, Cosnier S, Gondran C. Electrogeneration of a poly(pyrrole)-NTA chelator film for a reversible oriented immobilization of histidine-tagged proteins. *Journal of the American Chemical Society*. 2005;127:5752-5753.
193. Cernat A, Le Goff A, Holzinger M, Sandulescu R, Cosnier S. Micro to nanostructured poly(pyrrole-nitrilotriacetic acid) films via nanosphere templates: applications to 3D enzyme attachment by affinity interactions. *Analytical and Bioanalytical Chemistry*. 2014;406:1141-1147.
194. Baur J, Holzinger M, Gondran C, Cosnier S. Immobilization of biotinylated biomolecules onto electropolymerized poly(pyrrole-nitrilotriacetic acid) Cu^{2+} film. *Electrochemistry Communications*. 2010;12:1287-1290.
195. Schrader T, Koch S. Artificial protein sensors, *Molecular BioSystems*. 2007;3:241–248.
196. Feier B, Floner D, Cristea C, Săndulescu R, Geneste F. Development of a novel flow sensor for copper trace analysis by electrochemical reduction of 4-methoxybenzene diazonium salt. *Electrochemistry Communications*. 2013;31:13–15.
197. Cristea C, Feier B, Geneste F, Săndulescu R, Moinet C. New modified porous electrodes for the removal of heavy metal ions from aqueous solutions. *Journal of Environmental Protection and Ecology*. 2009;10(3):633-640.
198. Chow E, Ebrahimi D, Gooding JJ, Hibbert DB. Application of N-PLS calibration to the simultaneous determination of Cu, Cd^{2+} and Pb^{2+} using peptide modified electrochemical sensors. *Analyst*. 2006;131:1051–1057.
199. Chow E, Gooding JJ. Peptide Modified Electrodes as Electrochemical Metal Ion Sensors. *Electroanalysis*. 2006;18:1437-1448.
200. Holford TRJ, Davis F, Higson SPJ. Recent trends in antibody based sensors. *Biosensors and Bioelectronics*. 2012;34:12–24.
201. Song S, Wang L, Li J, Zhao J, Fan C. Aptamer-based biosensors. *Trends in Analytical Chemistry*. 2008;27(2):108-117.
202. Tombelli S, Minunni M, Mascini M. Analytical applications of aptamers. *Biosensors and Bioelectronics*. 2005;20:2424–2434.
203. Citartana M, Gopinathb SCB, Tominagab J, Tanc SC, Tang TH. Assays for aptamer-based platforms. *Biosensors and Bioelectronics*. 2012;34:1–11.
204. Chen H, Chen Q, Zhao Y, Zhang F, Yang F, Tang J, He P. Electrochemiluminescence aptasensor for adenosine triphosphate detection using host–guest recognition between metalocyclodextrin complex and aptamer. *Talanta*. 2014;121:229–233.
205. Chen Q, Chen H, Zhao Y, Zhang F, Yang F, Tang J, He P. A label-free electrochemiluminescence aptasensor for thrombin detection based on host–guest recognition between tris(bipyridine) ruthenium(II)- β -cyclodextrin and aptamer. *Biosensors and Bioelectronics*. 2014;54:547–552.
206. Fan H, Li H, Wang Q, He P, Fang Y. A host–guest-recognition-based electrochemical aptasensor for thrombin detection. *Biosensors and Bioelectronics*. 2012;35:33–36.
207. Jin F, Lian Y, Li J, Zheng J, Hu Y, Liu J, Huang J, Yang R. Molecule-binding dependent assembly of split aptamer and γ -cyclodextrin: A sensitive excimer signaling approach for aptamer biosensors. *Analytica Chimica Acta*. 2013;799:44–50.
208. Keawkim K, Chuanuwatanakul S, Chailapakul O, Motomizu S. Determination of lead and cadmium in rice samples by sequential injection/anodic stripping voltammetry using

- a bismuth film/crown ether/Nafion modified screen-printed carbon electrode. *Food Control*. 2013;31:14-21.
209. Lu J, He X, Zeng X, Wan Q, Zhang Z. Voltammetric determination of mercury (II) in aqueous media using glassy carbon electrodes modified with novel calix[4]arene. *Talanta*. 2003;59:553-560.
 210. El-Kosasy AM, Nebsen M, Abd El-Rahman MK, Salem MY, El-Bardicy MG. Comparative study of 2-hydroxy propyl beta cyclodextrin and calixarene as ionophores in potentiometric ion-selective electrodes for neostigmine bromide. *Talanta*. 2011;85:913– 918.
 211. Duțu G, Cristea C, Bodoki E., Hârceagă V, Saponar A, Popovici EJ, Săndulescu R. The electrochemical behavior of some local anesthetics on screen printed electrodes modified with calixarene. *Farmacia*. 2011;59(2):147–160.
 212. Villalonga R, Camacho C, Cao R, Hernandez J, Matias UC. Amperometric biosensor for xanthine with supramolecular architecture. *Chemical Communications*. 2007;9:942–944.
 213. Granadero D, Bordello J, Perez-Alvite MJ, Novo M, Al-Soufi W. Host-Guest complexation studied by fluorescence correlation spectroscopy: adamantane–cyclodextrin inclusion. *International Journal of Molecular Science*. 2010;11(1):173–188.
 214. Shown I, Ujihara M, Imae T. Sensitizing of pyrene fluorescence by β -cyclodextrin-modified TiO₂ nanoparticles. *Journal of Colloid and Interface Science*. 2010;352:232–237.
 215. Holzinger M, Le Goff A, Cosnier S. Supramolecular immobilization of bio-entities for bioelectrochemical applications. *New Journal of Chemistry*. 2014;38:5173-5180.
 216. Ogoshi T, Harada A. Chemical sensors based on cyclodextrin derivatives. *Sensors*. 2008;8:4961-4982.
 217. Davis ME, Brewster ME. Cyclodextrin-based pharmaceuticals: past, present and future. *Nature Reviews, Drug discovery*. 2004;3:1023-1035.
 218. Ortiz M, Fragoso A, O'Sullivan CK. Detection of Antigliadin Autoantibodies in Celiac Patient Samples Using a Cyclodextrin-Based Supramolecular Biosensor. *Analytical Chemistry*. 2011;83:2931–2938.
 219. Kandimalla VB, Ju HNX. Molecular imprinting: a dynamic technique for diverse applications in analytical chemistry. *Analytical and Bioanalytical Chemistry*. 2004;380:587–605.
 220. Marty JD, Mauzac M. Molecular Imprinting: State of the Art and Perspectives. *Advances in Polymer Science*. 2005;172:1–35.
 221. El-Kemarya M, Sobhya S, El-Dalyb S, Abdel-Shafi A. Inclusion of Paracetamol into β -cyclodextrin nanocavities in solution and in the solid stat. *Spectrochimica Acta Part A*. 2011;9:1904– 1908.
 222. Marian E, Jurca T, Vicaș L, Kacso I, Miclăuș M, Bratu I. Inclusion compounds of erythromycin with β -cyclodextrin. *Revista de Chimie-Bucharest*. 2011;62(11):1065–1068.
 223. Marian E, Mureșan M, Jurca T, Vicaș L. Evaluation of antimicrobial activity of some types of inclusion complexes of erythromycin with β -cyclodextrin on *Staphylococcus aureus*. *Farmacia*. 2013;61(3):518-525.
 224. Vicaș L, Bota S, Moisa C, Ganea M. Evaluation study of the inclusion complex of captopril- β -cyclodextrin. *Farmacia*. 2007;55(1):93–97.
 225. Arias MJ, Moyano JR, Munoz P, Gines JM, Justo A, Giordano F. Study of omeprazole-gamma-cyclodextrin complexation in the solid state. *Drug Development and Industrial Pharmacy*. 2000;26(3):253-259.
 226. Zheng L, Xiong L, Li J, Li X, Sun J, Yang S, Xia J. Synthesis of a novel β -cyclodextrin derivative with high solubility and the electrochemical properties of ferrocene-carbonyl-

- β -cyclodextrin inclusion complex as an electron transfer mediator. *Electrochemistry Communications*. 2008;10:340–345.
227. Bethanis K, Tzamalís P, Tsorteki F, Kokkinou A, Christoforides E, Mentzafos S. Structural study of the inclusion compounds of thymol, carvacrol and eugenol in β -cyclodextrin by X-ray crystallography. *Journal of Inclusion Phenomena and Macrocyclic Chemistry*. 2013;77:163–173.
228. Grandelli HE, Stickle B, Whittington A, Kiran E. Inclusion complex formation of β -cyclodextrin and Naproxen: a study on exothermic complex formation by differential scanning calorimetry. *Journal of Inclusion Phenomena and Macrocyclic Chemistry*. 2013;77:269–277.
229. Xu P, Jiang X, Zhou C, Tang K. Study on inclusion interaction of hydrophilic 2-chloromandelic acid with hydroxypropyl- β -cyclodextrin. *Journal of Inclusion Phenomena and Macrocyclic Chemistry*. 2013;77:447–453.
230. Funasaki N, Nagaoka M, Hirota S. Competitive potentiometric determination of binding constants between α -cyclodextrin and 1-alkanols. *Analytica Chimica Acta*. 2005;531:147–151.
231. Fritea L, Tertîş M, Topală LT, Săndulescu R. Electrochemical and spectral study of cyclodextrins interactions with some pharmaceutical substances. *Farmacia*. 2013;61(6):1054-1068.
232. Vilar M, Navarro M. Determination of cyclodextrin inclusion constant for aromatic carbonyl compounds through spectrophotometric and electrochemical methods. *Electrochimica Acta*. 2010;56:305–313.
233. Marian E. Complecşi ai unor elemente tranziţionale cu substanţe medicamentoase. Editura Politehnica, Timişoara, 2009.
234. Ferancová A, Bucková M, Korgová E, Korbut O, Gründler P, Wärmarm I, Štěpán R, Barek J, Zima J, Labuda J. Association interaction and voltammetric determination of 1-aminopyrene and 1-hydroxypyrene at cyclodextrin and DNA based electrochemical sensors. *Bioelectrochemistry*. 2005;67(2):191–197.
235. Zhang B, Huang D, Xu X, Alemu G, Zhang Y, Zhan F, Shen Y, Wang M. Simultaneous determination of dopamine, ascorbic acid, and uric acid using helical carbon nanotubes modified electrode. *Electrochimica Acta*. 2013;91:261–266.
236. Kannan P, Abraham JS. Determination of nanomolar uric and ascorbic acids using enlarged gold nanoparticles modified electrode. *Analytical Biochemistry*. 2009;386:65–72.
237. Ramirez-Berriozabal M, Galicia L, Gutierrez-Granados S, Sandoval CJ, Herrasti P. Selective electrochemical determination of uric acid in the presence of ascorbic acid using a carbon paste electrode modified with β -Cyclodextrin. *Electroanalysis*. 2008;2:1678–1683.
238. Zhang W, Yuan R, Chai Y-Q, Zhang Y, Chen S-H. A simple strategy based on lanthanum–multiwalled carbon nanotube nanocomposites for simultaneous determination of ascorbic acid, dopamine, uric acid and nitrite. *Sensors and Actuators B-Chemical*. 2012;166–167:601–607.
239. Atta NF, El-Kady MF, Galal A. Simultaneous determination of catecholamines, uric acid and ascorbic acid at physiological levels using poly(N-methylpyrrole)/Pd-nanoclusters sensor. *Analytical Biochemistry*. 2010;400:78–88.
240. Wang C, Yuan R, Chai Y, Chen S, Hu F, Zhang M. Simultaneous determination of ascorbic acid, dopamine, uric acid and tryptophan on gold nanoparticles/overoxidized-polyimidazole composite modified glassy carbon electrode. *Analytica Chimica Acta*. 2012;741:15–20.

241. Hu G, Ma Y, Guo Y, Shao S. Electrocatalytic oxidation and simultaneous determination of uric acid and ascorbic acid on the gold nanoparticles-modified glassy carbon electrode. *Electrochimica Acta*. 2008;53:6610–6615.
242. Ensafi AA, Taei M, Khayamian T. A differential pulse voltammetric method for simultaneous determination of ascorbic acid, dopamine, and uric acid using poly(3-(5-chloro-2-hydroxyphenylazo)-4,5-dihydroxynaphthalene-2,7-disulfonic acid) film modified glassy carbon electrode. *Journal of Electroanalytical Chemistry*. 2009;633:212–220.
243. Ensafi AA, Rezaei B, Mirahmadi ZSZ, Taei M. Simultaneous determination of ascorbic acid, epinephrine, and uric acid by differential pulse voltammetry using poly(3,3'-bis[N,N-bis(carboxymethyl)aminomethyl]-o-cresolsulfonophthalein) modified glassy carbon electrode. *Sensors and Actuators B*. 2010;150:321–329.
244. Zheng X, Zhou X, Ji X, Lin R, Lin W. Simultaneous determination of ascorbic acid, dopamine and uric acid using poly(4-aminobutyric acid) modified glassy carbon electrode. *Sensors and Actuators B*. 2013;178:359–365.
245. Sun C-L, Lee H-H, Yang J-M, Wu C-C. The simultaneous electrochemical detection of ascorbic acid, dopamine, and uric acid using graphene/size-selected Pt nanocomposites. *Biosensors and Bioelectronics*. 2011;26:3450–3455.
246. Sheng Z-H, Zheng X-Q, Xu J-Y, Bao W-J, Wang F-B, Xia X-H. Electrochemical sensor based on nitrogen doped graphene: Simultaneous determination of ascorbic acid, dopamine and uric acid. *Biosensors and Bioelectronics*. 2012;34:125–131.
247. Ping J, Wu J, Wang Y, Ying Y. Simultaneous determination of ascorbic acid, dopamine and uric acid using high-performance screen-printed graphene electrode. *Biosensors and Bioelectronics*. 2012;34:70-76.
248. Vulcu A, Grosan C, Muresan LM, Pruneanu S, Olenic L. Modified gold electrodes based on thiocytosine/guanine-gold nanoparticles for uric and ascorbic acid determination. *Electrochimica Acta*. 2013;88:839–846.
249. Ensafi AA, Taei M, Khayamian T, Arabzadeh A. Highly selective determination of ascorbic acid, dopamine, and uric acid by differential pulse voltammetry using poly(sulfonazo III) modified glassy carbon electrode. *Sensors and Actuators B*. 2010;147:213–221.
250. Huaqing B, Yanhui L, Shufeng L, Peizhi G, Zhongbin W, Chunxiao L, Jizhen Z, Zhao XS. Carbon-nanotube-modified glassy carbon electrode for simultaneous determination of dopamine, ascorbic acid and uric acid: The effect of functional groups. *Sensors and Actuators B*. 2012;171–172:1132–1140.
251. Mbougouena JCK, Kenfack IT, Walcarius A, Ngameni E. Electrochemical response of ascorbic and uric acids at organoclay film modified glassy carbon electrodes and sensing applications. *Talanta*. 2011;85:754–762.
252. Afrasiabi M, Kianipour S, Babaei A, Nasimi AA, Shabanian M. 2013. A new sensor based on glassy carbon electrode modified with nanocomposite for simultaneous determination of acetaminophen, ascorbic acid and uric acid. *Journal of Saudi Chemical Society*. Available at: <http://dx.doi.org/10.1016/j.jscs.2013.02.002>. Accessed April 30, 2014.
253. Zare HR, Nasirizadeh N. Simultaneous determination of ascorbic acid, adrenaline and uric acid at a hematoxylin multi-wall carbon nanotube modified glassy carbon electrode. *Sensors and Actuators B-Chemical*. 2010;143:666–672.
254. Sekli-Belaidi F, Temple-Boyer P, Gros P. Voltammetric microsensor using PEDOT-modified gold electrode for the simultaneous assay of ascorbic and uric acids. *Journal of Electroanalytical Chemistry*. 2010;647:159–168.

255. Prakash S, Chakrabarty T, Rajesh AM, Shahi VK. Investigation of polyelectrolyte for electrochemical detection of uric acid in presence of ascorbic acid. *Measurement*. 2012;45:500–506.
256. Colleran JJ, Breslin CB. Simultaneous electrochemical detection of the catecholamines and ascorbic acid at PEDOT/S- β -CD modified gold electrodes. *Journal of Electroanalytical Chemistry*. 2012;667:30–37.
257. Wu S, Wang T, Gao Z, Xu H, Zhou B, Wang C. Selective detection of uric acid in the presence of ascorbic acid at physiological pH by using a β -cyclodextrin modified copolymer of sulfanilic acid and N-acetylaniline. *Biosensors and Bioelectronics*. 2008;23:1776–1780.
258. Ferin R, Pavão ML, Baptista J. Rapid, sensitive and simultaneous determination of ascorbic and uric acids in human plasma by ion-exclusion HPLC-UV. *Clinical Biochemistry*. 2013;46:665–669.
259. Kandar R, Drábková P, Hampl R. The determination of ascorbic acid and uric acid in human seminal plasma using an HPLC with UV detection. *Journal of chromatography. B, Analytical technologies in the biomedical and life sciences*. 2011;879:2834–2839.
260. Li X, Franke AA. Fast HPLC–ECD analysis of ascorbic acid, dehydroascorbic acid and uric acid. *Journal of chromatography. B, Analytical technologies in the biomedical and life sciences*. 2009;877:853–856.
261. Sassolas A, Blum LJ, Leca-Bouvier BD. Immobilization strategies to develop enzymatic biosensors, *Biotechnology Advances*. 2012;30:489-511.
262. Sima V, Cristea C, Lăpăduș F, Marian IO, Marian A, Săndulescu S. Electroanalytical properties of a novel biosensor modified with zirconium alcoxide porous gels for the detection of acetaminophen. *Journal of Pharmaceutical and Biomedical Analysis*. 2008;48:1195–1200.
263. Sima V, Cristea C, Bodoki E, Dutu G, Sandulescu R. Screen-printed electrodes modified with HRP-zirconium alcoxide film for the development of a biosensor for acetaminophen detection. *Central European Journal of Chemistry*. 2010;8:1034-1040.
264. Fritea L, Tertiş M, Cristea C, Săndulescu R. New β -Cyclodextrin entrapped in polyethyleneimine film-modified electrodes for pharmaceutical compounds determination. *Sensors*. 2013;13:16312-16329.
265. Fritea L, Tertiş M, Cristea C, Cosnier S, Săndulescu R. Simultaneous Determination of Ascorbic and Uric Acids in Urine Using an Innovative Electrochemical Sensor Based on β -Cyclodextrin. *Analytical Letters*. 2015;48(1):89-99.
266. Colin-Orozco E, Corona-Avendano S, Ramirez-Silva MT, Romero-Romo M, Palomar-Pardave M. On the electrochemical oxidation of dopamine, ascorbic acid and uric acid onto a bare carbon paste electrode from a 0.1 M NaCl aqueous solution at pH 7. *International Journal of Electrochemical Science*. 2012;7:6097-6105.
267. Larkin PJ. *Infrared and Raman spectroscopy – Principles and spectral interpretation*. Waltman MA, USA, Elsevier, 2011.
268. Heise HM, Kuckuk R, Bereck A, Riegel D. Infrared spectroscopy and Raman spectroscopy of cyclodextrin derivatives and their ferrocene inclusion complexes. *Vibrational Spectroscopy*. 2010;53:19–23.
269. Krishna MPR, Sreelakshmi G, Muraleedharan CV, Joseph R. Water soluble complexes of curcumin with cyclodextrins: Characterization by FT-Raman spectroscopy. *Vibrational Spectroscopy*. 2012;62:77–84.
270. Rezaei NSM, Hoorfar M. Study of proton exchange membrane fuel cells using electrochemical impedance spectroscopy technique - A review. *Journal of Power Sources*. 2013;240:281-293.

271. Nijhuis CA, Boukamp BA, Ravoo BJ, Huskens J, Reinhoudt DN, Electrochemistry of ferrocenyl dendrimer- β -cyclodextrin assemblies at the interface of an aqueous solution and a molecular printboard. *The Journal of Physical Chemistry C*. 2007;111:9799-9810.
272. Kang J, Wen J, Jayaramb SH, Wang X, Chen S-C. Electrochemical characterization and equivalent circuit modeling of single-walled carbon nanotube (SWCNT) coated electrodes. *Journal of Power Sources*. 2013;234:208-221.
273. Wang Z, Dong X, Li J. An inlaying ultra-thin carbon paste electrode modified with functional single-wall carbon nanotubes for simultaneous determination of three purine derivatives. *Sensors and Actuators B-Chemical*. 2008;131:411-416.
274. Duțu G, Tertîș M, Săndulescu R, Cristea C. Differential pulse and square wave voltammetric methods for procaine hydrochloride determination using GCE and graphite based SPEs modified with p-tertbutyl-diester-calix[4]arene. *Revista de Chimie*. 2014;65(2):142-147.
275. Tertîș M, Florea A, Săndulescu R, Cristea C. Carbon based electrodes modified with horseradish peroxidase immobilized in conducting polymers for acetaminophen analysis. *Sensors*. 2013;13:4841-4854.
276. *Farmacopeea Română*, 10th ed.; Medicală: Bucharest, Romania. 2008:67-68;514-515.
277. *European Pharmacopoeia*, 7th ed.; EQCM; Strasbourg, France. 2011:1418.
278. Cristea AN. *Tratat de farmacologie*. ed. I, Editura Medicală București. 2008:834-837.
279. Kochmann S, Hirsch T, Wolfbeis OS. Graphenes in chemical sensors and biosensors. *TRAC-Trends in Analytical Chemistry*. 2012;39:87-113.
280. Sun Z, Vivekananthan J, Guschin DA, Huang X, Kuznetsov V, Ebbinghaus P, Sarfraz A, Muhler M, Schuhmann W. High-concentration graphene dispersions with minimal stabilizer: A scaffold for enzyme immobilization for glucose oxidation. *Chemistry: A European Journal*. 2014;20:5752-5761.
281. Cosnier S, Holzinger M. Design of carbon-nanotube-polymer frameworks by electropolymerization of SWCNTs-pyrrole derivatives. *Electrochimica Acta*. 2008;53:3948-3954.
282. Le Goff A, Holzinger M, Cosnier S. Characterization of multi-walled carbon nanotube electrodes functionalized by electropolymerized tris(pyrrole-ether bipyridine) ruthenium(II). *Electrochimica Acta*. 2011;56:3633-3640.
283. Gao F, Cai X, Wang X, Gao C, Liu S, Gao F, Wang Q. Highly sensitive and selective detection of dopamine in the presence of ascorbic acid at graphene oxide modified electrode. *Sensors and Actuators B*. 2013;186:380-387.
284. Gaied A, Jaballah N, Tounsi M, Braiek M, Jaffrezic-Renault N, Majdoub M. Selective detection of dopamine in presence of ascorbic acid by use of glassy-carbon electrode modified with amino- β -cyclodextrin and carbon nanotubes. *Electroanalysis*. 2014;26:1-8.
285. Huong, VT, Shimanouchi T, Quan DP, Umakoshi H, Viet PH, Kuboi R. Polymethylthiophene/Nafion-modified glassy carbon electrode for selective detection of dopamine in the presence of ascorbic acid. *Journal of Applied Electrochemistry*. 2009;39:2035-2042.
286. Ali SR, Ma Y, Parajuli RR, Balogun Y, Lai WYC, He H. A nonoxidative sensor based on a self-doped polyaniline/carbon nanotube composite for sensitive and selective detection of the neurotransmitter dopamine. *Analytical Chemistry*. 2007;79:2583-2587.
287. Chen J, Zhang J, Lin X, Wan H, Zhang S. Electrocatalytic oxidation and determination of dopamine in the presence of ascorbic acid and uric acid at a poly (4-(2-pyridylazo)-resorcinol) modified glassy carbon electrode. *Electroanalysis*. 2007;19:612-615.

288. Shervedani RK, Bagherzadeh M, Mozaffari SA. Determination of dopamine in the presence of high concentration of ascorbic acid by using gold cysteamine self-assembled monolayers as a nanosensor. *Sensors and Actuators B*. 2006;115:614–621.
289. Thiagarajan S, Chen S-M. Preparation and characterization of Pt Au hybrid film modified electrodes and their use in simultaneous determination of dopamine, ascorbic acid and uric acid. *Talanta*. 2007;74:212–222.
290. Tsai TH, Huang YC, Chen S-M, Ali MA, Hemaïd FMAA, Fabrication of Multifunctional Biosensor for the Determination of Hydrogen Peroxide, Dopamine and Uric Acid. *International Journal of Electrochemical Science*. 2011;6:6456-6468.
291. Zhang Y, Pan Y, Su S, Zhang L, Li S, Shao M. A novel functionalized single-wall carbon nanotube modified electrode and its application in determination of dopamine and uric acid in the presence of high concentrations of ascorbic acid. *Electroanalysis*. 2007;19:1695–1701.
292. Bujduveanu M-R, Yao W, Le Goff A, Gorgy K, Shan D, Diao G-W, Ungureanu E-M, Cosnier S. Multiwalled carbon nanotube-CaCO₃ nanoparticle composites for the construction of a tyrosinase-based amperometric dopamine biosensor. *Electroanalysis*. 2013;25(3):613–619.
293. Yang L, Liu D, Huang J, You T. Simultaneous determination of dopamine, ascorbic acid and uric acid at electrochemically reduced graphene oxide modified electrode. *Sensors and Actuators B*. 2014;193:166–172.
294. Kim Y-R, Bong S, Kang Y-J, Yang Y, Mahajan RK, Kim JS, Kim H. Electrochemical detection of dopamine in the presence of ascorbic acid using graphene modified electrodes. *Biosensors and Bioelectronics*. 2010;25:2366–2369.
295. Wu L, Feng L, Ren J, Qu X. Electrochemical detection of dopamine using porphyrin-functionalized graphene. *Biosensors and Bioelectronics*. 2012;34:57–62.
296. Wang Y, Li Y, Tang L, Lu J, Li J. Application of graphene-modified electrode for selective detection of dopamine. *Electrochemistry Communications*. 2009;11:889–892.
297. Zhuang Z, Li J, Xu R, Xiao D. Electrochemical detection of dopamine in the presence of ascorbic acid using overoxidized polypyrrole/graphene modified electrodes. *International Journal of Electrochemical Science*. 2011;6:2149–2161.
298. Du J, Yue R, Ren F, Yao Z, Jiang F, Yang P, Du Y. Simultaneous determination of uric acid and dopamine using a carbon fiber electrode modified by layer-by-layer assembly of graphene and gold nanoparticles. *Gold Bulletin*. 2013;46:137–144.
299. Zhang Y, Yuan R, Chai Y, Li W, Zhong X, Zhong H. Simultaneous voltammetric determination for DA, AA and NO²⁻ based on graphene/poly-cyclodextrin/MWCNTs nanocomposite platform. *Biosensors and Bioelectronics*. 2011;26:3977–3980.
300. Fritea L, Florea A, Tertîş M, Săndulescu R, Cristea C. Polymer based nanostructures for innovative bio and immunosensors development. *International Conference on Advancements of Medicine and Health Care through Technology “MediTech 2014” Proceedings, Simona Vlad, R.V. Ciupa (Eds), Springer, vol. 44, 129-134 ISBN 978-3-319-07652-2;*
301. Fritea L, Tertîş M, Cosnier S, Cristea C, Săndulescu R. A novel reduced graphene/b-cyclodextrin/tyrosinase biosensor for dopamine detection. *International Journal of Electrochemical Science*. 2015;10:7292-7302.
302. Guo Y, Guo S, Ren J, Zhai Y, Dong S, Wang E. Cyclodextrin functionalized graphene nanosheets with high supramolecular recognition capability: synthesis and host-guest inclusion for enhanced electrochemical performance, *ACS Nano*. 2010;4:4001-4010.
303. Fritea L, Le Goff A, Putaux J-L, Tertîş M, Cristea C, Săndulescu R, Cosnier S. Design of a reduced-graphene-oxide composite electrode from an electropolymerizable graphene aqueous dispersion using a cyclodextrine-pyrrole monomer. Application to dopamine biosensing. *Electrochimica Acta*. 2015;178:108-112.

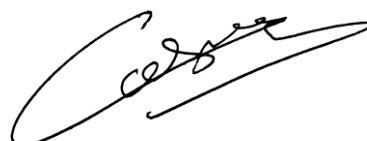
304. Cosnier S, Innocent C. A new strategy for the construction of a tyrosinase-based amperometric phenol and o-diphenol sensor. *Bioelectrochemistry and Bioenergetics*. 1993;31:147-160.
305. Guo Y, Guo S, Li J, Wang E, Dong S. Cyclodextrin–graphene hybrid nanosheets as enhanced sensing platform for ultrasensitive determination of carbendazim. *Talanta*. 2011;84:60–64.
306. Bustos-Ramírez K, Martínez-Hernández AL, Martínez-Barrera G, Icaza M, Castaño VM, Velasco-Santos C. Covalently Bonded Chitosan on Graphene Oxide via Redox Reaction. *Materials*. 2013;6:911-926.
307. Hu X, Qi R, Zhu J, Lu J, Luo Y, Jin J, Jiang P. Preparation and properties of dopamine reduced graphene oxide and its composites of epoxy. *Journal of Applied Polymer Science*. 2014;131(2), DOI: 10.1002/APP.39754.
308. Shan C, Yang H, Han D, Zhang Q, Ivaska A, Niu L. Water-Soluble Graphene Covalently Functionalized by Biocompatible Poly-L-lysine. *Langmuir*. 2009;25:12030-12033.
309. Shan C, Yang H, Song J, Han D, Ivaska A, Niu L. Direct electrochemistry of glucose oxidase and biosensing for glucose based on graphene. *Analytical Chemistry*. 2009;81:2378-2382.
310. Stankovich S, Piner RD, Chen X, Wu N, Nguyen ST, Ruoff RS. Stable aqueous dispersions of graphitic nanoplatelets via the reduction of exfoliated graphite oxide in the presence of poly(sodium 4-styrenesulfonate). *Journals of Material Chemistry*. 2006;16:155-158.
311. Pei S, Cheng H-M. The reduction of graphene oxide. *Carbon*. 2012;50:3210–3228.
312. Choi E-Y, Han TH, Hong J, Kim JE, Lee SH, Kim HW, Kim SO. Noncovalent functionalisation of graphene with end-functional polymers. *Journals of Material Chemistry*. 2010;20:1907–1912.
313. Terțiș M, Florea A, Feier B, Marian IO, Silaghi-Dumitrescu L, Cristea A, Săndulescu R, Cristea C. Electrochemical impedance studies on single and multi-walled carbon nanotubes-polymer nanocomposites for biosensors development. *Journal of Nanoscience and Nanotechnology*. 2015;15:3385-3393.
314. *Farmacopeea Română*, 10th ed., Editura Medicală: Bucharest, Romania, 2008:510-514, 524-525.
315. Clavier G, Audebert P. s-Tetrazines as building blocks for new functional molecules and molecular materials. *Chemical Reviews*. 2010;110:3299–3314.
316. Quinton C, Alain-Rizzo V, Dumas-Verdes C, Miomandre F, Audebert P. Tetrazine–triphenylamine dyads: Influence of the nature of the linker on their properties. *Electrochimica Acta*. 2013;110:693–701.
317. Kim Y, Kim E, Clavier G, Audebert P. New tetrazine-based fluoro-electrochromic window; modulation of the fluorescence through applied potential. *Chemistry Communications*. 2006;34:3612–3614.
318. Kim Y, Do J, Kim E, Clavier G, Galmiche L, Audebert P. Tetrazine-based electrofluoro-chromic windows: Modulation of the fluorescence through applied potential. *Journal of Electroanalytical Chemistry*. 2009;635:201–205.
319. Miomandre F, Méallet-Renault R, Vachon J-J, Pansua RB, Audebert P. Fluorescence microscopy coupled to electrochemistry: a powerful tool for the controlled electrochemical switch of fluorescent molecules. *Chemistry Communications*. 2008;16:1913-1915.
320. Qing Z, Audebert P, Clavier G, Miomandre F, Tang J, Vu TT, Méallet-Renault R. Tetrazines with hindered or electron withdrawing substituents: Synthesis, electrochemical and fluorescence properties. *Journal of Electroanalytical Chemistry*. 2009;632: 39–44.

321. Seo S, Kim Y, Zhou Q, Clavier G, Audebert P, Kim E. White electrofluorescence switching from electrochemically convertible yellow fluorescent dyad. *Advanced Functional Materials*. 2012;22:3556–3561.
322. Audebert P, Miomandre F, Clavier G, Vernières M-C, Badré S, Méallet-Renault R. Synthesis and properties of new tetrazines substituted by heteroatoms: Towards the world's smallest organic fluorophores. *Chemistry - A European Journal*. 2005;11:5667–5673.
323. Kaim W. The coordination chemistry of 1,2,4,5-tetrazines. *Coordination Chemistry Reviews*. 2002;230:127-139.
324. Saracoglu N. Recent advances and applications in 1,2,4,5-tetrazine chemistry. *Tetrahedron*. 2007;63:4199–4236.
325. Hu W-X, Rao G-W, Sun Y-Q. Synthesis and antitumor activity of s-tetrazine derivatives. *Bioorganic & Medicinal Chemistry Letters*. 2004;14:1177–1181.
326. Rao G-W, Wang C, Wang J, Zhao Z-G, Hu W-X. Synthesis, structure analysis, antitumor evaluation and 3D-QSAR studies of 3,6-disubstituted-dihydro-1,2,4,5-tetrazine derivatives. *Bioorganic & Medicinal Chemistry Letters*. 2013;23:6474–6480.
327. Jaiswal S, Varma PCR, O'Neill L, Duffy B, McHale P. An investigation of the biochemical properties of tetrazines as potential coating additives. *Materials Science and Engineering C*. 2013;33:1925–1934.
328. Devaraj NK, Upadhyay R, Haun JB, Hilderbrand SA, Weissleder R. Fast and sensitive pretargeted labeling of cancer cells through a tetrazine/trans-cyclooctene cycloaddition. *Angewandte Chemie International Edition*. 2009;48:7013–7016.
329. Devaraj NK, Weissleder R, Hilderbrand SA. Tetrazine-based cycloadditions: Application to pretargeted live cell imaging. *Bioconjugate Chemistry*. 2008;19:2297–2299.
330. Garau C, Quinonero D, Frontera A, Costa A, Ballester P, Dey PM. s-Tetrazine as a new binding unit in molecular recognition of anions. *Chemical Physics Letters*. 2003;370:7–13.
331. Hayden H, Gunko YK, Perova ST. Chemical modification of multi-walled carbon nanotubes using a tetrazine derivative. *Chemical Physics Letters*. 2007;435:84–89.
332. Li H, Zhou Q, Audebert P, Miomandre F, Allain C, Yang F, Tang J. New conducting polymers functionalized with redox-active tetrazines. *Journal of Electroanalytical Chemistry*. 2012;668:26–29.
333. Fritea L, Audebert P, Galmiche L, Gorgy K, Le Goff A, Săndulescu R, Cosnier S. First occurrence of tetrazines in aqueous solution. *Electrochemistry and fluorescence. ChemPhysChem*. 2015, accepted.
334. Zhong C, Mu T, Wang L, Fu E, Qin J. Unexpected fluorescent behavior of a 4-amino-1,8-naphthalimide derived β -cyclodextrin: conformation analysis and sensing properties. *Chemistry Communications*. 2009;27:4091–4093.
335. Campos IB, Brochsztain S. Inclusion complexes of cyclodextrins with 4-Amino-1,8-Naphthalimides. *Journal of Inclusion Phenomena and Macrocyclic Chemistry*. 2002;44:207–211.
336. Silva BPG, Marcon RO, Brochsztain S. Inclusion complexes of cyclodextrins with 4-amino-1,8-naphthalimides (part 2). *Journal of Inclusion Phenomena and Macrocyclic Chemistry*. 2010;68:313–322.
337. Gong Y-H, Miomandre F, Méallet-Renault R, Badré S, Galmiche L, Tang J, Audebert P, Clavier G. Synthesis and Physical Chemistry of s-Tetrazines: Which Ones are Fluorescent and Why?. *European Journal of Organic Chemistry*. 2009;35:6121-6128.
338. Dumas-Verdes C, Miomandre F, Lepicier E, Galangau O, Vu TT, Clavier G, Meallet-Renault R, Audebert P. BODIPY-Tetrazine Multichromophoric Derivatives. *European Journal of Organic Chemistry*. 2010;13:2525-2535.

339. Zhou Q, Audebert P, Clavier G, Méallet-Renault R, Miomandre F, Shaukat Z, Tang J. New Tetrazines Functionalized with Electrochemically and Optically Active Groups: Electrochemical and Photoluminescence Properties. *The Journal of Physical Chemistry C*. 2011;115:21899-21906.
340. Zhou Q, Clavier G, Mallet-Renault R, Miomandre F, Audebert P, Tang J. Bright fluorescence through activation of a low absorption fluorophore: the case of a unique naphthalimide–tetrazine dyad. *New Journal of Chemistry*. 2011;35:1678-1682.
341. Abruña HD. Coordination chemistry in two dimensions: Chemically modified electrodes. *Coordination Chemistry Reviews*. 1988;86:135–189.
342. Whittell G.R, Hager MD, Schubert US, Manners I. Functional soft materials from metallopolymers and metallosupramolecular polymers. *Nature Materials*. 2011;10:176–188.
343. Lapedes Am., Ashford DL, Hanson K, Torelli DA., Templeton JL, Meyer TJ. Stabilization of a ruthenium(II) polypyridyl dye on nanocrystalline TiO₂ by an electropolymerized overlayer. *Journal of the American Chemical Society*. 2013;135:15450–15458.
344. Yao WJ, Le Goff A, Spinelli N, Holzinger M, Diao G-W, Shan D, Defrancq E, Cosnier S. Electrogenerated trisbipyridyl Ru(II)-/nitritotriacetic-polypyrene copolymer for the easy fabrication of label-free photoelectrochemical immunosensor and aptasensor. Application to the determination of thrombin and anti-cholera toxin antibody. *Biosensors and Bioelectronics*. 2013;42:556–562.
345. Shan D, Qian B, Ding S-N, Zhu W, Cosnier S., Xue H-G. Enhanced solid-state electrochemiluminescence of tris(2,2'-bipyridyl)ruthenium(II) incorporated into electrospun nanofibrous Mat. *Analytical Chemistry*. 2010;82:5892–5896.
346. Moss JA, Stipkala JM, Yang JC, Bignozzi CA, Meyer GJ, Meyer TJ, Wen XG, Linton RW. Sensitization of nanocrystalline TiO₂ by electropolymerized thin film. *Chemistry of Materials*. 1998;10:1748–1750.
347. Le Goff A, Cosnier S. Photocurrent generation by MWCNTs functionalized with bis-cyclometallated Ir(III)- and trisbipyridyl ruthenium(II)- polypyrrole films. *Journal of Materials Chemistry*. 2011;21:3910–3915.
348. Le Goff A, Reuillard B, Cosnier S. A pyrene-substituted tris(bipyridine)osmium(II) complex as a versatile redox probe for characterizing and functionalizing carbon nanotube- and graphene-based electrodes. *Langmuir*. 2013;29(27):8736–8742.
349. Bartlett PN, Baumberg JJ, Birkin PR, Ghanem MA, Netti MC. Highly ordered macroporous gold and platinum films formed by electrochemical deposition through templates assembled from submicron diameter monodisperse polystyrene spheres. *Chemistry of Materials*. 2002;14:2199–2208.
350. Bartlett PN, Birkin PR, Ghanem MA. Electrochemical deposition of macroporous platinum, palladium and cobalt films using polystyrene latex sphere templates. *Chemistry Communications*. 2000;7:1671–1672.
351. Szamocki R, Reculosa S, Ravaine S, Bartlett PN, Kuhn A, Hempelmann R. Tailored mesostructuring and biofunctionalization of gold for increased electroactivity. *Angewandte Chemie*. 2006;45:1317–1321.
352. Cernat A, Griveau S, Martin P, Lacroix JC, Farcău C, Săndulescu R, Bedioui F. Electrografted nanostructured platforms for click chemistry. *Electrochemistry Communications*. 2012;23:141–144.
353. Santos L, Ghilane J, Lacroix J-C. Surface patterning based on nanosphere lithography and electroreduction of in situ generated diazonium cation. *Electrochemistry Communications*. 2012;18:20–23.

354. Sumida T, Wada Y, Kitamura T, Yanagida S. Electrochemical preparation of macroporous polypyrrole films with regular arrays of interconnected spherical voids. *Chemical Communications*. 2000;17:1613–1614.
355. Tian S, Wang J, Jonas U, Knoll W. Inverse opals of polyaniline and its copolymers prepared by electrochemical techniques. *Chemistry of Materials*. 2005;17:5726–5730.
356. Zhang G, Wang D. Colloidal lithography—the art of nanochemical patterning. *Chemistry - An Asian Journal*. 2009;4:236–245.
357. Fritea L, Haddache F, Reuillard B, Le Goff A, Gorgy K, Gondran C, Holzinger M, Săndulescu R, Cosnier S. Electrochemical nanopatterning of an electrogenerated photosensitive poly-[trisbipyridinyl-pyrrole ruthenium(II)] metallopolymer by nanosphere lithography. *Electrochemistry Communications*. 2014;46:75–78.

Dr. Serge COSNIER

A handwritten signature in black ink, appearing to read 'Serge Cosnier', written in a cursive style.